Stability and Power Sharing in Microgrids

vorgelegt von
Dipl.-Ing.
Johannes Schiffer
aus Stuttgart

von der Fakultät IV - Elektrotechnik und Informatik
der Technischen Universität Berlin
zur Erlangung des Akademischen Grades

Doktor der Ingenieurwissenschaften
- Dr.-Ing. -

genehmigte Dissertation

Promotionsausschuss:

Vorsitzender: Prof. Dr.-Ing. Clemens Gühmann
Gutachter: Prof. Dr.-Ing. Jörg Raisch
Gutachter: Dr. Romeo Ortega
Gutachter: Prof. Dr. Veit Hagenmeyer
Gutachter: Dr.-Ing. Tevfik Sezi
Tag der wissenschaftlichen Aussprache: 16. Juni 2015

Berlin 2015
D 83

Abstract

Motivated by environmental, economic and technological aspects, the penetration of renewable energy sources into the electrical networks is increasing worldwide. This fact requires a paradigmatic change in power system operation. One solution to facilitate this change are microgrids. In the present work, the problems of frequency stability, voltage stability and power sharing in microgrids are considered. More precisely, control concepts that address the aforementioned problems are investigated. The main contributions of the present work comprise: *(i)* A generic modular model of an uncontrolled microgrid is derived. *(ii)* A consensus-based distributed voltage control (DVC) is proposed, which guarantees a desired reactive power distribution in steady-state. In contrast with other control strategies available thus far, the control presented in this work only requires distributed communication among generation units, i.e., no central computing nor communication unit is needed. *(iii)* Conditions for local asymptotic stability of several microgrid configurations are derived. The considered networks comprise inverter-based microgrids operated with frequency and voltage droop control, as well as microgrids operated with frequency droop control and the proposed DVC. The conditions are established via converse Lyapunov theorems in combination with tools from linear algebra, as well as port-Hamiltonian systems. Most conditions are derived under the assumption of dominantly inductive power lines. *(iv)* Conditions are given under which the frequency droop control, respectively the proposed DVC, solve the problem of active, respectively reactive, power sharing in microgrids with dominantly inductive power lines. The claims are established by combining the aforementioned stability results with a design criterion for the controller gains and setpoints of the frequency droop control, respectively with the inherent properties of the DVC. *(v)* The analysis is validated via simulation on a microgrid based on the CIGRE benchmark medium voltage distribution network.

Kurzfassung

Aus ökologischen, ökonomischen und technologischen Gründen steigt der Anteil erneuerbarer Energien in elektrischen Netzen seit mehreren Jahren weltweit stetig an. Diese Entwicklung erfordert einen Paradigmenwechsel im Betrieb elektrischer Energienetze. Eine potentielle Lösung hierfür sind Microgrids. In der vorliegenden Arbeit werden die Probleme der Frequenzstabilität, der Spannungsstabilität sowie der Leistungsaufteilung in Microgrids betrachtet. Konkret werden Regelungskonzepte untersucht, die die oben genannten Probleme lösen sollen. Die vorliegende Arbeit enthält hierzu folgende Beiträge: *(i)* Es wird ein modulares Modell eines ungeregelten Microgrids hergeleitet. *(ii)* Es wird ein konsensbasiertes verteiltes Spannungsregelgesetz (VSR) vorgestellt, das eine gewünschte stationäre Blindleistungsaufteilung gewährleistet. Im Gegensatz zu anderen bisher verfügbaren Regelstrategien benötigt das vorliegende Regelgesetz lediglich verteilte Kommunikation zwischen den Erzeugungseinheiten, d.h. es ist keine zentrale Kommunikationseinheit notwendig. *(iii)* Es werden lokale Stabilitätsbedingungen für verschiedene Microgridkonfigurationen hergeleitet. Die betrachteten Netze umfassen wechselrichterbasierte Microgrids, die mit Frequenz- und Spannungs-Droop-Regelung betrieben werden, sowie Microgrids, die mit Frequenz-Droop-Regelung und dem vorgestellten VSR betrieben werden. Den meisten dieser Ergebnisse liegt die Annahme stark induktiver Stromleitungen zugrunde. *(iv)* Es werden Bedingungen aufgezeigt, unter denen die Frequenz-Droop-Regelung bzw. das vorgestellte VSR das Problem der Wirk- bzw. Blindleistungsaufteilung in Microgrids mit stark induktiven Stromleitungen löst. Hierzu werden die zuvor erwähnten Stabilitätsbedingungen mit einem Entwurfskriterium für die Reglerparameter der Frequenz-Droop-Regelung bzw. mit den inhärenten Eigenschaften des VSR kombiniert. *(v)* Die Analyse wird anhand von Simulationen auf Basis des CIGRE Benchmark Mittelspannungsverteilnetzes validiert.

To alicia.

Acknowledgements

The present thesis would not have been possible without the help, support and encouragement of many people.

First of all, I would like to thank Jörg Raisch for giving me the opportunity to pursue my PhD endeavour under his guidance and offering me a position as research assistant in his group. I am very grateful for the past four years and have greatly benefitted from his advice and expertise, not only regarding academic matters. Also, I very much appreciate the freedom he gave me to pursue my research according to my own interests.

Another big thanks goes to Romeo Ortega, who I first met at a HYCON2 workshop in Brussels in autumn of 2012. Since then, he has been an incredible source of inspiration, taught me many lessons on nonlinear systems and always encouraged me to explore new avenues—not least Mexican chapulines. I very much appreciate our professional and personal relationship.

Also, I am truely indebted to Tevfik Sezi. It was his commitment and interest in microgrids, which made this project and its funding possible. In particular, I am grateful for the many practical aspects that he pointed out during the course of these years, not only pertaining to my research, but also with regards to life in general.

Moreover, I wish to express my sincere gratitude to Anne-Kathrin Schmuck for all the invaluable advice and support that she provided at an inflection point of my scientific career.

Also, I would like to thank Adolfo Anta, who significantly smoothened my start into the academic world, as well as Veit Hagenmeyer and Clemens Gühmann for joining my PhD committee. Likewise, I would like to thank all my other collaborators and co-authors on different research topics Aleksandar Stanković, Alessandro Astolfi, Christian A. Hans, Daniele Zonetti, Darina Goldin, Denis Efimov, Thomas Seel and Truong Duc Trung for their

contributions, lessons, advice and comments at various stages of my work, as well as for fun times and many on- and off-topic discussions.

Moreover, I would like to thank all my colleagues at the Control Systems Group at TU Berlin, in particular my office mates Christian A. Hans, Steffen Hofmann, Vladislav Nenchev and Yashar Kouhi, as well as the proofreaders of this thesis Anne-Kathrin Schmuck, Behrang Monajemi-Nejad, Christian A. Hans and Thomas Seel. The past four years would have been far less enjoyable and instructive without you. Likewise, mention should be made of the wonderful espresso machine that significantly enhanced every single one of my days at the lab.

I would also like to thank my previous advisors Frank Allgöwer, Anders Robertsson, Anders Rantzer and Tobias Weissbach, who introduced me to the fields of control and system theory and their application to power systems. Furthermore, I would like to thank Kai Strunz for giving me the opportunity to foster my interest and knowledge on power systems and renewable energies. I am also grateful to Björn Heinbokel and Aris Gkountaras for sharing their helpful insights on inverters and Ulrich Münz for many enriching discussions.

Furthermore, I am very thankful to the Siemens AG and the Bundesministerium für Wirtschaft und Energie for their financial support.

Thanks to all my friends in Berlin, Stuttgart, Lund and the rest of the world for being there and sharing many memorable moments with me.

Last but not least, I would like to thank my parents Werner and Angelika, my sister Katharina (you are the only true doctor of us) and all my other family for their great support and understanding throughout these years. Especially, thank you Alicia for all the enriching chaos you brought and still bring into my life.

Contents

List of figures

Abbreviations

AC	alternating current
AVR	automatic voltage regulator
CHP	combined heat and power
CIGRE	Conseil International des Grands Réseaux Electriques
DAE	differential-algebraic equation
DC	direct current
DG	distributed generation
DSP	digital signal processor
DVC	distributed voltage control
EMF	electromotive force
FC	fuel cell
HV	high voltage
LTI	linear time invariant
LV	low voltage
MDREG	microgrid with distributed rotational and electronic generation
MIMO	multiple-input multiple-output
MV	medium voltage
ODE	ordinary differential equation
PCC	point of common coupling
PV	photovoltaic
RMS	root mean square
SG	synchronous generator
SISO	single-input single-output

VSI	voltage source inverter

Symbols

$\mathbb{N}$	set of positive natural numbers
$\mathbb{R}$	set of real numbers
$\mathbb{R}_{\geq 0}$	set of nonnegative real numbers
$\mathbb{R}_{>0}$	set of positive real numbers
$\mathbb{R}_{<0}$	set of negative real numbers
$\mathbb{T}$	set of real points on the unit circle (mod 2π)
$\mathbb{C}$	set of complex numbers
j	imaginary unit
$\mathcal{L}_\infty$	space of continuous bounded functions
∇f	transpose of the gradient of a function $f : \mathbb{R}^n \to \mathbb{R}$
$\|\cdot\|_1$	vector 1-norm
$\|\cdot\|_\infty$	vector ∞-norm
$\sigma(A)$	set of eigenvalues (spectrum) of a matrix $A \in \mathbb{C}^{n\times n}$
A^*	conjugate transpose of a matrix $A \in \mathbb{C}^{n\times n}$
$\|\mathcal{U}\|$	cardinality of a set $\mathcal{U}$
$i \sim \mathcal{U}$	given a set of, possibly unordered, natural numbers $\mathcal{U} = \{l, k, \ldots, m\}$, short-hand for "$i = l, k \ldots, n$"
α_i	phase angle of voltage at node i in an electrical network
B_{ik}	susceptance between nodes i and k in an electrical network
$\mathcal{C}_i$	set of neighboring nodes of node i in a communication network
χ_i	weighting coefficient for proportional reactive power sharing at node i in an electrical network
δ_i	phase angle of voltage at node i on a common reference frame
δ_{ik}	$\delta_i - \delta_k$
ω_i	angular frequency at node i in an electrical network
ω^d	angular frequency setpoint
G_{ik}	conductance between nodes i and k in an electrical network
γ_i	weighting coefficient for proportional active power sharing at node i in an electrical network
k_{P_i}	frequency droop gain of unit at node i in an electrical network
k_{Q_i}	voltage droop gain of unit at node i in an electrical network
$\mathcal{L}$	Laplacian matrix of a communication network
$\mathcal{N}$	set of network nodes

$\mathcal{N}_i$	set of neighboring nodes of node i in an electrical network
$\mathcal{N}_I$	set of network nodes at which inverter-interfaced units are connected
$\mathcal{N}_{SG}$	set of network nodes at which SG-interfaced units are connected
P_i	active power injection at node i in an electrical network
P_i^m	measured active power injection at node i in an electrical network
P_i^d	active power setpoint at node i in an electrical network
P_{M_i}	mechanical power applied to SG at node i in an electrical network
Q_i	reactive power injection at node i in an electrical network
Q_i^d	reactive power setpoint at node i in an electrical network
Q_i^m	measured reactive power injection at node i in an electrical network
S_i^N	nominal power rate of unit at node i in an electrical network
τ_{P_i}	low pass filter time constant of power measurement filter at node i in an electrical network
V_i	amplitude of voltage at node i in an electrical network
V_i^d	setpoint of voltage amplitude at node i in an electrical network
$Y_{ik} = G_{ik} + jB_{ik}$	admittance between nodes i and k in an electrical network
$\mathcal{Y}$	admittance matrix of an electrical network

1

Introduction

1.1 Motivation

The commercial use of electricity dates back to the late 1870s [1]. Since that time, the electric power industry has grown to become one of the world's largest industries [1]. Nowadays, without doubt, electric energy is the most fundamental energy carrier in modern industrialized societies [2, 3, 4].

Traditionally, the vast majority of the worldwide electricity generation has been contributed by steam turbines in combination with synchronous generators (SGs) [1, 4, 5]. Such systems are called thermal power plants and their basic functioning is as follows [5, 6]. A steam turbine converts thermal energy contained in pressurized steam into rotational mechanical energy. Then, an SG further transforms this mechanical energy into electrical energy via an electromagnetic process called induction. The required steam is usually obtained from combustion processes, which often use fossil fuels as heat sources. The most commonly used materials are coal, natural gas, nuclear fuel and oil [5, 6].

It is well-known that fossil-fueled thermal power generation highly contributes to greenhouse gas emissions [6, 7]. In addition, more and more scientific results, e.g., [8, 9, 10], substantiate claims that greenhouse gas emissions are one, if not the, key driver for climate change and global warming. Furthermore, the largest share of the greenhouse gas emissions is and has been contributed by developed countries [11].

As a consequence, many developed countries have agreed to reduce their greenhouse gas emissions. The most prominent treaty in this context is the well-known Kyoto Protocol to the United Nations Framework Convention on Climate Change from 1997

[12]. The Kyoto Protocol sets emissions targets for developed countries that are binding under international law [12, 13].

One possibility to reduce greenhouse gas emissions is the reduction of energy consumption. This can be achieved, e.g., by changing consumption patterns or increasing the efficiencies in production, transportation and consumption of energy. Another mechanism to reduce greenhouse gas emissions is to shift the energy production from fossil-fueled plants towards renewable energies [7]. Renewable energy is defined by the International Energy Association as "energy derived from natural processes (e.g., sunlight and wind) that are replenished at a faster rate than they are consumed" [14]. Common sources of renewable energy are, e.g., solar, wind, geothermal, hydro or biomass.

By now, most developed countries have set specific target goals regarding the share of renewable energies within their total energy consumption [15]. An outstanding example is the German "Energiewende" (engl. energy transition), which targets a 35% share of renewable generation by 2020 and a share of 80% by 2050 [16]. The European Union aims at achieving a total share of 20% of renewable energy generation by 2020, while at the same time reducing its greenhouse gas emissions by 30% compared to 1990 [17].

As a consequence of these political and environmental goals, the worldwide use of renewable energies has increased significantly in recent years [7, 15]. However, the increasing penetration of renewable energy sources not only changes the mix of the generation structure, but also strongly affects the power system structure and its operation as a whole [7, 18, 19]. One main reason for this is detailed in the following.

Typically, a power system is composed of a high voltage (HV) transmission system, as well as medium voltage (MV) and low voltage (LV) distribution systems. As mentioned above, traditional power generation has been based around thermal power plants, which are typically very large in terms of their generation power and therefore connected to the HV level. From there, the power is transported across the transmission and distribution systems to the end-consumer, mainly located at the MV and LV levels. Hence, traditional power system operation has mainly been concerned with a relatively small number of large power plants connected to the HV transmission system via SGs [6], as illustrated in Fig. 1.1a.

Unlike, fossil-fueled thermal power plants, most renewable power plants are relatively small-sized in terms of their generation power. This smaller scale is mainly due

to technical reasons. An important consequence of this smaller size is, that most renewable power plants are connected to the LV and MV levels. Such generation units are commonly denoted as distributed generation (DG) units [20]. Furthermore, it is obvious from the preceding discussion that a large number of DG units are required to replace one large thermal power plant. Hence, an increasing amount of renewable DG units not only reduces greenhouse gas emissions, but also highly affects the in-feed structure of existing power systems, see Fig. 1.1b. This fact requires a paradigmatic change in power system operation [7, 18, 19].

In addition, most renewable DG units are interfaced to the network via alternating current (AC) inverters. The physical characteristics of such power electronic devices largely differ from the characteristics of SGs. Therefore different control and operation strategies are needed in networks with a large amount of renewable DG [7, 21].

One potential solution to facilitate the aforementioned paradigmatic change in power system operation are microgrids [21, 22, 23, 24]. A microgrid gathers a combination of generation units, loads and energy storage elements at distribution level into a locally controllable system, which can be operated either in grid-connected mode or in islanded mode, i.e., in a completely isolated manner from the main transmission system. The microgrid concept has been identified as a key component in future electrical networks [18, 25].

Many new challenges arise in such networks. The present thesis is devoted to three fundamental challenges in the operation of microgrids, namely *(i)* frequency stability, *(ii)* voltage stability and *(iii)* power sharing. The relevance of the addressed problems and their inherent relation is detailed in Chapter 3.

1.2 Contributions

The main contributions of the present thesis are given below.

(i) A modular model of an uncontrolled microgrid is derived. The model is suitable for the purposes of network control design and subsequent stability analysis of the resulting closed-loop system. Compared to SG-based conventional power systems, inverter-interfaced DG units are the main generation units in microgrids. Hence, a detailed model derivation of such plants is given.

(ii) A consensus-based distributed voltage control (DVC) is proposed, which guarantees reactive power sharing in steady-state in meshed microgrids with arbitrary line admittances. Opposed to most other related communication-based control

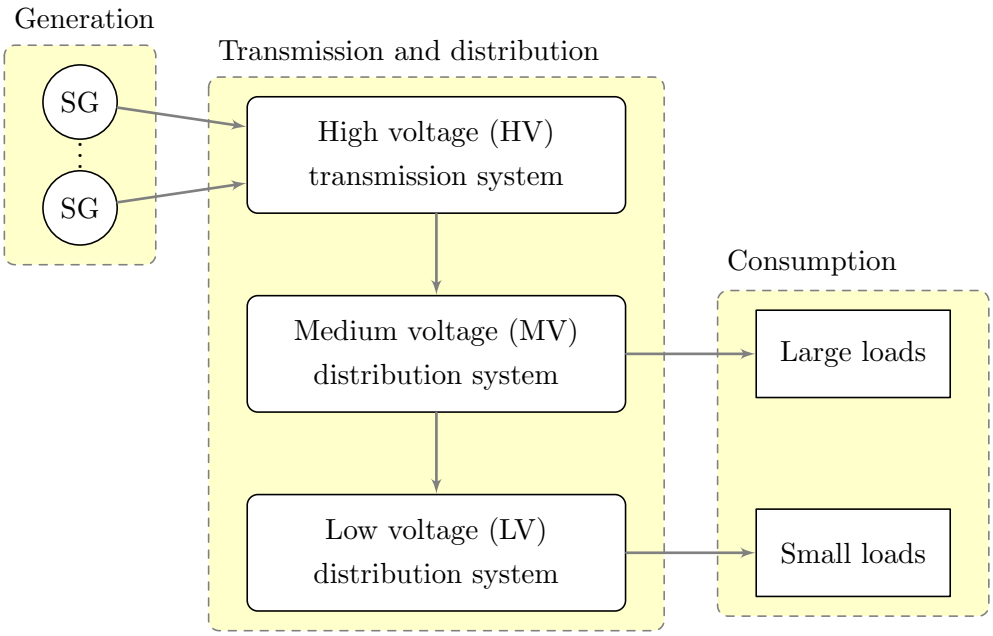

(a) Power system structure with mere conventional generation represented by synchronous generators (SGs)

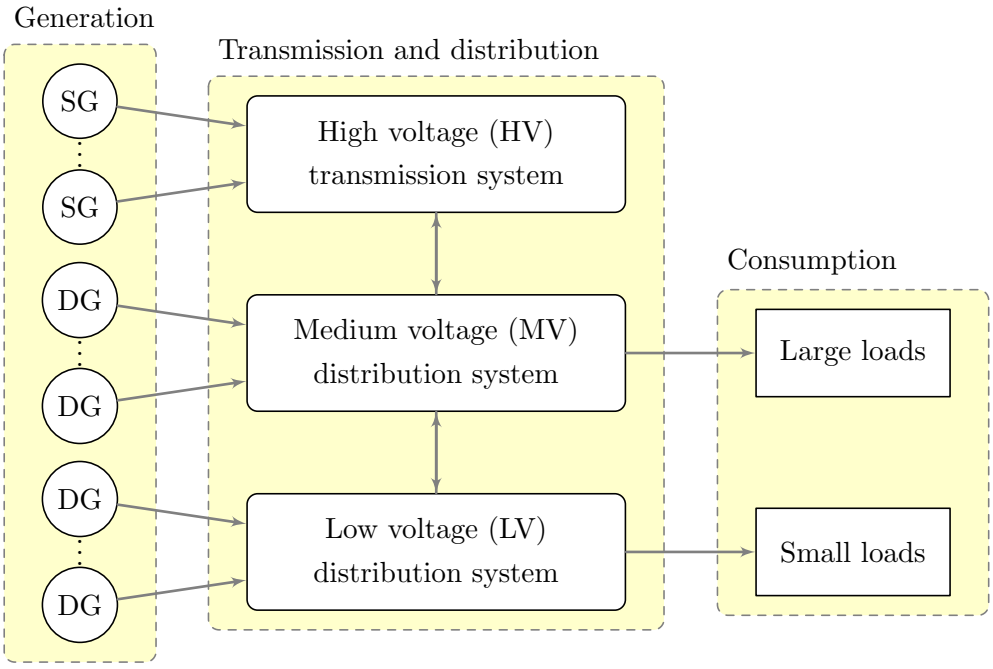

(b) Power system structure with large share of distributed generation (DG)

Figure 1.1: Change in power system structure due to increasing penetration of distributed generation. The symbol "SG" denotes conventional generation units; the symbol "DG" denotes distributed generation units. Fig. 1.1a illustrates the structure of a conventional power system. The generation units are located at the HV transmission level. The energy is transported one-directionally from the HV level to customers at the MV and LV levels. As depicted in Fig. 1.1b, the availability of DG units at the lower voltage levels changes the classical generation structure. Moreover, in such networks the energy flow may also be reversed.

concepts, e.g., [26, 27], the present approach only requires distributed communication among units, i.e., it neither requires a central communication or computing unit nor all-to-all communication among the DG units. Furthermore, it is proven that the choice of the control parameters uniquely determines the corresponding equilibrium point of the voltage and reactive power dynamics under the proposed DVC. The latter result is derived under the standard assumptions of dominantly inductive power lines and small angle differences [1, 28, 29].

(iii) Conditions for local asymptotic stability of several microgrid configurations are presented. In particular, the investigated networks include inverter-based microgrids operated with frequency and voltage droop control, as well as microgrids operated with frequency droop control and the proposed DVC. Most conditions are derived under the assumption of dominantly inductive power lines. The results are established by using tools from linear algebra, as well as port-Hamiltonian systems together with converse Lyapunov theorems.

(iv) It is shown that the problem of power sharing can be cast as an agreement problem. Furthermore, conditions are given, under which the frequency droop control, respectively the proposed DVC, solve the problem of active, respectively reactive, power sharing in microgrids with dominantly inductive power lines. The claims are established by combining the aforementioned stability results with a selection criterion on the gains and setpoints of the frequency droop control that ensures a desired active power sharing in steady-state, as well as with the inherent properties of the DVC.

(v) The provided analysis is illustrated in extensive simulation studies based on the Conseil International des Grands Réseaux Electriques (CIGRE) benchmark MV distribution network.

The thesis is organized in six chapters and a common conclusion. The main contents of each chapter are briefly outlined in the following.

Chapter 2 - Preliminaries in control theory and power systems. In this preliminary chapter, a series of standard results, definitions and models from the fields of control theory and power systems are reviewed. The given mathematical background focuses on the control theoretic concept of stability and presents some standard conditions for stability used to establish part of the results in this work. Furthermore,

some basics of algebraic graph theory, consensus protocols and matrix analysis are introduced. In addition, standard definitions and network models for AC three-phase electrical power systems are detailed. Finally, the concept of stability in power systems and microgrids is related to its control theoretic counterpart.

Chapter 3 - Problem statement. In this chapter, the microgrid concept is introduced and a formal definition of a microgrid is given. It is illustrated that the increasing penetration of DG units at the LV and MV levels leads to structural changes in today's power systems. The main associated technical challenges arising with these changes are discussed. The potentials and key features of microgrids in this context are pointed out and three fundamental problems in the operation of microgrids are introduced in detail. These are frequency stability, voltage stability and power sharing. In particular, the problem of power sharing is formulated as an agreement problem. The chapter is concluded with a brief overview of a hierarchical control architecture for microgrids.

Chapter 4 - Modeling of microgrids. A model of a microgrid with distributed rotational and electronic generation (MDREG), suitable for the purposes of control design, as well as subsequent frequency and voltage stability analysis, is derived. Therefore, unlike, e.g., in [30, 31, 32], a generic modular modeling approach is pursuit. The main model components are generation units interfaced to the network via AC inverters or SGs, as well as loads and power lines.

The modeling of SGs has a long history in the literature of power systems and is, hence, well-studied, see, e.g., [1, 3, 6]. On the contrary, modeling of inverters for the purpose of network stability analysis is a relatively young topic, see, e.g., [30, 33, 34, 35]. Therefore, in this chapter, a detailed model derivation of an inverter is provided. The basic functionality of an inverter is briefly reviewed, followed by a description of the two main operation modes of inverters in microgrid applications. The operation mode called grid-forming mode is identified as the main relevant operation mode in the context of network control and stability analysis. Hence, a suitable model of a grid-forming inverter represented by a controllable AC voltage source is derived. The main modeling assumptions are discussed and stated.

The model of an SG is introduced following standard modeling approaches from the literature on power systems, see, e.g., [1, 3, 6]. Finally, the network interconnections and loads are modeled based on the procedure outlined in Chapter 2 following the classical approach in conventional power system studies [1, 3, 6, 36].

Chapter 5 - Control concepts for microgrids and conditions for power sharing. Control concepts to address the aforementioned problems of frequency stability, voltage stability and power sharing are introduced. At first, the well-known droop control for SGs is reviewed [1, 6]. This control is widely used in SG-based power systems to achieve the control objectives of frequency stability and active power sharing. Building on the droop control for SGs, the frequency and voltage droop controls for inverter-interfaced DG units are introduced. These control laws have been widely proposed in the literature to operate grid-forming inverters in microgrids, see, e.g., [37, 38]. A thorough physical motivation for these control laws is given. Furthermore, a selection criterion on the setpoints and gains of the frequency droop controller is provided, which ensures a desired steady-state active power sharing in an MDREG. Unlike previous results, see, e.g., [28], the criterion holds independently of the line admittances.

Moreover, it is discussed that the voltage droop control [37] does, in general, not guarantee reactive power sharing. Consequently, a consensus-based DVC for inverter-interfaced DG units is proposed. It is proven that the DVC does guarantee reactive power sharing in steady-state independently of the line admittances. Furthermore, it is shown that—via a suitable feedback linearization—the proposed DVC can also be applied to SG-interfaced units in a straightforward manner.

Chapter 6 - Conditions for stability in microgrids. The closed-loop microgrid dynamics resulting by combining the microgrid model derived in Chapter 4 with the control laws introduced in Chapter 5 are undertaken a rigorous mathematical analysis. More precisely, the main contributions of this chapter are: *(i)* a necessary and sufficient condition for local frequency stability in a lossy[1] MDREG with constant voltage amplitudes is provided; *(ii)* a sufficient condition for global boundedness of trajectories of a lossy droop-controlled inverter-based microgrid with time-varying frequencies and voltage amplitudes is given; *(iii)* for the same system and under the assumption of lossless admittances, sufficient conditions for local asymptotic stability are derived using a port-Hamiltonian framework; *(iv)* under the assumptions of dominantly inductive power lines and small phase angle differences between the output voltages of the DG units, it is proven that the equilibrium point of the closed-loop voltage and reactive power dynamics of a microgrid operated with the DVC is uniquely determined by the choice of the control parameters; *(v)* a necessary and sufficient condition for local

[1] A lossy MDREG is an MDREG with nonzero transfer conductances.

exponential stability of this equilibrium point is given; *(vi)* a necessary and sufficient condition for local exponential stability of a microgrid operated with frequency droop control and DVC is provided. The latter result is established without the assumption of small phase angle differences. Finally, *(vii)* solutions to the problems of active and reactive power sharing are given by combining the results of the present chapter with those of Chapter 5.

Chapter 7 - Illustrative simulation examples. The analytic results of the previous chapters are illustrated via two extensive simulation studies based on the meshed CIGRE benchmark MV distribution network. At first, a simulation scenario in which all grid-forming DG units are operated with the standard droop controllers is considered. The study mainly serves to evaluate the following three aspects: *(i)* the conservativeness of the derived sufficient stability condition; *(ii)* its robustness with respect to model uncertainties; *(iii)* the suitability of the droop controllers to achieve a desired power sharing. In the second simulation study the performance of the voltage droop control is compared to that of the DVC proposed in this work. This second study also serves to evaluate the compatibility of the DVC with the usual frequency droop control.

Chapter 8 - Discussion and conclusion. The main results are summarized and future research directions are discussed.

1.3 Related work

Today's electrical power systems are very large, complex and highly nonlinear systems [3, 4, 6]. They possess a huge variety of actuators and operational constraints, while persistently being subjected to disturbances. Typical disturbances in power systems are, e.g., changes in load, outages of power plants, or failures in transformer substations and power lines [39]. Hence, the task of guaranteeing a stable, reliable and efficient operation of a power system is tremendous. This fact becomes even more obvious by noting that already a local instability can lead to a cascade of failures, which can cause severe blackouts affecting millions of people [40, 41].

It is, therefore, not surprising that the stability analysis of power systems has a long research tradition with its beginning dating back to the 1920s [42, 43]. Nevertheless, the stability analysis of power systems and the design of stabilizing feedback controllers for power systems are still open and very active research fields, see, e.g., the recent works

[44, 45, 46, 47, 48, 49, 50, 51, 52]. An excellent review of the research history on power system stability analysis is given, e.g., in [6, Chapter 1].

Compared to the physical system considered in the present work, all of the research activities indicated above are restricted to power systems with SG-interfaced generation units located at the transmission level. It is, however, important to note that the results in, e.g., [45, 48], are established by means of the interconnection and damping assignment passivity-based control approach [53]. The approach of [53] is also followed in the present work to obtain a sufficient stability condition for a lossless droop-controlled microgrid.

Furthermore, although the aforementioned frequency and voltage droop control laws are widely discussed and promoted in the literature, see, e.g., [34, 38, 54], the available results on performance of droop-controlled microgrids are limited in the following four regards.

(i) Stability analysis of droop-controlled microgrids has traditionally been carried out by means of detailed numerical small-signal analysis as well as extensive simulations and experimental studies aiming to characterize a range for the droop gains guaranteeing system stability [30, 33, 34, 55, 56, 57, 58, 59, 60, 61, 62].

(ii) So far, most research on stability and power sharing of microgrids has focused on purely inverter-based systems, see, e.g., [28, 29, 63, 64] and all of the aforementioned references. However, from a practical perspective, most present and near-future applications concern networks of mixed generation structure including SGs and inverter-interfaced distributed resources. Recall that such microgrids are denoted by MDREGs in this work. In MDREGs, SGs may for example be used in combination with diesel engines or gas turbines [65]. Stability and performance of such systems remain largely unexplored from a system theoretic point of view. In [30, 31] and [32], MDREGs that consist of two inverters and one to two SGs are investigated via simulations complemented by a numerical small-signal stability analysis. Furthermore, the problems of frequency stability, power sharing and optimal dispatch in radial MDREGs have recently been investigated in [66]. However, the analysis therein is restricted to first-order inverter and SG models, as well as conducted under the assumptions of constant voltage amplitudes and lossless line admittances.

(iii) As pointed out in [38], most work on microgrid stability has so far focused on microgrids with radial topologies, while stability of microgrids with meshed topolo-

gies and decentralized controlled units is still an open research area. For radial lossless microgrids, and under the assumption of constant voltage amplitudes, analytic conditions for proportional active power sharing and synchronization of lossless microgrids with first-order inverter models have been recently derived in [28]. Note that, under the assumption of constant voltage amplitudes, the dynamics of droop-controlled microgrids can be cast within the framework of complex oscillators networks [66, 67, 68]. The aforementioned results in [28, 66], as well as those in the related previous work [69], are established by exploring this fact. Conditions for voltage stability for a lossless parallel microgrid with one common load have been derived in [29].

For general meshed microgrids operated with frequency droop control, an iterative numerical procedure to evaluate local stability has been proposed in [62]. This approach is based on bifurcation theory. In [70], the authors provide a decentralized LMI-based control design for lossy meshed inverter-based networks guaranteeing overall network stability for a nonlinear model considering variable voltage amplitudes and phase angles, while accounting for power sharing. Under the assumptions of constant voltage amplitudes, lossless power lines and first-order inverter models, sufficient conditions for frequency synchronization, i.e., convergence to one common frequency, are given in [63]. Furthemore, conservative sufficient conditions for frequency synchronization and voltage stability of lossy droop-controlled microgrids with first-order inverter models are provided in [64], by using ideas from [50].

(iv) The voltage droop control [37] exhibits a significant drawback: it does in general not guarantee a desired reactive power sharing, i.e., it does, in general, not achieve the desired control goal, as discussed, e.g., in [29, 71, 72, 73]. Moreover, to the best of the author's knowledge, no theoretically or experimentally well-founded selection criteria are known for the parameters of the voltage droop control which would ensure at least a guaranteed minimum (quantified) performance in terms of reactive power sharing.

As a consequence, several other or modified (heuristic) decentralized voltage control strategies have been proposed in the literature, e.g., [29, 59, 72, 73, 74, 75, 76]. Most of this work is restricted to networks of inverters connected in parallel. Moreover, typically only networks composed of two DG units are considered. With most approaches the control performance in terms of reactive power sharing with

respect to the original control [37] is improved. However, no general conditions or formal guarantees for reactive power sharing are given. A quantitative analysis of the error in power sharing is provided in [72] for the control proposed therein. Other related work is [77, 78], where a secondary voltage control scheme is proposed that regulates all voltage amplitudes to a common reference value. In that case, in general, no reactive power sharing is achieved. In [79, 80] distributed control schemes for the problem of optimal reactive power compensation are presented. The study therein is limited to the steady-state behavior, i.e., the considered time-scale is much larger than in the present work. Furthermore, the DG units are modeled as constant power or PQ buses. Hence, the units considered in [79, 80] are operated as grid-feeding and not as grid-forming units, see, e.g., [35, 81].

As a consequence of the preceding discussion, conditions for stability of generic meshed microgrids are derived in this work. The closed-loop systems considered in the analysis comprise frequency-droop controlled MDREGs with constant voltage amplitudes, as well as droop-controlled inverter-based microgrids with time-varying frequencies and voltage amplitudes.

Furthermore, a consensus-based DVC, which guarantees reactive power sharing in steady-state is proposed. Unlike in other related work on distributed voltage control, e.g., [82, 83, 84], for the case of dominantly inductive power lines, a rigorous mathematical analysis of the closed-loop microgrid dynamics under the proposed DVC is carried out in the present thesis.

The consensus protocol used to design the DVC is based on the weighted average consensus protocol [85]. This protocol is closely related to the well-known average consensus protocol [85]. It should, however, be noted that the average consensus protocol has been extended in several other regards. These include, but are not limited to, directed networks [86, 87], dynamic network topologies [88, 89], time-discrete protocols [86, 90, 91], consensus under communication time-delays [88, 92, 93, 94, 95, 96, 97], second-order protocols with homogeneous interaction topologies [98, 99, 100], second-order protocols with heterogeneous interaction topologies [101, 102], nonlinear protocols [97, 103, 104, 105] and higher-order agent dynamics [97, 99, 106, 107, 108]. Given the vast amount of recent results on different types of consensus protocols for multi-agent networks, the preceding list of references is by no means intended to be complete,

but rather to offer a glimpse into the rich literature on consensus protocols. A recent overview on progress in the study of multi-agent systems is given, e.g., in [109].

It is also worth noting that the network interconnection among the different loads and generation units in a power system can typically be modeled by a graph. Moreover, the problem of frequency stability can be formulated as an output agreement problem, see, e.g., [110, 111]. These two facts establish a natural link between the theoretical framework provided by consensus protocols and the analysis and control of power systems [112]. Therefore, consensus protocols have recently been applied to a number of problems and applications in power systems and microgrids. For example, in [50, 67, 68, 113, 114] conditions for frequency synchronization in power systems composed of highly-overdamped SGs are derived. To establish their claims, the authors make use, among others, of results on convergence of nonlinear consensus protocols reported in [103]. Furthermore, assuming a linear power system model, second-order consensus protocols have been applied in [115, 116] to address the problem of secondary frequency control in large power systems. Ideas of consensus protocols are also used in [117] to prove convergence of SG-based power systems. In addition, the authors of [117] provide several estimates of the region of attraction of a given steady-state.

Likewise, the aforementioned works on conditions for stability in lossless inverter-based microgrids [28, 69, 118] employ a graph-theoretic notation. In addition, in [28, 118, 119] the problem of secondary frequency control in droop-controlled inverter-based microgrids has been studied using tools of graph theory and consensus protocols. Similarly, the previously mentioned secondary frequency and voltage control schemes for inverter-based microgrids proposed in [77, 78, 120] are designed based on the weighted average consensus protocol [85]. Also the author's work [121] employs a graph theoric notation to study the problem of frequency synchronization in microgrids in which the agents have second-order dynamics.

The DVC proposed in this work further explores the illustrated links between consensus protocols and the control of power systems. More precisely, it is shown that the problem of power sharing can be cast as an agreement problem. However, unlike the usual agreement problems in multi-agent systems discussed, e.g., in [85, 109], power sharing is not a strict state nor output agreement problem. On the contrary, the agreement subspace is spanned by a set of algebraic nonlinear state-dependent equations, which describe the weighted steady-state power flows in the network.

1.4 Publications

A large share of this thesis is based on the following publications (listed in chronological order), to all of which the author of the present work has made substantial contributions.

- J. Schiffer, A. Anta, T. D. Trung, J. Raisch, and T. Sezi. **On power sharing and stability in autonomous inverter-based microgrids**. In *51st Conference on Decision and Control*, pages 1105–1110, Maui, HI, USA, 2012,
- J. Schiffer, D. Goldin, J. Raisch, and T. Sezi. **Synchronization of droop-controlled microgrids with distributed rotational and electronic generation**. In *52nd Conference on Decision and Control*, pages 2334–2339, Florence, Italy, 2013,
- J. Schiffer, T. Seel, J. Raisch, and T. Sezi. **A consensus-based distributed voltage control for reactive power sharing in microgrids**. In *13th European Control Conference*, pages 1299–1305, Strasbourg, France, 2014,
- J. Schiffer, R. Ortega, A. Astolfi, J. Raisch, and T. Sezi. **Stability of synchronized motions of inverter-based microgrids under droop control**. In *19th IFAC World Congress*, pages 6361–6367, Cape Town, South Africa, 2014,
- J. Schiffer, R. Ortega, A. Astolfi, J. Raisch, and T. Sezi. **Conditions for stability of droop-controlled inverter-based microgrids**. *Automatica*, **50**(10):2457–2469, 2014,
- J. Schiffer, R. Ortega, C. Hans, and J. Raisch. **Droop-controlled inverter-based microgrids are robust to clock drifts**. In *American Control Conference*, pages 2341–2346, Chicago, IL, USA, 2015,
- J. Schiffer, T. Seel, J. Raisch, and T. Sezi. **Voltage stability and reactive power sharing in inverter-based microgrids with consensus-based distributed voltage control**. *IEEE Transactions on Control Systems Technology*, 2015. To appear,
- J. Schiffer, D. Zonetti, R. Ortega, A. Stanković, J. Raisch, and T. Sezi. **Modeling of microgrids - from fundamental physics to phasors and voltage sources**. 2015. Submitted.

1.5 Outline

The thesis is organized as follows. Background information on the main mathematical methods used to establish the results in this work, as well as on electrical engineering are given in Chapter 2. The microgrid concept and the specific problem statement of this work are discussed in Chapter 3. In Chapter 4, a suitable model of an uncontrolled microgrid is derived. Control concepts for microgrids are presented in Chapter 5. A rigorous mathematical analysis of the closed-loop microgrid dynamics, resulting by combining the derived model with the proposed control schemes, is given in Chapter 6. The theoretical analysis is illustrated via simulations in Chapter 7. In Chapter 8, conclusions are drawn and future research directions are discussed.

2

Preliminaries in control theory and power systems

2.1 Introduction

This preliminary chapter is structured as follows. Basic notation used within the present work is introduced in Section 2.2. Subsequently, relevant background information of the field of control theory is given in Section 2.3 and some preliminaries in electrical power systems are recalled in Section 2.4.

2.2 Notation

The set of positive natural numbers is denoted by $\mathbb{N}$, the set of real numbers by $\mathbb{R}$ and the set of complex numbers by $\mathbb{C}$. It is convenient to define the sets $\mathcal{N} := \{1, 2, \ldots, n\}$, $n \in \mathbb{N}$, $\mathbb{R}_{\geq 0} := \{x \in \mathbb{R} | x \geq 0\}$, $\mathbb{R}_{>0} := \{x \in \mathbb{R} | x > 0\}$, $\mathbb{R}_{<0} := \{x \in \mathbb{R} | x < 0\}$ and $\mathbb{T} := \{x \in \mathbb{R} \,|\, 0 \leq x < 2\pi\}$. For a set $\mathcal{U}$, $|\mathcal{U}|$ denotes its cardinality. For a set of, possibly unordered, positive natural numbers $\mathcal{V} = \{l, k, \ldots, n\}$, the short-hand $i \sim \mathcal{V}$ denotes $i = l, k, \ldots, n$. For $z \in \mathbb{C}$, $\Re(z)$ denotes the real part of z and $\Im(z)$ its imaginary part. Let j denote the imaginary unit. Let $x := \mathrm{col}(x_i) \in \mathbb{C}^n$ denote a vector with entries $x_i \in \mathbb{C}$, $i \sim \mathcal{N}$, $\underline{0}_n$ the vector of all zeros, $\underline{1}_n$ the vector with all ones, $\mathbf{I}_n$ the $n \times n$ identity matrix, $\mathbf{0}_{n \times n}$ the $n \times n$ matrix of all zeros and $\mathrm{diag}(a_i)$, $i \sim \mathcal{N}$, an $n \times n$ diagonal matrix with entries $a_i \in \mathbb{C}$. Likewise, $\mathrm{blkdiag}(A_i) \in \mathbb{C}^{n \times n}$ denotes a block-diagonal matrix with entries $A_i \in \mathbb{C}^{l \times l}$. Let $x \in \mathbb{C}^n$ and $y \in \mathbb{C}^m$, then $v = \mathrm{col}(x, y) \in \mathbb{C}^{n+m}$ denotes the column vector with entries $v_i = x_i$, $i = 1, \ldots, n$ and $v_{n+k} = y_k$, $k = 1, \ldots, m$. The conjugate transpose of a matrix $A \in \mathbb{C}^{n \times n}$ is denoted by A^*. A complex-valued matrix

A is said to be Hermitian if $A = A^*$. If $A = -A^*$, then A is said to be skew-Hermitian. A (skew)-Hermitian matrix, which has only real entries is said to be (skew)-symmetric. A Hermitian matrix $A \in \mathbb{C}^{n\times n}$ is said to be positive definite if $x^\top Ax > 0$ for all $x \in \mathbb{C}^n \setminus \{\underline{0}_n\}$. This property is also denoted by $A = A^* > 0$. If $x^\top Ax \geq 0$ for all $x \in \mathbb{C}^n \setminus \{\underline{0}_n\}$, A is said to be positive semidefinite, or, equivalently, $A = A^* \geq 0$. Note that if $A = A^\top \in \mathbb{R}^{n\times n}$, the condition $x^\top Ax > (\geq)0$ for all $x \in \mathbb{R}^n \setminus \{\underline{0}_n\}$ implies that A is positive (semi)definite. Furthermore, for $x \in \mathbb{C}^n$, $\|x\|$ denotes an arbitrary vector norm, $\|x\|_1 := \sum_{i\sim\mathbb{N}} |x_i|$ denotes the vector 1-norm and $\|x\|_\infty := \max(|x_1|, \ldots, |x_n|)$ the vector ∞-norm. The operator $\otimes$ denotes the Kronecker product. Unless specified differently, $t \in \mathbb{R}$ denotes the time. Finally, ∇f denotes the transpose of the gradient of a function $f : \mathbb{R}^n \to \mathbb{R}$.

To simplify notation the time argument of all signals is omitted, whenever clear from the context.

2.3 Preliminaries in control theory

In this section, some standard control theoretic concepts and results are recalled. Namely, a brief introduction to nonlinear dynamical systems is given in Section 2.3.1; Lyapunov stability is reviewed in Section 2.3.2; in Section 2.3.3, main properties of the class of port-Hamiltonian systems are shortly discussed. The presentation of the aforementioned topics is strongly oriented on [127, Chapter 2.3], [128, Chapter 4] and [129, Chapters 3 and 4]. For further information on control theory, as well as for proofs of the given mathematical statements, the reader is referred to, e.g., [127, 128, 129, 130].

In addition, the Routh-Hurwitz criterion for polynomials with complex coefficients is introduced in Section 2.3.4. Subsequently, basics on algebraic graph theory and consensus protocols for multi-agent systems are recalled in Section 2.3.5. A brief review of relevant properties of the numerical range of a matrix is given in Section 2.3.6.

Note that the introduced basics on algebraic graph theory, as well as the numerical range of a matrix do not strictly belong to the field of control theory. However, they are used in this work as tools to derive control theoretic results and therefore included in the present section.

2.3.1 Nonlinear dynamical systems

The class of systems relevant in the context of this work are dynamical systems modeled by first-order ordinary differential equations (ODEs)

$$\begin{aligned} \dot{x}(t) &= f(t, x(t), u(t)), \\ y(t) &= h(t, x(t), u(t)), \end{aligned} \tag{2.1}$$

with initial time $t_0 \in \mathbb{R}$, state signal $x : [t_0, \infty) \to \mathbb{X} \subseteq \mathbb{R}^n$, input signal $u : [t_0, \infty) \to \mathbb{U} \subseteq \mathbb{R}^p$, output signal $y : [t_0, \infty) \to \mathbb{Y} \subseteq \mathbb{R}^m$, as well as functions $f : [t_0, \infty) \times \mathbb{X} \times \mathbb{U} \to \mathbb{R}^n$ and $h : [t_0, \infty) \times \mathbb{X} \times \mathbb{U} \to \mathbb{Y}$.

A representation of a dynamical system in the form (2.1) is called a state-space model. The state vector x represents the memory that the system (2.1) has of its past. The input u represents exogeneous signals, which can be applied to the system (2.1), for example, to influence its behavior. The output y denotes particular variables, e.g., physically measurable variables or meaningful variables for the performance evaluation of the system (2.1). The output vector y is optional. Therefore, if not needed, the output y is not specified in the following.

A special subclass of systems described by (2.1) is the class of dynamical systems, where the function f does not explicitly depend on the time t and, in addition, no input vector is present. Then, the system (2.1) (without output y) reduces to

$$\dot{x}(t) = f(x(t)). \tag{2.2}$$

The system (2.2) is said to be an autonomous, or time-invariant, system. It is assumed in the following that f is locally Lipschitz continuous, i.e., to each $x \in \mathbb{X}$ there exists a neighborhood U_0 of x and a constant $k_0 \in \mathbb{R}_{>0}$, such that

$$\|f(x_1) - f(x_2)\| \leq k_0 \|x_1 - x_2\|,$$

for all $x_1 \in U_0$ and all $x_2 \in U_0$. This implies existence and uniqueness of solutions of (2.2), at least for small times [128, Theorem 3.1]. The solution of (2.2) starting at x_0 at time t_0 is denoted by $x(\cdot; x_0, t_0)$, i.e., $x(t_0; x_0, t_0) = x_0$.

A particular property of autonomous systems is that their solutions are invariant to a time shift, i.e., for all $T \in \mathbb{R}_{>0}$ and for all $t \in [t_0, \infty)$, $x(t+T; x_0, t_0+T) = x(t; x_0, t_0)$. Therefore, without loss of generality, $t_0 = 0$ is assumed and the notation $x(\cdot; x_0)$ is used instead of $x(\cdot; x_0, 0)$.

An important concept associated with the system (2.2) is that of an equilibrium point. A solution $x(\cdot; x^s)$ is said to be an equilibrium point of (2.2) if $x(t; x^s) = x^s$ for all $t \geq 0$. Clearly,

$$\underline{0}_n = f(x^s).$$

Physically, an equilibrium may describe, for example, a desired operating point of a dynamical system. The system (2.2) may possess one equilibrium point, several equilibrium points or a continuum of equilibrium points. An equilibrium point is called isolated if in its neighborhood there exists no other equilibrium point.

2.3.2 Lyapunov stability

Lyapunov stability is a widely used concept in control theory. In particular, Lyapunov stability is an important property of an equilibrium point of a dynamical system. This is formalized in the definition below.

Definition 2.3.1. *Let x^s be an interior point of $\mathbb{X}$ and an equilibrium point of the system (2.2), i.e., $f(x^s) = \underline{0}_n$. Thus, $x(t; x^s) = x^s$ for all $t \geq 0$. Let $x_0 \in \mathbb{X}$. The equilibrium point x^s is said to be*

- *stable, if for each positive real constant ϵ there is a real constant $\delta = \delta(\epsilon) > 0$ such that*
$$\|x_0 - x^s\| < \delta \quad \Rightarrow \quad \|x(t; x_0) - x^s\| < \epsilon, \quad \forall t \geq 0,$$
- *unstable, if it is not stable,*
- *asymptotically stable, if it is stable and there exists a real constant $r > 0$ such that*
$$\|x_0 - x^s\| < r \quad \Rightarrow \quad \lim_{t\to\infty} x(t; x_0) = x^s,$$
- *globally asymptotically stable, if $\mathbb{X} = \mathbb{R}^n$, x^s is stable and*
$$\lim_{t\to\infty} x(t; x_0) = x^s, \quad \forall x_0 \in \mathbb{R}^n,$$
- *exponentially stable, if there exist positive real constants α, γ and r such that*
$$\|x_0 - x^s\| < r \;\Rightarrow\; \|x(t; x_0) - x^s\| \leq \gamma e^{-\alpha t}\|x_0 - x^s\|, \quad \forall t \geq 0,$$
- *globally exponentially stable, if $\mathbb{X} = \mathbb{R}^n$, x^s is stable and there exist positive real constants α and γ such that*
$$\|x(t; x_0) - x^s\| \leq \gamma e^{-\alpha t}\|x_0 - x^s\|, \quad \forall x_0 \in \mathbb{R}^n, \quad \forall t \geq 0.$$

Remark 2.3.2. Let $x^s \in \mathbb{X}$ be an equilibrium point of the system (2.2). If x^s is (asymptotically, exponentially) stable, but not globally (asymptotically, exponentially) stable, then it is often called a locally (asymptotically, exponentially) stable equilibrium point.

Any nonzero equilibrium point x^s can be shifted to the origin by a change of variables, i.e., $z = x - x^s$. Hence, without loss of generality, it is assumed in the following that $x^s = \underline{0}_n$, i.e., the considered equilibrium point is the origin. The next result is known as Lyapunov's stability theorem.

Theorem 2.3.3. *[128, Theorem 4.1] Let $x^s = \underline{0}_n$ be an interior point of $\mathbb{X}$ and an equilibrium point of (2.2). If there exists a neighborhood $\mathbb{D} \subseteq \mathbb{X}$ of x^s and a continuously differentiable function $V : \mathbb{D} \to \mathbb{R}$ such that*

$$V(0) = 0 \quad \textit{and} \quad V(x) > 0 \quad \forall x \in \mathbb{D} \setminus \{0\}, \tag{2.3}$$

$$\dot{V}(x) \leq 0 \quad \forall x \in \mathbb{D}, \tag{2.4}$$

then $x^s = \underline{0}_n$ is a stable equilibrium point. Moreover, if

$$\dot{V}(x) < 0 \quad \forall x \in \mathbb{D} \setminus \{0\}, \tag{2.5}$$

then $x^s = \underline{0}_n$ is an asymptotically stable equilibrium point.

A function $V : \mathbb{D} \to \mathbb{R}$ satisfying conditions (2.3) is said to be positive definite [128, Chapter 4]. It is said to be positive semidefinite, if it satisfies the (weaker) conditions $V(0) = 0$ and $V(x) \geq 0$ for all nonzero $x \in \mathbb{D}$. Likewise, a function $V(x)$ is said to be negative (semi)definite, if $-V(x)$ is positive (semi)definite. A function $V : \mathbb{D} \to \mathbb{R}$ satisfying conditions (2.3) and (2.4) is called a Lyapunov function.

Situations may occur where $\dot{V}(x)$ is only negative semidefinite. Then, Theorem 2.3.3 can not be applied to establish asymptotic stability of x^s. The theorem below, known as LaSalle's Invariance Principle, allows to generalize the second part of Theorem 2.3.3 to cases where $\dot{V}(x)$ is only negative semidefinite.

Definition 2.3.4. *[128, Chapter 4.2] Let $\mathbb{M} \subseteq \mathbb{X}$. The set $\mathbb{M}$ is said to be positively invariant with respect to (2.2) if*

$$x_0 \in \mathbb{M} \quad \Rightarrow \quad x(t; x_0) \in \mathbb{M}, \quad \forall t \geq 0.$$

Theorem 2.3.5. *[128, Theorem 4.4] Let $\mathbb{B} \subseteq \mathbb{X}$ be a compact set that is positively invariant with respect to (2.2). Let $V : \mathbb{X} \to \mathbb{R}$ be a continuously differentiable function such that $\dot{V}(x) \leq 0$ for all $x \in \mathbb{B}$. Define $\mathbb{E} \subseteq \mathbb{B}$ by $\mathbb{E} = \{x \in \mathbb{B} \mid \dot{V}(x) = 0\}$. Let $\mathbb{M}$ be the largest invariant set in $\mathbb{E}$. Then, whenever $x_0 \in \mathbb{B}$, the solution $x(t; x_0)$ approaches $\mathbb{M}$ as $t \to \infty$.*

Combining Theorems 2.3.3 and 2.3.5 yields the following corollary, also known as the theorem of Barbashin and Krasovskii.

Corollary 2.3.6. *[128, Corollary 4.1] Let $x^s = \underline{0}_n$ be an interior point of $\mathbb{X}$ and an equilibrium point of (2.2). Suppose that there exists a neighborhood $\mathbb{D} \subseteq \mathbb{X}$ of x^s and a continuously differentiable positive definite function $V : \mathbb{D} \to \mathbb{R}$ such that $\dot{V}(x) \leq 0$ for all $x \in \mathbb{D}$. Let $\mathbb{E} = \{x \in \mathbb{D} \mid \dot{V}(x) = 0\}$ and suppose that no solution can stay in $\mathbb{E}$ other than the trivial solution $x(t; \underline{0}_n) = \underline{0}_n$ for all $t \geq 0$. Then, the origin is asymptotically stable.*

This section is concluded with a converse Lyapunov theorem for exponential stability.

Definition 2.3.7. *[128, Chapter 4.3] Let $A \in \mathbb{R}^{n \times n}$ and denote the eigenvalues of A by λ_i, $i = 1, \ldots, m$, $m \in \mathbb{N}$, $m \leq n$. Then, A is said to be Hurwitz if $\Re(\lambda_i) < 0$, $i = 1, \ldots, m$.*

Theorem 2.3.8. *[128, Corollary 4.3] Let $x^s = \underline{0}_n$ be an interior point of $\mathbb{X}$ and an equilibrium point of (2.2). Let*

$$A = \frac{\partial f}{\partial x}\Big|_{x=x^s}.$$

If and only if A is Hurwitz, x^s is an exponentially stable equilibrium point of the nonlinear system (2.2).

2.3.3 Port-Hamiltonian systems

In this section, the class of port-Hamiltonian systems is briefly introduced. Furthermore, following [129, Chapters 3 and 4] some basic properties and notions associated with port-Hamiltonian systems are presented.

The class of port-Hamiltonian systems comprises all dynamical systems, which can be written in the following form

$$\begin{aligned} \dot{x} &= (J(x) - R(x))\, \nabla H + g(x)u, \quad x \in \mathbb{X} \subseteq \mathbb{R}^n, \quad u \in \mathbb{R}^m, \\ y &= g^\top(x) \nabla H, \quad y \in \mathbb{R}^m, \end{aligned} \tag{2.6}$$

where the matrix $J(x)$ has entries depending smoothly on x and $J(x) = -J(x)^\top$, i.e., $J(x)$ is skew-symmetric. Furthermore, the matrix $R(x)$ satisfies $R(x) \geq 0$ for all $x \in \mathbb{X}$ and the entries of $R(x)$ depend smoothly on x. Usually, $J(x)$ is called interconnection matrix and $R(x)$ is called damping matrix. The continuously differentiable function $H : \mathbb{X} \to \mathbb{R}$ is called Hamiltonian. Recall that ∇H denotes the transpose of the gradient of the function H. Commonly, u and y are called the input, respectively output, port.

Calculating the time-derivative of the Hamiltonian H along the flow of the system (2.6), yields the following power balance equation

$$\begin{aligned} \dot{H} = \nabla H^\top \dot{x} &= \nabla H^\top \left((J(x) - R(x)) \nabla H + g(x)u \right) \\ \Leftrightarrow \quad \underbrace{\dot{H}}_{\text{stored power}} &= \underbrace{-\nabla H^\top R(x) \nabla H}_{\text{dissipated power}} + \underbrace{u^\top y}_{\text{supplied power}} \leq u^\top y. \end{aligned}$$

In light of this fact, combining Theorems 2.3.3 and 2.3.5 yields the following well-known result relating port-Hamiltonian systems and stability.

Lemma 2.3.9. *[129, Lemma 3.2.4] Let $H : \mathbb{X} \to \mathbb{R}$ be a continuously differentiable Hamiltonian function for (2.6). Suppose that x^s is an interior point of $\mathbb{X}$ and a strict local minimum of $H(x)$. Then, x^s is a stable equilibrium point of the unforced system*

$$\dot{x} = (J(x) - R(x)) \nabla H$$

with Lyapunov function $V(x) = H(x) - H(x^s) > 0$ for all $x \in \mathbb{D} \setminus \{x^s\}$ and $V(x^s) = 0$, where $\mathbb{D} \subseteq \mathbb{X}$ is a neighborhood of x^s. Furthermore, suppose that no other solution than $x(t; x^s) = x^s$ remains in $\{x \in \mathbb{D} \mid \dot{H}(x) = 0\}$ for all $t \geq 0$. Then, x^s is an asymptotically stable equilibrium point.

An alternative formulation of Lemma 2.3.9 can be stated by using the property of zero-state detectability of a dynamical system.

Definition 2.3.10. *[129, Definition 3.2.7] The system (2.6) is zero-state detectable if $u(t) = \underline{0}_m$ and $y(t) = \underline{0}_m$, $\forall t \geq 0$, implies $\lim_{t\to\infty} x(t) = \underline{0}_n$.*

Lemma 2.3.11. *Let $H : \mathbb{X} \to \mathbb{R}$ be a continuously differentiable Hamiltonian function for (2.6). Suppose that x^s is an interior point of $\mathbb{X}$ and a strict local minimum of $H(x)$. Suppose that the unforced system*

$$\dot{x} = (J(x) - R(x)) \nabla H$$

is zero-state detectable with output $\bar{y} = R(x)\nabla H$. Then, x^s is an asymptotically stable equilibrium point of the unforced system.

Proof. The proof is based on that of [129, Lemma 3.2.8]. By Lemma 2.3.9, x^s is a stable equilibrium point of $\dot{x} = (J(x) - R(x))\nabla H$. Taking $u = \underline{0}_m$ in (2.6) yields

$$\dot{H} = \nabla H^\top \dot{x} = -\nabla H^\top R(x) \nabla H \leq -\epsilon \|\bar{y}\|$$

with $\epsilon \in \mathbb{R}_{>0}$ and asymptotic stability follows by LaSalle's Invariance Principle, since $\dot{H} = 0$ implies $R(x)\nabla H = \underline{0}_n$, hence $\bar{y} = \underline{0}_n$. □

2.3.4 Routh-Hurwitz criterion for polynomials with complex coefficients

The Routh-Hurwitz criterion for a polynomial with real coefficients derived in [131, 132] is a well-known mathematical test providing necessary and sufficient conditions for all roots of the polynomial to have a negative real part. It is therefore frequently used in the stability analysis of linear time invariant (LTI) systems.

The extension of the Routh-Hurwitz criterion to polynomials with complex coefficients given in [133] is less known. Nevertheless, it provides a simple test to establish part of the results in this thesis. The results of [133] have also recently been used, e.g., in [134, 135, 136, 137, 138, 139]. The main result of [133] is as follows.

Theorem 2.3.12. *[133, Theorem 3.2] Let $P(z)$ denote the polynomial*

$$P(z) = z^n + \alpha_1 z^{n-1} + \alpha_2 z^{n-2} + \ldots + \alpha_n, \quad n \geq 0,$$

where $\alpha_k = p_k + jq_k \in \mathbb{C}$, $k = 1, \ldots, n$. The polynomial $P(z)$ has all its zeros in the open left-half plane if and only if the determinants

$$\Delta_1 = p_1 > 0,$$

$$\Delta_k = \begin{vmatrix} p_1 & p_3 & p_5 & \cdots & p_{(2k-1)} & -q_2 & -q_4 & \cdots & -q_{(2k-2)} \\ 1 & p_2 & p_4 & \cdots & p_{(2k-2)} & -q_1 & -q_3 & \cdots & -q_{(2k-3)} \\ 0 & p_1 & p_3 & \cdots & p_{(2k-3)} & 0 & -q_2 & \cdots & -q_{(2k-4)} \\ 0 & 1 & p_2 & \cdots & p_{(2k-4)} & 0 & -q_1 & \cdots & -q_{(2k-5)} \\ & & & \cdots & & & & \cdots & \\ 0 & & & \cdots & p_k & 0 & & \cdots & -q_{(k-1)} \\ 0 & q_2 & q_4 & \cdots & q_{(2k-2)} & p_1 & p_3 & \cdots & p_{(2k-3)} \\ 0 & q_1 & q_3 & \cdots & q_{(2k-3)} & 1 & p_2 & \cdots & p_{(2k-4)} \\ 0 & 0 & q_2 & \cdots & q_{(2k-4)} & 0 & p_1 & \cdots & p_{(2k-5)} \\ 0 & 0 & q_1 & \cdots & q_{(2k-5)} & 0 & 1 & \cdots & p_{(2k-6)} \\ & & & \cdots & & & & \cdots & \\ 0 & & & \cdots & q_k & 0 & & \cdots & p_{(k-1)} \end{vmatrix}, \quad k = 2, 3, \ldots, n,$$

where $p_r = q_r = 0$ for $r > n$, are all positive.

In the case where $q_k = 0$, $k = 1, \ldots, n$, Theorem 2.3.12 reduces to the usual Hurwitz criterion [133]. For the special case of a quadratic polynomial with complex coefficients, Theorem 2.3.12 simplifies to the following corollary.

Corollary 2.3.13. *Let $P(z)$ denote the polynomial*

$$P(z) = z^2 + \alpha_1 z + \alpha_2,$$

where $\alpha_k = p_k + jq_k \in \mathbb{C}$, $k = 1, 2$. The polynomial $P(z)$ has all its zeros in the open left-half plane if and only if

$$\Delta_1 = p_1 > 0, \quad \Delta_2 = \begin{vmatrix} p_1 & 0 & -q_2 \\ 1 & p_2 & -q_1 \\ 0 & q_2 & p_1 \end{vmatrix} = p_1^2 p_2 + p_1 q_1 q_2 - q_2^2 > 0.$$

2.3.5 Algebraic graph theory and consensus protocols

Graph theory is mainly used in the present work as a tool to describe the high-level properties of distributed communication networks. Therefore, some notation and preliminary results from algebraic graph theory are recalled in Section 2.3.5.1. Furthermore, consensus protocols are introduced in Section 2.3.5.2. These offer interesting possibilities for designing distributed control laws with the purpose of achieving an agreement on certain variables in a network with different agents. Specifically, in this work a consensus-based DVC is proposed, which achieves the objective of reactive power sharing.

For further information on graph theory, the reader is referred to, e.g., [140] and references therein. More details on consensus protocols for multi-agent systems are given, e.g., in [85, 99, 141, 142] and references therein.

2.3.5.1 Algebraic graph theory

A weighted directed graph of order $n \in \mathbb{N}$ is a 3-tuple $\mathcal{G} := (\mathcal{V}, \mathcal{E}, w)$, where $\mathcal{V} := \{1, 2, \ldots, n\}$ is the set of nodes, $\mathcal{E} \subseteq \mathcal{V} \times \mathcal{V}$ is the set of edges, i.e., ordered pairs of nodes (i, k) and $w : \mathcal{E} \to \mathbb{R}_{>0}$ is a weight function. In the case of multi-agent systems, each node in the graph typically represents an individual agent. For the purpose of the present work, an agent represents a DG unit. If there is an edge $e_l = (i, k)$ from node i to node k, then i is called the source and k the sink of the l-th edge, i.e., i can send

information to k. It is assumed that the graph contains no self-loops, i.e., there is no edge $e_l = (i, i)$. The set of neighbors of a node k contains all i for which $e_l = (i, k) \in \mathcal{E}$.

The node-edge incidence matrix $\mathcal{B} \in \mathbb{R}^{|\mathcal{V}|\times|\mathcal{E}|}$ of a directed graph $\mathcal{G}$ is defined element-wise as $b_{il} = 1$, if node i is the source of the l-th edge e_l, $b_{il} = -1$, if i is the sink of e_l and $b_{il} = 0$ otherwise. The $|\mathcal{V}| \times |\mathcal{V}|$ adjacency matrix $\mathcal{A}$ has entries $a_{ik} = w(i, k)$ if there is an edge $e_l = (k, i)$ from k to i with edge weight $w_l = w(i, k)$ and $a_{ik} = 0$ otherwise. The degree of a node i is given by $d_i = \sum_{k\sim\mathcal{V}} a_{ik}$. With $\mathcal{D} := \mathrm{diag}(d_i) \in \mathbb{R}^{n\times n}$, the Laplacian matrix of a graph is given by $\mathcal{L} := \mathcal{D} - \mathcal{A}$.

Based on their interconnection properties, graphs can be divided into two main groups: undirected and directed graphs, the main properties of which are stated below.

Undirected graphs

In an undirected graph the set of edges is undirected. Therefore, the l-th edge connecting nodes i and k is denoted as $e_l = (i, k) = (k, i)$ and its edge weight by $w_l = w(i, k) = w(k, i)$. The node-edge incidence matrix $\mathcal{B}$ of an undirected graph is obtained by associating an arbitrary ordering to the edges. The Laplacian matrix of an undirected graph is symmetric positive semidefinite [140, Chapter 13]. A path in an undirected graph is an ordered sequence of nodes such that any pair of consecutive nodes in the sequence is connected by an edge. $\mathcal{G}$ is called connected if for all pairs $(i, k) \in \mathcal{V} \times \mathcal{V}$, $i \neq k$, there exists a path from i to k. Given an undirected graph, zero is a simple eigenvalue of its Laplacian matrix $\mathcal{L}$ if and only if the graph is connected. Moreover, a corresponding right eigenvector to this simple zero eigenvalue is then $\underline{1}_n$, i.e., $\mathcal{L}\underline{1}_n = \underline{0}_n$ [140, Chapter 13]. Furthermore, $\mathcal{L} = \mathcal{B}\mathrm{diag}(w_l)\mathcal{B}^\top$, $l = 1, \ldots, |\mathcal{E}|$.

Directed graphs

The diagonal entries of the Laplacian matrix $\mathcal{L}$ of a directed graph are nonnegative, its off-diagonal entries are nonpositive and its row sums are zero. All eigenvalues of $\mathcal{L}$ have nonnegative real part [141, Chapter 3]. In a directed graph, a path between two nodes is an ordered sequence of nodes, such that each ordered pair (k, i) in the sequence is adjacent, i.e., the corresponding entry a_{ik} in the adjacency matrix is nonzero. $\mathcal{G}$ is called strongly connected if for all $i \in \mathcal{V}$ and $k \in \mathcal{V}$, there exists a path from i to k [141]. Given a weighted directed graph, zero is a simple eigenvalue of its Laplacian $\mathcal{L}$ if the graph is strongly connected, but the converse is not true [142].

The following lemmata on properties of Laplacian matrices are used in this work.

Lemma 2.3.14. *[102] Let $\mathcal{L} \in \mathbb{R}^{n\times n}$ be the Laplacian matrix of a weighted directed graph. There is no vector $v \in \mathbb{C}^n$ satisfying*

$$\mathcal{L}v = \underline{1}_n.$$

Lemma 2.3.15. *Let $\mathcal{L} \in \mathbb{R}^{n\times n}$ be the Laplacian matrix of a weighted directed graph. Then,*

$$\mathcal{L}\begin{bmatrix} \mathbf{I}_{n-1} & -\underline{1}_{n-1} \\ \underline{0}_{n-1}^\top & 0 \end{bmatrix} = \mathcal{L}.$$

Proof. Recall that the row sums of a Laplacian matrix are zero, i.e., $\sum_{k=1}^{n} l_{ik} = 0$, where $l_{ik} \in \mathbb{R}$ are the elements of the i-th row of $\mathcal{L}$. Hence,

$$\operatorname{col}(l_{ik})^\top \begin{bmatrix} -\underline{1}_{n-1} \\ 0 \end{bmatrix} = -\sum_{k=1}^{n-1} l_{ik} = l_{in}, \quad i \sim \mathcal{N},$$

and the claimed equivalence follows immediately. □

2.3.5.2 Consensus protocols

Consensus protocols for multi-agent networked systems have become an increasingly popular research field in control theory during the past decade. This interest is not the least due to the large area of potential applications of consensus protocols, which include distributed formation control, synchronization in networks of oscillators and flocking theory among others [85].

To reach consensus in a network of agents means that the agents "reach an agreement regarding a certain quantity of interest that depends on the state of all agents" [85]. The interaction rule specifying the information exchange between an agent and its neighbors is called consensus protocol (or algorithm) [85]. An important property of consensus protocols is that, in general, they are distributed protocols. That is, in order to reach an agreement among the agents neither a central communication or computing unit nor all-to-all communication among the agents is required.

Consider a network formed by $n \in \mathbb{N}$ agents. Denote the set of network nodes by $\mathcal{N}$. Suppose the interaction topology of the network is described by an undirected weighted graph $\mathcal{G} = (\mathcal{N}, \mathcal{E}, w)$. Suppose moreover that the graph is connected. Let the dynamics of the i-th agent with state $x_i : \mathbb{R}_{\geq 0} \to \mathbb{R}$ and input $u_i : \mathbb{R}_{\geq 0} \to \mathbb{R}$ be given by

$$\dot{x}_i = u_i, \quad i \sim \mathcal{N}.$$

Then, the most basic consensus protocol guaranteeing convergence to a common state value is given by [85]

$$\dot{x}_i = \sum_{k\sim\mathcal{N}} a_{ik}(x_k - x_i), \quad i \sim \mathcal{N}, \tag{2.7}$$

where a_{ik} denotes the (i,k)-th entry of the adjacency matrix $\mathcal{A}$ of the graph $\mathcal{G}$. The above consensus protocol can equivalently be written in matrix form as

$$\dot{x} = -\mathcal{L}x, \tag{2.8}$$

where $x = \mathrm{col}(x_i) \in \mathbb{R}^n$ and $\mathcal{L}$ is the Laplacian matrix of the graph $\mathcal{G}$. Recalling that $\mathcal{L}\underline{1}_n = \underline{0}_n$ and hence $\underline{1}_n^\top \mathcal{L} = \underline{0}_n^\top$, reveals the following important property of the consensus algorithm (2.8)

$$\underline{1}_n^\top \dot{x} = -\underline{1}_n^\top \mathcal{L}x = \underline{0}_n^\top x \quad \Rightarrow \quad \sum_{i\sim\mathcal{N}} \dot{x}_i = 0,$$

i.e., the sum of the states of all agents is invariant [85].

The preceding discussion leads to the following result.

Lemma 2.3.16. *[85] Let $\mathcal{G}(\mathcal{N},\mathcal{E},w)$ be a connected undirected graph. Let $x(t;x_0)$ denote the solution of* (2.8) *with initial condition $x_0 \in \mathbb{R}^n$. Then, the algorithm* (2.8) *asymptotically solves an average-consensus problem, i.e.,*

$$\lim_{t\to\infty} x(t;x_0) = \alpha \underline{1}_n, \quad \alpha = \frac{1}{|\mathcal{N}|}\sum_{i\sim\mathcal{N}} x_i(0).$$

Let $K \in \mathbb{R}^{n\times n}$ be a diagonal matrix with positive real diagonal entries k_i, $i \sim \mathcal{N}$. In the context of the present work, a relevant extension of the protocol (2.8) is the weighted average consensus protocol given by [85]

$$\dot{x} = -K\mathcal{L}x. \tag{2.9}$$

Rewriting the consensus protocol (2.9) for the agent at the i-th node with $\gamma_i := \frac{1}{k_i}$ yields

$$\gamma_i \dot{x}_i = \sum_{k\sim\mathcal{N}} a_{ik}(x_k - x_i).$$

Hence, γ_i can be interpreted as a variable rate of integration [85]. Further properties of the protocol (2.9) are discussed in Section 5.3, where the protocol (2.9) is used to design a DVC guaranteeing reactive power sharing.

2.3.6 Numerical range of a matrix

Based on [143, Chapter 1], the numerical range (or field of values) of a matrix together with some useful properties relating the spectrum of a matrix to its numerical range are introduced. For further information on matrix analysis, the reader is referred to, e.g., [143, 144].

Definition 2.3.17. *[143, Chapter 1] Let $A \in \mathbb{C}^{n\times n}$. The numerical range or field of values of A is defined as*

$$W(A) := \{x^*Ax \mid x \in \mathbb{C}^n,\, x^*x = 1\}.$$

For a matrix $A \in \mathbb{C}^{n\times n}$, let $\sigma(A) := \{\lambda \in \mathbb{C} \mid \det(\lambda \mathbf{I}_n - A) = 0\}$ denote its spectrum. It holds that $\sigma(A) \subseteq W(A)$. If A is Hermitian, i.e., $A = A^*$, then $W(A) \subset \mathbb{R}$ and $\min(\sigma(A)) \leq W(A) \leq \max(\sigma(A))$. Let $A_{\text{sy}} = \frac{1}{2}(A + A^*)$, respectively $A_{\text{sk}} = \frac{1}{2}(A - A^*)$ be the Hermitian, respectively skew-Hermitian, part of A. Then $\Re(W(A)) = W(A_{\text{sy}})$ and $\Im(W(A)) = W(A_{\text{sk}})$.

The following result is used in this thesis.

Lemma 2.3.18. *[143, Corollary 1.7.7] Let $A \in \mathbb{C}^{n\times n}$ and $B \in \mathbb{C}^{n\times n}$, with B positive semidefinite. Then,*

$$\sigma(AB) \subseteq W(A)W(B) := \{\lambda = ab \mid a \in W(A), b \in W(B)\}.$$

2.4 Preliminaries in power systems

Worldwide, a very common method of AC power generation, transmission and distribution is electric three-phase power [145]. Therefore, this work focuses on the analysis of three-phase electrical systems operated with AC. For information on the history of power systems, as well as on advantages of three-phase AC systems over other solutions, such as, e.g., single-phase AC systems or direct current (DC) systems, the reader is referred to, e.g., [4, 5, 145].

The present section aims at giving a comprehensive and compact overview of the most relevant physical models, definitions, notions and assumptions used in this thesis to model three-phase AC microgrids. The introduced contents apply equivalently to the modeling of general three-phase power systems. As a matter of fact, the presented modeling procedure and definitions are based on standard reference text books in power systems and power electronics, e.g., [1, 3, 4, 5, 6, 15, 146, 147, 148, 149].

The remainder of this section is outlined as follows. At first, relevant properties and characteristics of three-phase AC power systems are presented in Section 2.4.1. Subsequently, in Section 2.4.2 the $dq0$-transformation is introduced. Following [15, 147], instantaneous power is defined in Section 2.4.3 and a short overview of this, still today, controversial research field is given. The fundamental network model describing the current and power flows between units in an electrical network is presented in Section 2.4.4. Finally, definitions of stability in power systems and microgrids are given in Section 2.4.5. To a large extent, this section is taken from [126].

2.4.1 Three-phase AC electrical power systems

Some basic definitions for AC electrical networks are introduced.

Definition 2.4.1. *[150] A signal $x : \mathbb{R}_{\geq 0} \to \mathbb{R}$ is said to be an AC signal if it satisfies the following conditions.*

1. *It is periodic with period $T \in \mathbb{R}_{>0}$,* i.e.*,*

$$x(t) = x(t + nT), \quad \forall n \in \mathbb{N}, \quad \forall t \geq 0.$$

2. *Its arithmetic mean is zero,* i.e.*,*

$$\int_t^{t+T} x(\tau) d\tau = 0 \quad \forall t \geq 0.$$

Definition 2.4.2. *A signal $x : \mathbb{R}_{\geq 0} \to \mathbb{R}^3$ is said to be a three-phase AC signal if it is of the form*

$$x_{ABC} = \begin{bmatrix} x_A \\ x_B \\ x_C \end{bmatrix},$$

where $X_A : \mathbb{R}_{\geq 0} \to \mathbb{R}$, $X_B : \mathbb{R}_{\geq 0} \to \mathbb{R}$ and $X_C : \mathbb{R}_{\geq 0} \to \mathbb{R}$ are AC signals.

A special kind of three-phase AC signals are symmetric AC three-phase signals, defined below.

Definition 2.4.3. *[147, Chapter 2] A three-phase AC signal $x_{abc} : \mathbb{R}_{\geq 0} \to \mathbb{R}^3$ is said to be symmetric if it can be described by*

$$x_{abc}(t) = \begin{bmatrix} x_a(t) \\ x_b(t) \\ x_c(t) \end{bmatrix} = A(t) \begin{bmatrix} \sin(\delta(t)) \\ \sin(\delta(t) - \frac{2\pi}{3}) \\ \sin(\delta(t) + \frac{2\pi}{3}) \end{bmatrix},$$

where $A : \mathbb{R}_{\geq 0} \to \mathbb{R}_{\geq 0}$ is called the amplitude and $\delta : \mathbb{R}_{\geq 0} \to \mathbb{T}$ is called the phase angle of the signal.

Clearly, from the preceding definition, a symmetric three-phase AC signal x_{abc} can be described completely by two signals: its angle δ and its amplitude A[1].

Definition 2.4.4. *[147, Chapter 2] A three-phase AC signal is said to be asymmetric if it is not symmetric.*

Definition 2.4.5. *[149, Chapter 3] A three-phase AC electrical system is said to be symmetrically configured if a symmetrical feeding voltage yields a symmetrical current and vice versa.*

Definition 2.4.6. *[149, Chapter 3] A three-phase AC power system is said to be operated under symmetric conditions if it is symmetrically configured and symmetrically fed.*

Examples of symmetric and asymmetric three-phase AC signals[2] are given in Fig. 2.1. The signals in Fig. 2.1a and Fig. 2.1b are symmetric, while the signal in Fig. 2.1c is not, because the phases are not shifted equally by $\frac{2\pi}{3}$. The signal in Fig. 2.1d is also asymmetric, since the different phases are superposed asymmetrically with signals oscillating at higher frequencies. Such signals are, e.g., obtained by superposing a symmetric three-phase signal with harmonic signals, which oscillate with a higher frequency than the fundamental frequency. Such three-phase signals can, for example, be caused by nonlinear loads, i.e., loads that draw nonsinusoidal currents [147].

Remark 2.4.7. Note that for any three-phase symmetric signal x_{abc}

$$x_a + x_b + x_c = 0,$$

i.e., a symmetric three-phase signal can be described in a two-dimensional space, see also [148, Chapter 2.3].

Remark 2.4.8. The terms "balanced" and "unbalanced" are frequently used as synonyms of "symmetric", respectively "asymmetric" in the literature [4, 147].

Remark 2.4.9. Three-phase electrical power systems consist of three main conductors in parallel. Each of these conductors carries an AC current. A three-phase system can be arranged in Δ- or Y-configuration, see Fig. 2.2. The latter is also called wye-configuration. Frequently, in a system with Y-configuration an additional fourth

[1] Recall that to simplify notation the time argument of all signals is omitted, whenever clear from the context. The same applies to the definition of signals, i.e., a signal $x : \mathbb{R}_{\geq 0} \to \mathbb{R}$, is defined equally as $x \in \mathbb{R}$, whenever clear from the context.

[2] In this work only AC systems and signals are considered. Therefore, the qualifier AC is dropped from now on.

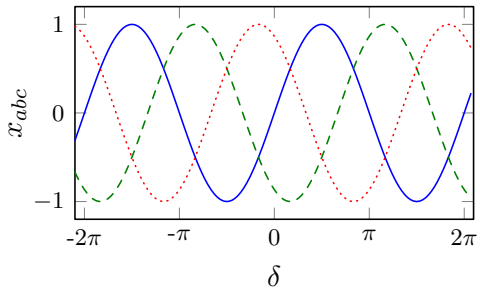

(a) Symmetric three-phase AC signal with constant amplitude

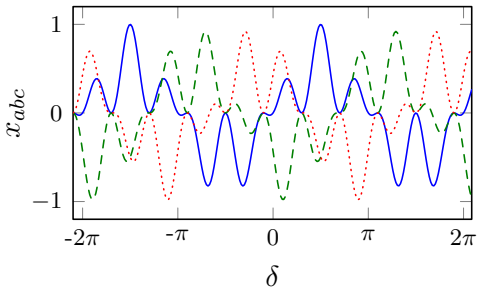

(b) Symmetric three-phase AC signal with time-varying amplitude

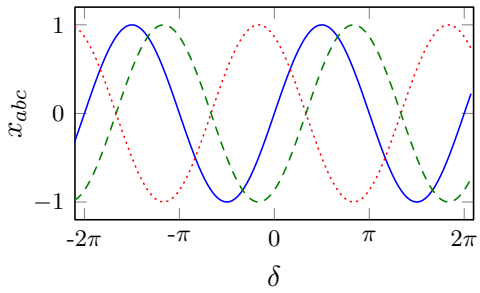

(c) Asymmetric three-phase AC signal with phases not shifted equally by $\frac{2\pi}{3}$

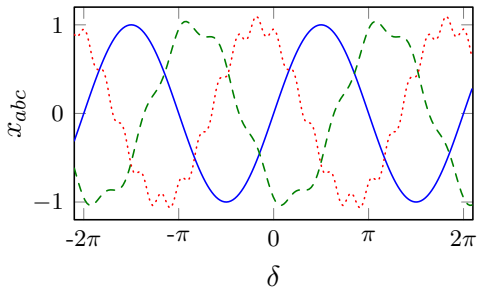

(d) Asymmetric three-phase AC signal resulting of an asymmetric superposition of a symmetric signal with signals oscillating at higher frequencies

Figure 2.1: Symmetric and asymmetric AC three-phase signals. The lines correspond to x_a '—', x_b '- -', x_c '...'.

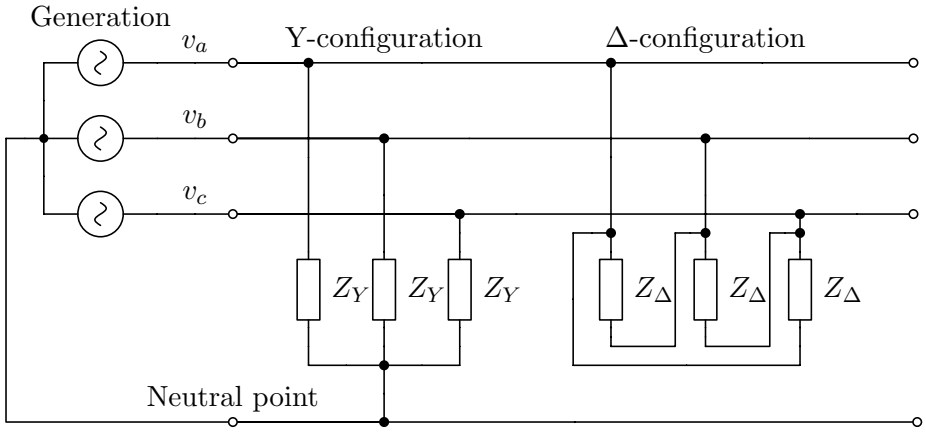

Figure 2.2: Standard Y- and Δ-configurations of three-phase AC power systems based on [149, Chapter 3].

grounded neutral conductor is used to reduce transient overvoltages and to carry asymmetric currents [4, Chapter 2], see Fig. 2.2. Such systems are typically called three-phase four-wire systems. Most three-phase power systems are four-wire Y-connected systems with grounded neutral conductor [4, Chapter 2]. However, it can easily be shown that, under symmetric operating conditions, this fourth wire does not carry any current and can therefore be neglected [4, Chapter 2].

2.4.2 $Dq0$-transformation

An important coordinate transformation known as $dq0$-transformation in the literature [3, 6, 15, 148, 151, 152, 153] is introduced.

Definition 2.4.10. *[3, Chapter 4], [6, Chapter 11] Let $x : \mathbb{R}_{\geq 0} \to \mathbb{R}^3$ and $\varrho : \mathbb{R}_{\geq 0} \to \mathbb{T}$. Consider the mapping $T_{dq0} : \mathbb{T} \to \mathbb{R}^{3\times 3}$,*

$$T_{dq0}(\varrho(t)) := \sqrt{\frac{2}{3}} \begin{bmatrix} \cos(\varrho(t)) & \cos(\varrho(t) - \frac{2}{3}\pi) & \cos(\varrho(t) + \frac{2}{3}\pi) \\ \sin(\varrho(t)) & \sin(\varrho(t) - \frac{2}{3}\pi) & \sin(\varrho(t) + \frac{2}{3}\pi) \\ \frac{\sqrt{2}}{2} & \frac{\sqrt{2}}{2} & \frac{\sqrt{2}}{2} \end{bmatrix}. \tag{2.10}$$

Then, $f_{dq0} : \mathbb{R}^3 \times \mathbb{T} \to \mathbb{R}^3$,

$$f_{dq0}(x(t), \varrho(t)) = T_{dq0}(\varrho(t))x(t) \tag{2.11}$$

is called $dq0$-transformation.

Note that the mapping (2.10) is unitary, i.e., $T_{dq0}^\top = T_{dq0}^{-1}$. From a geometrical point of view, the $dq0$-transformation is a concatenation of two rotational transformations,

see, e.g., [152] for further details. The variables in the transformed coordinates are often denoted by $dq0$-variables. Since this transformation was first introduced (with a slightly different scaling factor) by Robert H. Park in 1929 [151] it is also called Park transformation [15, Appendix A].

The $dq0$-transformation offers various advantages when analyzing and working with power systems and is therefore widely used in power systems and power electronics applications [3, 15, 147, 148, 152]. For example, the $dq0$-transformation permits, through appropriate choice of ϱ, to map sinusoidal signals to constant signals. This simplifies the control design and analysis in power systems, which is the main reason why the transformation (2.11) is introduced in the present case. In addition, the transformation (2.11) exploits the fact that, in a power system operated under symmetric conditions, a three-phase signal can be represented by two quantities, cf. Remark 2.4.7. To see this, let $x_{abc} : \mathbb{R}_{\geq 0} \to \mathbb{R}^3$ be a symmetric three-phase signal with amplitude $A : \mathbb{R}_{\geq 0} \to \mathbb{R}_{\geq 0}$ and phase angle $\delta : \mathbb{R}_{\geq 0} \to \mathbb{T}$. Applying the mapping (2.10) with some angle $\varrho : \mathbb{R}_{\geq 0} \to \mathbb{T}$ to x_{abc} yields

$$x_{dq0} = \begin{bmatrix} x_d \\ x_q \\ x_0 \end{bmatrix} = T_{dq0}(\varrho) x_{abc} = \sqrt{\frac{3}{2}} A \begin{bmatrix} \sin(\delta - \varrho) \\ \cos(\delta - \varrho) \\ 0 \end{bmatrix}. \tag{2.12}$$

Hence, $x_0 = 0$ for all $t \geq 0$. In this work, only symmetric three-phase signals are considered. Due to (2.12), it is therefore convenient to introduce the mapping $T_{dq} : \mathbb{T} \to \mathbb{R}^{2\times 3}$,

$$T_{dq}(\varrho(t)) := \sqrt{\frac{2}{3}} \begin{bmatrix} \cos(\varrho(t)) & \cos(\varrho(t) - \frac{2}{3}\pi) & \cos(\varrho(t) + \frac{2}{3}\pi) \\ \sin(\varrho(t)) & \sin(\varrho(t) - \frac{2}{3}\pi) & \sin(\varrho(t) + \frac{2}{3}\pi) \end{bmatrix}, \tag{2.13}$$

with $\varrho : \mathbb{R}_{\geq 0} \to \mathbb{T}$. Applying the mapping (2.13) to the symmetric three-phase signal x_{abc} defined above yields

$$x_{dq} = \begin{bmatrix} x_d \\ x_q \end{bmatrix} = T_{dq}(\varrho) x_{abc} = \sqrt{\frac{3}{2}} A \begin{bmatrix} \sin(\delta - \varrho) \\ \cos(\delta - \varrho) \end{bmatrix}. \tag{2.14}$$

Remark 2.4.11. There are several variants of the mapping (2.10) available in the literature. They may differ from the mapping (2.10) in the order of the rows and the sign of the entries in the second row of the matrix given in (2.10), see, e.g., [3, 148, 153]. However, all representations are equivalent in the sense that they can all be represented by T_{dq0} as given in (2.10) by choosing an appropiate angle $\varrho : \mathbb{R}_{\geq 0} \to \mathbb{T}$ and, possibly, rearranging the row order of the matrix T_{dq0}. The same applies to the mapping T_{dq} given in (2.13).

2.4.3 Instantaneous power

Power is one of the most important quantities in control, monitoring and operation of electrical networks. The first theoretical contributions to the definition of the power flows in an AC network date back to the early 20th century. However, these first definitions are restricted to sinusoidal steady-state conditions and based on the root mean square (RMS) values of currents and voltages. As a consequence, these definitions of electric power are not well-suited for the purposes of network control under time-varying operating conditions [147].

The extension of the definition of electrical power to time-varying operating conditions is called "instantaneous power theory" in the power system and power electronics community [15, 147]. The development of this theory already begun in the 1930s with the study of active and nonactive components of currents and voltages [154]. Among others, further relevant contributions are [155, 156, 157, 158, 159, 160, 161].

Today, it is widely agreed by reasearchers and practitioners [15, 158, 160] that the definitions of instantaneous power proposed in [157] and contained in [147] are well-suited for describing the power flows in three-phase three-wire systems and symmetric three-phase four-wire systems. However, a proper definition of instantaneous power in asymmetric three-phase four-wire systems with nonzero neutral current and voltage is still a controversial open field of research [15, 147, 162, 163]. A good overview of the research history on instantaneous power theory is given in [15, Appendix B].

Consider a symmetric three-phase voltage, respectively current, given by

$$v_{abc} = \sqrt{2}V \begin{bmatrix} \sin(\alpha) \\ \sin(\alpha - \frac{2\pi}{3}) \\ \sin(\alpha + \frac{2\pi}{3}) \end{bmatrix}, \quad i_{abc} = \sqrt{2}I \begin{bmatrix} \sin(\beta) \\ \sin(\beta - \frac{2\pi}{3}) \\ \sin(\beta + \frac{2\pi}{3}) \end{bmatrix}, \tag{2.15}$$

where $\alpha : \mathbb{R}_{\geq 0} \to \mathbb{T}$, respectively $\beta : \mathbb{R}_{\geq 0} \to \mathbb{T}$, is the phase angle and $\sqrt{2}V : \mathbb{R}_{\geq 0} \to \mathbb{R}_{\geq 0}$, respectively $\sqrt{2}I : \mathbb{R}_{\geq 0} \to \mathbb{R}_{\geq 0}$, the amplitude of the respective three-phase signal. As shown in Section 2.4.2, applying the transformation (2.13) to the signals given in (2.15) yields, cf. (2.14),

$$v_{dq} = \begin{bmatrix} V_d \\ V_q \end{bmatrix} = \sqrt{3}V \begin{bmatrix} \sin(\alpha - \varrho) \\ \cos(\alpha - \varrho) \end{bmatrix}, \quad i_{dq} = \begin{bmatrix} I_d \\ I_q \end{bmatrix} = \sqrt{3}I \begin{bmatrix} \sin(\beta - \varrho) \\ \cos(\beta - \varrho) \end{bmatrix}. \tag{2.16}$$

Based on the preceding discussion, the following definitions of instantaneous active, reactive and apparent power under symmetric, but not necessarily steady-state, conditions are used in this work.

Definition 2.4.12. *[147, 157] Let $v_{qd}(t)$ and $i_{qd}(t)$ be given by (2.16). The instantaneous three-phase active power is defined as*

$$P(t) := v_{dq}^{\top}(t) i_{dq}(t) = V_d(t) I_d(t) + V_q(t) I_q(t).$$

The instantaneous three-phase reactive power is defined as

$$Q(t) := v_{dq}^{\top}(t) \begin{bmatrix} 0 & 1 \\ -1 & 0 \end{bmatrix} i_{dq}(t) = V_d(t) I_q(t) - V_q(t) I_d(t).$$

Finally, the instantaneous three-phase apparent power is defined as

$$S(t) := P(t) + jQ(t),$$

where j denotes the imaginary unit.

From the above definition, straight-forward calculations together with standard trigonometric identities yield

$$P(t) = 3V(t)I(t)\cos(\alpha(t) - \beta(t)), \quad Q(t) = 3V(t)I(t)\sin(\alpha(t) - \beta(t)).$$

It follows that whenever v_{abc} and i_{abc} given in (2.15) possess constant amplitudes, as well as the same frequency, i.e., $\dot{\alpha} = \dot{\beta}$, all quantities P, Q and S are constant. Moreover, then the given definitions of power are in accordance to the conventional definitions of power in a symmetric steady-state [4, 5, 147]. For further information on definitions and physical interpretations of instantaneous power, also under asymmetric conditions, the reader is referred to, e.g., [15, 147, 158, 160, 164, 165].

Since this work is mainly concerned with dynamics of generation units, all powers are expressed in "Generator Convention" [4, Chapter 2], also called "Generator Reference Arrow System". That is, delivered active power is positive, while absorbed active power is negative. Furthermore, capacitive reactive power is counted positively and inductive reactive power is counted negatively.

Remark 2.4.13. In [147, 157] the instantaneous power is defined using representations of voltage and current in *alpha-beta*-coordinates [147, 148]. The definitions of power given in Definition 2.4.12 in *dq*-coordinates are equivalent to the representation in *alpha-beta*-coordinates [3, 6, 15]. For the purposes of the present work, the definition in *dq*-coordinates is more convenient.

2.4.4 Modeling of electrical networks

This section is inspired by [1, 3, 5, 6, 146, 166] and presents the physical model used in this work to describe the current and power flows among different nodes in a microgrid. The model is derived from fundamental laws of physics and therefore also applies to generic power systems. At first, some basic notation in electrical circuits is introduced.

Definition 2.4.14. *[150] Let $C \in \mathbb{R}_{>0}$, $L \in \mathbb{R}_{\geq 0}$ and $\omega \in \mathbb{R}_{>0}$ be constants denoting a capacitance, an inductance and a frequency. The capacitive reactance is defined as*

$$X_C := -\frac{1}{\omega C} \in \mathbb{R}_{<0}.$$

The inductive reactance is defined as

$$X_L := \omega L \in \mathbb{R}_{\geq 0}.$$

Definition 2.4.15. *[150] Let $R \in \mathbb{R}_{\geq 0}$ and $X \in \mathbb{R}$ be constants denoting a resistance, respectively a reactance. The constant complex impedance Z is defined as $Z := R + jX \in \mathbb{C}$. For $Z \neq 0$, the constant complex admittance Y is defined as*

$$Y := \frac{1}{Z} = \frac{R}{R^2 + X^2} + j\frac{-X}{R^2 + X^2} := G + jB \in \mathbb{C}.$$

Furthermore, $G = \frac{R}{R^2+X^2} \in \mathbb{R}_{\geq 0}$ is called conductance and $B = \frac{-X}{R^2+X^2} \in \mathbb{R}$ is called susceptance.

Remark 2.4.16. For ease of notation, also $Y = 0$ is employed at times, though the above definition does not naturally comprise this case.

Remark 2.4.17. In power system analysis, currents and voltages are often expressed as complex quantities (see, e.g., the model derivation in the next section). Then, the impedance of an element of an electrical circuit represents the voltage-to-current ratio of that element at a specific frequency ω.

2.4.4.1 Relation of voltage and current on a power line

The different components in a power system are usually connected via power lines. A standard model for a power line is the π-model illustrated in Fig. 2.3a. The π-model consists of a series RL element connected in parallel with R and C shunt-elements, i.e., grounded R and C elements [1, 4, 5, 146, 166]. For short power lines on the transmission and distribution level the shunt-elements can often be neglected [1, 4, 5, 146, 166]. Then, a power line can be modeled by a series RL element as shown in Fig. 2.3b.

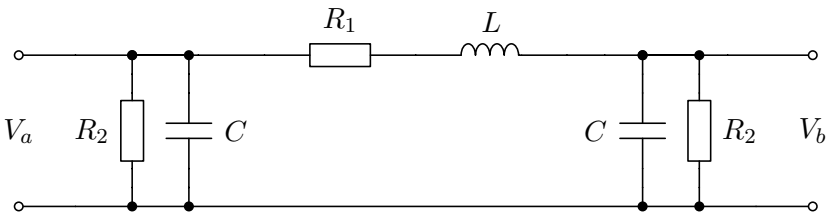

(a) π-model of a power line

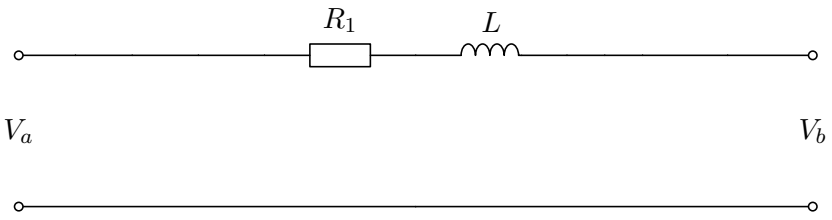

(b) RL model of a power line

Figure 2.3: Common power line models

The model given in Fig. 2.3b is also a valid representation of an equivalent circuit of a power transformer under the standard assumptions of small core losses and small core magnetization losses [4, Chapter 3], [167, Chapter 3]. Power transformers are used to transform AC voltages and currents to suitable efficient levels for power transmission, distribution and utilization [4, Chapter 3].

The analysis in this work is restricted to symmetric network operating conditions. Moreover, in a microgrid the lines are typically short. Therefore, the following assumption is made.

Assumption 2.4.18. *All power lines and transformers can be represented by symmetric three-phase RL elements.*

In light of Assumption 2.4.18 and to ease presentation, the term power lines is solely used to refer to the network interconnections in the following.

Consider a three-phase symmetric power line each phase of which is composed of a constant ohmic resistance $R \in \mathbb{R}_{>0}$ in series with a constant inductance $L \in \mathbb{R}_{>0}$. Recall the symmetric three-phase voltage v_{abc} and current i_{abc} defined in (2.15). Let v_{abc} denote the voltage drop across the line and i_{abc} denote the current flowing over the line. Then, the dynamic relation between v_{abc} and i_{abc} can be described by the following ODE [3, Chapter 9]

$$L\frac{di_{abc}}{dt} = -Ri_{abc} + v_{abc}. \tag{2.17}$$

Recall the dq-transformation T_{dq} introduced in (2.13) and let ω^{com} be a real constant[1]. Let

$$\phi := \text{mod}_{2\pi}\left(\omega^{\text{com}} t\right) \in \mathbb{T}, \tag{2.18}$$

where the operator[2] $\text{mod}_{2\pi}(\cdot)$ is added to respect the topology of $\mathbb{T}$. Applying the transformation T_{dq} with transformation angle ϕ to the signals v_{abc} and i_{abc} in (2.17) gives

$$\hat{v}_{dq} := T_{dq}(\phi) v_{abc} = \begin{bmatrix} \hat{V}_d \\ \hat{V}_q \end{bmatrix}, \quad \hat{i}_{dq} := T_{dq}(\phi) i_{abc} = \begin{bmatrix} \hat{I}_d \\ \hat{I}_q \end{bmatrix}, \tag{2.19}$$

where the superscript " $\hat{\cdot}$ " is introduced to denote signals in dq-coordinates with respect to the angle ϕ. This notation is used in the subsequent section, where a model of an electrical network is derived by using several dq-transformation angles. Furthermore, following standard notation in power systems, the constant $\dot{\phi} = \omega^{\text{com}}$ is referred to as "the rotational speed of the common reference frame". Note that

$$\frac{d\hat{i}_{dq}}{dt} = \frac{dT_{dq}(\phi)}{dt} i_{abc} + T_{dq}(\phi) \frac{di_{abc}}{dt} = \dot{\phi} \begin{bmatrix} -\hat{I}_q \\ \hat{I}_d \end{bmatrix} + T_{dq}(\phi) \frac{di_{abc}}{dt} = \omega^{\text{com}} \begin{bmatrix} -\hat{I}_q \\ \hat{I}_d \end{bmatrix} + T_{dq}(\phi) \frac{di_{abc}}{dt}.$$

Hence, (2.17) reads in dq-coordinates as

$$L \frac{d\hat{i}_{dq}}{dt} = -R\hat{i}_{dq} + L\omega^{\text{com}} \begin{bmatrix} -\hat{I}_q \\ \hat{I}_d \end{bmatrix} + \hat{v}_{dq}. \tag{2.20}$$

For the purpose of deriving an interconnected network model suitable for stability analysis, it is customary to make the following assumption [1, 3, 146].

Assumption 2.4.19. *The dynamics of the power lines are negligible.*

Assumption 2.4.19 is standard in power system analysis [1, 3, 4, 5, 6, 146]. The usual justification of Assumption 2.4.19 is that the line dynamics evolve on a much faster time-scale than the dynamics of the generation sources, i.e., $0 < L < \epsilon$, where L is the line inductance and ϵ is a small positive real parameter. Therefore, the line dynamics can be neglected in the network model [168, 169].

A theoretical legitimation of Assumption 2.4.19 can be given via singular perturbation arguments [128, Chapter 11], [170]. If some of the time-derivatives of the states of a model of a dynamical system are multiplied by a small positive real parameter, then the model is said to be a "singular perturbation model" [128, Chapter 11]. In

[1] In general, one could also choose a time-varying signal ω^{com}. However, for the subsequent model derivation, it is more convenient to let ω^{com} be a constant.

[2] The operator $\text{mod}_{2\pi}\{\cdot\} : \mathbb{R} \to [0, 2\pi)$, is defined as follows: $y = \text{mod}_{2\pi}\{x\}$ yields $y = x - k2\pi$ for some integer k, such that $y \in [0, 2\pi)$.

that case, the set of states the time derivatives of which are multiplied by the small parameter are called "fast" dynamics, while the remaining states are called "slow" dynamics. The main idea of the singular perturbation approach is to analyze the system dynamics on different time-scales. As a consequence and under certain conditions (see, e.g., [128, Chapter 11] for details), the behavior of the "slow" dynamics can then be studied by approximating the "fast" dynamics by their corresponding algebraic steady-state equations. In the present case, the "fast" dynamics represent the line dynamics and the "slow" dynamics are the dynamics of the generation units. A rigorous singular perturbation analysis is, in general, technically very involved and therefore omitted here. Instead, the reader is referred to [171] and, e.g., [146, 172, 173] for an in-depth discussion of the application of the singular perturbation approach to power systems. It should, however, be noted that Assumption 2.4.19 also applies to the model of inverter-interfaced DG units derived in this work, i.e., the dynamics of the model of an inverter-interfaced DG unit are typically slower than the power line dynamics (2.20) (see also Section 4.2).

Furthermore, to the best of the author's knowledge, although being pursued for long time, up to day there are only very few well-funded results on stability of generic power systems and, specifically, microgrids, which are not derived under Assumption 2.4.19. Some existing results together with their limitations are reviewed in Section 8.2.

Under Assumption 2.4.19 and recalling the definition of a reactance given in Definition 2.4.14, the ODE (2.20) reduces to the algebraic equation

$$\hat{v}_{dq} = L\omega^{\mathrm{com}} \begin{bmatrix} \hat{I}_q \\ -\hat{I}_d \end{bmatrix} + R\hat{i}_{dq} = X \begin{bmatrix} \hat{I}_q \\ -\hat{I}_d \end{bmatrix} + R\hat{i}_{dq}. \tag{2.21}$$

Note that the reactance X is calculated at the frequency ω^{com}, which, under Assumption 2.4.19, should be chosen as the (constant) synchronous frequency of the network—denoted by $\omega^s \in \mathbb{R}$ in the following[1]. Typically, $\omega^s \in 2\pi[45, 65]$ rad/s. For ease of notation, it is convenient to represent the quantities

$$\hat{v}_{dq}(t) = \begin{bmatrix} \hat{V}_d(t) \\ \hat{V}_q(t) \end{bmatrix} \in \mathbb{R}^2, \quad \hat{i}_{dq}(t) = \begin{bmatrix} \hat{I}_d(t) \\ \hat{I}_q(t) \end{bmatrix} \in \mathbb{R}^2,$$

as complex numbers, i.e.,

$$\hat{V}_{qd}(t) := \hat{V}_q(t) + j\hat{V}_d(t) \in \mathbb{C}, \quad \hat{I}_{qd}(t) := \hat{I}_q(t) + j\hat{I}_d(t) \in \mathbb{C}. \tag{2.22}$$

[1] Under Assumption 2.4.19, (2.21) is the equilibrium of the "fast" line dynamics (2.20) [128, Chapter 11]. Hence, in order for the currents $\hat{i}_{dq}$ and voltages $\hat{v}_{dq}$ to be constant in steady-state, ω^{com} has to be chosen equivalently to the synchronous steady-state network frequency, see also (2.14).

By making use of (2.22), (2.21) can be expressed as

$$\hat{V}_q + j\hat{V}_d = (R + jX)(\hat{I}_q + j\hat{I}_d), \tag{2.23}$$

or, more compactly, with $Z = R + jX$,

$$\hat{V}_{qd} = Z\hat{I}_{qd}, \tag{2.24}$$

which is an algebraic relation of the current flow $\hat{I}_{qd}$ and voltage drop $\hat{V}_{qd}$ on a power line with impedance Z.

The form (2.22) is a very popular representation in the power community and the complex quantities $\hat{V}_{qd}$ and $\hat{I}_{qd}$ are often denoted as phasors [3, 148]. Furthermore, by using Euler's formula [174], (2.22) can also be rewritten in polar form. Note, however, that, unlike, e.g., [3, 148], other authors define a phasor as a complex sinusoidal quantity with a constant frequency [4]. Therefore, in order to avoid confusions, the term "phasor" is not used in this work.

2.4.4.2 Current and power flows in an electrical network

Building on the results of the previous section, a network model describing the current and power flows between nodes in an electrical network is derived. These relations are of further interest in the context of the present work, since the current and power flows describe the interactions among different generation sources and loads in a power system. The network model is elaborated under Assumptions 2.4.18 and 2.4.19 and, hence, static. In general, the different DG units (and sometimes also some loads) connected at the different nodes in the network are modeled by dynamical systems. These models are discussed in detail in Chapter 4.

Consider an electrical network formed by $n \in \mathbb{N}$ nodes and denote the set of network nodes by $\mathcal{N} = \{1, 2, \ldots, n\}$ as defined in Section 2.2. Associate to each node i in the network a symmetric three-phase voltage $v_{abc_i} : \mathbb{R}_{\geq 0} \to \mathbb{R}^3$ with amplitude $\sqrt{\frac{2}{3}}V_i : \mathbb{R}_{\geq 0} \to \mathbb{R}_{\geq 0}$ and phase angle $\alpha_i : \mathbb{R}_{\geq 0} \to \mathbb{T}$, i.e.,

$$v_{abc_i} = \sqrt{\frac{2}{3}}V_i \begin{bmatrix} \sin(\alpha_i) \\ \sin(\alpha_i - \frac{2\pi}{3}) \\ \sin(\alpha_i + \frac{2\pi}{3}) \end{bmatrix}. \tag{2.25}$$

In addition, associate to each node $i \in \mathcal{N}$ a symmetric three-phase current $i_{abc_i} : \mathbb{R}_{\geq 0} \to \mathbb{R}^3$, which represents the current injected by the generation unit, respectively the current drawn by the load, at node i. A schematic representation of an exemplary

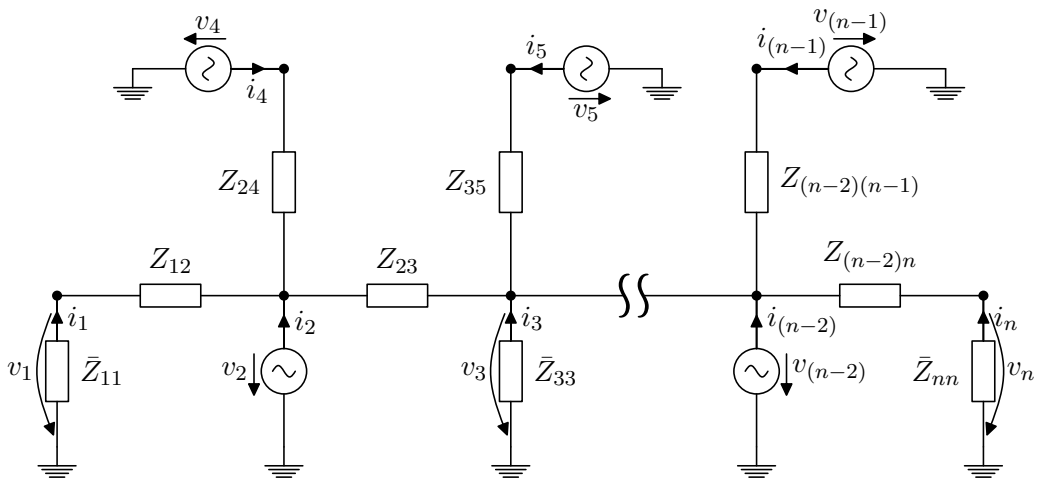

Figure 2.4: Schematic single-phase representation of an electrical network with $n \in \mathbb{N}$ nodes. The AC voltage sources $v_i : \mathbb{R}_{\geq 0} \to \mathbb{R}$, $i \sim \mathcal{N}$, denote either generation units or loads with exogeneous AC current injection, respectively consumption, $i_i : \mathbb{R}_{\geq 0} \to \mathbb{R}$. In addition, some loads are represented by shunt-impedances $\bar{Z}_{ii} \in \mathbb{C}$, while power lines are represented by the impedances $Z_{ik} \in \mathbb{C}$, $i \sim \mathcal{N}$, $k \sim \mathcal{N}_i$.

electrical network is given in Fig. 2.4. Therein, some loads are represented by shunt-impedances, i.e., impedances to ground—a commonly used load model in power system studies [1, 4, 6].

Following [3, Chapter 9], a two-step procedure is carried out to obtain the network equations that establish the desired relations between voltages and currents in the network. These can subsequently be used to obtain the power flow equations. Typically, the voltages are states of the individual dynamical subsystems connected at the network nodes and representing generation units (or loads), while the currents are not. From a control theoretic point of view, it is therefore desirable to describe the current and power flows by means of the voltages, i.e., to describe the network interconnections by means of the state variables of the different subsystems.

Recall the mapping T_{dq} given in (2.13) and perform the following two steps.

1. Transform each v_{abc_i}, $i \sim \mathcal{N}$, into "local" dq-coordinates by means of the mapping T_{dq} with some continuously differentiable transformation angle $\theta_i : \mathbb{R}_{\geq 0} \to \mathbb{T}$, $i \sim \mathcal{N}$. This yields

$$\boxed{v_{dq_i} = \begin{bmatrix} V_{d_i} \\ V_{q_i} \end{bmatrix} = T_{dq}(\theta_i) v_{abc_i} = V_i \begin{bmatrix} \sin(\alpha_i - \theta_i) \\ \cos(\alpha_i - \theta_i) \end{bmatrix}.} \tag{2.26}$$

   Note that the factor $\sqrt{\frac{2}{3}}$ in the amplitude of the three-phase signal v_{abc_i} vanishes

when transforming the signal into dq-coordinates, i.e., the amplitude of the signal v_{dq_i} is V_i. Furthermore, since the angles θ_i, $i \sim \mathcal{N}$, can be chosen arbitrarily for each node, this first transformation step is usually referred to as a "transformation to local dq-coordinates" and the angle θ_i is called "local reference angle" [3]. Its main purpose is to simplify the interconnection of the respective node voltage v_{dq_i} at the i-th bus with the dynamic model of the unit connected at that bus. This purpose typically also determines the choice of the angle θ_i, $i \sim \mathcal{N}$[1].

Applying the same transformation to i_{abc_i}, $i \sim \mathcal{N}$, yields

$$i_{dq_i} = \begin{bmatrix} I_{d_i} \\ I_{q_i} \end{bmatrix} = T_{dq}(\theta_i) i_{abc_i}. \tag{2.27}$$

It is convenient to define, cf. (2.22) and (2.24),

$$V_{qd_i} := V_{q_i} + jV_{d_i}, \quad I_{qd_i} := I_{q_i} + jI_{d_i}, \quad i \sim \mathcal{N},$$

and denote the vectors of all currents and voltages in local dq-coordinates by

$$\boxed{V_{qd} := \mathrm{col}(V_{qd_i}) \in \mathbb{C}^n, \quad I_{qd} := \mathrm{col}(I_{qd_i}) \in \mathbb{C}^n.} \tag{2.28}$$

Note that from a control or network theoretic point of view v_{dq_i} and i_{dq_i}, respectively V_{qd_i} and I_{qd_i}, $i \sim \mathcal{N}$, represent the port variables of the respective dynamical subsystem connected at the i-th node.

2. Transform all variables v_{dq_i} and i_{dq_i}, $i \sim \mathcal{N}$, given in (2.26) and (2.27) to a "common reference frame". This second step seeks to describe all port variables v_{dq_i} and i_{dq_i}, $i \sim \mathcal{N}$, in one common coordinate system and, hence, to facilitate the derivation of the power flows in the network by means of the variables v_{dq_i}, $i \sim \mathcal{N}$.

   To this end, recall the rotational speed of the common reference frame given by the real constant ω^{com} in (2.18) and set

$$\delta_i := \theta_{0_i} + \int_0^t (\dot{\theta}_i - \omega^{\mathrm{com}}) d\tau \in \mathbb{T}, \quad i \sim \mathcal{N}, \tag{2.29}$$

   where θ_i is the angle used in the transformation (2.26), $\dot{\theta}_i$ its time-derivative and $\theta_{0_i} \in \mathbb{T}$ its initial condition. For example, a typical choice for ω^{com} would be the

[1] If there are merely static components connected at the i-th node, e.g., in the case of a load represented by a constant shunt-admittance, then it is convenient to set $\theta_i = \alpha_i$.

frequency of the operating point of interest. Let $\varpi : \mathbb{R}_{\geq 0} \to \mathbb{T}$ and consider the mapping $T_\delta : \mathbb{T} \to \mathbb{R}^{2\times 2}$,

$$T_\delta(\varpi) := \begin{bmatrix} \cos(\varpi) & \sin(\varpi) \\ -\sin(\varpi) & \cos(\varpi) \end{bmatrix}, \tag{2.30}$$

which applied to any $x \in \mathbb{R}^2$ represents a rotational transformation. Applying T_δ with δ_i defined in (2.29) to the voltage v_{dq_i} at the i-th node gives

$$\hat{v}_{dq_i} = \begin{bmatrix} \hat{V}_{d_i} \\ \hat{V}_{q_i} \end{bmatrix} := T_\delta(\delta_i) \begin{bmatrix} V_{d_i} \\ V_{q_i} \end{bmatrix}. \tag{2.31}$$

Note that, by construction,

$$T_{dq}(\phi) = T_\delta(\delta_i) T_{dq}(\theta_i)$$

and, hence,

$$\hat{v}_{dq_i} = T_{dq}(\phi) v_{abc_i} = T_\delta(\delta_i) T_{dq}(\theta_i) v_{abc_i} = T_\delta(\delta_i) v_{dq_i} = V_i \begin{bmatrix} \sin(\alpha_i - \phi) \\ \cos(\alpha_i - \phi) \end{bmatrix},$$

where v_{dq_i} is given in (2.26) and $\hat{v}_{dq_i}$ in (2.31), see Fig. 2.5. For ease of notation, it is convenient to use the following equivalent representation of (2.31)

$$\hat{V}_{qd_i} := \hat{V}_{q_i} + j\hat{V}_{d_i} = (\cos(\delta_i) + j\sin(\delta_i)) V_{qd_i} = e^{j\delta_i} V_{qd_i}, \tag{2.32}$$

where $V_{qd_i} = V_{q_i} + jV_{d_i}$. Equivalently, let

$$\hat{I}_{qd_i} := \hat{I}_{q_i} + j\hat{I}_{d_i} = e^{j\delta_i} I_{qd_i}. \tag{2.33}$$

In the following, (2.32) and (2.33) are used to derive mathematical expressions describing the current and power flows in the network as functions of the voltages V_{qd} given in (2.26) and the angles δ_i, $i \sim \mathcal{N}$, defined in (2.29). To this end, it is convenient to describe the network topology by an undirected graph with set of nodes $\mathcal{N}$, see Section 2.3.5.1. Denote the set of power lines interconnecting the different network nodes $i \in \mathcal{N}$ by $\mathcal{E}$. Associate to each power line $e_l \in \mathcal{E}$ a line current $i_{\ell,abc,l} : \mathbb{R}_{\geq 0} \to \mathbb{R}^3$, $l = 1, \ldots, |\mathcal{E}|$. With Assumption 2.4.18, consider a three-phase symmetric power line $e_l \in \mathcal{E}$ connecting nodes $i \in \mathcal{N}$ and $k \in \mathcal{N}$. Then, each phase of the power line e_l is composed of a constant ohmic resistance $R_l \in \mathbb{R}_{>0}$ in series with a constant inductance $L_l \in \mathbb{R}_{>0}$. Without loss of generality, an arbitrary order is associated to the edges e_l,

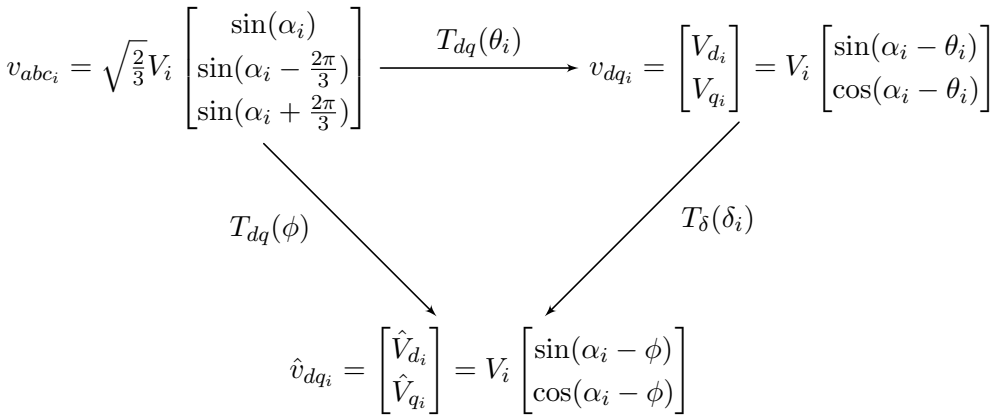

Figure 2.5: Illustration of the different coordinate frames used to derive the model of an electrical network given in (2.44). The signal $v_{abc_i} : \mathbb{R}_{\geq 0} \to \mathbb{R}^3$ denotes the three-phase voltage at the i-th bus with phase angle $\alpha_i : \mathbb{R}_{\geq 0} \to \mathbb{T}$ and amplitude $V_i : \mathbb{R}_{\geq 0} \to \mathbb{R}_{\geq 0}$, $i \sim \mathcal{N}$, see (2.25). The mappings T_{dq} and T_{δ} are given in (2.13), respectively (2.30). The angle $\delta_i : \mathbb{R}_{\geq 0} \to \mathbb{T}$ is defined in (2.29). Note that, by construction, $\mathrm{mod}_{2\pi}(\theta_i - \delta_i) = \mathrm{mod}_{2\pi}(\omega^{\mathrm{com}} t) = \phi$, where the real constant ω^{com} denotes the speed of the common dq-reference frame.

$l = 1, \ldots, |\mathcal{E}|$. Physically, this is equivalent to assigning an arbitrary direction to the line currents $i_{\ell,abc,l}$. By recalling (2.17), defining

$$v_{abc} := \mathrm{col}(v_{abc,i}) \in \mathbb{R}^{3|\mathcal{N}|}, \quad i_{abc} := \mathrm{col}(i_{abc,i}) \in \mathbb{R}^{3|\mathcal{N}|}, \quad i_{\ell,abc} := \mathrm{col}(i_{\ell,abc,l}) \in \mathbb{R}^{3|\mathcal{E}|},$$
$$L := \mathrm{diag}(L_l) \in \mathbb{R}^{|\mathcal{E}|\times|\mathcal{E}|}, \quad R := \mathrm{diag}(R_l) \in \mathbb{R}^{|\mathcal{E}|\times|\mathcal{E}|}$$

and denoting by $\mathcal{B} \in \mathbb{R}^{|\mathcal{N}|\times|\mathcal{E}|}$ the node-edge incidence matrix of the electrical network, the current flows in the network are given by

$$(L \otimes \mathbf{I}_3)\frac{di_{\ell,abc}}{dt} = -(R \otimes \mathbf{I}_3)i_{\ell,abc} + (\mathcal{B}^\top \otimes \mathbf{I}_3)v_{abc}. \tag{2.34}$$

Furthermore, from Kirchhoff's current law [4, Chapter 2]

$$i_{abc} = (\mathcal{B} \otimes \mathbf{I}_3)i_{\ell,abc}, \tag{2.35}$$

i.e., the sum of all currents at each node is zero.

Recall (2.20) and define the nodal voltages v_{abc} and current injections i_{abc}, as well as the network line currents $i_{\ell,abc}$ in common dq-coordinates by $\hat{v}_{dq} \in \mathbb{R}^{2|\mathcal{N}|}$, $\hat{i}_{dq} \in \mathbb{R}^{2|\mathcal{N}|}$, respectively $\hat{i}_{\ell,dq} \in \mathbb{R}^{2|\mathcal{E}|}$. With

$$\mathcal{X} := \mathrm{diag}\left(L_l \omega^{\mathrm{com}} \begin{bmatrix} 0 & -1 \\ 1 & 0 \end{bmatrix}\right) \in \mathbb{R}^{2|\mathcal{E}|\times 2|\mathcal{E}|}, \tag{2.36}$$

(2.34) and (2.35) become in common dq-coordinates

$$\begin{aligned}(L \otimes \mathbf{I}_2)\frac{d\hat{i}_{\ell,dq}}{dt} &= (-(R \otimes \mathbf{I}_2) + \mathcal{X})\,\hat{i}_{\ell,dq} + (\mathcal{B}^\top \otimes \mathbf{I}_2)\hat{v}_{dq},\\ \hat{i}_{dq} &= (\mathcal{B} \otimes \mathbf{I}_2)\hat{i}_{\ell,dq}.\end{aligned} \tag{2.37}$$

Under Assumption 2.4.19, (2.37) reduces to the algebraic relation, see (2.21),

$$\hat{i}_{dq} = (\mathcal{B} \otimes \mathbf{I}_2)\left((R \otimes \mathbf{I}_2) - \mathcal{X}\right)^{-1}(\mathcal{B}^\top \otimes \mathbf{I}_2)\hat{v}_{dq}, \tag{2.38}$$

or, equivalently, by defining $X := \operatorname{diag}(X_l) = \operatorname{diag}(L_l\omega^{\mathrm{com}}) \in \mathbb{R}^{|\mathcal{E}|\times|\mathcal{E}|}$ and using complex notation (see (2.24))

$$\hat{I}_{qd} = \mathcal{B}\,(R + jX)^{-1}\,\mathcal{B}^\top \hat{V}_{qd}. \tag{2.39}$$

Define the admittance matrix of the electrical network by

$$\mathcal{Y} := \mathcal{B}\,(R + jX)^{-1}\,\mathcal{B}^\top \in \mathbb{C}^{|\mathcal{N}|\times|\mathcal{N}|} \tag{2.40}$$

and

$$G_{ii} := \Re(\mathcal{Y}_{ii}), \quad B_{ii} := \Im(\mathcal{Y}_{ii}), \quad Y_{ik} := G_{ik} + jB_{ik} := -\mathcal{Y}_{ik}, \quad i \neq k. \tag{2.41}$$

Moreover, it follows immediately that

$$\mathcal{Y}_{ik} = \begin{cases} 0 & \text{if nodes } i \text{ and } k \text{ are not connected} \\ -(R_l + jX_l)^{-1} & \text{if nodes } i \text{ and } k \text{ are connected by line } l \end{cases} \tag{2.42}$$

and

$$G_{ii} + jB_{ii} = \sum_{l\sim L_i}(R_l + jX_l)^{-1}, \tag{2.43}$$

where L_i denotes the set of edges associated to node i. Inserting (2.32) and (2.33) into (2.39) yields

$$\boxed{I_{qd} = \operatorname{diag}\left(e^{-j\delta_i}\right)\mathcal{Y}\operatorname{diag}\left(e^{j\delta_i}\right)V_{qd}.} \tag{2.44}$$

Recall that V_{qd} and I_{qd} defined in (2.26) and (2.27) are expressed in local dq-coordinates. Hence, (2.44) is the desired relation between currents and voltages in the network. Via straightforward calculations, (2.44) can be written component-wise as

$$\begin{aligned}&I_{qd_i} = I_{q_i} + jI_{d_i},\\ &I_{q_i}(\delta_1,\dots,\delta_n,V_{d_1},\dots,V_{d_n},V_{q_1},\dots,V_{q_n}) = G_{ii}V_{q_i} - B_{ii}V_{d_i}\\ &+\sum_{k\sim\mathcal{N}_i}\left(B_{ik}\cos(\delta_{ik}) - G_{ik}\sin(\delta_{ik})\right)V_{d_k} - \sum_{k\sim\mathcal{N}_i}\left(G_{ik}\cos(\delta_{ik}) + B_{ik}\sin(\delta_{ik})\right)V_{q_k},\\ &I_{d_i}(\delta_1,\dots,\delta_n,V_{d_1},\dots,V_{d_n},V_{q_1},\dots,V_{q_n}) = G_{ii}V_{d_i} + B_{ii}V_{q_i}\\ &-\sum_{k\sim\mathcal{N}_i}\left(G_{ik}\cos(\delta_{ik}) + B_{ik}\sin(\delta_{ik})\right)V_{d_k} - \sum_{k\sim\mathcal{N}_i}\left(B_{ik}\cos(\delta_{ik}) - G_{ik}\sin(\delta_{ik})\right)V_{q_k},\end{aligned} \tag{2.45}$$

$i \sim \mathcal{N}$, where, for ease of notation, angle differences are written as $\delta_{ik} := \delta_i - \delta_k$. Furthermore, the power flows in the network can be derived in a straightforward manner from (2.44), respectively (2.45), as follows. Recall that the instantaneous active and reactive powers P_i and Q_i at the i-th node are given, according to Definition 2.4.12, by

$$\begin{aligned} P_i =& V_{d_i} I_{d_i} + V_{q_i} I_{q_i}, \\ Q_i =& V_{d_i} I_{q_i} - V_{q_i} I_{d_i}. \end{aligned} \tag{2.46}$$

Hence, inserting (2.45) in (2.46) gives

$$\begin{aligned} P_i(\delta_1, \ldots, \delta_n, V_{d_1}, \ldots, V_{d_n}, V_{q_1}, \ldots, V_{q_n}) &= G_{ii}(V_{d_i}^2 + V_{q_i}^2) \\ &- \left(\sum_{k \sim \mathcal{N}_i} G_{ik} \cos(\delta_{ik}) + B_{ik} \sin(\delta_{ik}) \right) (V_{d_k} V_{d_i} + V_{q_k} V_{q_i}) \\ &- \left(\sum_{k \sim \mathcal{N}_i} B_{ik} \cos(\delta_{ik}) - G_{ik} \sin(\delta_{ik}) \right) (V_{q_k} V_{d_i} - V_{d_k} V_{q_i}), \\ Q_i(\delta_1, \ldots, \delta_n, V_{d_1}, \ldots, V_{d_n}, V_{q_1}, \ldots, V_{q_n}) &= -B_{ii}(V_{d_i}^2 + V_{q_i}^2) \\ &+ \left(\sum_{k \sim \mathcal{N}_i} B_{ik} \cos(\delta_{ik}) - G_{ik} \sin(\delta_{ik}) \right) (V_{d_k} V_{d_i} + V_{q_k} V_{q_i}) \\ &- \left(\sum_{k \sim \mathcal{N}_i} G_{ik} \cos(\delta_{ik}) + B_{ik} \sin(\delta_{ik}) \right) (V_{q_k} V_{d_i} - V_{d_k} V_{q_i}), \end{aligned} \tag{2.47}$$

which are the desired power flow equations corresponding to the i-th node.

2.4.4.3 Kron reduction of electrical networks

Consider an electrical network, in which some loads are represented by shunt-admittances, see Fig. 2.4. Denote the set of network nodes by $\mathcal{N}$, the set of nodes with shunt-admittances by $\mathcal{N}_L \subset \mathcal{N}$ and that of all other network nodes by $\mathcal{N}_R := \mathcal{N} \setminus \mathcal{N}_L$. Denote the nodal voltages and currents at nodes $i \sim \mathcal{N}_L$ in common dq-coordinates by

$$\hat{V}_{L,qd} = \mathrm{col}(\hat{V}_{L,qd_i}) \in \mathbb{C}^{|\mathcal{N}_L|}, \quad \hat{I}_{L,qd} = \mathrm{col}(\hat{I}_{L,qd_i}) \in \mathbb{C}^{|\mathcal{N}_L|}.$$

Denote the remaining nodal voltages and currents at nodes $i \sim \mathcal{N}_R$ in common dq-coordinates by $\hat{V}_{R,qd} \in \mathbb{C}^{|\mathcal{N}_R|}$, respectively $\hat{I}_{R,qd} \in \mathbb{C}^{|\mathcal{N}_R|}$. With Assumptions 2.4.18 and 2.4.19, let $\bar{Y}_{ii} = \bar{G}_{ii} + j\bar{B}_{ii} \in \mathbb{C}$ be the shunt-admittance at the i-th node, $i \in \mathcal{N}_L$, and define

$$\bar{\mathcal{Y}} := \mathrm{diag}(\bar{Y}_{ii}) \in \mathbb{C}^{|\mathcal{N}_L| \times |\mathcal{N}_L|}. \tag{2.48}$$

Then, the following relation holds (in "Generator convention", see Section 2.4.3)

$$\hat{I}_{L,qd} = -\bar{\mathcal{Y}}\hat{V}_{L,qd}.$$

Recall the electric admittance matrix $\mathcal{Y} \in \mathbb{C}^{|\mathcal{N}|\times|\mathcal{N}|}$ defined in (2.40). Partition $\mathcal{Y}$ in accordance to the sets $\mathcal{N}_L$ and $\mathcal{N}_R$, i.e.,

$$\begin{bmatrix} \hat{I}_{R,qd} \\ \hat{I}_{L,qd} \end{bmatrix} = \begin{bmatrix} \hat{I}_{R,qd} \\ -\bar{\mathcal{Y}}\hat{V}_{L,qd} \end{bmatrix} = \begin{bmatrix} \mathcal{Y}_{\mathcal{N}_R\mathcal{N}_R} & \mathcal{Y}_{\mathcal{N}_R\mathcal{N}_L} \\ \mathcal{Y}_{\mathcal{N}_R\mathcal{N}_L}^\top & \mathcal{Y}_{\mathcal{N}_L\mathcal{N}_L} \end{bmatrix} \begin{bmatrix} \hat{V}_{R,qd} \\ \hat{V}_{L,qd} \end{bmatrix}. \tag{2.49}$$

Suppose that $\mathcal{Y}_{\mathcal{N}_L\mathcal{N}_L} + \bar{\mathcal{Y}}$ is nonsingular. This assumption holds for most electrical networks [175]. In particular, the lemma below shows that this assumption holds for all networks with RL power lines (i.e., the class of networks considered in this work), which are connected in a graph-theoretical sense, see Section 2.3.5.1.

Lemma 2.4.20. *Let $\mathcal{Y} \in \mathbb{C}^{n\times n}$ be the admittance matrix of an electrical network satisfying Assumption 2.4.18. Let $\mathcal{Y}$ be partitioned as in* (2.49) *and $\bar{\mathcal{Y}}$ be given by* (2.48)*. Suppose that the network is connected. Then, $\mathcal{Y}_{\mathcal{N}_L\mathcal{N}_L} + \bar{\mathcal{Y}}$ is nonsingular.*

Proof. Recall the definition of $\mathcal{Y}$ in (2.40). With Assumption 2.4.18, all lines are composed of RL elements. Therefore, (2.41) - (2.43) together with the fact that the network is connected by assumption imply that (see (2.40))

$$\Re(\mathcal{Y}_{ii}) = -\sum_{k\sim\mathcal{N}} \Re(\mathcal{Y}_{ik}) > 0, \quad i \sim \mathcal{N},$$

that

$$x^\top (\mathcal{Y} + \mathcal{Y}^*)\, x > 0, \quad \forall x \in \mathbb{R}^n \setminus \{\gamma \underline{1}_n\}, \quad \gamma \in \mathbb{R}, \tag{2.50}$$

and that $\mathcal{Y}_{\mathcal{N}_R\mathcal{N}_L} \neq \mathbf{0}_{\mathcal{N}_R\times\mathcal{N}_L}$. Consequently,

$$\Re(\mathcal{Y}_{ii}) \geq -\sum_{k\sim\mathcal{N}_L} \Re(\mathcal{Y}_{ik}), \quad i \sim \mathcal{N}_L,$$

with strict inequality for at least one $i \in \mathcal{N}_L$. This, together with (2.50), implies that

$$x^\top \left(\mathcal{Y}_{\mathcal{N}_L\mathcal{N}_L} + \mathcal{Y}^*_{\mathcal{N}_L\mathcal{N}_L}\right) x > 0, \quad \forall x \in \mathbb{R}^{\mathcal{N}_L} \setminus \{\underline{0}_{\mathcal{N}_L}\}.$$

It is straightforward to see that

$$x^\top \left(\bar{\mathcal{Y}} + \bar{\mathcal{Y}}^*\right) x \geq 0, \quad \forall x \in \mathbb{R}^{\mathcal{N}_L} \setminus \{\underline{0}_{\mathcal{N}_L}\}.$$

Thus,

$$x^\top \left(\left(\mathcal{Y}_{\mathcal{N}_L\mathcal{N}_L} + \bar{\mathcal{Y}}\right) + \left(\mathcal{Y}_{\mathcal{N}_L\mathcal{N}_L} + \bar{\mathcal{Y}}\right)^*\right) x > 0, \quad x \in \mathbb{R}^{\mathcal{N}_L} \setminus \{\underline{0}_{\mathcal{N}_L}\},$$

and, by the properties of the numerical range of a matrix, see Section 2.3.6,

$$\Re\left(\sigma\left(\mathcal{Y}_{\mathcal{N}_L\mathcal{N}_L} + \bar{\mathcal{Y}}\right)\right) \subset \mathbb{R}_{>0},$$

completing the proof. □

For $\mathcal{Y}_{\mathcal{N}_L\mathcal{N}_L} + \bar{\mathcal{Y}}$ being nonsingular, solving the second row of (2.49) for $\hat{I}_{L,qd}$ and inserting the result in the first row of (2.49), yields

$$\hat{I}_{R,qd} = \left(\mathcal{Y}_{\mathcal{N}_R\mathcal{N}_R} - \mathcal{Y}_{\mathcal{N}_R\mathcal{N}_L}\left(\mathcal{Y}_{\mathcal{N}_L\mathcal{N}_L} + \bar{\mathcal{Y}}\right)^{-1}\mathcal{Y}_{\mathcal{N}_R\mathcal{N}_L}^{\top}\right)\hat{V}_{R,qd} := \mathcal{Y}_{\mathcal{R}}\hat{V}_{R,qd}.$$

This network reduction is called Kron reduction [1, 176] and $\mathcal{Y}_{\mathcal{R}}$ is the admittance matrix of the Kron-reduced network. Kron reduction is frequently used in power system analysis, since it allows to equivalently represent a system of differential-algebraic equations (DAEs) as a set of pure ODEs. For this purpose, the Kron reduction is also employed in the present work.

2.4.5 Stability in power systems and microgrids

The notions of stability used within the power systems community often differ significantly from those in the control systems community presented in Section 2.3.2. Moreover, even within the power systems community different types and notions of stability are used incoherently [39]. Therefore, the problem of stability definition and classification in power systems has been adressed in [39]. In accordance with [39], the following definition of power system stability is employed in this work.

Definition 2.4.21. *[39] Power system stability is the ability of an electric power system, for a given initial operating condition, to regain a state of operating equilibrium after being subjected to a physical disturbance, with most system variables bounded so that practically the entire system remains intact.*

With respect to the control theoretic definition of stability given in Definition 2.3.1, Definition 2.4.21 is to be understood as follows [39]. Consider a power system and suppose that it is subjected to a physical disturbance. Examples for typical disturbances in a power system are load changes, loss of generation units or short circuits. The system's response to the disturbance may include the disconnection of some system components from the system (e.g., by protection relays). Hence, the system topology after the disturbance may not be identical to that before the disturbance. If after the disturbance has occured, almost all system components remain connected with their corresponding variables being bounded and the power system reaches a—typically new—operating equilibrium[1], then the power system is said to be stable. Thus, Definition 2.4.21 is

[1]Often, the qualifiers prefault, fault and postfault are used to refer to a power system before, during and after a fault [6]. Faults (e.g., a short circuit or a line tripping) are a particular class of disturbances in power systems.

consistent with the definition of asymptotic stability given in Definition 2.3.1, in that the new equilibrium point (if it exists) is required to be asymptotically stable in the sense of Definition 2.3.1. In the remainder of this work a generic microgrid is said to be stable if it satisfies Definition 2.4.21.

Due to the high complexity and nonlinearity of power systems, it is in general convenient to further classify different types of instability that a power system may undergo as a consequence of different types of disturbances. The following definitions of frequency, rotor angle and voltage stability are used in this work.

Definition 2.4.22. *[39] Frequency stability refers to the ability of a power system to regain a steady frequency following a severe system upset resulting in significant imbalance between generation and load.*

Definition 2.4.23. *[39] Rotor angle stability refers to the ability of synchronous machines of an interconnected power system to regain synchronism after being subjected to a disturbance.*

Definition 2.4.24. *[39] Voltage stability is the ability of a power system to regain steady voltages at all buses in the system after being subjected to a disturbance from a given initial operating point.*

It is important to stress that the given definitions are usually made in order to facilitate the stability analysis of power systems by reducing the complexity of the problem [39]. However, the different types of defined stability are not necessarily independent from each other. It is therefore fundamental to consider different types of stability, when assessing the overall system stability [39].

A detailed review of further classifications of power system stability is given in [39]. However, many of the classifications therein are tailored to large HV power systems operated with SGs and may therefore not apply directly to MDREGs or purely inverter-based microgrids. For this reason, no further classification of different types of microgrid stability is pursued here.

2.5 Summary

In this chapter basic notation used throughout this work has been introduced. Furthermore, relevant background information on the employed mathematical notions and tools has been provided. More precisely, the given overview has comprised stability for dynamical systems, as well as graph theory, consensus protocols, the numerical range of

a matrix and an extension of the Routh-Hurwitz criterion for polynomials with complex coefficients.

In addition, main characteristis of three-phase AC power systems together with a standard definition of instantaneous power and a standard algebraic network model describing the current and power flows among different nodes in a power network have been presented. The chapter has been concluded with a definition of stability of power systems, which is consistent with the usual definition of asymptotic stability in control theory.

3

Problem statement

3.1 Introduction

As discussed in Chapter 1, the increasing penetration of renewable DG units leads to significant changes in the generation structure of power systems. To successfully address these structural changes and the resulting challenges, new operation strategies are needed [21]. In this chapter, the microgrid concept is introduced as one approach to address these issues and facilitate the integration of renewable DG units into the electrical grid. Furthermore, the potentials and key features of microgrids are highlighted.

In addition, three key challenges arising in microgrids are introduced in detail. These are frequency stability, voltage stability and power sharing. In particular, it is shown that the problem of power sharing can be formulated as an agreement problem. Furthermore, the separation of the control tasks in a microgrid into several control layers is motivated. The most common hierarchical control scheme for microgrids is discussed and related to the hierarchical control scheme in conventional power systems. Finally, the aforementioned main problems addressed in this work are classified within the presented control hierarchy.

The remainder of this chapter is structured as follows. Based on [126], the microgrid concept is presented in Section 3.2. Three fundamental challenges in microgrids, to which this work is devoted to, are introduced in Section 3.3. The chapter is concluded in Section 3.4 with a brief review of the predominant hierarchical control scheme for microgrids available in the literature.

3.2 The microgrid concept

3.2.1 Definition of a microgrid

Microgrids have attracted a wide interest in different research and application communities over the last decade [23, 28, 34]. However, the term "microgrid" is not uniformly defined in the literature [4, 21, 22, 23, 24, 177]. Based on [21, 23], the following definition of an AC microgrid is employed in this work.

Definition 3.2.1. *An AC electrical network is said to be an AC microgrid if it satisfies the following conditions.*

1. *It is a connected subset of the LV or MV distribution system of an AC electrical power system.*
2. *It possesses a single point of connection to the remaining electrical power system. This point of connection is called point of common coupling (PCC).*
3. *It gathers a combination of generation units, loads and energy storage elements.*
4. *It possesses enough generation and storage capacity to supply most of its loads autonomously during at least some period of time.*
5. *It can be operated either connected to the remaining electrical network or as an independent island network. The first operation mode is called grid-connected mode and the second operation mode is called islanded, stand-alone or autonomous mode.*
6. *In grid-connected mode, it behaves as a single controllable generator or load from the viewpoint of the remaining electrical system.*
7. *In islanded mode, frequency, voltage and power can be actively controlled within the microgrid.*

According to Definition 3.2.1, the main components in a microgrid are DG units, loads and energy storage elements. Typical DG units in microgrids are renewable DG units, such as photovoltaic (PV) units, wind turbines, fuel cells (FCs), as well as microturbines or reciprocating engines in combination with SGs. The latter two can either be powered with biofuels or fossil fuels [4, 178]. Some DG units may also be operated as combined heat and power (CHP) plants allowing to recover part of the waste heat generated in the combustion process [4].

Typical loads in a microgrid are residential, commercial and industrial loads [22, 24, 178]. It is also foreseen to categorize the loads in a microgrid with respect to their priorities, e.g., critical and non-critical loads. This enables load shedding as a possible operation option in islanded-mode [22, 178].

Finally, storage elements play a key-role in microgrid operation [4, 178]. They are especially useful in balancing the power fluctuations of intermittent renewable sources and, hence, to contribute to network control. Possible storage elements are, e.g., batteries, flywheels or supercapacitors. The combination of renewable DGs and storage elements is also an important assumption for the inverter models used in this work, see Section 4.2.

Most of the named DG and storage units are either DC sources (PV, FC, batteries) or are often operated at variable or high-speed frequency (wind turbines, microturbines, flywheels). Therefore, they have to be connected to an AC network via AC or DC-AC inverters [15, 21]. For ease of notation, such devices are simply called "inverters" in the following. An illustration of an exemplary microgrid is given in Fig. 3.1.

Given the early stage of research and development on control concepts for microgrids, to the best of the author's knowledge, worldwide no commercial microgrid with large amount of renewable DG exists up to date. However, there are several test-sites and experimental microgrids around the globe, see, e.g., the survey papers [23, 178, 179, 180].

Remark 3.2.2. While not comprised in Definition 3.2.1, true island power systems are sometimes also called microgrids in the literature [23]. This can be justified by the fact that islanded power systems operating with a large share of renewable energy sources face similar technical challenges as microgrids. Nevertheless, an island power system differs from a microgrid in that it can not be frequently connected to and disconnected from a larger electrical network [21].

Remark 3.2.3. Microgrids can also be implemented as DC systems [181, 182, 183]. Definition 3.2.1 can easily be adapted to this scenario by removing the property "frequency control" in item 7. Recent reviews of the main differences and challenges for AC and DC microgrids are given, e.g., in [180, 184, 185].

3.2.2 Microgrid characteristics and challenges

Microgrids represent a promising solution to facilitate the local integration of DG units into the electrical grid [18, 22, 23, 24]. The following three points are among the main motivating facts for the need of such concepts.

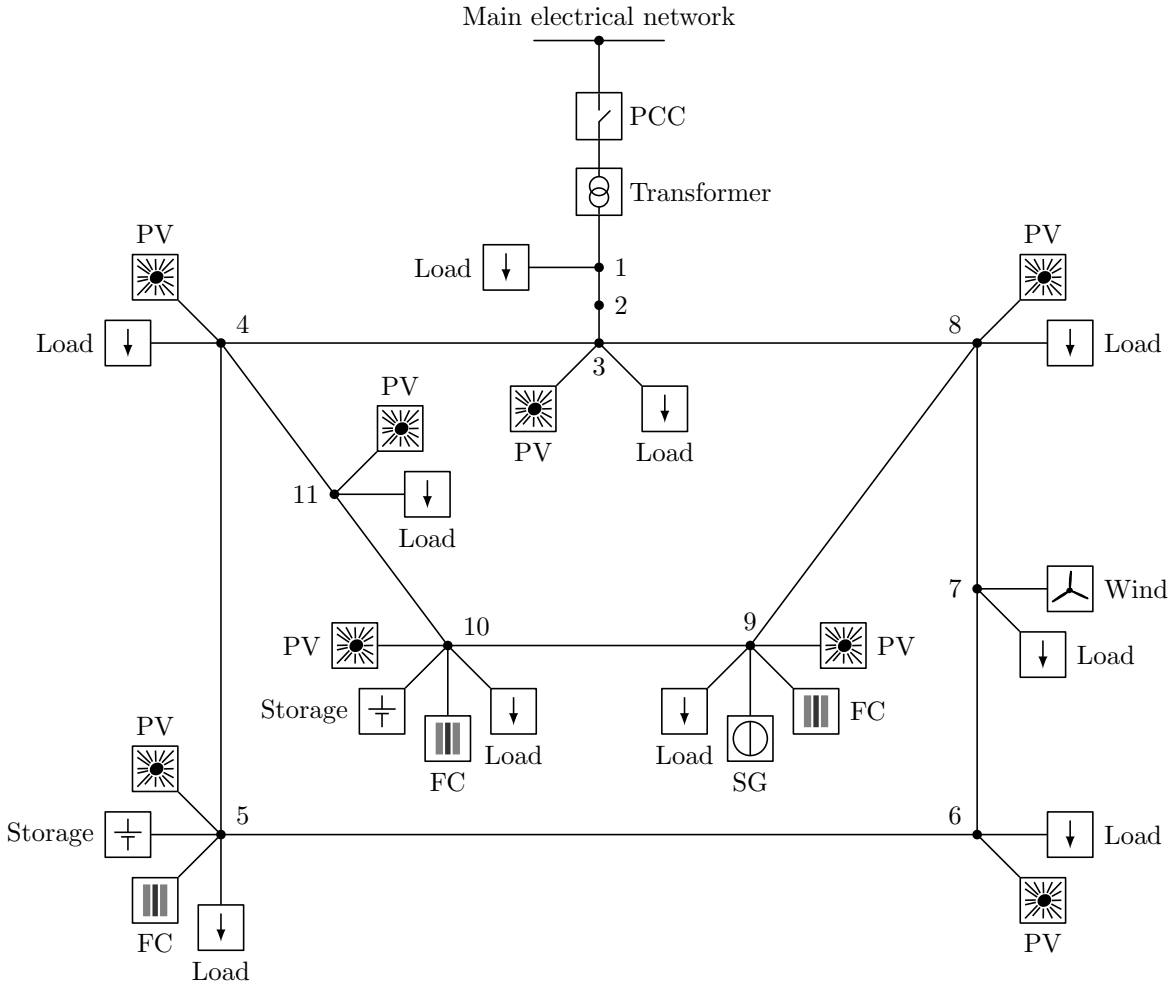

Figure 3.1: Schematic representation of a microgrid. The microgrid is composed of several DG units, loads and storage devices. The DG units are inverter-interfaced photovoltaic (PV), fuel cell (FC) and wind power plants. In addition, a power generation unit is connected to the network via a synchronous generator (SG). The point of connection of the microgrid to the main network is denoted by point of common coupling (PCC).

(i) The penetration of renewable energy sources into the electrical networks is increasing worldwide. This process is motivated by political, environmental, economic and technological aspects [7, 18].

(ii) Most renewable sources are intermittent small-scale DG units connected at the LV and MV levels, while conventional power plants are mostly located at the HV level [21, 23, 24].

(iii) A large portion of these DG units are connected to the network via inverters. The physical characteristics of inverters largely differ from the characteristics of conventional electrical generators, i.e., SGs [21, 24].

These facts have the following implications for power system control and operation.

(i) The power generation structure is moving from large, centralized plants to a mixed generation pool consisting of conventional large plants and smaller DG units.

(ii) Several DG units are required to replace one large conventional power plant. Hence, the number of generation units in the power system increases.

(iii) Especially, the number of generation units present in the network at LV and MV level increases drastically.

(iv) With increasing penetration of inverter-based sources accompanied by a reduction of conventional power plants, ancillary services [186], such as frequency and voltage control, have to be provided, at least partially, by inverter-interfaced sources.

(v) The control and operation strategies have to take into account the physical characteristics of inverters, as well as the intermittency of many renewable sources.

In summary, with higher penetration of renewable sources, the power generation structure becomes far more complex and the dynamics of the generation units change. Additionally, power generation becomes more uncertain and takes increasingly place at the LV and MV levels. Hence, new solutions and strategies to operate the electric power system that ensure a reliable and stable operation by taking into account the characteristics of renewable inverter-interfaced DG units are needed [21].

In this context, the microgrid concept has been identified as a key component in future electrical networks [4, 18, 19]. As detailed in Definition 3.2.1, a microgrid is a cluster of a larger electrical network. The main operation strategy for a microgrid is as follows [22, 23]. During normal operating conditions, the microgrid is connected in parallel to the remaining electrical power system. In the case of a disturbance, e.g., a short circuit or an outage of a large generation unit, the microgrid disconnects from the rest of the electrical power system and keeps operating in islanded-mode. Whenever

the disturbance is cleared, the microgrid may be reconnected to the main network. In addition, the microgrid can also be disconnected if the power quality[1] in the main grid falls below certain thresholds. This process is called intentional disconnection or islanding.

Hence, the microgrid concept offers various features to contribute to a successful integration of a large share of inverter-based DG units into the electrical network. Some of the key properties of microgrids in this context are listed below [4, 18, 23, 24, 25].

(i) Power quality is increased, e.g., by locally controlling the frequency and voltage in the microgrid or by intentional islanding.

(ii) The control burden on the higher voltage levels can be reduced by performing control actions already locally.

(iii) Local power balancing reduces network losses.

(iv) Clustering a large electrical network into several microgrids reduces the complexity of the individual systems in consideration. This simplifies control and operation tasks.

(v) In grid-connected mode, different microgrids forming an electrical network are coupled with each other. Then, as illustrated in Fig. 3.2, each microgrid represents a single entity from the point of view of all other microgrids in the network. This simplifies the coordination of several interconnected microgrids within one electrical network.

In order for microgrids to be able to reliably and safely provide the aforementioned services, several technical, economic and regulatory challenges have to be met [4, 18, 21, 22, 23, 24, 38]. Given the technical character of this thesis, the listing of challenges presented next is limited to technical aspects. For further information on market and regulatory challenges, the reader is referrred to, e.g., [4, 24, 38]. Among the most relevant technical tasks to be considered are:

(i) Frequency stability;

(ii) Voltage stability;

(iii) Desired power sharing in steady-state;

(iv) Operational compatibility of inverter-interfaced and SG-interfaced units;

(v) Seamless switching from grid-connected to islanded-mode and vice-versa;

[1] Power quality is a measure for the fitness of electrical power delivered to consumers. It comprises the following criteria: continuity of service, variation in voltage magnitude, frequency stability, unbalances and harmonic content [187].

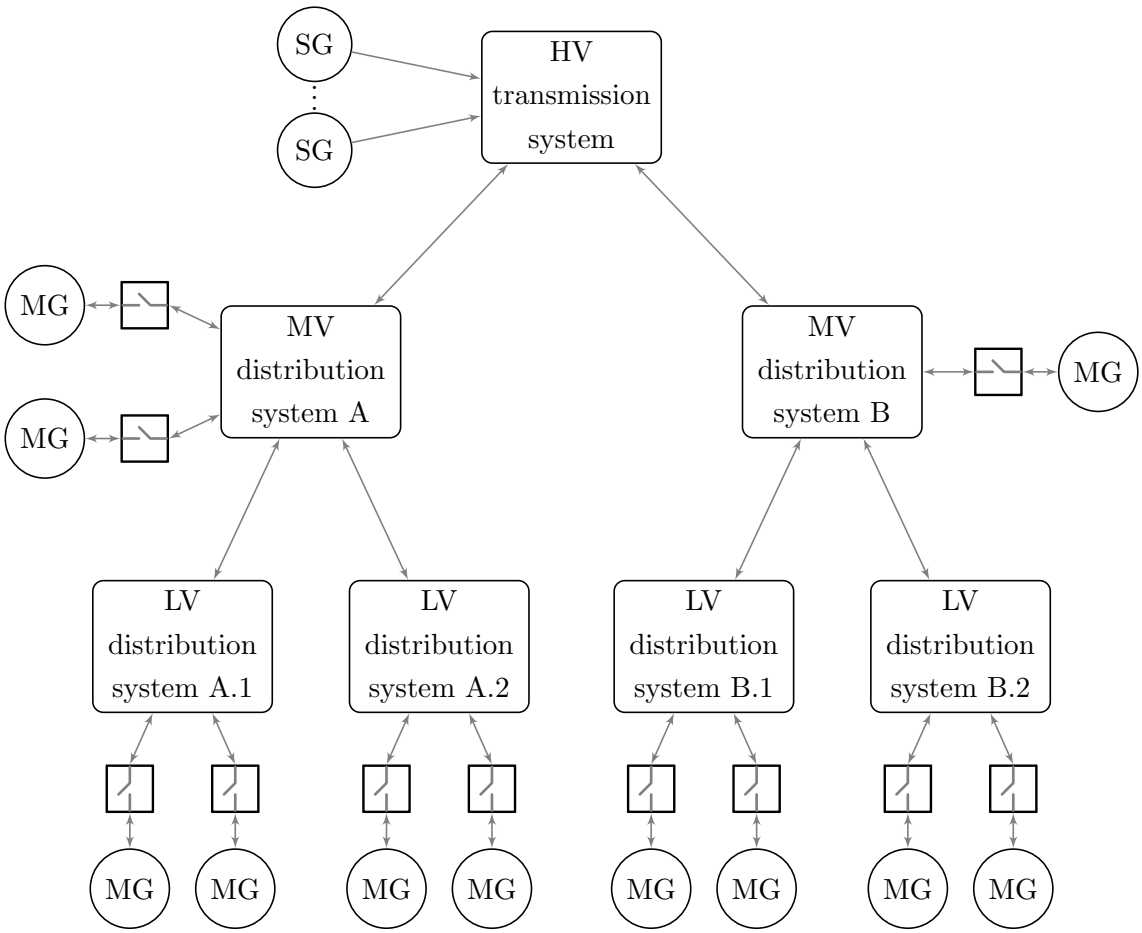

Figure 3.2: Example of an electrical network composed of several interconnected microgrids (MGs). Large units, such as, e.g., hydro power plants or pump storage plants, may be connected at the HV level and are represented by synchronous generators (SGs). Note that by Definition 3.2.1, the switch between a microgrid and the main grid is defined as part of a microgrid. Nevertheless, the switches are shown explicitly in the above illustration to emphasize their role in a coupled network of interconnected microgrids. In grid-connected operation, the switch at each microgrid is closed. Then, each microgrid is seen as a single load or generator from all other microgrids. In case of a severe disturbance in the network, each microgrid can disconnect itself from the main network and operate in stand-alone mode.

(vi) Protection systems and provision of short-circuit current by inverter-interfaced sources;

(vii) Robustness with respect to uncertainties;

(viii) Optimal dispatch.

In this work, the challenges *(i)*-*(iii)* are addressed, while also taking challenge *(iv)* into account. These problems together with their practical relevance are detailed in the next section.

3.3 Stability and power sharing

As mentioned above, three key problems in microgrids to which this thesis is devoted to are introduced and motivated in detail in this section. More precisely, the addressed problems are *(i)* frequency stability, *(ii)* voltage stability and *(iii)* power sharing. The presentation of these problems is based on [1, 3, 39, 71, 122].

3.3.1 Frequency and voltage stability

In conventional power systems, power generation sources are connected to the network via SGs. The main task of SGs in AC electrical networks is to transform rotational mechanical energy into electrical energy. This energy conversion process is achieved via electromagnetic induction, i.e., the rotation of the magnetic field of the rotor (driven by a mechanical input) induces a three-phase voltage within the stator winding.

As a consequence, SGs provide an AC voltage at their terminals. Recall from Section 2.4.1, that a symmetric three-phase voltage can be described completely by two variables: its angle and its amplitude. If an SG is operated in such way that it actively sets the values of the frequency, i.e., the time-derivative of the angle, and the amplitude of the voltage at its terminals, then the SG is said to be operated as a grid-forming unit [81]. Alternatively, an SG can also be controlled in such way that it injects a prespecified amount of active and reactive power into the network. An SG operated in such way is called a grid-feeding or PQ unit [35, 81].

Grid-forming units are essential components in power systems. They have the task to provide a synchronous frequency and a certain voltage level at all buses in the network, i.e., to provide a stable operating point. Analyzing under which conditions such an operating point can be provided and maintained, naturally leads to the problems of frequency and voltage stability, see Definitions 2.4.22 and 2.4.24.

If all SGs in an AC electrical network rotate at the same speed, then the network is said to be synchronized. If the network is synchronized, then the rotor field and the field at the machine terminal of each SG in the network rotate at the same speed with a constant phase difference between both fields. The angle describing this phase difference is usually called rotor angle or power-angle in the literature [1, 3, 39]. Clearly, if the network is synchronized, then the rotor angle of each SG in the network is constant.

Therefore, in AC electrical networks with conventional power generation units, the problem of rotor angle stability [39] is of great relevance, see Definition 2.4.23. The problem of rotor angle stability after a large disturbance in the network is often called the problem of transient stability [39].

Note moreover that it is usually not desired that the voltages at all terminals synchronize to exactly the same three-phase signal. On the contrary, it is desired that all terminal voltages synchronize to a common frequency, but exhibiting phase differences between each other. Manipulation of these phase differences, e.g., via a suitable control, allows to shape the power flows in the network, cf. (2.47).

As discussed previously, in microgrids a large number of renewable DG units are typically interfaced to the network via inverters and only a small amount, if any, of generation sources is connected to the network via SGs. Therefore, in microgrids grid-forming capabilities have often also to be provided by inverter-interfaced sources [24, 35].

Given the different physical characteristics of inverters in comparison to SGs, new control concepts for microgrids guaranteeing (under certain conditions) a stable operating point are needed. These concepts have to be compatible to the operation of SGs and, since the microgrid has to be able to operate in grid-connected mode, also to the operation of larger electrical networks.

In addition, in grid-connected mode, control actions and power demand in the microgrid can be supported by the main grid. However, in islanded-operation mode, all control capabilities have to be provided by units within the microgrid. Moreover, in islanded power systems, any kind of disturbance causing a substantial change of load or generation can affect frequency stability [39, 188]. Hence, the problems of frequency and voltage stability become especially crucial in microgrids operated in islanded-mode. Therefore, the stability analysis carried out in this thesis focuses on microgrids in islanded-mode.

3.3.2 Power sharing

Besides frequency and voltage stability, power sharing is an important performance criterion in the operation of microgrids [21, 24, 35, 81]. Here, power sharing is understood as the ability of the local controls of the individual generation sources to achieve a desired steady-state distribution of the power outputs of all generation sources *relative* to each other, while satisfying the load demand in the network. The relevance of this control objective lies within the fact that it allows to prespecify the utilization of the generation units in operation, e.g., to prevent overloading [24]. In addition, thereby high-circulating currents in the network can be avoided [38].

The concept of proportional power sharing is formalized via the following definition.

Definition 3.3.1. *Consider an AC electrical network, e.g., an AC microgrid. Denote its set of nodes by* $\mathcal{N} = \{1, 2, \dots, n\}$, $n \in \mathbb{N}$. *Consider two units connected at nodes* $i \in \mathcal{N}$, *respectively* $k \in \mathcal{N}$. *Let* γ_l *and* χ_l *denote constant positive real weighting factors and* P_l^s, *respectively* Q_l^s, *the steady-state active, respectively reactive, power flow,* $l \in \{i, k\}$. *Then, the units at nodes* i *and* k *are said to share their active, respectively reactive, powers proportionally according to* γ_i *and* γ_k, *respectively* χ_i *and* χ_k, *if*

$$\frac{P_i^s}{\gamma_i} = \frac{P_k^s}{\gamma_k}, \quad \textit{respectively} \quad \frac{Q_i^s}{\chi_i} = \frac{Q_k^s}{\chi_k}.$$

Remark 3.3.2. A practical choice for γ_i and χ_i would, for example, be $\gamma_i = \chi_i = S_i^N$, where $S_i^N \in \mathbb{R}_{>0}$ is the nominal power rating of the DG unit at node $i \in \mathcal{N}$.

The problems of active and reactive power sharing can be formalized as follows.

Problem 3.3.3. *Consider an AC electrical network, e.g., an AC microgrid, and denote its set of nodes by* $\mathcal{N} = \{1, 2, \dots, n\}$, $n \in \mathbb{N}$. *Let the associated vectors of phase angles and voltages be given by* $\delta \in \mathbb{T}^n$, *respectively* $V_{qd} \in \mathbb{C}^n$, *cf.* (2.28). *Let* $\mathcal{N}_G \subseteq \mathcal{N}$ *denote a set of nodes, such that at each node* $i \in \mathcal{N}_G$ *a generation and/or storage unit is connected. Recall from* (2.47) *that* $P_i(\delta, V_{qd})$ *denotes the active power flow associated to the* i*-th unit,* $i \in \mathcal{N}_G$. *Furthermore, let* $P_G = col(P_i) \in \mathbb{R}^{|\mathcal{N}_G|}$, $i \sim \mathcal{N}_G$. *Associate to each unit a positive real weighting coefficient* γ_i, $i \sim \mathcal{N}_G$. *Let* $U = diag(1/\gamma_i)$. *The problem of active power sharing is said to be solved for the* $|\mathcal{N}_G|$ *units if and only if* $P_G(\delta, V_{qd})$ *is bounded and*

$$\lim_{t \to \infty} U P_G(\delta, V_{qd}) = \upsilon \underline{1}_{|\mathcal{N}_G|}, \tag{3.1}$$

with real constant υ.

Problem 3.3.4. *Consider an AC electrical network, e.g., an AC microgrid, and denote its set of nodes by* $\mathcal{N} = \{1, 2, \ldots, n\}$, $n \in \mathbb{N}$. *Let the associated vectors of phase angles and voltages be given by* $\delta \in \mathbb{T}^n$, *respectively* $V_{qd} \in \mathbb{C}^n$, *cf.* (2.28). *Let* $\mathcal{N}_G \subseteq \mathcal{N}$ *denote a set of nodes, such that at each node* $i \in \mathcal{N}_G$ *a generation and/or storage unit is connected. Recall from* (2.47) *that* $Q_i(\delta, V_{qd})$ *denotes the reactive power flow associated to the i-th unit,* $i \in \mathcal{N}_G$. *Furthermore, let* $Q_G = col(Q_i) \in \mathbb{R}^{|\mathcal{N}_G|}$, $i \sim \mathcal{N}_G$. *Associate to each unit a positive real weighting coefficient* χ_i, $i \sim \mathcal{N}_G$. *Let* $D = diag(1/\chi_i)$. *The problem of reactive power sharing is said to be solved for the* $|\mathcal{N}_G|$ *units if and only if* $Q_G(\delta, V_{qd})$ *is bounded and*

$$\lim_{t\to\infty} DQ_G(\delta, V_{qd}) = \beta \underline{1}_{|\mathcal{N}_G|}, \tag{3.2}$$

with real constant β.

Combining Problems 3.3.3 and 3.3.4, yields the power sharing problem.

Problem 3.3.5. *Consider an AC electrical network, e.g., an AC microgrid, and denote its set of nodes by* $\mathcal{N} = \{1, 2, \ldots, n\}$, $n \in \mathbb{N}$. *Let* $\mathcal{N}_G \subseteq \mathcal{N}$ *denote a set of nodes, such that at each node* $i \in \mathcal{N}_G$ *a generation and/or storage unit is connected. The problem of power sharing is said to be solved if and only if the Problems 3.3.3 and 3.3.4 are solved jointly for the* $|\mathcal{N}_G|$ *units.*

Suppose δ and V_{qd} are states (or outputs) of agents—each represented by a dynamical system—connected at the nodes of the considered network. In a microgrid, agents typically represent DG units (or loads). It then follows from the formulation of Problem 3.3.5, that the problem of power sharing is an agreement problem, see Section 2.3.5.

Two important aspects, when considering the practical interest of power sharing are: *(i)* the power losses over a power line are given by $Ri^\top i$, where $i : \mathbb{R}_{\geq 0} \to \mathbb{R}^3$ is the current flowing on the line and $R \in \mathbb{R}_{>0}$ is the resistance of the line; *(ii)* the larger the line impedance is, the larger the voltage difference at two connected buses has to be in order to have a significant effect on the power flows.

Because of *(i)*, power sharing is only a relevant control objective in networks with relatively small resistances between the different nodes in the network, since with increasing line resistances the power losses also increase. To illustrate the second claim, consider a dominantly inductive power line with admittance $Y_{ik} \in \mathbb{C}$ connecting two nodes $i \in \mathcal{N}$ and $k \in \mathcal{N}$. Let the voltage amplitudes and phase angles at these nodes be given by $V_{qd_i} = V_{q_i} + j0 : \mathbb{R}_{\geq 0} \to \mathbb{R}_{\geq 0}$ and $\delta_i : \mathbb{R}_{\geq 0} \to \mathbb{T}$, respectively $V_{qd_k} = V_{q_k} + j0 : \mathbb{R}_{\geq 0} \to \mathbb{R}_{\geq 0}$ and $\delta_k : \mathbb{R}_{\geq 0} \to \mathbb{T}$, cf. Section 2.4.4. Suppose the phase

angle difference is small, i.e., $\|\delta_i - \delta_k\| < \epsilon$ for some small real constant ϵ. Then, with $\delta_{ik} = \delta_i - \delta_k$, the following approximations can be made

$$Y_{ik} = G_{ik} + jB_{ik} \approx jB_{ik}, \quad \sin(\delta_{ik}) \approx \delta_{ik}, \quad \cos(\delta_{ik}) \approx 1 \tag{3.3}$$

and the active and reactive power flows given in (2.47) between nodes i and k simplify to

$$\begin{aligned} P_{ik} &= -B_{ik}V_{q_i}V_{q_k}\delta_{ik}, \\ Q_{ik} &= -B_{ik}V_{q_i}^2 + B_{ik}V_{q_i}V_{q_k} = -B_{ik}V_{q_i}(V_{q_i} - V_{q_k}). \end{aligned} \tag{3.4}$$

Moreover, the voltage amplitudes are usually required to remain within a certain range—typically $0.9 < |V_{q_i}| < 1.1$ pu and $0.9 < |V_{q_k}| < 1.1$ pu for normalized voltage amplitudes, see, e.g., [189]. Hence, the active power flow P_{ik} is mainly influenced by the phase angle difference δ_{ik} and the reactive power flow Q_{ik} by the voltage difference $V_{q_i} - V_{q_k}$.

In HV transmission systems, typically the power lines are dominantly inductive and relatively long. Hence, the resistance between generation units is relatively small and the inductance is rather large, i.e., $|B_{ik}| \ll 1$. In that case, it follows from (3.4) that a significant voltage difference $V_{q_i} - V_{q_k}$ is required in order to obtain a significant change in the reactive power flow. Thus, the criterion $0.9 < |V_{q_i}| < 1.1$ pu may be violated and controlling the reactive power flow by manipulation of the voltage difference $V_{q_i} - V_{q_k}$ is not feasible. Therefore, in transmission systems usually only active power sharing is a desired control objective, while reactive power sharing is not a feasible target. A similar reasoning can be made for active power sharing in dominantly resistive networks with large resistances, e.g., by inspection of the power flow equations (2.47) for such a scenario.

In microgrids, however, the electrical distance between units is typically small. Consequently, active and reactive power sharing are, in general, relevant control objectives [21, 24, 35, 81]. Close electrical proximity usually implies close geographical distance between the different units, which facilitates the practical implementation of a distributed communication network. This fact is explored in Section 5.3, where a consensus-based DVC for reactive power sharing in microgrids with dominantly inductive power lines is proposed based on [122, 125].

3.4 Control hierarchies in microgrids

Given the complexity, for example, in terms of the number of network components, time-scales of dynamics and operational goals in microgrids, an evident approach is to separate the individual control tasks into several hierarchical control levels. This is also the standard approach in the control of conventional power systems. Since the available hierarchical control concepts for microgrids are strongly inspired by those of conventional power systems, the hierarchical control architecture of the latter is briefly reviewed.

In conventional power systems, the set of controls the main task of which is to achieve rotor angle and frequency stability is called frequency control. Frequency control is typically divided into several control hierarchies and performed at the HV level by SGs. The frequency control hierarchies presented next are based on the current grid-code of the European Network of Transmission System Operators for Electricity (ENTSO-E) [190].

- Primary control (also: droop control). Decentralized proportional control aiming at frequency stabilization and achievement of an active power balance.
- Secondary control. Distributed communication-based control with integral behavior to eliminate stationary frequency deviations, as well as power flow imbalances between the different control areas.
- Minute reserve/tertiary control. Replacement of secondary control in the event of a long-standing power imbalance.

Note that, depending on the grid code of the respective network operator, the minute reserve/tertiary control level is not always considered part of the frequency control hierarchy, see, e.g., [4, 6]. In addition, the term "tertiary control" is sometimes used in the literature to denote the economic dispatch problem, see, e.g., [6, 66].

Voltage control is typically carried out by taking local control actions—on the HV level by adjusting the excitation voltage of the SGs; on the MV and LV level by means of transformers or compensation devices [1].

Inspired by the hierarchical control layers for conventional power systems, there is ongoing effort on establishing a similar hierarchical control architecture in microgrids [35, 38, 180, 191, 192]. It is worth noting that a definition of a control hierarchy for a microgrid is not necessary for the present work, since the considered problems of

frequency and voltage stability, as well as the achievement of a desired power balance are usually associated with primary control tasks [38, 180, 191, 192]. Nevertheless, a classification suggested by the authors of [38, 120, 191, 192] is given in the following for the sake of completeness, see Fig. 3.3 for an illustration.

- Primary control. Frequency and voltage stability; achievement of a desired power distribution to reduce circulating active and reactive power flows; mimic the behavior of SG-dominated networks.
- Secondary control. Compensation of frequency and voltage amplitude deviations caused by the primary control.
- Tertiary control. Optimal dispatch; additionally, in grid-connected mode: elimination of power flow imbalances between the microgrid and the main grid at the point of common coupling (PCC).

Note that the optimal dispatch problem is included in the control tasks associated with the tertiary control layer. Also, it is worth pointing out that, given the fairly recent interest in microgrids and the lack of commercially implemented microgrids, there is not yet an equivalent uniformly accepted definition of a hierarchical control architecture for microgrids. For example, the recent work [66] suggests to relax the strict separation of control tasks and time-scales in microgrid operation.

The author of the present work expects that further research and standardization efforts of academics and practitioners together with regulatory institutions are needed to establish a rigorous definition of control hierarchies and their respective tasks in microgrids, see also the discussion on this aspect in [193].

3.5 Summary

In this chapter the microgrid concept has been introduced and the main problems addressed in this work have been formulated. More precisely, a microgrid has been defined as a locally controllable subset of a distribution system. Furthermore, it has been shown that microgrids possess numerous key features, which help to face the ongoing structural changes of power systems worldwide. Two of these features are that microgrids facilitate the integration of large amounts of DG units and, at the same time, reduce the control burden of the main grid.

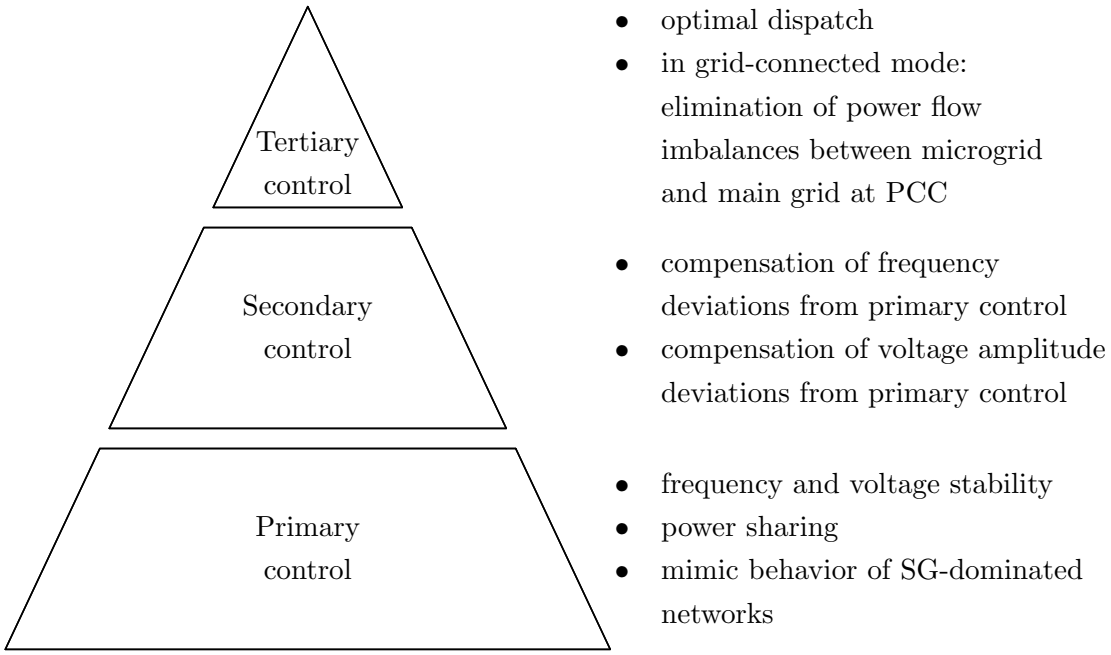

Figure 3.3: Example of a hierarchical control architecture for microgrids based on [38, 180, 191, 192]. The definition of the control layers and their associated control tasks is strongly inspired by the hierarchical control architecture for frequency control in large transmission systems, see, e.g., [4, 6, 190].

Furthermore, it has been argued that inverter-interfaced DG units have to contribute to frequency and voltage regulation in microgrids by operating as grid-forming units. However, the physical characteristics of inverters largely differ from those of SGs, which are used in conventional power systems as grid-forming units. As a consequence, new control concepts for microgrids are needed.

In this context, three fundamental challenges arising in microgrids and addressed in this work have been discussed, namely *(i)* frequency stability, *(ii)* voltage stability and *(iii)* power sharing. In particular, it has been shown, that power sharing essentially is an agreement problem.

Finally, it has been argued that the complexity—regarding components and timescales—of microgrids, motivates a hierarchical control design. A possible control hierarchy of microgrids has been presented based on the state-of-the-art in the literature. Within the framework of this hierarchal control architecture, all control problems addressed in this thesis are located at the primary control level.

4

Modeling of microgrids

4.1 Introduction

In the previous chapter, the relevance of microgrids in the context of electrical networks with large share of renewable DG units has been discussed. Furthermore, some of the most relevant associated challenges have been pointed out. Building on this discussion and based on [126], the main contribution of the present chapter is the derivation of a suitable mathematical model of an uncontrolled microgrid. Compared to related work on modeling of MDREGs, e.g., [30, 31, 32], a generic modular modeling approach is taken. This makes the derived model amenable for control design and straightforward derivation of closed-loop model representations for network analysis.

Based on Section 3.2, the derived model consists of several main components. More precisely, these are inverter-interfaced DG and storage units, DG units connected to the network via SGs, as well as loads and power lines.

The remainder of this chapter is outlined as follows. At first, the model of an inverter is derived in Section 4.2. Subsequently, the model of an SG is given in Section 4.3. This modeling chapter is concluded in Section 4.4 with the network and load models.

4.2 Inverter model

This section is dedicated to the model derivation of an inverter in a microgrid. Recall that a large share of renewable DG units are DC power sources or operated at high or variable frequency and, therefore, connected to an AC network via inverters [21]. Consequently, as outlined in Section 3.2, inverters are key components of microgrids.

The basic functionality of an inverter is illustrated in Fig. 4.1. The main elements of inverters are power semiconductor devices [167, 194]. An exemplary basic hardware topology of the electric circuit of a two-level three-phase inverter constructed with insulated-gate bipolar transistors (IGBTs) and antiparallel diodes is shown in Fig. 4.2. The conversion process from DC to AC is usually achieved by adjusting the on- and off-times of the transistors. These on- and off-time sequences are typically determined via a modulation technique, such as, e.g., puls-width-modulation (PWM) [167, 194]. To improve the quality of the AC waveform, e.g., to reduce the harmonics, the generated AC signal is typically processed through a low-pass filter constructed with RLC elements. Further information on the hardware design of inverters and related controls is given, e.g., in [148, 167, 194].

The remainder of this section is structured as follows. The main operation modes of inverters in microgrids are reviewed in Section 4.2.1. Then, based on [70, 71, 126] a suitable model of a three-phase inverter is derived in Section 4.2.2. More precisely, at first, the model of a single inverter is given and the main modeling assumptions are outlined. Subsequently, the validity of the proposed model with respect to the effect of clock drifts of the digital signal processor (DSP) used to operate the inverter is discussed. Finally, in Section 4.2.3, the proposed model is transformed into dq-coordinates, cf. Section 2.4.2, in order to interconnect it with a network composed of several units.

4.2.1 Common operation modes of inverters in microgrids

In microgrids, two main operation modes for inverters can be distinguished [81, 184]: grid-forming and grid-feeding mode. The latter is sometimes also called grid-following mode [24] or PQ control [35], whereas the first is also referred to as voltage source inverter (VSI) control [35]. The main characteristics of these two different operation modes are as follows [24, 35, 81, 184].

1. Grid-forming mode (also: VSI control).

   The inverter (shown in Fig. 4.2) is controlled in such way that its output voltage $v_{abc} : \mathbb{R}_{\geq 0} \to \mathbb{R}^3$, $v_{abc} = \mathrm{col}(v_a, v_b, v_c)$ can be specified by the designer. This is typically achieved via a cascaded control scheme consisting of an inner current control and an outer voltage control as shown in Fig. 4.3 based on [81]. The feedback signal of the current control loop is the current through the filter inductance

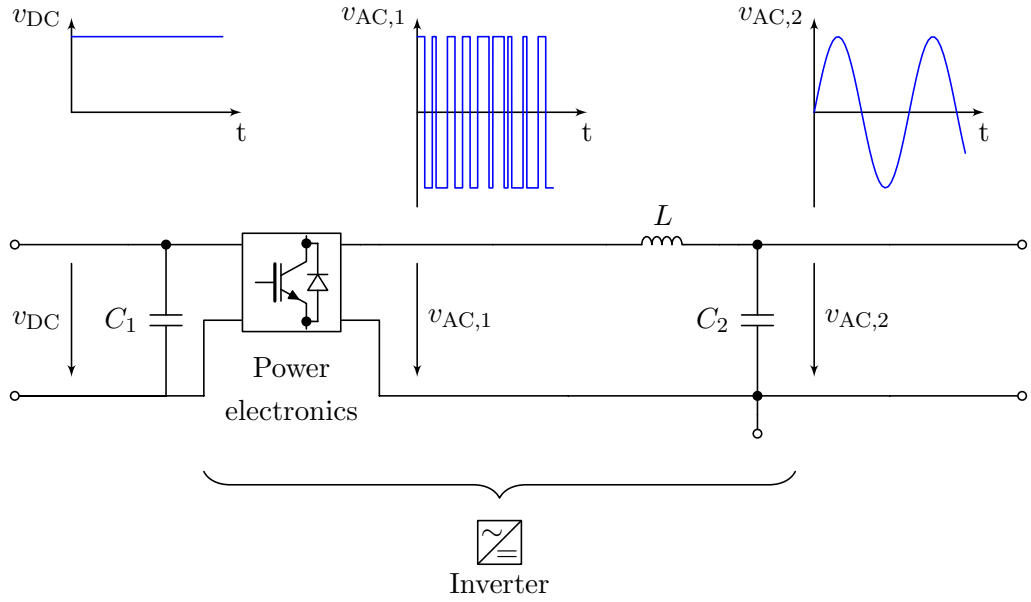

Figure 4.1: Schematic representation of a DC-AC voltage conversion by a DC-AC inverter. The DC signal $v_{\mathrm{DC}} : \mathbb{R}_{\geq 0} \to \mathbb{R}$ on the left side is converted into an AC signal via power semiconductor devices. The generated AC signal $v_{\mathrm{AC},1} : \mathbb{R}_{\geq 0} \to \mathbb{R}^3$ at the output of the power electronics is not sinusoidal. Therefore, an LC filter is connected in series with the power electronics to obtain a sinusoidal ouput voltage $v_{\mathrm{AC},2} : \mathbb{R}_{\geq 0} \to \mathbb{R}^3$ with low harmonic content.

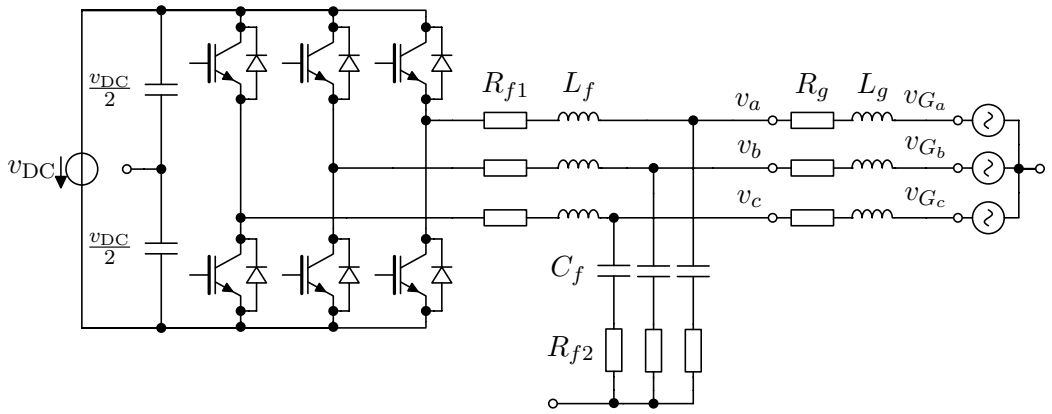

Figure 4.2: Typical circuit of a two-level three-phase inverter with LC output filter to convert a DC into a three-phase AC voltage. The inverter is constructed with insulated-gate bipolar transistors (IGBTs) and antiparallel diodes. The DC voltage is denoted by $v_{\mathrm{DC}} : \mathbb{R}_{\geq 0} \to \mathbb{R}$, the three-phase AC voltage generated by the inverter with $v_{abc} : \mathbb{R}_{\geq 0} \to \mathbb{R}^3$, $v_{abc} = \mathrm{col}(v_a, v_b, v_c)$ and the three-phase grid-side AC voltage by $v_{G,abc} : \mathbb{R}_{\geq 0} \to \mathbb{R}^3$, $v_{G,abc} = \mathrm{col}(v_{G_a} v_{G_b}, v_{G_c})$. The components of the output filter are an inductance $L_f \in \mathbb{R}_{>0}$, a capacitance $C_f \in \mathbb{R}_{>0}$ and two resistances $R_{f_1} \in \mathbb{R}_{>0}$, respectively $R_{f_2} \in \mathbb{R}_{>0}$. Typically, the resistance $R_g \in \mathbb{R}_{>0}$ and the inductance $L_g \in \mathbb{R}_{>0}$ represent a transformer or an output impedance. At the open connectors denoted by "**o**" the circuit can be grounded if desired.

$i_{f,abc} : \mathbb{R}_{\geq 0} \to \mathbb{R}^3$ and the inverter output voltage is the feedback signal of the voltage control loop. The inner loop of the control cascade is not necessary to control the output voltage of the inverter and can also be omitted. Nevertheless, it is often included to improve the control performance and to ensure the current limitations of the inverter are not violated.

2. Grid-feeding mode (also: grid-following mode, PQ control).

   The inverter is operated as power source, i.e., it provides a prespecified amount of active and reactive power to the grid. The active and reactive power setpoints are typically provided by a higher-level control or energy management system, see, e.g., [79, 81, 195]. Also in this case, a cascaded control scheme is usually implemented to achieve the desired closed-loop behavior of the inverter, as illustrated in Fig. 4.4. As in the case of a grid-forming inverter, the inner control loop is a current control the feedback signal of which is the current through the filter inductance $i_{f,abc} : \mathbb{R}_{\geq 0} \to \mathbb{R}^3$. However, the outer control loop is not a voltage, but a power (or, sometimes, a current) control. The feedback signals of the power control are the active and reactive power provided by the inverter.

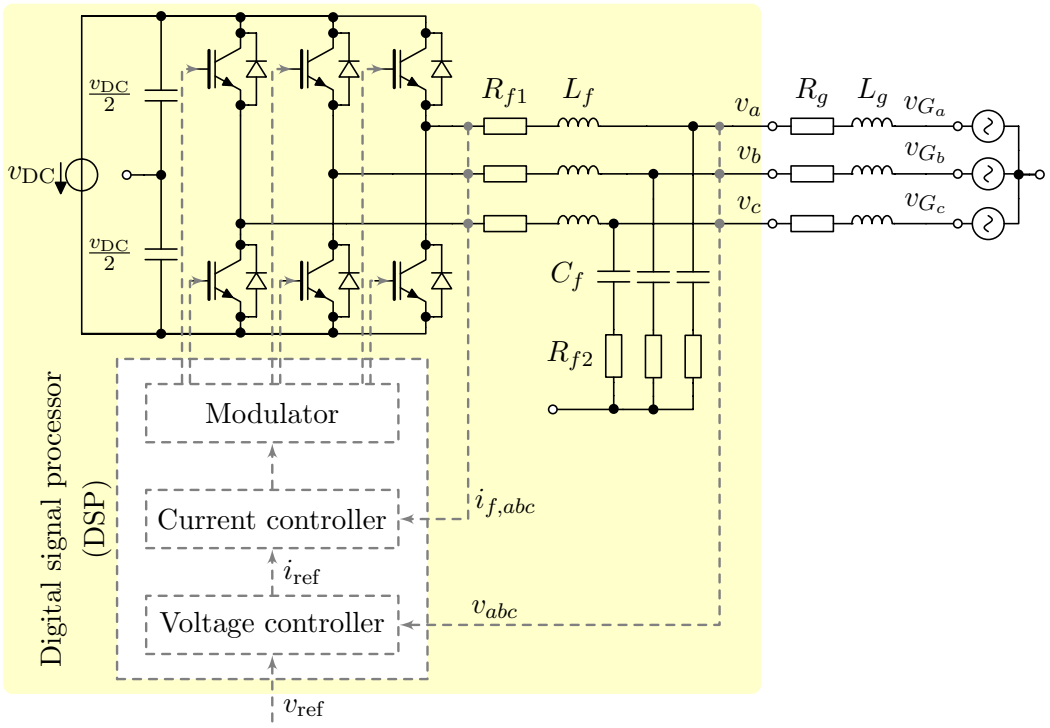

Figure 4.3: Schematic representation of an inverter operated in grid-forming mode based on [81]. Bold lines represent electrical connections, while dashed lines represent signal connections. The current through the filter inductance is denoted by $i_{f,abc} : \mathbb{R}_{\geq 0} \to \mathbb{R}^3$ and the inverter output voltage by $v_{abc} : \mathbb{R}_{\geq 0} \to \mathbb{R}^3$. Both quantities are fed back to a cascaded control consisting of an outer voltage and an inner current control. The reference signal $v_{\mathrm{ref}} : \mathbb{R}_{\geq 0} \to \mathbb{R}^3$ for the voltage controller is set by the designer, respectively a higher-level control. The IGBTs of the inverter are then controlled via signals generated by a modulator. The control structure can also be reduced to a pure voltage control.

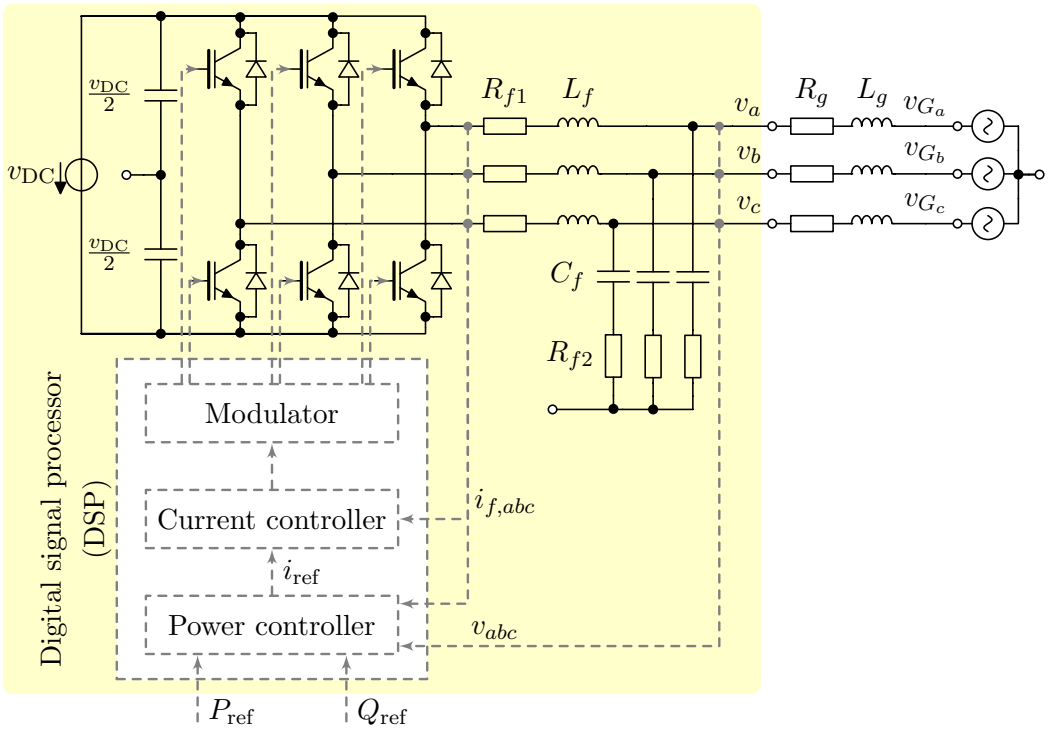

Figure 4.4: Schematic representation of an inverter operated in grid-feeding mode based on [81]. Bold lines represent electrical connections, while dashed lines represent signal connections. As in Fig 4.3, the current through the filter inductance is denoted by $i_{f,abc}$: $\mathbb{R}_{\geq 0} \to \mathbb{R}^3$ and the inverter output voltage by v_{abc} : $\mathbb{R}_{\geq 0} \to \mathbb{R}^3$. In grid-feeding mode, both quantities are fed back to a cascaded control consisting of an outer power and an inner current controller. The reference active and reactive powers $P_{\mathrm{ref}} \in \mathbb{R}$, respectively $Q_{\mathrm{ref}} \in \mathbb{R}$, are set by the designer or a higher-level control.

In both abovementioned operation modes, the current and voltage control loops are, in general, designed with the objectives of rejecting high frequency disturbances, enhancing the damping of the output $LC(L)$ filter and providing harmonic compensation [34, 59, 196, 197]. Furthermore, nowadays, most inverter-based DG units, such as PV or wind plants, are operated in grid-feeding mode [81]. However, as discussed in Section 3.3, grid-forming units are essential components in AC power systems, since they are responsible for frequency and voltage regulation in the network. Therefore, in microgrids with a large share of renewable inverter-based DG units, grid-forming capabilities often also have to be provided by inverter-interfaced sources [24, 35].

Remark 4.2.1. Some authors [81, 184] also introduce a third operation mode for inverters called grid-supporting mode. According to [81], a grid-supporting inverter participates in frequency and voltage regulation by adjusting its power output. In [184] a grid-supporting inverter is defined as an inverter, which not only provides power to the grid, but also ancillary services. The latter include voltage and frequency regulation [186]. Nevertheless, this last category is not necessary to classify typical operation modes of inverters in microgrids in the context of this work, since grid-supporting inverters are grid-forming inverters equipped with an additional outer control-loop to determine the reference output voltage. Such outer control-loops are discussed and designed in Chapter 5. Therefore, the term "grid-supporting inverter" is not used in the following.

Remark 4.2.2. In addition to the two control schemes introduced above, there also exist other approaches to operate inverters in microgrid applications. For example, [198, 199, 200] propose to design the inverter control based on the model of an SG with the aim of making the inverter mimic as close as possible the behavior of an SG. However, to the best of the author‘s knowledge, these approaches do not consider additional aspects, such as harmonic compensation or improved damping. Furthermore, to the best of the author‘s knowledge, they are not as commonly used as the control schemes shown in Fig. 4.3 and Fig. 4.4.

4.2.2 Model of a single grid-forming inverter

As described in Section 3.3, the derivation of control concepts for grid-forming inverters in microgrids together with the provision of conditions under which a desired stable operating point can be achieved is a very intriguing and challenging problem to which a large part of this thesis is devoted. Therefore, with respect to the operation mode of inverters, the focus in this work is on inverters operated in grid-forming mode. The

power, respectively current, injections of DG units operated in grid-feeding mode are considered as negative loads in this work, see Chapter 7 for details.

4.2.2.1 Model of a single grid-forming inverter as AC voltage source

A suitable model of a grid-forming inverter for the purpose of control design and stability analysis of microgrids is derived. There are many control schemes available to operate an inverter in grid-forming mode, such as PI control in dq-coordinates [34], proportional resonant control [201, 202] or repetitive control [203, 204] among others. An overview of the most common control schemes with an emphasis on H_∞ repetitive control is given in [148]. For a comparison of different control schemes, the reader is referred to, e.g., [205].

Due to the large variety of available control schemes, it is difficult to determine a standard closed-loop model of an inverter operated in grid-forming mode together with its inner control and output filter. Therefore, the approach taken in this work is to represent such a system as a generic dynamical system. Note that the operation of the IGBTs of an inverter occurs typically at very high switching frequencies (2-20 kHz) compared to the network frequency (45-65 Hz). It is therefore common practice [21, 34, 35, 59, 203, 206] to model an inverter in network studies with continuous dynamics by using the averaged switch modeling technique [194, 207], i.e., by averaging the internal inverter voltage and current over one switching period.

Consider an inverter located at the i-th node of a given microgrid. Denote the three-phase symmetric output voltage provided by the inverter by $v_{abc_i} : \mathbb{R}_{\geq 0} \to \mathbb{R}^3$ with phase angle $\alpha_i : \mathbb{R}_{\geq 0} \to \mathbb{T}$ and amplitude $\sqrt{\frac{2}{3}}V_i : \mathbb{R}_{\geq 0} \to \mathbb{R}_{\geq 0}$, i.e.,

$$v_{abc_i} = \sqrt{\frac{2}{3}}V_i \begin{bmatrix} \sin(\alpha_i) \\ \sin(\alpha_i - \frac{2\pi}{3}) \\ \sin(\alpha_i + \frac{2\pi}{3}) \end{bmatrix}. \tag{4.1}$$

Furthermore, denote by $\omega_i := \dot{\alpha}_i$ the frequency of the voltage v_{abc_i}. Denote the state signal of the inverter with its inner control and output filter by $x_{I_i} : \mathbb{R}_{\geq 0} \to \mathbb{R}^m$, its input signal by $v_{\mathrm{ref}_i} : \mathbb{R}_{\geq 0} \to \mathbb{R}^3$ and suppose its output signal is v_{abc_i}, see Fig. 4.3. Furthermore, let the grid-side current be given by $i_{abc_i} : \mathbb{R}_{\geq 0} \to \mathbb{R}^3$. Note that i_{abc_i} represents a disturbance for the inner control system of the inverter. Let $f_i : \mathbb{R}^m \times \mathbb{R}^3 \times \mathbb{R}^3 \to \mathbb{R}^m$ and $h_i : \mathbb{R}^m \times \mathbb{R}^3 \to \mathbb{R}^3$ denote continuously differentiable functions and ν_i denote a nonnegative real constant. Then, the closed-loop inverter dynamics with

inner control and output filter can be represented in a generic manner as

$$\begin{aligned} \nu_i \dot{x}_{I_i} &= f_i(x_{I_i}, v_{\mathrm{ref}_i}, i_{abc_i}), \\ v_{abc_i} &= h(x_{I_i}, v_{\mathrm{ref}_i}). \end{aligned} \tag{4.2}$$

As mentioned previously, one key objective of this work is to design suitable higher-level controls to provide a reference voltage v_{ref_i} for the system (4.2). Within the hierarchical control scheme discussed in Section 3.4, this next higher control level corresponds to the primary control layer of a microgrid. Let $z_{I_i} : \mathbb{R}_{\geq 0} \to \mathbb{R}^p$ denote the state signal of this higher-level control system, $u_{I_i} : \mathbb{R}_{\geq 0} \to \mathbb{R}^q$ its input signal and v_{ref_i} its output signal. Furthermore, let $g_i : \mathbb{R}^p \times \mathbb{R}^q \to \mathbb{R}^p$ and $w_i : \mathbb{R}^p \times \mathbb{R}^q \to \mathbb{R}^3$ be continuously differentiable functions. Then, the outer control system of the inverter can be described by

$$\begin{aligned} \dot{z}_{I_i} &= g_i(z_{I_i}, u_{I_i}), \\ v_{\mathrm{ref}_i} &= w_i(z_{I_i}, u_{I_i}). \end{aligned} \tag{4.3}$$

Combining (4.2) and (4.3) yields the overall inverter dynamics

$$\begin{aligned} \dot{z}_{I_i} &= g_i(z_{I_i}, u_{I_i}), \\ \nu_i \dot{x}_{I_i} &= f_i(x_{I_i}, w_i(z_{I_i}, u_{I_i}), i_{abc_i}), \\ v_{abc_i} &= h_i(x_{I_i}, w_i(z_{I_i}, u_{I_i})). \end{aligned} \tag{4.4}$$

The following assumptions on the inverter represented by (4.4) are made.

Assumption 4.2.3. *$\nu_i = 0$ in (4.4). Furthermore, $v_{abc_i} = w_i(z_{I_i}, u_{I_i})$.*

Assumption 4.2.4. *Whenever the inverter connects an intermittent renewable generation source, e.g., a photovoltaic plant or a wind plant, to the network, it is equipped with some sort of fast-reacting storage (e.g., a flywheel or a battery).*

Assumption 4.2.4 implies that the inverter can increase and decrease its power output within a certain range. This is necessary if the inverter should be able to provide a controllable voltage for all $t \geq 0$. Furthermore, since the storage element is assumed to be fast-reacting, the DC-side dynamics can be neglected in the model.

Assumption 4.2.3 is equivalent to the assumption that the inner current and voltage controllers track the voltage and current references ideally, meaning fast and exact. Usually, the current and voltage controllers in (4.2) (see also Fig. 4.3) are designed such the resulting closed-loop system (4.2) has a very large bandwidth compared to the control system located at the next higher control level represented by (4.3) [33, 35, 59].

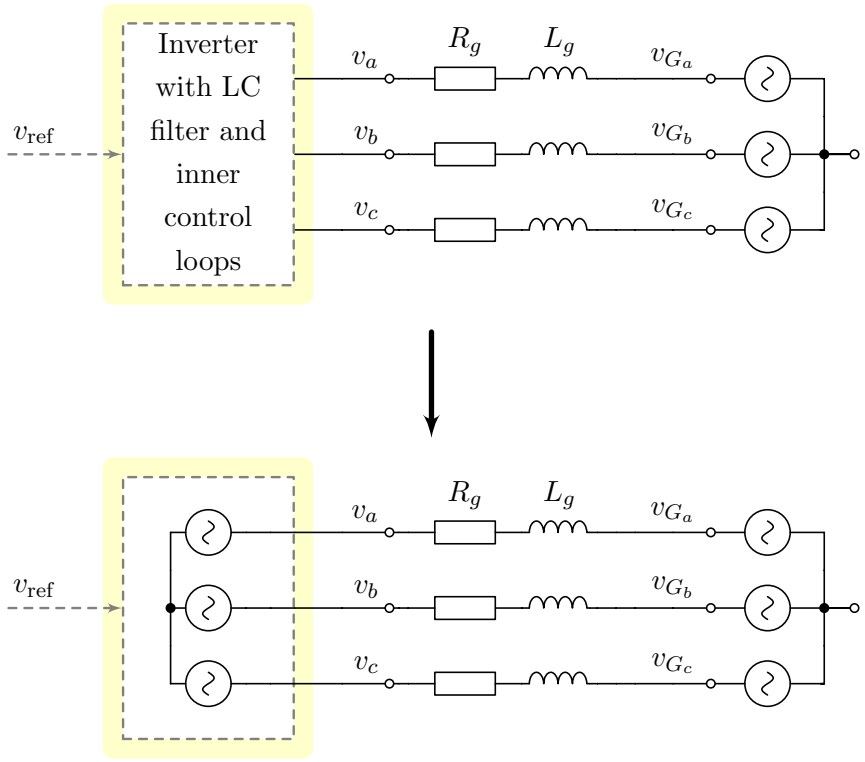

Figure 4.5: Simplified idealized representation of an inverter operated in grid-forming mode as ideal controllable voltage source. Bold lines represent electrical connections, while dashed lines represent signal connections. Typically, the switching frequency of the transistors is high (2-20 kHz) compared to the network frequency (45-65 Hz). In addition, the current and voltage controllers displayed in Fig. 4.3 are tuned such that their bandwidth is relatively large. Hence, with Assumptions 4.2.4 and 4.2.3 the system shown in Fig. 4.3 can be modeled as a controllable ideal AC voltage source.

If this time-scale separation is followed in the design of the system (4.4), the first part of Assumption 4.2.3 can be mathematically formalized by invoking the singular perturbation theory [128, Chapter 11], [170], see also Section 2.4.4. The second part of Assumption 4.2.3 expresses the fact that the inner control system (4.2) is assumed to track the reference $v_{\text{ref}_i} = w_i(z_{I_i}, u_{I_i})$ exactly, independently of the disturbance i_{abc_i}.

Typical values for the bandwidth of (4.2) reported in [34, 59] are in the range of $400-600$ Hz, while those of (4.3) are in the range of $2-10$ Hz. Note that Assumption 4.2.3 also further justifies Assumption 2.4.19, i.e., that the line and transformer dynamics can be neglected in the modeling and analysis, since these are typically at least as fast as those of the internal inverter controls (4.2), see, e.g., [33, 34].

Under Assumptions 4.2.4 and 4.2.3, the system (4.4) reduces to

$$\begin{aligned} \dot{z}_{I_i} &= g_i(z_{I_i}, u_{I_i}), \\ v_{abc_i} &= w_i(z_{I_i}, u_{I_i}). \end{aligned} \tag{4.5}$$

The model (4.5) represents the inverter in grid-forming mode at the i-th node as an AC voltage source, the amplitude and frequency of which can be defined by the designer. The system (4.5) is a very commonly used model of a grid-forming inverter in microgrid control design and analysis [21, 24, 28, 29, 35, 81, 208]. The model simplification from (4.4) to (4.5) is illustrated in Figure 4.5.

In the remainder of this work, a particular structure of (4.5) is used. As discussed in Section 2.4.1, a symmetric three-phase voltage can be completely described by its phase angle and its amplitude. In addition, it is usually preferred to control the frequency of the inverter output voltage, instead of the phase angle. Hence, a suitable model of the inverter at the i-th node with output voltage v_{abc_i} is given by [70, 71]

$$\begin{aligned} \dot{\alpha}_i &= \omega_i = u_i^{\delta}, \\ V_i &= u_i^{\mathrm{V}}, \\ v_{abc_i} &= v_{abc_i}(\alpha_i, V_i), \end{aligned} \tag{4.6}$$

where v_{abc_i} is given in (4.1) and $u_i^{\delta} : \mathbb{R}_{\geq 0} \to \mathbb{R}$ and $u_i^{V} : \mathbb{R}_{\geq 0} \to \mathbb{R}$ are control signals. It is also assumed that the active and reactive power output is measured and processed through a filter [33, 34]

$$\begin{aligned} \tau_{P_i} \dot{P}_i^m &= -P_i^m + P_i, \\ \tau_{P_i} \dot{Q}_i^m &= -Q_i^m + Q_i, \end{aligned} \tag{4.7}$$

where P_i and Q_i are the active and reactive power injections of the inverter, $P_i^m : \mathbb{R}_{\geq 0} \to \mathbb{R}$ and $Q_i^m : \mathbb{R}_{\geq 0} \to \mathbb{R}$ their measured values and $\tau_{P_i} \in \mathbb{R}_{>0}$ is the time constant of the low pass filter.

The model (4.6) together with (4.7) is the particular inverter model used in this work. Note that whenever the measured and filtered power signals are used as feedback signals in the controls u_i^{δ}, respectively u_i^{V}, the bandwidth of the overall control system is limited by the bandwidth of the measurement filter. This is the case for all control laws investigated and designed in the present work. Hence, if $\tau_{P_i} \gg \nu_i$, then Assumption 4.2.3 is justified [33, 59].

4.2.2.2 Comments on the model of a single grid-forming inverter as AC voltage source

Before proceeding, a fundamental aspect regarding the inverter model (4.6), (4.7) has to be discussed. Consider a microgrid with purely inverter-based grid-forming units, i.e., grid-forming units represented as ideal fully controllable AC voltage sources. Suppose you are given the problem of controlling these voltage sources such that the network synchronizes. An obvious straightforward approach is to set the inputs of all voltage sources to a common frequency and a constant, possibly non-uniform, amplitude. Then, by simple laws of physics and mathematics, the network is synchronized already at its initialization and will remain synchronized for all times. Moreover, the steady-state current and power flows in the network are determined by the choices of the amplitudes, as well as the initial conditions of the phase angles and the network parameters.

Hence, one may ask whether the problems of frequency and voltage stability in such a microgrid are essential at all. If the assumption that all grid-forming inverters are ideal voltage sources would exactly match the real world, the answer would be negative. However, in practice this is not true and even if it would be true, such an operation is not desirable from a practical point of view. The main reasons for this are three-fold.

First, in many practical setups, each individual inverter is operated with its own processor. It is well-known that the clocks used to generate the time signals of the individual processors differ from each other due to clock drifts [209, 210, 211]. As a consequence, it has been argued in [38, 81, 212] that apart from sensor uncertainties, the presence of clock drifts is the main reason why inverters operated with fixed electrical frequency cannot operate in parallel—unless the network possesses a very accurate clock synchronization system, which is often not the case in practice [38]. An example of two three-phase voltage sources with non-synchronized clocks connected in parallel over an RL-line is given in Fig. 4.6a. Both voltage sources V_a and V_b are operated with a fixed amplitude of one and a desired electrical frequency of $\omega^d = 2\pi 50$ rad/s. Both initial angles are set to zero. The frequency of each DSP used to control the voltage sources is assumed with 10 kHz. Furthermore, it is assumed that the clock of the voltage source V_a exhibits a relative drift of 10^{-6} [213]. The active power flow between both sources is shown in Fig. 4.6b. Clearly, the power oscillates drastically. Since the power flows are functions of the angles, see (2.47), this behavior is due to the fact that the frequencies of the voltage sources are not synchronized.

Second, by fixing frequency, voltage amplitudes and initial conditions of the phase angles to constant values, the network operator looses all controllability over the current and power flows in the network. Hence, the control objective of power sharing can, in general, not be achieved. Moreover, as mentioned previously, such an operation may lead to very high uncontrolled current flows in the network.

Third, from a practical consideration, most present and near-future applications concern MDREGs, i.e., networks of mixed generation structure including SGs and inverter-interfaced distributed resources. Consequently, the operation mode of inverters in grid-forming mode has to be compatible to that of SGs. The operation of SGs with constant fixed speed, or equivalently frequency, is called isochronous operation [1, Chapter 11]. However, in practice it is not possible to operate several SGs in one network in isochronous mode due to sensor and actuator inacurracies [1, Chapter 11].

4.2.2.3 Model of a grid-forming inverter with inaccurate clock

Due to its relevance in terms of synchronization and stability, the problem of clock drifts is discussed more in detail. This discussion is mainly taken from [124]. In a practical setup, the dynamics (4.6), (4.7) together with the controllers generating the signals u_i^δ and u_i^V are implemented on a processor by means of numerical integration. After each integration step, the generated values of the angle δ_i and the voltage amplitude V_i are passed to the internal controllers of the inverter at the i-th node. These internal controls then ensure that the inverter provides the desired three-phase sinusoidal voltage at its terminals, see (4.4) or Fig. 4.3.

For each unit in the network, the time step used to perform this numerical integration stems from the internal clock of the processor of that same unit. Following standard terminology and to avoid confusions with the electrical frequency, we denote by clock rate the frequency at which the processor is running. The clock rate is usually determined by some sort of resonator, e.g., a crystal oscillator. Almost all resonators suffer from precision inaccuracies [209, 213, 214, 215], which are typically classified into short- and long-term inaccuracy. While many resonators generally exhibit an excellent short-term accuracy, they do suffer from long-term effects, such as aging [214]. Furthermore, in general, no two resonators generate the exact same clock rates. Additionally, the clock rates are affected by environmental changes, such as pressure or temperature [215]. As a consequence, the clocks of different units in the network are

not synchronized per se. In particular, this implies that the numerical integration required to implement (4.6), (4.7) is carried out using different integration times at the different units in the network.

In the following, an equivalent model to (4.6), (4.7) is derived for the case of an inverter with a processor with an inaccurate clock. For an illustration of the influence of the clock inaccuracy on the numerical integration of (4.6), (4.7), consider the well-known Euler method [216] as an exemplary numerical integration method[1]. Let $x \in \mathbb{R}^n$, $f : \mathbb{R} \times \mathbb{R}^n \to \mathbb{R}^n$ and consider the ODE

$$\dot{x}(t) = f(t, x(t)), \quad x(t_0) = x_0.$$

Fix an initial time $t_0 \in \mathbb{R}$ and an integration step size $h \in \mathbb{R}_{>0}$. Let $k \in \mathbb{N}$ be the k-th integration step. Then

$$t^k = t_0 + kh \tag{4.8}$$

and the integration step of the Euler method from t^k to $t^{k+1} = t^k + h$ is given by [216]

$$x^{k+1} = x^k + hf(t^k, x^k). \tag{4.9}$$

Recall that every inverter in a microgrid is operated using its own local clock, i.e., at each inverter the integration (4.9) is carried out using the time signal provided by the local clock. As outlined above, almost all real clocks exhibit a certain (though often small) inaccuracy. In usual data-sheets, this clock drift is specified relative to the nominal clock rate [213]. To see how such a relative clock drift affects the time signal provided by a processor clock, denote an exemplary nominal clock rate by $f_c \in \mathbb{R}_{>0}$ and its relative drift by $\upsilon \in \mathbb{R}$. Typically, $|\upsilon| \leq 10^{-5}$ [213]. Then, the actual sampling interval $\Delta t_c \in \mathbb{R}_{>0}$ with respect to the nominal sampling interval $\Delta \bar{t}_c = 1/f_c$ of the corresponding processor is given by

$$\begin{aligned} \Delta t_c &= \frac{1}{f_c(1+\upsilon)} = \left(1 - \frac{\upsilon}{1+\upsilon}\right) \Delta \bar{t}_c = (1+\epsilon)\Delta \bar{t}_c, \\ \epsilon &:= -\frac{\upsilon}{1+\upsilon}. \end{aligned} \tag{4.10}$$

Note that both the step size h in (4.8) and the time signal provided by the processor (given, e.g., by (4.8)) are multiples of the sampling time Δt_c in (4.10). Denote by $t \in \mathbb{R}$ the nominal network time, by $t_0 \in \mathbb{R}$ the nominal network initial time, by $h \in \mathbb{R}_{>0}$ the

[1] The model derivation applies equivalently to other numerical integration methods, at the cost of a more complex notation.

step size in nominal time, by $t_i \in \mathbb{R}$ the local time of the clock of the i-th inverter, by $t_{i_0} \in \mathbb{R}$ its initial time and by $h_i \in \mathbb{R}_{>0}$ its step size. Furthermore, denote the relative drift of the clock of the i-th inverter by the parameter $\upsilon_i \in \mathbb{R}$. Due to the good short-term accuracy of many resonators, it is assumed in the following that υ_i is a small, but unknown constant parameter satisfying $|\upsilon_i| \ll 1$. Furthermore, a possible constant local clock offset $\bar{\zeta}_i \in \mathbb{R}$ is taken into account. Without loss of generality, it is convenient to write $\bar{\zeta}_i$ as $\bar{\zeta}_i = t_0\epsilon_i + \zeta_i$, $\zeta_i \in \mathbb{R}$. Hence, with (4.10), t_{i_0} and h_i can be expressed as

$$t_{i_0} = t_0 + \bar{\zeta}_i = t_0(1+\epsilon_i) + \zeta_i, \quad h_i = h(1+\epsilon_i).$$

Then

$$t_i^k = t_{i_0} + kh_i = t^k(1+\epsilon_i) + \zeta_i,$$

with t^k given in (4.8). It follows that, for sufficiently fast sampling times, the clock drift of the processor of the i-th inverter can formally be included in the continuous-time model (4.6), (4.7) by an appropriate time-scaling, i.e.,

$$t_i = (1+\epsilon_i)t + \zeta_i. \tag{4.11}$$

Note that the clock model (4.11) is identical to that used to investigate clock synchronization in [210, 211]. Furthermore,

$$\frac{d(\cdot)}{dt_i} = \frac{1}{(1+\epsilon_i)}\frac{d(\cdot)}{dt} = (1+\upsilon_i)\frac{d(\cdot)}{dt}. \tag{4.12}$$

Suppose the time derivatives in (4.6), (4.7) are expressed with respect to the local time t_i of the i-th inverter. Inserting (4.12) in (4.6), (4.7) yields

$$\begin{aligned}
(1+\upsilon_i)\dot{\alpha}_i &= u_i^\delta, \\
(1+\upsilon_i)\tau_{P_i}\dot{P}_i^m &= -P_i^m + P_i, \\
V_i &= u_i^V, \\
(1+\upsilon_i)\tau_{P_i}\dot{Q}_i^m &= -Q_i^m + Q_i, \\
v_{abc_i} &= v_{abc_i}(\alpha_i, V_i),
\end{aligned} \tag{4.13}$$

where the time derivatives are now expressed with respect to the nominal time t. Furthermore, without loss of generality, the local clock offset ζ_i can be included in the initial conditions of the system (4.13).

All control laws introduced in this work are—to a certain extent—robust with respect to the uncertain parameter υ_i. Here, robustness is understood in the sense that

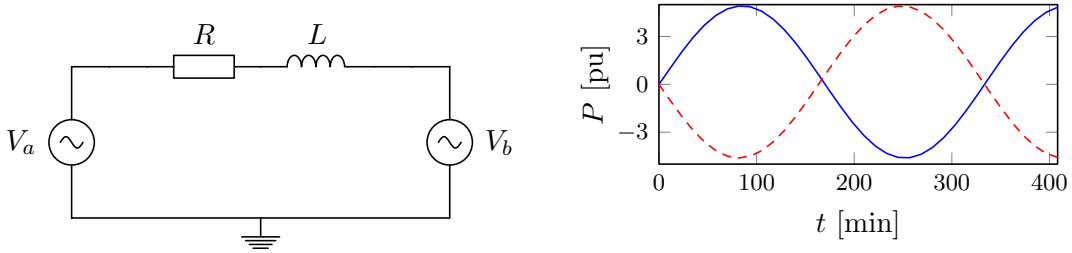

(a) Equivalent single-phase circuit of two voltage sources in parallel

(b) Active power flows of the voltage sources V_a '–' and V_b '- -'. Clearly, the active power flows oscillate, since the frequencies of the voltage sources are not synchronized.

Figure 4.6: Example of the effect of clock-drifts between two voltage sources in parallel

the control goals (stability and power sharing) can still be achieved for small (in magnitude) values of υ_i. Therefore, the nominal model (4.6), (4.7) is used instead of the model (4.13) in the following to represent the inverter at the i-th node. Whenever necessary, the claimed robustness property is pointed out. In particular, for the results in Section 6.4, a detailed proof is given in [124].

Remark 4.2.5. Besides clock drifts, digital control usually introduces time delays [217, 218, 219]. According to [219], the main reasons for this are 1) sampling of control variables, 2) calculation time of the digital controller and 3) generation of the pulse-width-modulation. The reader is referred to, e.g., [219] for further details. These time delays may have a deteriorating effect on the control performance of a microgrid. Motivated by this phenomenon, recently the input-to-state stability (ISS) theory for multistable systems [220] has been extended to multistable systems with delay [221]. Based on the proposed approach, also some preliminary results in form of a condition for asymptotic phase-locking in a microgrid composed of two droop-controlled inverters with delay are derived in [221]. The analysis is conducted for a simplified inverter model under the assumptions of constant voltage amplitudes and ideal clocks, as well as negligible dynamics of the internal inverter filter and controllers. In that scenario, the delay merely affects the phase angle of the inverter output voltage. The authors of [221] plan to extend the analysis conducted in [221] to more complex inverter models with delays and, e.g., time-varying voltages or internal filter and controllers.

4.2.3 Model of a grid-forming inverter connected to a network

The interconnection of the inverter model (4.6), (4.7) with the network equations (2.44) is established by proceeding as outlined in Section 2.4.4. Hence, at first, the node

voltage v_{abc_i} is transformed into local dq-coordinates. To this end, recall the mapping T_{dq} defined in (2.13) and let

$$\theta_i := \alpha_i,$$

where α_i is the phase angle of the three-phase voltage at the i-th node defined in (4.1). Then, the bus voltage v_{abc_i} in local dq-coordinates is given by (cf. (2.26))

$$v_{dq_i} := T_{dq}(\theta_i) v_{abc_i} = \begin{bmatrix} V_{d_i} \\ V_{q_i} \end{bmatrix} = V_i \begin{bmatrix} 0 \\ 1 \end{bmatrix} \in \mathbb{R}^2 \tag{4.14}$$

or, equivalently, by

$$V_{qd_i} := V_{q_i} + j0 = V_i \in \mathbb{R}_{\geq 0}.$$

Second, V_{qd_i} is transformed to a common reference frame. Let

$$\delta_i := \alpha_{0_i} + \int_0^t (\dot{\alpha}_i - \omega^{\text{com}})\, d\tau = \alpha_{0_i} + \int_0^t (\omega_i - \omega^{\text{com}})\, d\tau \in \mathbb{T}, \tag{4.15}$$

where the real constant ω^{com} denotes the rotational speed of the common reference frame and $\alpha_{0_i} \in \mathbb{T}$ the initial condition of α_i. On the common reference frame, the voltage is then given by (cf. (2.32))

$$\hat{V}_{qd_i} := \hat{V}_{q_i} + j\hat{V}_{d_i} = e^{j\delta_i} V_{qd_i} = e^{j\delta_i} V_i.$$

Consequently, the model (4.6), (4.7) can be represented on the common reference frame by

$$\boxed{\begin{aligned} \dot{\delta}_i = \omega_i - \omega^{\text{com}} &= u_i^{\delta} - \omega^{\text{com}}, \\ \tau_{P_i} \dot{P}_i^m &= -P_i^m + P_i, \\ V_i &= u_i^V, \\ \tau_{P_i} \dot{Q}_i^m &= -Q_i^m + Q_i. \end{aligned}} \tag{4.16}$$

With $V_{d_i} = 0$ and $V_{q_i} = V_i$, cf. (4.14), the active and reactive power flows P_i and Q_i are given from Definition 2.4.12 by[1]

$$P_i = V_{q_i} I_{q_i} = V_i I_{q_i},$$
$$Q_i = -V_{q_i} I_{d_i} = -V_i I_{d_i}.$$

Remark 4.2.6. Consider a microgrid and suppose it possesses a desired steady-state motion at some constant frequency $\omega^s \in \mathbb{R}_{>0}$. For the purpose of stability analysis of this steady-state motion, a typical choice for the common reference speed is $\omega^{\text{com}} = \omega^s$.

[1] As detailed in Section 2.4.4.2, the power flows describe the interactions between nodes in an electrical network. For the particular models of DG units derived in this chapter, an explicit expression of the power flow equations is given in Section 4.4 based on (2.47).

4.3 Synchronous generator model

As outlined in Chapter 1 and detailed in Section 3.2, from a practical consideration, most present and near-future applications of microgrids concern networks of mixed generation structure including SGs and inverter-interfaced distributed units. Such systems are called MDREGs in this work.

Generally speaking, an SG consists of two main components, a rotor and a stator, see Fig. 4.7. The rotor is driven by a mechanical torque, which in MDREGs is typically provided by a diesel engine or gas turbine [65]. Usually, the rotor possesses a field winding, which carries a DC current supplied by an excitation system. The resulting rotating magnetic field induces AC voltages in the stator windings. The stator windings are distributed such that a magnetic field, which rotates at a constant speed, induces a symmetric three-phase voltage. Based on [6], in Fig. 4.7, the field winding is denoted by $F_{1,2}$, while the stator windings are denoted by $a_{1,2}$, $b_{1,2}$ and $c_{1,2}$.

The usual model derivation of an SG in the literature, see, e.g., [1, 3, 6, 146], follows that of an inverter outlined in Section 4.2, i.e., at first the model of a single SG is derived in local dq-coordinates and then this model is subsequently transformed to a common reference frame in order to be able to connect it to a network composed of several units. Since modeling of SGs is a well-studied topic, see, e.g., [1, 3, 6, 146], a detailed model derivation is omitted here and a standard third-order model of an SG is directly given on a common reference frame. In addition, as commonly done in stability analysis of power systems, the dynamics of the mechanical part of the power generation unit are neglected [1, 3, 6, 146].

At first, the main relevant variables to describe the dynamics of an SG are introduced. Consider an SG connected at the i-th node of a given microgrid. Let the corresponding symmetric three-phase voltage at that node be given by $v_{abc_i} : \mathbb{R}_{\geq 0} \to \mathbb{R}^3$. This voltage is usually called terminal voltage. Note that unlike for an inverter, in the case of an SG the phase angle of the terminal voltage v_{abc_i} is, for physical reasons, not a feasible control variable.

Furthermore, it is convenient to introduce the electromotive force (EMF) $e_{abc_i} : \mathbb{R}_{\geq 0} \to \mathbb{R}^3$ of the SG. Recall that an EMF is the voltage developed by a source of electrical energy [222]. In the case of an SG, the term EMF is typically used to describe the electrical voltage induced in the stator winding of the SG through rotation of the magnetic field of the rotor [6, Chapter 11].

Associate an angle $\theta_i : \mathbb{R}_{\geq 0} \to \mathbb{T}$ to the SG and call this angle "shaft angle" [3, 6]. Furthermore, let $\omega_i := \dot{\theta}_i$ denote the rotational speed of the rotor of the SG. Recall the mapping T_{dq} defined in (2.13). Following Section 2.4.4, denote the terminal voltage, respectively the EMF, in local dq-coordinates by (cf. (2.26))

$$v_{dq_i} := T_{dq}(\theta_i) v_{abc_i} \in \mathbb{R}^2, \quad e_{dq_i} := T_{dq}(\theta_i) e_{abc_i} \in \mathbb{R}^2$$
$$V_{qd_i} := V_{q_i} + jV_{d_i} \in \mathbb{C}, \quad E_{qd_i} := E_{q_i} + jE_{d_i} \in \mathbb{C}.$$

For the presentation of a third-order model of an SG, the following standard assumption is made [3, 6].

Assumption 4.3.1. *$E_{d_i} = 0$ for all $t \geq 0$, $i \sim \mathcal{N}_{SG}$.*

Assumption 4.3.1 is, generally, justified by the fact that the EMF of the SG acts mainly along the q-axis [3, Chapter 4]. Furthermore, for ease of notation let

$$\boxed{V_i := E_{q_i}, \quad i \sim \mathcal{N}_{SG}.} \tag{4.17}$$

Next, $E_{q_i} = V_i$ is transformed to a common reference frame. As done for the inverter model in Section 4.2.3, let

$$\delta_i := \theta_{0_i} + \int_0^t \left(\dot{\theta}_i - \omega^{\text{com}} \right) d\tau = \theta_{0_i} + \int_0^t \left(\omega_i - \omega^{\text{com}} \right) d\tau \in \mathbb{T}, \tag{4.18}$$

where the real constant ω^{com} denotes the rotational speed of the common reference frame and $\theta_{0_i} \in \mathbb{T}$ the initial condition of θ_i. On the common reference frame, the EMF is then given by (cf. (2.32))

$$\hat{E}_{qd_i} := \hat{E}_{q_i} + j\hat{E}_{d_i} = e^{j\delta_i} E_{qd_i} = e^{j\delta_i} V_i.$$

An illustration of the stator and rotor of an SG is given in Fig. 4.7 based on [6, Chapter 11]. The figure shows the axes denoting the abc-coordinates corresponding to the three-phase stator armature winding, the dq-axes, as well as the shaft angle θ_i. Note that the positioning of the dq-axes and the denomination of the angles is not uniform in the literature, see, e.g., [3, 146].

Recall that the network equations have been derived in Section 2.4.4 in terms of the terminal voltage in local coordinates V_{qd_i}. The following relation between V_{qd_i} and $E_{q_i} = V_i$, see (4.17), is useful [1, 3, 6, 146]

$$\begin{bmatrix} V_{d_i} \\ V_{q_i} \end{bmatrix} = \begin{bmatrix} -R_i & -X'_{q_i} \\ X'_{d_i} & -R_i \end{bmatrix} \begin{bmatrix} I_{d_i} \\ I_{q_i} \end{bmatrix} + \begin{bmatrix} 0 \\ E_{q_i} \end{bmatrix}, \tag{4.19}$$

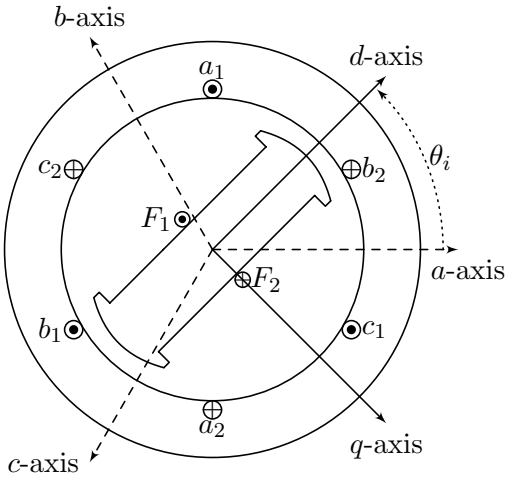

Figure 4.7: Representation of the axes and the shaft angle of an SG based on [6]. The *abc*-axes correspond to the *abc*-coordinates of the voltages and currents of the three-phase stator armature winding. The excitation winding is denoted by $F_{1,2}$, while the stator windings are denoted by $a_{1,2}$, $b_{1,2}$ and $c_{1,2}$. The *dq*-axes denote the rotating axes of the *dq*-frame corresponding to the transformation $T_{dq_i}(\theta_i)$. The angle θ_i moves at the speed of the rotor of the i-th SG.

where $I_{d_i} : \mathbb{R}_{\geq 0} \to \mathbb{R}$ is the d-axis current, $I_{q_i} : \mathbb{R}_{\geq 0} \to \mathbb{R}$ the q-axis current, $R_i \in \mathbb{R}_{>0}$ the resistance of the symmetric stator phases, $X'_{d_i} \in \mathbb{R}_{>0}$ the d-axis transient inductance and $X'_{q_i} \in \mathbb{R}_{>0}$ the q-axis transient inductance. By transforming the relation (4.19) to the common reference frame and including it in the network admittance matrix $\hat{\mathcal{Y}}(\delta)$ given in (2.44), the network interconnection of the SG is represented in terms of the EMF $E_{q_i} = V_i$ in local *dq*-coordinates. Whenever an SG is connected to the network, it is assumed that this process has been carried out.

Then, the SG at the i-th node can be represented by the following standard third-order model [1, 3, 6, 146]

$$\boxed{\begin{aligned} \dot{\delta}_i &= \omega_i - \omega^{\text{com}}, \\ M_i \dot{\omega}_i &= -D_i(\omega_i - \omega^d) + P_{M_i} - P_i, \\ \tau_{d0_i} \dot{V}_i &= -V_i + (X_{d_i} - X'_{d_i}) I_{d_i} + E_{f_i}, \end{aligned}} \tag{4.20}$$

where $P_{M_i} : \mathbb{R}_{\geq 0} \to \mathbb{R}$ is the mechanical power, P_i the electrical power, $M_i \in \mathbb{R}_{>0}$ the inertia coefficient, $\omega^d \in \mathbb{R}$ the nominal speed and $D_i \in \mathbb{R}_{>0}$ a damping term. Furthermore, $\tau_{d0_i} \in \mathbb{R}_{>0}$ is the d-axis transient open-circuit time constant, $X_{d_i} \in \mathbb{R}_{>0}$ the d-axis inductance and $E_{f_i} : \mathbb{R}_{\geq 0} \to \mathbb{R}$ the excitation voltage. Here, P_{M_i} and E_{f_i} are control inputs.

Neglecting transient saliency, i.e., the effects of the rotor saliency on the active power, [3, 6, 146], the instantaneous active power P_i can be expressed according to Definition 2.4.12 as

$$P_i = V_i I_{q_i}.$$

The model (4.20) is widely used in stability analysis of power systems, see, e.g., [36, 48, 51, 223, 224, 225, 226, 227, 228, 229, 230, 231]. For a detailed derivation of the model (4.20), as well as the underlying assumptions and limitations, the reader is referred to standard power systems text books, e.g., [1, 3, 6, 146].

4.4 Network and load model

The load model considered in this work is discussed in Section 4.4.1. The network model of a generic meshed microgrid is derived in Section 4.4 following the procedure depicted in Section 2.4.4.

4.4.1 Load model

Accurate load modeling is a very important, but also very difficult task in power system analysis [1, 232]. The main reason for this is that there are typically many different kinds of loads connected within one power system or microgrid, see, e.g., [1, Chapter 7]. As a consequence, often simplified load models are employed in power system studies [1, Chapter 7]. Commonly, load models are classified into static and dynamic load models [1, 6, 232, 233]. Into which category a particular load belongs can, e.g., be determined as follows [232, Chapter 4]. Most often, the power consumed by a load depends on the voltage. This dependence can be permanent, then the load is purely static, or it may change over time, then the load is dynamic. The frequency-dependency of a load can be determined in an equivalent fashion.

The analysis in this work follows the classical approach in conventional power system studies [3, 6, 36, 146] that loads are represented by constant impedances, i.e., a particular class of static loads is considered[1]. According to [1, 6], in the absence of detailed load information, this is the most commonly accepted static load model for

[1]The author is aware that different types of loads may have different effects on network stability and that not all loads can be accurately represented by constant impedance loads. Therefore, the presented results may be inaccurate for other type of load models, such as dynamic loads [232]. Stability analysis of microgrids under consideration of other load models is discussed as a future direction of research in Section 8.2.

reactive power. The same references agree that the active power is most commonly represented as a constant current load[1].

4.4.2 Network model

Modeling loads as impedances leads to a set of (nonlinear) DAEs, where the differential equations describe the dynamics of the generation units, while the algebraic equations correspond to the loads. Then, a standard network reduction (called Kron reduction, see Section 2.4.4.3) can be performed to eliminate all algebraic equations corresponding to loads and to obtain a set of differential equations. In the following, it is assumed that this process has been carried out and the Kron-reduced network is used.

The Kron-reduced microgrid is formed by $n := n_1 + n_2 \geq 1$, $n_1 \in \mathbb{N}$, $n_2 \in \mathbb{N}$, nodes, of which $\mathcal{N}_I := \{1, \dots, n_1\}$ represent DG units interfaced via inverters modeled by (4.16) and $\mathcal{N}_{SG} := \{(n_1 + 1), \dots, n\}$ are DG units interfaced via SGs modeled by (4.20). As before, the set of network nodes is denoted by $\mathcal{N} := \mathcal{N}_I \cup \mathcal{N}_{SG}$.

Recall from Section 2.4.4 that two nodes i and k of the microgrid are connected via a complex nonzero admittance $Y_{ik} := G_{ik} + jB_{ik} \in \mathbb{C}$ with conductance $G_{ik} \in \mathbb{R}_{>0}$ and susceptance $B_{ik} \in \mathbb{R}_{<0}$ and that $Y_{ik} := 0$ whenever i and k are not directly connected. Furthermore, recall that the set of neighbors of a node $i \in \mathcal{N}$ is denoted by $\mathcal{N}_i := \{k \mid k \in \mathcal{N},\ k \neq i\ , Y_{ik} \neq 0\}$. The representation of loads as constant impedances in the original network leads to shunt-admittances at at least some of the nodes in the Kron-reduced network, i.e., $\bar{Y}_{ii} = \bar{G}_{ii} + j\bar{B}_{ii} \neq 0$ for some $i \in \mathcal{N}$, where $\bar{G}_{ii} \in \mathbb{R}_{>0}$ is the shunt-conductance and $\bar{B}_{ii} \in \mathbb{R}$ denotes the shunt-susceptance. The assumption below on the shunt-susceptances is made.

Assumption 4.4.1. $\bar{B}_{ii} \leq 0$, $i \sim \mathcal{N}$.

The restriction to inductive loads, i.e., $\bar{B}_{ii} \leq 0$, $i \sim \mathcal{N}$, is justified as follows. The admittance loads in the Kron-reduced network are a conglomeration of the individual loads in the original network, see Remark 2.4.4.3. Therefore, assuming purely inductive loads in the Kron-reduced network can be interpreted as assuming that the original network is not overcompensated, i.e., that the overall load possesses inductive character. Furthermore, capacitive shunt-admittances in distribution systems mainly stem from capacitor banks used to compensate possibly strong inductive behavior of loads. In conventional distribution systems, these devices are additionally inserted in the system

[1] An extension of the results derived in this work to constant current loads is under current investigation.

to improve its performance with respect to reactive power consumption [1, 234]. This is needed because there is no generation located close to the loads. However, in a microgrid the generation units are located close to the loads. Hence, the availability of generation units at distribution level is likely to replace the need for capacitor banks, see also [234].

The admittance matrix of the electrical network (see Section 2.4.4.2) is denoted by $\mathcal{Y}_{\mathcal{R}} \in \mathbb{C}^{n\times n}$ with entries

$$\mathcal{Y}_{Rii} := \bar{G}_{ii} + j\bar{B}_{ii} + \sum_{k\sim\mathcal{N}_i} (G_{ik} + jB_{ik}) := G_{ii} + jB_{ii}, \quad \mathcal{Y}_{Rik} := -G_{ik} - jB_{ik}, \quad i \neq k.$$

Hence, with Assumption 4.4.1,

$$G_{ii} \geq \sum_{k\sim\mathcal{N}_i} G_{ik}, \quad |B_{ii}| \geq \sum_{k\sim\mathcal{N}_i} |B_{ik}|, \quad i \sim \mathcal{N}. \tag{4.21}$$

In addition, the following assumption on the network topology is made.

Assumption 4.4.2. *The microgrid is connected, i.e., for all pairs $(i,k) \in \mathcal{N}\times\mathcal{N}$, $i \neq k$, there exists an ordered sequence of nodes from i to k such that any pair of consecutive nodes in the sequence is connected by a power line represented by an admittance.*

Assumption 4.4.2 is reasonable for a microgrid, unless severe line outages separating the system into several disconnected parts occur.

Recall the active and reactive power flows in an electrical network given in (2.47). Moreover, recall that for the inverter model (4.16) $V_{d_i} = 0$ and $V_{q_i} = V_i$, $i \sim \mathcal{N}_I$, respectively for the SG model (4.20) $E_{d_k} = 0$, $E_{q_k} = V_k$, $k \sim \mathcal{N}_{SG}$. Moreover, recall that, with Assumptions 2.4.18 and 4.4.1, $B_{ii} < 0$ and $B_{ik} \leq 0$, $i \sim \mathcal{N}$, $k \sim \mathcal{N}$. Finally, recall that ω_i denotes the absolute frequency of the voltage generated by the inverter, respectively the rotational speed of the SG, at the i-th node and that δ_i, $i \sim \mathcal{N}$, is given by (4.15), respectively (4.18), as

$$\delta_i = \delta_{0_i} + \int_0^t (\omega_i - \omega^{\text{com}})\, d\tau \in \mathbb{T}, \quad i \sim \mathcal{N},$$

where $\delta_{0_i} \in \mathbb{T}$ is a constant. Then, the expressions for the currents I_{q_i} and I_{d_i} at the i-th node given by (2.45) reduce to

$$\begin{aligned} I_{q_i}(\delta_1,\ldots,\delta_n,V_1,\ldots,V_n) &= G_{ii}V_i - \sum_{k\sim\mathcal{N}_i} \left(G_{ik}\cos(\delta_{ik}) + B_{ik}\sin(\delta_{ik})\right) V_k, \\ I_{d_i}(\delta_1,\ldots,\delta_n,V_1,\ldots,V_n) &= B_{ii}V_i + \sum_{k\sim\mathcal{N}_i} \left(G_{ik}\sin(\delta_{ik}) - B_{ik}\cos(\delta_{ik})\right) V_k. \end{aligned} \tag{4.22}$$

Furthermore, with $V_{d_i} = 0$ and $V_{q_i} = V_i$, $i \sim \mathcal{N}_I$, respectively $E_{d_k} = 0$ and $E_{q_k} = V_k$, $k \sim \mathcal{N}_{SG}$, the active and reactive power flows at the i-th node, $i \in \mathcal{N}$, given in (2.47) simplify to

$$\begin{aligned}
P_i(\delta_1, \ldots, \delta_n, V_1, \ldots, V_n) &= V_i I_{q_i} \\
&= G_{ii} V_i^2 - \left(\sum_{k \sim \mathcal{N}_i} G_{ik} \cos(\delta_{ik}) + B_{ik} \sin(\delta_{ik}) \right) V_i V_k, \\
&= G_{ii} V_i^2 - \left(\sum_{k \sim \mathcal{N}_i} G_{ik} \cos(\delta_{ik}) - |B_{ik}| \sin(\delta_{ik}) \right) V_i V_k, \\
Q_i(\delta_1, \ldots, \delta_n, V_1, \ldots, V_n) &= -V_i I_{d_i} \\
&= -B_{ii} V_i^2 - \left(\sum_{k \sim \mathcal{N}_i} G_{ik} \sin(\delta_{ik}) - B_{ik} \cos(\delta_{ik}) \right) V_i V_k, \\
&= |B_{ii}| V_i^2 - \left(\sum_{k \sim \mathcal{N}_i} G_{ik} \sin(\delta_{ik}) + |B_{ik}| \cos(\delta_{ik}) \right) V_i V_k.
\end{aligned} \tag{4.23}$$

It is convenient to rewrite the power flows given by (4.23) in a more compact form. To this end, let the admittance magnitude $|Y_{ik}|$ and the admittance angle ϕ_{ik} be given by

$$|Y_{ik}| := \sqrt{G_{ik}^2 + B_{ik}^2} \in \mathbb{R}_{\geq 0}, \quad \phi_{ik} := \arctan\left(\frac{G_{ik}}{B_{ik}}\right) \in \mathbb{T}, \quad i \sim \mathcal{N}, \quad k \sim \mathcal{N}_i.$$

Let $\beta \in \mathbb{T}$ and a, b, c be real constants. Then, by making use of the following trigonometric identities

$$\begin{aligned}
a \sin(\beta) + b \cos(\beta) &= \sqrt{a^2 + b^2} \sin\left(\beta + \arctan\left(\frac{b}{a}\right)\right), \quad a > 0, \\
\arctan(-c) &= -\arctan(c), \\
\sin\left(\beta + \frac{\pi}{2}\right) &= \cos(\beta), \\
\arctan\left(\frac{1}{c}\right) &= \operatorname{sign}(c)\frac{\pi}{2} - \arctan(c), \quad c \neq 0,
\end{aligned}$$

the power flows (4.23) at the i-th node can be expressed compactly as

$$\boxed{\begin{aligned}
P_i(\delta_1, \ldots, \delta_n, V_1, \ldots, V_n) &= G_{ii} V_i^2 + \sum_{k \sim \mathcal{N}_i} |Y_{ik}| V_i V_k \sin(\delta_{ik} + \phi_{ik}), \\
Q_i(\delta_1, \ldots, \delta_n, V_1, \ldots, V_n) &= |B_{ii}| V_i^2 - \sum_{k \sim \mathcal{N}_i} |Y_{ik}| V_i V_k \cos(\delta_{ik} + \phi_{ik}),
\end{aligned}} \tag{4.24}$$

which is a very common form of the power flow equations.

4.5 Summary

In this chapter a comprehensive mathematical model of a microgrid suitable for network control design and network analysis has been derived. The model comprises individual dynamic models of inverter-interfaced DG units, SG-interfaced DG units, as well as a network model containing loads.

In particular, the basic physical structure of an inverter has been reviewed. It has been shown that, typically, inverters in microgrids are operated either in grid-forming or in grid-feeding mode. Both operation modes have been described in detail. Subsequently, inverters in grid-forming mode have been identified as key components in microgrids with large share of renewable DG units. As a consequence, a model of an inverter in grid-forming mode has been derived. Furthermore, it has been shown that, under certain assumptions, a grid-forming inverter can be modeled as an AC voltage source. This model of a grid-forming inverter is used in the remainder of this work.

In addition, the standard one-axis model of a SG has been introduced following the usual modeling procedure in the literature, see, e.g., [3, 6]. Finally, based on Section 2.4.4, a suitable network model of a microgrid has been derived, in which loads are represented as constant impedances.

5

Control concepts for microgrids and conditions for power sharing

5.1 Introduction

As discussed in Chapter 3, the present thesis is devoted to three main problems in the operation of microgrids: frequency stability, voltage stability and power sharing. In the previous chapter, an appropriate model of a microgrid to investigate these problems has been derived. Based on this model, control concepts to address the aforementioned problems are introduced, respectively designed, in the present chapter.

The theoretical analysis in this chapter is focused on the control objective of power sharing. For a rigorous mathematical analysis of the closed-loop microgrid dynamics under the different control schemes introduced in the following, the reader is referred to Chapter 6. In particular, therein conditions for frequency and voltage stability are derived. Furthermore, the performance of the different control schemes is illustrated and compared via extensive simulation studies in Chapter 7.

The main contributions of the present chapter are two-fold.

(i) **Droop control for SGs and inverters**

The popular droop control laws are introduced. More precisely, by using the traditional droop control for SGs [1, 3, 6] as point of departure, the most commonly employed frequency and voltage droop controls for inverter-interfaced DG units—originally proposed in [37]—are motivated and presented.

Furthermore, it is shown that the dynamics of a regulated SG and an inverter equipped with the typically proposed frequency droop control combined with a low pass filter, e.g., for power measurement [33, 34], are equivalent. Altough several

authors have proposed to make inverters resemble the input/output behavior of SGs [198, 200], to the best of the author's knowledge, this observation has first been stated in the author's work [121] in a mathematically rigorous fashion. Based on this result, compact closed-loop representations of an MDREG, as well as a purely inverter-based microgrid, both operated with droop control, are derived. Moreover, based on [71, 121, 123], a selection criterion on the droop gains and setpoints, similar to the one given in [28], is provided, that ensures active power sharing in steady-state. Compared to [28], the proof is extended to lossy networks, i.e., networks with nonzero conductances.

(ii) **Distributed voltage control (DVC) for reactive power sharing**
A main limitation of the voltage control proposed in [37] is discussed. Namely, this voltage droop control does in general not guarantee a desired reactive power sharing [29, 71, 73]. Recall from Section 1.3, that also for modified voltage control schemes reported in the literature, e.g., [29, 59, 72, 73, 74, 75, 76], no general conditions or formal guarantees for reactive power sharing are given.
Therefore, based on [122, 125], a consensus-based DVC for inverter-based microgrids is proposed. Moreover, following [235], it is shown that the DVC can also be applied to SGs via an appropriate feedback linearization, as previously used, e.g., in [51, 231]. Subsequently, a closed-loop representation of a microgrid operated with frequency droop control and the suggested DVC is derived. Finally, it is proven that the proposed DVC does indeed guarantee reactive power sharing in steady-state.

The remainder of this chapter is outlined as follows. The droop control laws for SGs and inverters are presented and motivated in Section 5.2. The DVC is introduced in Section 5.3.

5.2 Frequency and voltage droop control

The contents of this section are as follows. The droop control schemes are introduced in Section 5.2.1 for SGs and in Section 5.2.2 for inverters. Furthermore, in Section 5.2.3, closed-loop representations of droop-controlled microgrids are derived by combining the droop controls with the microgrid model presented in Chapter 4. In Section 5.2.4, a selection criterion for the control parameters of the frequency droop controls for SGs and inverters is provided, which ensures a desired active power sharing in steady-state. The presentation below is based on [71, 121].

5.2.1 Droop control for synchronous generators

A control technique widely used to address the problems of active power sharing and frequency regulation in conventional power systems is droop control, also referred to as power-speed characteristic [1, Chapter 11]. In droop control, the current value of the rotational speed of each SG in the network is monitored locally to derive how much mechanical power each SG needs to provide. From a control perspective, droop control is a decentralized proportional controller, where the control gain (known as droop gain) specifies the steady-state power distribution in the network. The qualifier "decentralized" is used here to emphasize that only local measurements are used as feedback signals.

Recall the model of an SG given in (4.20). Suppose an SG is connected at the i-th node of a microgrid, $i \in \mathcal{N}_{SG}$. If the turbine is connected to a governing system allowing to set the turbine mechanical power output P_{M_i}, then the SG is called a regulated machine. Assuming a linear relationship between the valve position and the mechanical power as well as ideal governor dynamics and noting that the mechanical speed $\omega_{M_i} : \mathbb{R}_{\geq 0} \to \mathbb{R}$ is connected to the electrical frequency ω_i via $\omega_i = (p_i/2)\omega_{M_i}$ with $p_i \in \mathbb{R}_{>0}$ being the number of machine poles, droop control can be represented as $u_{G_i} : \mathbb{R}_{\geq 0} \to \mathbb{R}$ [1, Chapter 11], [6, Chapter 2]

$$\boxed{u_{G_i} = P_{M_i} = P_{M_i}^d - \frac{1}{\tilde{k}_{P_i}} \left(\omega_i - \omega^d\right),} \tag{5.1}$$

where $\omega^d \in \mathbb{R}_{>0}$ is the nominal (reference) frequency and the constant $P_{M_i}^d \in \mathbb{R}_{>0}$ is the reference setpoint for the mechanical power. Hence, (5.1) is a proportional control law with input signal $(\omega_i - \omega^d)$, gain $1/\tilde{k}_{P_i} \in \mathbb{R}_{>0}$ and output P_{M_i}.

Remark 5.2.1. The desired power setpoint for the mechanical power $P_{M_i}^d$, $i \sim \mathcal{N}_{SG}$, is assumed to be transmitted to each SG by a higher-level control, i.e., typically a secondary control or energy management system. See Section 3.4 for further details on control hierarchy in power systems and microgrids.

5.2.2 Droop control for inverters

Inspired by the droop control (5.1) employed for SGs, researchers have proposed to apply a similar control scheme to inverters, see [37] and, e.g., [30, 33, 54, 55, 56, 60, 61, 236]. The main motivation for this is two-fold. First, and as discussed above, droop control is a decentralized proportional control, which uses the network frequency as an

implicit communication (respectively feedback) link to adjust the active power outputs of the different SGs in a network. It, hence, is a modular and easy to implement plug-and-play-like control scheme, in the sense that no centrally coordinated network control design is required. Second, differently from SGs, inverters do not have an inherent physical relation between frequency and generated active power, see, e.g., the model of an inverter given in (4.16). The frequency droop control aims at artificially creating such a relation, since it is desired in many applications [212].

Furthermore, in large SG-based HV transmission systems droop control is usually only applied to obtain a desired active power distribution, while the voltage amplitude at a generator bus is regulated to a nominal voltage setpoint via an automatic voltage regulator (AVR) acting on the excitation system of the SG [6, Chapter 2.3.2.2]. Unlike in HV transmission systems, in microgrids the power lines are typically relatively short. Then, the AVR employed at the transmission level is, in general, not appropriate because slight differences in voltage amplitudes can cause high power flows, see also Section 3.3.2. Therefore, droop control is typically also applied to set the voltage with the objective to achieve a desired reactive power distribution in microgrids. The most common (heuristic) approach is to set the voltage amplitude via a proportional control, the feedback signal of which is the reactive power generation relative to a reference setpoint [37, 38]. Hence, this control is usually called voltage droop control.

The rationale behind the frequency and voltage droop controllers is as follows [37, 38]. For small angular deviations δ_{ik}, it follows that $\sin(\delta_{ik}) \approx \delta_{ik}$ while $\cos(\delta_{ik}) \approx 1$. Hence, as discussed in Section 3.3.2, for dominantly inductive networks, i.e., $G_{ik} \approx 0$, from the power equations (4.24) it is clear that the reactive power is mostly influenced by changes in the voltage, while the active power depends "more directly" on angular deviations. Consequently, the frequencies ω_i and voltage amplitudes V_i of the inverters ($i \sim \mathcal{N}_I$) are modified depending on the deviations (with respect to a desired value) of the active and reactive powers, respectively.

Recall the model of an inverter given in (4.16). Suppose an inverter is connected at the i-th node of a microgrid, $i \in \mathcal{N}_I$. Following the heuristics outlined previously, simple proportional controllers, called **frequency**, respectively **voltage, droop control** hereafter, are then implemented as

$$\boxed{u_i^\delta = \omega^d - k_{P_i}(P_i^m - P_i^d),} \tag{5.2}$$

$$\boxed{u_i^V = V_i^d - k_{Q_i}(Q_i^m - Q_i^d),} \tag{5.3}$$

where $\omega^d \in \mathbb{R}_{>0}$ is the desired (nominal) frequency, $V_i^d \in \mathbb{R}_{>0}$ the desired (nominal) voltage amplitude, $k_{P_i} \in \mathbb{R}_{>0}$, respectively $k_{Q_i} \in \mathbb{R}_{>0}$, the frequency, respectively voltage, droop gain, $P_i^m : \mathbb{R}_{\geq 0} \to \mathbb{R}$ and $Q_i^m : \mathbb{R}_{\geq 0} \to \mathbb{R}$ are the measured active and reactive powers and $P_i^d \in \mathbb{R}$ and $Q_i^d \in \mathbb{R}$ their desired setpoints.

From the preceding discussion, it is clear that the control laws (5.2)-(5.3) are heuristic control laws derived under the assumption of a dominantly inductive network, i.e., for power lines with small R/X ratios. They are (by far) the most commonly used ones in this scenario. However, if the network lines possess large resistive components, the standard droop control laws (5.2)-(5.3) exhibit limitations [38]. In this case, several modified droop controls [72, 237, 238] have been proposed. Even in the presence of non-negligible line resistances the application of the droop controls of [33, 37] can be justified, on one hand, via the virtual impedance approach [239] while, on the other hand, by invoking their analogy to conventional droop control [212] of SG-based grids, cf. (5.1). The latter fact implies that the control laws (5.2)-(5.3) are well compatible with the operation of conventional power systems [212]. Recall from Section 3.2 that this is an important criterion in the operation of microgrids. Therefore, the analysis in this work is restricted to the control laws (5.2)-(5.3), commonly referred to as "conventional droop control".

Note that, from a control theoretic perspective, the design of the droop controls (5.2)-(5.3) is very similar to a common control design approach for multiple-input multiple-output (MIMO) systems. Namely, to reformulate a MIMO control design problem as a set of decoupled single-input single-output (SISO) control design problems by identifying suitable input/output-pairings of the plant under consideration. This parallel is further discussed in Section 6.6.

Remark 5.2.2. As stated in Remark 5.2.1 for the case of SGs, the desired power setpoints for active and reactive power P_i^d and Q_i^d, $i \sim \mathcal{N}_I$, are assumed to be transmitted to each inverter by a high-level control, i.e., typically a secondary control or energy management system, see, e.g., [79, 195].

Remark 5.2.3. Since an inverter may connect a pure storage device, e.g., a battery, to the network, P_i^d, $i \in \mathcal{N}_I$, can also take negative values. In that case, the storage device is charged depending on the excess power available in the network and thus functions as a frequency and voltage dependent load. In the sequel, such an operation mode is referred to as charging mode.

5.2.3 Closed-loop microgrid under droop control

The closed-loop models for a droop-controlled inverter and a droop-controlled SG are derived based on the models and controls introduced previously. In addition, based on [121] the equivalence of the dynamics of a regulated SG and an inverter equipped with the typically proposed frequency droop control (5.2) combined with a low pass filter, e.g., for power measurement [33], is established.

5.2.3.1 Closed-loop microgrid with distributed rotational and electronic generation under frequency droop control

In the case of droop-controlled MDREGs, the focus of the analysis in the present section and in Chapter 6 is on the dynamics of the DG units with respect to active power and frequency. For that scenario, the assumption below is made.

Assumption 5.2.4. *All voltage amplitudes V_i, $i \sim \mathcal{N}$, are positive real constants for all $t \geq 0$.*

Note that Assumption 5.2.4 is a standard assumption in stability analysis of power systems and microgrids, see, e.g., [28, 36, 50, 113, 121, 176, 240]. Under Assumption 5.2.4 the **closed-loop model of the frequency droop-controlled inverter** at the i-th node, $i \in \mathcal{N}_I$, is obtained by replacing (5.2) in (4.16) as

$$\boxed{\begin{aligned} \dot{\delta}_i &= \omega^d - k_{P_i}(P_i^m - P_i^d) - \omega^{\text{com}}, \\ \tau_{P_i}\dot{P}_i^m &= -P_i^m + P_i, \end{aligned}} \tag{5.4}$$

where $P_i(\delta_1, \ldots, \delta_n)$ is given by (4.24). Moreover, under Assumption 5.2.4 and by defining

$$k_{P_i} := \frac{\tilde{k}_{P_i}}{1 + \tilde{k}_{P_i} D_i},$$

the **closed-loop model of the droop-controlled SG** at the i-th node, $i \in \mathcal{N}_{SG}$, is given by combining (4.20) and (5.1) as

$$\boxed{\begin{aligned} \dot{\delta}_i &= \omega_i - \omega^{\text{com}}, \\ M_i\dot{\omega}_i &= -\frac{1}{k_{P_i}}(\omega_i - \omega^d) + P_{M_i}^d - P_i, \end{aligned}} \tag{5.5}$$

where $P_i(\delta_1, \ldots, \delta_n)$ is given by (4.24).

In the following, it is shown—via an affine state transformation—that the input-output dynamics of a droop-controlled SG given by (5.5) and a frequency droop-controlled inverter given by (5.4) are identical with respect to the input-output pair

(P_i, δ_i). To see this, define the states, input and output of the frequency droop-controlled inverter (5.4) as

$$x_{\mathrm{Inv},i} := \begin{bmatrix} \delta_i \\ P_i^m \end{bmatrix}, \quad u_{\mathrm{Inv},i} := P_i, \quad y_{\mathrm{Inv},i} := \delta_i,$$

and write the constants ω^{com}, ω^d and $k_{P_i} P_i^d$ in vector form as

$$d_{\mathrm{Inv},i} := \begin{bmatrix} \omega^{\mathrm{com}} \\ \omega^d + k_{P_i} P_i^d \end{bmatrix}.$$

Define the corresponding quantities for the droop-controlled SG (5.5) as

$$x_{\mathrm{SG},i} := \begin{bmatrix} \delta_i \\ \omega_i \end{bmatrix}, \quad u_{\mathrm{SG},i} := P_i, \quad y_{\mathrm{SG},i} := \delta_i, \quad d_{\mathrm{SG},i} := \begin{bmatrix} \omega^{\mathrm{com}} \\ \omega^d + k_{P_i} P_{M_i}^d \end{bmatrix}. \tag{5.6}$$

Then, (5.4) can be written as

$$\begin{aligned} \dot{x}_{\mathrm{Inv},i} &= A_{\mathrm{Inv},i} x_{\mathrm{Inv},i} + B_{\mathrm{Inv},i} u_{\mathrm{Inv},i} + D_{\mathrm{Inv},i} d_{\mathrm{Inv},i}, \\ y_{\mathrm{Inv},i} &= C_{\mathrm{Inv},i} x_{\mathrm{Inv},i} \end{aligned} \tag{5.7}$$

with

$$A_{\mathrm{Inv},i} = \begin{bmatrix} 0 & -k_{P_i} \\ 0 & -\frac{1}{\tau_{P_i}} \end{bmatrix}, \quad B_{\mathrm{Inv},i} = \begin{bmatrix} 0 \\ \frac{1}{\tau_{P_i}} \end{bmatrix}, \quad D_{\mathrm{Inv},i} = \begin{bmatrix} -1 & 1 \\ 0 & 0 \end{bmatrix}, \quad C_{\mathrm{Inv},i} = \begin{bmatrix} 1 & 0 \end{bmatrix}.$$

Likewise, (5.5) can be written as

$$\begin{aligned} \dot{x}_{\mathrm{SG},i} &= A_{\mathrm{SG},i} x_{\mathrm{SG},i} + B_{\mathrm{SG},i} u_{\mathrm{SG},i} + D_{\mathrm{SG},i} d_{\mathrm{SG},i}, \\ y_{\mathrm{SG},i} &= C_{\mathrm{SG},i} x_{\mathrm{SG},i} \end{aligned} \tag{5.8}$$

with

$$A_{\mathrm{SG},i} = \begin{bmatrix} 0 & 1 \\ 0 & -\frac{1}{M_i k_{P_i}} \end{bmatrix}, \quad B_{\mathrm{SG},i} = \begin{bmatrix} 0 \\ -\frac{1}{M_i} \end{bmatrix}, \quad D_{\mathrm{SG},i} = \begin{bmatrix} -1 & 0 \\ 0 & \frac{1}{M_i k_{P_i}} \end{bmatrix}, \quad C_{\mathrm{SG},i} = \begin{bmatrix} 1 & 0 \end{bmatrix}.$$

Consider the affine state-transformation

$$\bar{x}_{\mathrm{Inv},i} = T_{\mathrm{Inv},i} x_{\mathrm{Inv},i} + \begin{bmatrix} 0 & 0 \\ 0 & 1 \end{bmatrix} d_{\mathrm{Inv},i}, \quad T_{\mathrm{Inv},i} = \begin{bmatrix} 1 & 0 \\ 0 & -k_{P_i} \end{bmatrix}. \tag{5.9}$$

In the coordinates $\bar{x}_{\mathrm{Inv},i}$, (5.7) becomes

$$\begin{aligned} \dot{\bar{x}}_{\mathrm{Inv},i} &= \bar{A}_{\mathrm{Inv},i} \bar{x}_{\mathrm{Inv},i} + \bar{B}_{\mathrm{Inv},i} u_{\mathrm{Inv},i} + \bar{D}_{\mathrm{Inv},i} d_{\mathrm{Inv},i}, \\ y_{\mathrm{Inv},i} &= C_{\mathrm{Inv},i} \bar{x}_{\mathrm{Inv},i} \end{aligned} \tag{5.10}$$

with

$$\bar{A}_{\mathrm{Inv},i} = T_{\mathrm{Inv},i} A_{\mathrm{Inv},i} T_{\mathrm{Inv},i}^{-1} = \begin{bmatrix} 0 & 1 \\ 0 & -\frac{1}{\tau_{P_i}} \end{bmatrix}, \quad \bar{B}_{\mathrm{Inv},i} = T_{\mathrm{Inv},i} B_{\mathrm{Inv},i} = \begin{bmatrix} 0 \\ -\frac{k_{P_i}}{\tau_{P_i}} \end{bmatrix},$$
$$\bar{D}_{\mathrm{Inv},i} = -\bar{A}_{\mathrm{Inv},i} \begin{bmatrix} 0 & 0 \\ 0 & 1 \end{bmatrix} + T_{\mathrm{Inv},i} D_{\mathrm{Inv},i} = \begin{bmatrix} 0 & -1 \\ 0 & \frac{1}{\tau_{P_i}} \end{bmatrix} + \begin{bmatrix} -1 & 1 \\ 0 & 0 \end{bmatrix} = \begin{bmatrix} -1 & 0 \\ 0 & \frac{1}{\tau_{P_i}} \end{bmatrix}.$$

Furthermore, by defining

$$\tau_{P_i} := k_{P_i} M_i, \quad P_i^d := P_{M_i}^d, \quad i \sim \mathcal{N}_{SG}, \tag{5.11}$$

the dynamics (5.8) take exactly the form (5.10). Hence, the input-output dynamics of a droop-controlled SG and a frequency droop-controlled inverter are identical with respect to the input-output pair (P_i, δ_i). Consequently, (5.10) is used in the following to describe either of the abovementioned closed-loop systems. Furthermore, in analogy to (5.6), the second element of the state vector $\bar{x}_{\mathrm{Inv},i}$ is denoted by ω_i, $i \sim \mathcal{N}_I$.

To simplify notation let

$$\begin{aligned} \delta :=& \mathrm{col}(\delta_i) \in \mathbb{T}^n, \quad \omega := \mathrm{col}(\omega_i) \in \mathbb{R}^n, \\ P^d :=& \mathrm{col}(P_i^d) \in \mathbb{R}^n, \quad P := \mathrm{col}(P_i) \in \mathbb{R}^n, \\ T :=& \mathrm{diag}(\tau_{P_i}) \in \mathbb{R}^{n \times n}, K_P := \mathrm{diag}(k_{P_i}) \in \mathbb{R}_{>0}^{n \times n}. \end{aligned} \tag{5.12}$$

Then, the system given by (5.10) can be compactly written as

$$\boxed{\begin{aligned} \dot{\delta} &= \omega - \underline{1}_n \omega^{\mathrm{com}}, \\ T\dot{\omega} &= -\omega + \underline{1}_n \omega^d - K_P(P - P^d), \end{aligned}} \tag{5.13}$$

with power flows $P(\delta)$ given in (4.24). Furthermore, a power rating $S_i^N \in \mathbb{R}_{>0}$, $i \sim \mathcal{N}$, is associated to each generation source.

Remark 5.2.5. It follows from (5.10) that if one main control design intention for an inverter operated in grid-forming mode is to achieve a behavior with respect to frequency similar to that of an SG, the rather simple structure given in (5.4) is sufficient and no additional components are required. Moreover, (5.10) together with (5.11) reveal that the time constant τ_{P_i} of the low pass filter can be used as additional design parameter to shape the desired "virtual" inertia coefficient M_i of the inverter. Methods to emulate additional characteristics of SGs are proposed, e.g., in [198, 199, 200].

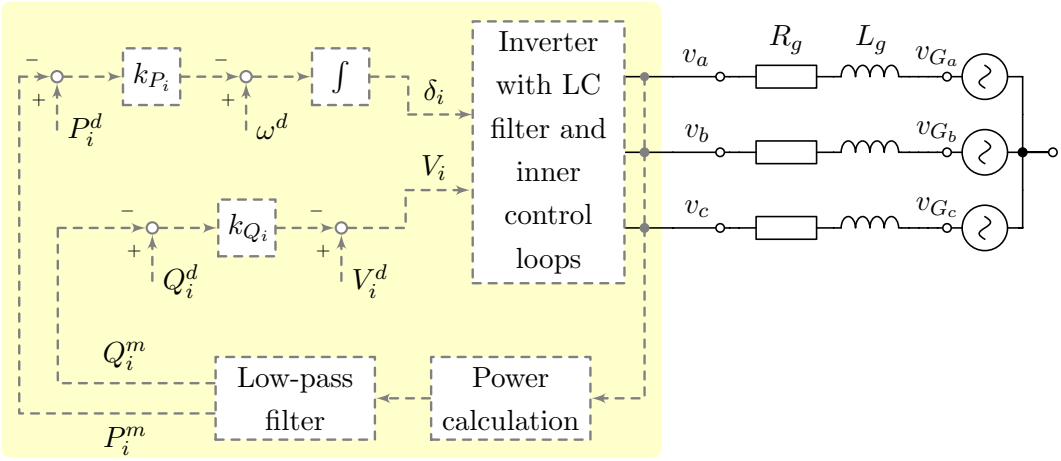

Figure 5.1: Block diagram of a droop-controlled inverter at node $i \in \mathcal{N}_I$ modeled by (5.14). Bold lines represent power connections, while dashed lines represent signal connections. The parameters are as follows: $\omega^d \in \mathbb{R}_{>0}$ is the desired (nominal) frequency, $V_i^d \in \mathbb{R}_{>0}$ the desired (nominal) voltage amplitude, $k_{P_i} \in \mathbb{R}_{>0}$, respectively $k_{Q_i} \in \mathbb{R}_{>0}$, the frequency, respectively voltage, droop gain, $P_i^m : \mathbb{R}_{\geq 0} \to \mathbb{R}$ and $Q_i^m : \mathbb{R}_{\geq 0} \to \mathbb{R}$ are the measured powers and $P_i^d \in \mathbb{R}$ and $Q_i^d \in \mathbb{R}$ their desired setpoints.

5.2.3.2 Closed-loop inverter-based microgrid under droop control

In the previous section, a model of an MDREG has been derived under the assumption of constant voltage amplitudes. Next, this assumption is dropped and a model of an inverter-based microgrid, i.e., $\mathcal{N} = \mathcal{N}_I$, containing inverter models with variable frequencies, as well as variable voltage amplitudes is derived.

The **closed-loop model of the droop-controlled inverter** at the i-th node, $i \in \mathcal{N}$, is obtained by replacing (5.2) and (5.3) in (4.16) as

$$\begin{aligned} \dot{\delta}_i &= \omega^d - k_{P_i}(P_i^m - P_i^d) - \omega^{\text{com}}, \\ \tau_{P_i}\dot{P}_i^m &= -P_i^m + P_i, \\ V_i &= V_i^d - k_{Q_i}(Q_i^m - Q_i^d), \\ \tau_{P_i}\dot{Q}_i^m &= -Q_i^m + Q_i, \end{aligned} \tag{5.14}$$

where $P_i(\delta_1, \ldots, \delta_n, V_1, \ldots, V_n)$ and $Q_i(\delta_1, \ldots, \delta_n, V_1, \ldots, V_n)$ are given by (4.24). A block diagram of an inverter modeled by (4.16) and controlled with the droop control (5.2) and (5.3) is shown in Fig. 5.1.

Based on (5.14), (5.9) and (5.10), the closed-loop model of a droop-controlled inverter used for the analysis, is also established via a change of coordinates. To this end, note that the system (5.14) can be viewed as being composed of two subsystems,

the first of which is given by

$$\begin{aligned} \dot{\delta}_i &= \omega^d - k_{P_i}(P_i^m - P_i^d) - \omega^{\text{com}}, \\ \tau_{P_i}\dot{P}_i^m &= -P_i^m + P_i \end{aligned} \tag{5.15}$$

with states (δ_i, P_i^m), input $P_i(\delta_1, \ldots, \delta_n, V_1, \ldots, V_n)$ and output δ_i, and the second of which is given by

$$\begin{aligned} V_i &= V_i^d - k_{Q_i}(Q_i^m - Q_i^d), \\ \tau_{P_i}\dot{Q}_i^m &= -Q_i^m + Q_i, \end{aligned} \tag{5.16}$$

with state Q_i^m, input $Q_i(\delta_1, \ldots, \delta_n, V_1, \ldots, V_n)$ and output V_i.

By noting that (5.15) is identical to (5.7), the coordinate transformation (5.9) is employed to perform the change of coordinates of the subsystem (5.15). This yields (5.10). In a similar manner, define for the second subsystem (5.16)

$$x_{V,i} := Q_i^m, \quad u_{V,i} := Q_i, \quad y_{V,i} := V_i, \quad d_{V,i} := V_i^d + k_{Q_i}Q_i^d$$

and write (5.16) as

$$\begin{aligned} \dot{x}_{V,i} &= A_{V,i}x_{V,i} + B_{V,i}u_{V,i}, \\ y_{V_i} &= C_{V,i}x_{V,i} + D_{V,i}d_{V,i}, \end{aligned} \tag{5.17}$$

where

$$A_{V,i} = -\frac{1}{\tau_{P_i}}, \quad B_{V,i} = \frac{1}{\tau_{P_i}}, \quad C_{V,i} = -k_{Q_i}, \quad D_{V,i} = 1.$$

With the affine change of coordinates

$$\bar{x}_{V,i} = T_{V,i}x_{V,i} + d_{V,i}, \quad T_{V,i} = -k_{Q_i},$$

(5.17) reads

$$\begin{aligned} \dot{\bar{x}}_{V,i} &= \bar{A}_{V,i}\bar{x}_{V,i} + \bar{B}_{V,i}u_{V,i} + \bar{D}_{V,i}d_{V,i}, \\ y_{V_i} &= \bar{C}_{V,i}\bar{x}_{V,i}, \end{aligned} \tag{5.18}$$

where

$$\begin{aligned} \bar{A}_{V,i} &= T_{V,i}A_{V,i}T_{V,i}^{-1} = A_{V,i}, \quad \bar{B}_{V,i} = T_{V,i}B_{V,i} = -\frac{k_{Q_i}}{\tau_{P_i}}, \\ \bar{C}_{V,i} &= C_{V,i}T_{V,i}^{-1} = 1, \quad \bar{D}_{V,i} = -T_{V,i}A_{V,i}T_{V,i}^{-1}D_{V,i} = \frac{1}{\tau_{P_i}}. \end{aligned}$$

Hence, (5.14) can equivalently be written as

$$\boxed{\begin{aligned} \dot{\delta}_i &= \omega_i - \omega^{\text{com}}, \\ \tau_{P_i}\dot{\omega}_i &= -\omega_i + \omega^d - k_{P_i}(P_i - P_i^d), \\ \tau_{P_i}\dot{V}_i &= -V_i + V_i^d - k_{Q_i}(Q_i - Q_i^d), \end{aligned}} \tag{5.19}$$

which is the model of a droop-controlled inverter used in the subsequent analysis. To simplify notation recall $\mathcal{N} = \mathcal{N}_I$, as well as (5.12) and let

$$\begin{aligned} V :=& \mathrm{col}(V_i) \in \mathbb{R}^n_{\geq 0}, \quad V^d := \mathrm{col}(V_i^d) \in \mathbb{R}^n_{>0} \\ Q^d :=& \mathrm{col}(Q_i^d) \in \mathbb{R}^n, \quad Q := \mathrm{col}(Q_i) \in \mathbb{R}^n, \\ K_Q :=& \mathrm{diag}(k_{Q_i}) \in \mathbb{R}^{n\times n}_{>0}. \end{aligned} \tag{5.20}$$

Then, the system given by (5.19) and (4.24) can be compactly written as

$$\boxed{\begin{aligned} \dot{\delta} &= \omega - \underline{1}_n \omega^{\mathrm{com}}, \\ T\dot{\omega} &= -\omega + \underline{1}_n \omega^d - K_P(P - P^d), \\ T\dot{V} &= -V + V^d - K_Q(Q - Q^d), \end{aligned}} \tag{5.21}$$

with power flows $P(\delta, V)$ and $Q(\delta, V)$ given in (4.24). Furthermore, a power rating $S_i^N \in \mathbb{R}_{>0}$, $i \sim \mathcal{N}$, is associated to each generation source.

5.2.4 Active power sharing under frequency droop control

In [28], a criterion on the frequency droop gains and setpoints has been derived such that the generation units share the active power according to their power ratings in steady-state. This is a desired control goal in many applications. However, it has been argued in [62] that system operators may not always seek to achieve a power sharing in proportion to the power ratings of the units. Instead, they may also wish to take into account other technical, economic or environmental criteria, such as fuel consumption, generation costs or emission costs, see also [241].

In this regard, the ideas derived in [28] are easily applied to proportional active power sharing with respect to a user-defined criterion, cf. Definition 3.3.1. Compared to [28], the proof is extended to lossy networks, i.e., networks with nonzero conductances, as well as to MDREGs. It turns out that the same criterion ensures that storage devices in charging mode, i.e., $P_i^d < 0$ for some $i \in \mathcal{N}_I$, are charged proportionally.

Lemma 5.2.6. *Consider the system* (5.13), (4.24)*, respectively* (5.21), (4.24)*. Assume that it possesses a steady-state motion with constant frequency $\omega^s \in \mathbb{R}$. Then all generation units the power outputs of which satisfy*[1] *$\mathrm{sign}(P_i^s) = \mathrm{sign}(P_k^s)$, achieve proportional active power sharing if the gains k_{P_i} and k_{P_k} and the active power setpoints P_i^d and P_k^d are chosen such that*

$$k_{P_i}\gamma_i = k_{P_k}\gamma_k \text{ and } k_{P_i}P_i^d = k_{P_k}P_k^d, \tag{5.22}$$

$i \sim \mathcal{N}$ and $k \sim \mathcal{N}$.

[1] Recall from Definition 3.3.1 that the superscript s denotes signals in steady-state.

Proof. The claim follows in a straightforward manner from [28], where it has been shown for first-order inverter models and $\gamma_i = S_i^N$, $P_i^d > 0$, $P_i^s > 0$, $i \sim \mathcal{N}$. For a constant steady-state frequency $\omega_i = \omega^s$, $i \sim \mathcal{N}$, it follows from (5.13), (4.24) that

$$\dot{\omega}_i = 0 = -\omega^s + \omega^d - k_{P_i}(P_i^s - P_i^d), \quad i \sim \mathcal{N}.$$

Hence, under conditions (5.22), along the steady-state motion,

$$\frac{P_i^s}{\gamma_i} = \frac{-\omega^s + \omega^d + k_{P_i} P_i^d}{k_{P_i}\gamma_i} = \frac{-\omega^s + \omega^d + k_{P_k} P_k^d}{k_{P_k}\gamma_k} = \frac{P_k^s}{\gamma_k},$$

where $i \in \mathcal{N}$ and $k \in \mathcal{N}$ with $\operatorname{sign}(P_i^s) = \operatorname{sign}(P_k^s)$. □

Remark 5.2.7. The conditions in Lemma 5.2.6 also imply that storage devices in charging mode are charged proportionally.

Remark 5.2.8. In the present case, active power sharing can be achieved without the need of any explicit communication exchange. This is explained by the fact that the frequency serves as an implicit communication signal.

Remark 5.2.9. Note that proportional active power sharing is achieved by Lemma 5.2.6 independently of the admittance values of the network. However, in a highly ohmic network, the droop control laws (5.2)-(5.3) may induce high fluctuating currents due to the stronger coupling of phase angles and reactive power, see (4.24). Then, additional methods such as the virtual output impedance [239] or alternative droop control laws [72] could be employed instead of (5.2)-(5.3).

Remark 5.2.10. Recall the inverter model (4.13), which takes into account the drift of the internal clock of the inverter at the i-th node, $i \in \mathcal{N}_I$. It is easy to see that (5.10) and, equivalently, the (δ, ω)-dynamics of (5.19) then become

$$\begin{aligned} (1+\upsilon_i)\dot{\delta}_i &= \omega_i - \omega^{\mathrm{com}}, \\ (1+\upsilon_i)\tau_{P_i}\dot{\omega}_i &= -\omega_i + \omega^d - k_{P_i}(P_i - P_i^d), \end{aligned} \tag{5.23}$$

where υ_i denotes the constant[1] relative drift of the clock of the i-th inverter. Suppose that the constant synchronization frequency of the system (5.23), (4.24) is given by $\omega^N \in \mathbb{R}_{>0}$. As shown in [124], it follows from inspection of (5.23) that under the presence of a clock drift

$$\dot{\delta}_i^s = \frac{\omega_i^s - \omega^{\mathrm{com}}}{(1+\upsilon_i)} = \omega^N \quad \Rightarrow \quad \omega_i^s = \omega^{\mathrm{com}} + (1+\upsilon_i)\omega^N, \quad i \sim \mathcal{N}_I, \tag{5.24}$$

Hence, (5.24) shows that if inverters with clock drifts are modeled by (5.23), then the internal synchronization frequencies ω_i^s, $i \sim \mathcal{N}_I$, of the inverters are scaled by the factors $(1+\upsilon_i)$ with respect to the network synchronization frequency ω^N.

[1] Over large periods of time, i.e., several weeks or months, the relative clock drift υ_i may vary depending, e.g., on the ambient temperature or aging effects.

Remark 5.2.11. The presence of unknown constant clock drifts also has a deteriorating effect on the active power sharing accuracy. To see this, consider a microgrid in which the inverters are modeled by (5.23), (4.24). Consider a pair of nodes $(i,k) \in \mathcal{N}_I \times \mathcal{N}_I$, $i \neq k$, the power outputs of which satisfy $\operatorname{sign}(P_i^s) = \operatorname{sign}(P_k^s)$ and the parameters of which have been selected according to (5.22). Recall that υ_i and υ_k denote the nonzero constant unknown clock drifts. Suppose the network possesses a synchronized motion with constant synchronization frequency $\omega^N \in \mathbb{R}_{>0}$. Then, together with (5.24), the ratio of the weighted active power outputs of the two inverters along a synchronized motion is given by

$$\frac{P_i^s/\gamma_i}{P_k^s/\gamma_k} = \frac{(-\omega_i^s + k_{P_i} P_i^d + \omega^d) k_{P_k} \gamma_k}{(-\omega_k^s + k_{P_k} P_k^d + \omega^d) k_{P_i} \gamma_i} = \frac{-\upsilon_i \omega^N + c}{-\upsilon_k \omega^N + c} \neq 1, \tag{5.25}$$

where $c := k_{P_i} P_i^d + \omega^d - \omega^N - \omega^{\mathrm{com}} = k_{P_k} P_k^d + \omega^d - \omega^N - \omega^{\mathrm{com}}$. However, since in general $|\upsilon_i| \ll 1$ and $|\upsilon_k| \ll 1$, (5.25) also shows that the introduced error in power sharing is negligible in most practical scenarios. Therefore, the selection criteria (5.22) seem also appropriate in the presence of clock drifts.

5.3 Distributed voltage control and reactive power sharing

As described in Section 5.2.2, the voltage droop control law (5.3) follows a similar heuristic approach as the frequency droop control law (5.2), aiming at obtaining a desired reactive power distribution in a steady-state. Recall that the physical motivation for the control laws (5.2) and (5.3) is based on the power flow over a dominantly inductive power line. However, even in this scenario, the voltage droop control (5.3) does, in general, not achieve a desired reactive power sharing, see, e.g., [29, 71, 72, 73]. This, possibly unexpected, behavior of the voltage droop control (5.3) is explained as follows. The conditions for proportional active power sharing in Lemma 5.2.6 are derived using the fact that the frequency of a steady-state motion of the system (5.13), (4.24) is equal all over the network, i.e., $\omega_i^s = \omega_k^s = \ldots = \omega^s$, and serves thus as a common communication signal. This is not the case for the voltage, since, in general, $V_i^s \neq V_k^s$ for $i \in \mathcal{N}$, $k \in \mathcal{N}$. In addition, V_i^s, $i \sim \mathcal{N}$, are not known beforehand and change depending on the load demand in the network (if set with the voltage droop control (5.3)).

Therefore, a consensus-based DVC, which guarantees reactive power sharing in steady-state is proposed in the following. The suggested DVC has originally been introduced in [122, 125] for grid-forming inverters. In addition, based on [235], it is

shown that, via a suitable partial feedback linearization, the proposed DVC can easily be extended to SGs.

The remainder of this section is based on [122, 125, 235] and outlined as follows. The communication topology is depicted in Section 5.3.1. The proposed DVC for an inverter is presented in Section 5.3.2. Given the different dynamics of SGs compared to inverters, the DVC is adapted to SGs in Section 5.3.3. The closed-loop microgrid dynamics obtained by combining the inverter, respectively SG, model with the corresponding frequency droop control and DVC are given in Section 5.3.4. Finally, it is proven in Section 5.3.5 that the proposed DVC guarantees reactive power sharing in steady-state.

5.3.1 Communication topology

The proposed voltage control is distributed and requires communication among generation units in the network. To describe the high-level properties of the communication network, a graph theoretic notation—as introduced in Section 2.3.5—is used.

It is assumed that the communication network is represented by an undirected, unweighted and connected graph $\mathcal{G} = (\mathcal{V}, \mathcal{E})$. Furthermore, it is assumed that the graph contains no self-loops, i.e., there is no edge $e_l = (i, i)$, $i \sim \mathcal{N}$. Recall that a node represents an individual agent. In the present case, this is a power generation source. If there is an edge between two nodes i and k, then i and k can exchange their local measurements with each other. The set of neighbors of the i-th node is denoted by $\mathcal{C}_i$. The nodes in the communication and in the electrical network are identical, i.e., $\mathcal{N} = \mathcal{V}$. Note that the communication topology may, but does not necessarily have to, coincide with the topology of the electrical network, i.e., it is allowed that $\mathcal{C}_i \neq \mathcal{N}_i$ for any $i \in \mathcal{V}$.

5.3.2 Distributed voltage control for inverters

Recall that, as discussed in Section 3.3.2, for dominantly inductive networks, i.e., $G_{ik} \approx 0$, and for small angular deviations, i.e., $\delta_{ik} \approx 0$, the reactive power flow of the i-th node Q_i given in (4.24) reduces to $Q_i : \mathbb{R}^n_{\geq 0} \to \mathbb{R}$,

$$Q_i(V_1, \ldots, V_n) = |B_{ii}|V_i^2 - \sum_{k \sim \mathcal{N}_i} |B_{ik}|V_i V_k. \tag{5.26}$$

Clearly, the reactive power Q_i can then be controlled by controlling the voltage amplitudes V_i and V_k, $k \sim \mathcal{N}_i$. Therefore, inspired by consensus-algorithms, see Section 2.3.5

or, e.g., [85], the following **distributed voltage control (DVC)** u_i^V is proposed for an inverter at node $i \in \mathcal{N}$

$$\begin{aligned} u_i^V(t) &:= V_i^d - k_i \int_0^t e_i(\tau) d\tau, \\ e_i(t) &:= \sum_{k \sim \mathcal{C}_i} \left(\frac{Q_i^m(t)}{\chi_i} - \frac{Q_k^m(t)}{\chi_k} \right) = \sum_{k \sim \mathcal{C}_i} (\bar{Q}_i(t) - \bar{Q}_k(t)), \end{aligned} \tag{5.27}$$

where $V_i^d \in \mathbb{R}_{>0}$ is the desired (nominal) voltage amplitude and $k_i \in \mathbb{R}_{>0}$ is a feedback gain. For convenience, the weighted reactive power flows $\bar{Q}_i := Q_i^m/\chi_i$, $i \sim \mathcal{N}$, have been defined. Recall that $\mathcal{C}_i$ is the set of neighbor nodes of node i in the graph induced by the communication network, i.e., the set of nodes that node i can exchange information with. The control scheme is illustrated for an inverter at node $i \in \mathcal{N}$ in Fig. 5.2. It is proven in Section 5.3.5 that the control (5.27) does guarantee proportional reactive power sharing in steady-state.

Note that opposed to the voltage droop control (5.3), the control law (5.27) does not require setpoints Q_i^d, $i \sim \mathcal{N}_I$, for the reactive power output, which, as discussed previously, are difficult to obtain in practice.

Remark 5.3.1. The proposed voltage control law (5.27) is a *distributed* control, which requires communication exchange. Most control approaches proposed so far to achieve proportional reactive power sharing, e.g., [26, 27], require a central control and/or communication unit or all-to-all communication among all inverters. On the contrary, for the control (5.27) proposed here, the only requirement on the communication topology is that the graph induced by the communication network is connected.

Remark 5.3.2. Consider a scenario in which there exists a high-level control that can generate setpoints $Q_i^d \in \mathbb{R}$, $i \sim \mathcal{N}_I$, for the reactive power injections. A possible high-level control is, for example, the one proposed in [80]. The control (5.27) can easily be combined with such high-level control by setting e_i given in (5.27) to

$$e_i = \sum_{k \sim \mathcal{C}_i} \left(\frac{(Q_i^m - Q_i^d)}{\chi_i} - \frac{(Q_k^m - Q_k^d)}{\chi_k} \right). \tag{5.28}$$

This implies that the inverters share their absolute reactive power injections with respect to individual setpoints in steady-state.

Remark 5.3.3. In addition to reactive power sharing, it usually is desired that the voltage amplitudes V_i, $i \sim \mathcal{N}_I$, remain within certain boundaries. With the above control law (5.27), where the voltage amplitudes are actuator signals, this can, e.g., be ensured by saturating the control signal u_i^V. For mathematical simplicity, this is not considered in the present analysis.

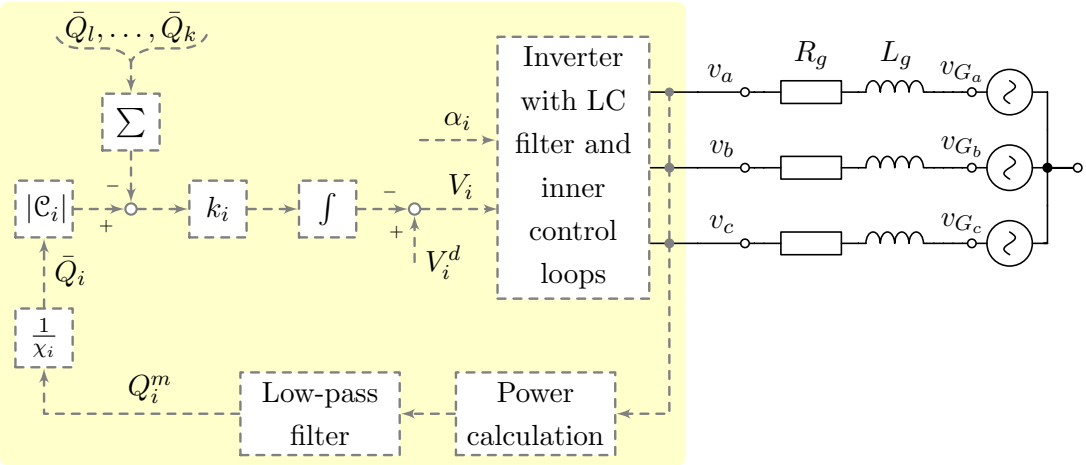

Figure 5.2: Block diagram of the proposed DVC (5.27) for an inverter at node $i \in \mathcal{N}_I$. Bold lines represent power connections, while dashed lines represent signal connections. $V_i : \mathbb{R}_{\geq 0} \to \mathbb{R}_{\geq 0}$ is the voltage amplitude, $V_i^d \in \mathbb{R}_{>0}$ its desired (nominal) value, $Q_i^m : \mathbb{R}_{\geq 0} \to \mathbb{R}$ is the measured reactive power and $\bar{Q}_i : \mathbb{R}_{\geq 0} \to \mathbb{R}$ the weighted reactive power, where $\chi_i \in \mathbb{R}_{>0}$ is the weighting coefficient to ensure proportional reactive power sharing and $k_i \in \mathbb{R}_{>0}$ is a feedback gain. Furthermore, $\bar{Q}_l, \ldots, \bar{Q}_k$ are the weighted reactive power measurements of the inverter outputs at the neighbor nodes $\mathcal{C}_i = \{l, \ldots, k\}$ provided by the communication system.

Remark 5.3.4. Communication delays or failures, such as package losses, are not considered in this work. As in any communication-based control, such events can be critical. In the present case, the voltage amplitude is an actuator signal. Hence, it could, for example, be set to a constant value in case of a severe communication failure.

The closed-loop model of a grid-forming inverter modeled by (4.16) operated with the frequency droop control (5.2) and the suggested DVC (5.27) is obtained as follows. By differentiating $V_i = u_i^V$ with respect to time, combining (5.27) and (4.16) and recalling (5.10), the **closed-loop dynamics of the inverter at the i-th node**, $i \in \mathcal{N}_I$, are given by

$$\boxed{\begin{aligned} \dot{\delta}_i &= \omega_i - \omega^{\text{com}}, \\ \tau_{P_i}\dot{\omega}_i &= -\omega_i + \omega^d - k_{P_i}(P_i - P_i^d), \\ \dot{V}_i &= -k_i e_i = -k_i \sum_{k \sim \mathcal{C}_i} \left(\frac{Q_i^m}{\chi_i} - \frac{Q_k^m}{\chi_k} \right), \\ \tau_{P_i}\dot{Q}_i^m &= -Q_i^m + Q_i, \end{aligned}} \tag{5.29}$$

and the interaction between nodes is modeled by (4.24). Note that $V_i(0) = V_i^d$ is determined by the control law (5.27).

5.3.3 Distributed voltage control for synchronous generators

Based on [235], it is shown how the DVC for grid-forming inverters given in (5.27) can also be applied to SGs modeled by (4.20). The key idea of the approach is to render the voltage dynamics of an SG given by (4.20) identical to those of an inverter modeled by (4.16) via a partial feedback linearization. Then, identical mathematical tools as employed for the analysis of purely inverter-based microgrids in [122, 125] can be used to analyze the dynamics of MDREGs under the DVC.

Partial feedback linearization is widely employed in control design of SGs, see, e.g., [51, 224, 225, 227, 228, 231]. Following [51, 231], the assumption below is made.

Assumption 5.3.5. *The parameters X_{d_i}, X'_{d_i} and τ_{d0_i} are exactly known, $i \sim \mathcal{N}_{SG}$. Moreover, V_i and I_{d_i} are measurable, $i \sim \mathcal{N}_{SG}$.*

The validity of Assumption 5.3.5 is justified as follows. Usually, the values for X_{d_i}, X'_{d_i} and τ_{d0_i} are provided by manufacturers of SGs in the respective data-sheet. Hence, these values are tpyically available. The output current and voltages at the terminals of the SG are typically also measured. Furthermore, the shaft angle θ_i can also be measured. Hence, I_{d_i} can be made available[1]. The EMF, denoted here by V_i, can not be measured directly. However, if θ_i is measured, V_i can be calculated from the terminal voltage by means of (4.19) since the values of R_i and X'_{q_i} are usually also provided by the manufacturer.

Consider the following partial linearizing feedback

$$E_{f_i} := V_i - (X_{d_i} - X'_{d_i})I_{d_i} + \tau_{d0_i}\vartheta_i^V, \tag{5.30}$$

with $\vartheta_i^V : \mathbb{R}_{\geq 0} \to \mathbb{R}$. Applying the control law (5.30) under Assumption 5.3.5 to the SG dynamics (4.20) yields

$$\begin{aligned} \dot{\delta}_i &= \omega_i - \omega^{\text{com}}, \\ M_i\dot{\omega}_i &= -D_i\omega_i + P_{M_i} - P_i, \\ \dot{V}_i &= \vartheta_i^V. \end{aligned} \tag{5.31}$$

[1]The quantity I_{d_i} describes the current flow along the d-axis of the i-th machine. Note that the expression for I_{d_i} given in (4.22) is a function of the variables δ_i, and V_i, $i \sim \mathcal{N}$, where each δ_i is expressed on the common network reference frame. This is done in order be able to interconnect the i-th machine with the network model, cf. Section 2.4.4. However, in practice, if the shaft angle θ_i and the three-phase current i_{abc_i} at the machine terminal are measured, then I_{d_i} can directly be computed as $I_{dq_i} = T_{dq}(\theta_i)i_{abc_i}$.

For the purpose of reactive power sharing and as done in the case of an inverter, cf. (4.16), it is assumed that reactive power output is measured and processed through a filter, i.e.,

$$\tau_{Q_i}\dot{Q}_i^m = -Q_i^m + Q_i, \tag{5.32}$$

where Q_i is the reactive power output of the SG at the i-th node, $Q_i^m : \mathbb{R}_{\geq 0} \to \mathbb{R}$ its measured value and $\tau_{Q_i} \in \mathbb{R}_{>0}$ is the time constant of the low pass filter.

Following (5.27), a **DVC for an SG** with dynamics given by (5.31) is proposed as

$$\boxed{\vartheta_i^V := -k_i e_i = -k_i \sum_{k\sim\mathcal{C}_i} \left(\frac{Q_i^m}{\chi_i} - \frac{Q_k^m}{\chi_k} \right) = -k_i \sum_{k\sim\mathcal{C}_i} (\bar{Q}_i - \bar{Q}_k),} \tag{5.33}$$

where $k_i \in \mathbb{R}_{>0}$ is a feedback gain, χ_i and χ_k are weighting coefficients and $\mathcal{C}_i$ denotes the set of neighbors of node i in the communication network.

Combining (5.31), (5.32) and (5.33), as well as recalling (5.10) to simplify notation, yields the following **closed-loop model of the SG with droop control** (5.1) **and DVC** (5.33) at the i-th node

$$\boxed{\begin{aligned} \dot{\delta}_i &= \omega_i - \omega^{\text{com}}, \\ \tau_{P_i}\dot{\omega}_i &= -\omega_i + \omega^d - k_{P_i}(P_i^d - P_i^d), \\ \dot{V}_i &= -k_i e_i = -k_i \sum_{k\sim\mathcal{C}_i} \left(\frac{Q_i^m}{\chi_i} - \frac{Q_k^m}{\chi_k} \right), \\ \tau_{Q_i}\dot{Q}_i^m &= -Q_i^m + Q_i, \end{aligned}} \tag{5.34}$$

which is identical to the closed-loop inverter dynamics (5.29). Furthermore, P_i and Q_i are given by (4.24).

Note that opposed to the case of an inverter, for an SG $V_i(0)$ is, in general, not a control parameter. However, it is practically feasible to make the following assumption.

Assumption 5.3.6. *The operator can determine positive initial conditions $V_i(0) = V_i^d \in \mathbb{R}_{>0}$ for the voltages V_i, $i \sim \mathcal{N}_{SG}$.*

Assumption 5.3.6 is feasible, because in a practical scenario an SG is at first synchronized to an existing and running network via a specific synchronization control unit. Typically, this control not only synchronizes the SG speed to the network frequency, but also regulates the voltage amplitude at the generator terminals to a desired value. After this synchronization process, the DVC would be switched on by the operator and from there on set the EMF (represented by $\dot{V}_i$ in (5.34)) of the SG, e.g., to react to

disturbances such as changes in load. Furthermore, recall that the EMF of the SG is related to its terminal voltage by (4.19). Consequently, $V_i(0) = V_i^d \in \mathbb{R}_{>0}$ is a control parameter under Assumption 5.3.6.

Remark 5.3.7. It is emphasized that the feedback linearization (5.30) is merely introduced for mathematical convenience, i.e., to facilitate the mathematical analysis of the closed-loop system carried out in Section 6.5. A DVC for SGs, which does not require such—sometimes delicate—partial feedback linearization is a subject of current investigation.

5.3.4 Closed-loop microgrid dynamics under frequency droop control and distributed voltage control

To compactly write the closed-loop system given by (5.29), (5.34) and (4.24), it is convenient to recall (5.20) and introduce

$$\begin{aligned} T_P :=& \operatorname{diag}(\tau_{P_i}) \in \mathbb{R}^{n_1 \times n_1}, \quad T_Q := \operatorname{diag}(\tau_{Q_i}) \in \mathbb{R}^{n_2 \times n_2}, \quad T_F := \operatorname{diag}(T_P, T_Q) \in \mathbb{R}^{n \times n}, \\ D :=& \operatorname{diag}(1/\chi_i) \in \mathbb{R}^{n \times n}, \quad K := \operatorname{diag}(k_i) \in \mathbb{R}^{n \times n}. \end{aligned} \tag{5.35}$$

Furthermore, denote by $\mathcal{L} \in \mathbb{R}^{n \times n}$ the Laplacian matrix of the communication network. Then, the system given by (5.29), (5.34) and (4.24) can be compactly written as

$$\boxed{\begin{aligned} \dot{\delta} &= \omega - \underline{1}_n \omega^{\text{com}}, \\ T\dot{\omega} &= -\omega + \underline{1}_n \omega^d - K_P(P - P^d), \\ \dot{V} &= -K\mathcal{L}DQ^m, \\ T_F \dot{Q}^m &= -Q^m + Q, \end{aligned}} \tag{5.36}$$

with power flows P and Q given in (4.24). Furthermore, as done in the previous section, a power rating $S_i^N \in \mathbb{R}_{>0}$, $i \sim \mathcal{N}$, is associated to each generation source. Recall that under Assumption 5.3.6 the initial conditions for each element of V are determined by the control law (5.27), $i \sim \mathcal{N}_I$, respectively by the operator $i \sim \mathcal{N}_{SG}$, i.e., $V(0) = V^d := \operatorname{col}(V_i^d)$, $i \sim \mathcal{N}$.

5.3.5 Reactive power sharing and a voltage conservation law

The next result proves that the proposed DVC does indeed guarantee proportional reactive power sharing in steady-state. The claim below holds independently of the line admittances.

Claim 5.3.8. *Consider the closed-loop system* (5.36), (4.24)*. It achieves proportional reactive power sharing in steady-state in the sense of Definition 3.3.1.*

Proof. Set $\dot{V} = 0$ in (5.36). Note that, since $\mathcal{L}$ is the Laplacian matrix of an undirected connected graph, it has a simple zero eigenvalue with a corresponding right eigenvector $\beta \underline{1}_n$, $\beta \in \mathbb{R} \setminus \{0\}$. All its other eigenvalues are positive real. Moreover, K is a diagonal matrix with positive diagonal entries and from (5.36) in steady-state $Q^s = Q^{m,s}$. Hence, for $\beta \in \mathbb{R} \setminus \{0\}$ and $i \sim \mathcal{N}$, $k \sim \mathcal{N}$,

$$\underline{0}_n = -K\mathcal{L}DQ^s \Leftrightarrow DQ^s = \beta \underline{1}_n \Leftrightarrow \frac{Q_i^s}{\chi_i} = \frac{Q_k^s}{\chi_k}. \tag{5.37}$$

□

Remark 5.3.9. Because of (5.37), all entries of $Q^{m,s} = Q^s(V^s)$ must have the same sign. For dominantly inductive power lines and loads, only $Q^{m,s} = Q^s(V^s) \in \mathbb{R}^n_{>0}$ is practically relevant.

Remark 5.3.10. Note that Claim 5.3.8 holds independently of the specific choice of K and independently of possible clock drifts (see Section 4.2).

The following fact reveals an important property of the system (5.36), (4.24).

Fact 5.3.11. *The flow of the system* (5.36), (4.24) *satisfies for all* $t \geq 0$ *the conservation law*

$$\|K^{-1}V(t)\|_1 = \sum_{i=1}^{n} \frac{V_i(t)}{k_i} = \xi(V(0)), \tag{5.38}$$

where the positive real parameter $\xi(V(0))$ *is given by*

$$\xi(V(0)) = \|K^{-1}V(0)\|_1 = \sum_{i=1}^{n} \frac{V_i^d}{k_i}. \tag{5.39}$$

Proof. Recall that $\mathcal{L}$ is the Laplacian matrix of an undirected connected graph. Consequently, $\mathcal{L}$ is symmetric positive semidefinite and possesses a simple zero eigenvalue with corresponding right eigenvector $\underline{1}_n$, i.e., $\mathcal{L} = \mathcal{L}^\top$ and $\mathcal{L}\underline{1}_n = \underline{0}_n$. Hence, $\underline{1}_n^\top \mathcal{L} = \underline{0}_n^\top$. Multiplying the third equation in (5.36) from the left with $\underline{1}_n^\top K^{-1}$ yields

$$\underline{1}_n^\top K^{-1}\dot{V} = \underline{0}_n^\top DQ^m \quad \Rightarrow \quad \sum_{i=1}^{n} \frac{\dot{V}_i}{k_i} = 0. \tag{5.40}$$

Integrating (5.40) with respect to time and using (5.39) yields (5.38). □

Fact 5.3.11 has the following important practical implication: by interpreting the control gains k_i as weighting coefficients, expression (5.38) is—up to a scaling factor—equivalent to the weighted average voltage amplitude $\bar{V}(t)$ in the network, i.e.,

$$\bar{V}(t) := \frac{1}{n}\sum_{i=1}^{n}\frac{V_i(t)}{k_i}.$$

By Fact 5.3.11, it then follows that for all $t \geq 0$

$$\bar{V}(t) := \bar{V}(0) = \frac{\xi(V(0))}{n} = \frac{1}{n}\sum_{i=1}^{n}\frac{V_i^d}{k_i}. \tag{5.41}$$

Hence, the parameters V_i^d and k_i, $i \sim \mathcal{N}$, offer useful degrees of freedom for a practical implementation of the DVC (5.27), respectively (5.30) and (5.33). For example, a typical choice for V_i^d would be $V_i^d = V_N$, $i \sim \mathcal{N}$, where $V_N \in \mathbb{R}_{>0}$ denotes the nominal voltage amplitude. By setting $k_i = 1$, $i \sim \mathcal{N}$, (5.41) becomes

$$\bar{V}(t) := \frac{1}{n}\sum_{i=1}^{n}V_i(t) = V_N, \tag{5.42}$$

i.e., the average voltage amplitude $\bar{V}(t)$ of all generator buses in the network is for all $t \geq 0$ equivalent to the nominal voltage amplitude V_N.

Remark 5.3.12. Note that achieving (5.42) for $t \to \infty$ is exactly the control goal of the distributed voltage control proposed in [82], Section IV-B. As has just been shown, for $V_i^d = V_N$, $k_i = 1$, $i \sim \mathcal{N}$, the DVC (5.27), respectively (5.30) and (5.33), not only guarantees compliance of (5.42) for $t \to \infty$, but for all $t \geq 0$. In addition, by Claim 5.3.8 the DVC (5.27), respectively (5.30) and (5.33), guarantees a desired reactive power sharing in steady-state.

Remark 5.3.13. Note that the possible clock drifts discussed in Section 4.2 would merely appear as additional scaling parameters in (5.42).

5.4 Summary

In this chapter, feasible control laws for microgrids to address the problem of power sharing, as well as those of frequency and voltage stability have been discussed. At first, the droop control for SGs has been introduced. This control law is widely used in conventional power systems to address the problems of frequency control and active power sharing. Furthermore, the most common frequency and voltage droop control laws for inverter-interfaced DG units have been presented and the physical heuristics

motivating these control laws have been outlined. In addition, a selection criterion on the gains and setpoints of the droop control ensuring active power sharing in steady-state has been provided. The condition is independent of the line admittances.

Moreover, it has been discussed that the voltage droop control does, in general, not achieve the control objective of reactive power sharing. As a consequence, a consensus-based DVC for inverter-interfaced DG units has been proposed. It has been proven that the DVC does indeed guarantee reactive power sharing in steady-state. Finally, it has been shown that the proposed DVC can easily be applied to SG-interfaced units via an appropriate feedback-linearizing control law.

6

Conditions for stability in microgrids

6.1 Introduction

This chapter is devoted to the stability analysis of microgrids operated with the control laws presented in Chapter 5. As in any conventional power system, stability is understood in the sense of achieving asymptotic synchronization of the frequencies of all DG units and asymptotic convergence of their voltage amplitudes to constant values, cf. Section 2.4.5. Most results of the present chapter are based on or taken from the author's works [71, 121, 122, 123, 125].

In light of the limitations of available stability results for microgrids discussed in Section 1.3, the main contributions of the present chapter are three-fold.

(i) **Conditions for frequency stability in MDREGs**

A necessary and sufficient condition for local frequency stability of a generic meshed islanded MDREG operated with the frequency droop controls (5.1), respectively (5.2), is derived. Transfer conductances are explicitly considered, while voltage amplitudes are assumed to be constant.

Since the synchronization frequency is the same for all DG units and their dynamics depend on the angle differences, it is possible to translate—via a time-dependent coordinate shift—the synchronization objective into a (standard) equilibrium stabilization problem. This approach is adopted in the present work. Furthermore, by combining the obtained stability results with Lemma 5.2.6, a solution to Problem 3.3.3, i.e., the problem of active power sharing, in lossless MDREGs is provided.

The given results are based on the author's work [121]. Moreover, the analysis is inspired by the recent interest in graph theory and second-order consensus algorithms for multi-agent systems. It is, hence, carried out using tools of linear algebra. Second-order consensus algorithms have been used to study synchronization of harmonic oscillators [242] and have recently also been applied to frequency restoration in conventional power systems [115, 116].

(ii) **Conditions for stability of inverter-based droop-controlled microgrids with variable frequencies and voltages**

Sufficient conditions on the control parameters that ensure local stability of lossless droop-controlled inverter-based microgrids operated with the control laws given in (5.2)-(5.3) are derived. Hereby, networks with general meshed topology and third-order inverter models with variable frequencies as well as variable voltage amplitudes are considered.

Recall that the frequency synchronization objective can be transformed into a (standard) equilibrium stabilization problem. By taking this approach, the indicated results are established by means of the interconnection and damping assignment passivity-based control approach of [53]. More precisely, the lossless microgrid is represented in port-Hamiltonian form, see Section 2.3.3. This allows to easily identify the energy-Lyapunov function and give conditions for stability of the synchronization equilibrium state.

In contrast to [28, 29, 121], no assumptions of constant voltage amplitudes or small phase angle differences between the output voltages of the DG units are made.

(iii) **Closed-loop analysis of inverter-based droop-controlled microgrids operated with frequency droop control and DVC**

Since the voltage droop control (5.3) does, in general, not achieve a desired reactive power sharing, a novel distributed consensus-based DVC has been proposed in this work, see (5.27). Unlike in other related work on distributed voltage control, e.g., [82, 83, 84], a rigorous mathematical analysis of the closed-loop voltage and reactive power dynamics under the proposed DVC is carried out in the present case. More precisely, based on [122, 125], it is proven that the choice of the control parameters uniquely determines the corresponding equilibrium point. Furthermore, a necessary and sufficient condition for local exponential stability of that equilibrium point is given. The two latter results are derived under the stan-

dard assumptions of lossless line admittances and small angle differences [1, 29]. In addition, by combining these results, a condition is provided, under which the DVC solves Problem 3.3.4. Recall that Problem 3.3.4 is the problem of reactive power sharing. Then, the assumption of small angle differences is dropped and a necessary and sufficient condition for local exponential stability of a microgrid operated with the frequency droop control (5.2) and the DVC (5.27) is derived. The latter result is used to provide a solution to Problem 3.3.5 (the problem of joint active and reactive power sharing).

The remainder of the present chapter is outlined as follows. Some preliminary assumptions on the microgrid models used at several points in this chapter are discussed in Section 6.2. Under the assumption of constant voltage amplitudes, conditions for stability of lossy MDREGs operated with frequency droop control are derived in Section 6.3. Section 6.4 is devoted to the analysis of droop-controlled inverter-based microgrids with time-varying voltages and frequencies. Finally, a detailed closed-loop analysis of an inverter-based microgrid operated with frequency droop control and DVC is given in 6.5.

6.2 Preliminaries

Within this chapter, only DG units with positive voltage amplitudes $V_i : \mathbb{R}_{\geq 0} \to \mathbb{R}_{>0}$, $i \sim \mathcal{N}$, are considered. This is motivated by the fact that $V_i = 0$ implies that the i-th DG unit does not provide any power to the network, see (4.24). Hence, $V_i = 0$ can be interpreted as if the i-th DG unit was not connected to the network. In that case, the network with set of nodes $\mathcal{N} \setminus \{i \in \mathcal{N} \,|\, V_i = 0\}$ is considered instead of the network with set of nodes $\mathcal{N}$ and $V_i = 0$, $i \in \mathcal{N}$.

Most of the results in this chapter are derived for lossless microgrids. The assumption of lossless line admittances may be justified as follows [28, 71, 122, 125]. In MV and LV networks, the line impedance is usually not purely inductive, but has a non-negligible resistive part. On the other hand, the inverter output impedance is typically inductive (due to the output inductor and/or the possible presence of an output transformer). Under these circumstances, the inductive parts dominate the resistive parts in the admittances for some particular microgrids, especially on the MV level.

Only such microgrids are considered whenever lossless admittances are assumed and the inverter output admittances (together with possible transformer admittances) are absorbed into the line admittances, while neglecting all resistive effects.

More precisely, to establish the stability results in Section 6.4, the following assumption on the network admittances is made[1].

Assumption 6.2.1. *$G_{ik} = 0$ and $B_{ik} \leq 0$, $i \sim \mathcal{N}$, $k \sim \mathcal{N}$.*

By making use of Assumption 6.2.1, the power flow equations (4.24) reduce to

$$\begin{aligned} P_i &= \sum_{k \sim \mathcal{N}_i} |B_{ik}| V_i V_k \sin(\delta_{ik}), \\ Q_i &= |B_{ii}| V_i^2 - \sum_{k \sim \mathcal{N}_i} |B_{ik}| V_i V_k \cos(\delta_{ik}). \end{aligned} \tag{6.1}$$

Remark 6.2.2. The need to introduce the, sometimes unrealistic, assumption of lossless admittances has a long history in power systems studies. It appears in transient stability studies, where the presence of transfer conductances hampers the derivation of energy-Lyapunov functions [36]. Although there has been progress in addressing this issue [44, 50], to the best of the author's knowledge, no analytic solution for power systems with variable frequencies as well as variable voltage amplitudes is available. See also [48] for an illustration of the deleterious effect of line losses on field excitation controller design.

Remark 6.2.3. In the case of the Kron-reduced network, the author is aware that, in general, the reduced network admittance matrix does not permit to neglect the conductances and the given stability results might, therefore, be inaccurate [36]. Alternatively, one could consider the idealized scenario in which part of the inverter-interfaced storage devices are being charged, hence acting as loads and all constant impedance loads are neglected. Another approach is to use other, possibly dynamic, load models instead of constant impedances in the so-called structure preserving power system models. However, in the presence of variable voltages, the load models are usually, somehow artificially, adapted to fit the theoretical framework used for the construction of energy-Lyapunov functions, see, e.g., [47, 243].

Unlike in Section 6.4, the linearization of the power flow equations is used in Section 6.3.4 and Section 6.5 to derive conditions for local stability in microgrids with dominantly inductive power lines. In that case it is feasible to slightly relax Assumption 6.2.1 and allow $G_{ii} \neq 0$ for all or some $i \in \mathcal{N}$. Recall that a shunt conductance G_{ii} represents a load in the Kron-reduced network. Hence, the following assumption is employed[2].

[1] Recall that Assumption 2.4.18 together with Assumption 4.4.1 implies that $B_{ik} \leq 0$, $i \sim \mathcal{N}$, $k \sim \mathcal{N}$. For clarity of presentation, this implication is also included in Assumption 6.2.1.

[2] Recall that Assumption 2.4.18 together with Assumption 4.4.1 implies that $B_{ik} \leq 0$, $i \sim \mathcal{N}$, $k \sim \mathcal{N}$. For clarity of presentation, this implication is also included in Assumption 6.2.4.

Assumption 6.2.4. *$G_{ik} = 0$, $i \neq k$ and $B_{ik} \leq 0$, $i \sim \mathcal{N}$, $k \sim \mathcal{N}$.*

Under Assumption 6.2.4, the power flow equations (4.24) reduce to

$$\begin{aligned} P_i &= G_{ii}V_i^2 + \sum_{k\sim\mathcal{N}_i} |B_{ik}|V_iV_k \sin(\delta_{ik}), \\ Q_i &= |B_{ii}|V_i^2 - \sum_{k\sim\mathcal{N}_i} |B_{ik}|V_iV_k \cos(\delta_{ik}). \end{aligned} \tag{6.2}$$

Furthermore, the following standard decoupling assumption, see, e.g., [1, 29, 125], is used to establish part of the results in Section 6.5[1].

Assumption 6.2.5. $\delta_{ik}(t) \approx 0 \quad \forall t \geq 0,\ i \sim \mathcal{N},\ k \sim \mathcal{N}_i$.

Under Assumption 6.2.5, $\cos(\delta_{ik}(t)) \approx 1$, for all $t \geq 0$ and $i \sim \mathcal{N}$, $k \sim \mathcal{N}_i$. Consequently, together with Assumption 6.2.1, the reactive power flow at node $i \in \mathcal{N}$ reduces to $Q_i : \mathbb{R}^n_{>0} \to \mathbb{R}$,

$$Q_i(V_1, \ldots, V_n) = |B_{ii}|V_i^2 - \sum_{k\sim\mathcal{N}_i} |B_{ik}|V_iV_k. \tag{6.3}$$

This preliminary section is concluded with the following lemma, used at various occasions within the present chapter. Let $\mathcal{T} : \mathbb{T}^n \to \mathbb{R}^{n\times n}$ with

$$\begin{aligned} (\mathcal{T}(\delta))_{ii} &:= -B_{ii}, \\ (\mathcal{T}(\delta))_{ik} &:= B_{ik}\cos(\delta_{ik}), \quad i \neq k. \end{aligned} \tag{6.4}$$

Lemma 6.2.6. *Consider the mapping $\mathcal{T}(\delta)$ defined in* (6.4) *with Assumptions 2.4.18 and 4.4.1. Then, $v^\top \mathcal{T}(\delta) v > 0$ for all $v \in \mathbb{R}^n \setminus \{\underline{0}_n\}$ and all $\delta \in \mathbb{T}^n$.*

Proof. Recall that $B_{ik} = B_{ki}$. Hence, $\mathcal{T}(\delta)$ is symmetric. Furthermore, recall that $B_{ii} = \bar{B}_{ii} + \sum_{k\sim\mathcal{N}_i} B_{ik}$ and (4.21). Let $\delta^s \in \mathbb{T}^n$ such that $\delta^s_{ik} = 0$ for all $i \sim \mathcal{N}$, $k \sim \mathcal{N}_i$. It is then easily verified that, with the standing assumptions, the matrix

$$\mathcal{T}(\delta^s) - \operatorname{diag}(|\bar{B}_{ii}|),$$

is a symmetric weighted Laplacian matrix. Recall that the microgrid is connected by assumption. Consequently, $\mathcal{T}(\delta^s) - \operatorname{diag}(|\bar{B}_{ii}|)$ possesses a simple zero eigenvalue with a corresponding right eigenvector $\underline{1}_n$ and all its other eigenvalues are positive real, i.e., for any $v \in \mathbb{R}^n \setminus \{\beta\underline{1}_n\}$, $\beta \in \mathbb{R}$,

$$\big(\mathcal{T}(\delta^s) - \operatorname{diag}(|\bar{B}_{ii}|)\big)\,\underline{1}_n = \underline{0}_n, \quad v^\top \big(\mathcal{T}(\delta^s) - \operatorname{diag}(|\bar{B}_{ii}|)\big)\, v \in \mathbb{R}_{>0}. \tag{6.5}$$

[1] These results in Section 6.5 also hold for arbitrary, but constant angle differences, i.e., $\delta_{ik}(t) := \delta_{ik}$ $\forall t \geq 0$, $\delta_{ik} \in \mathbb{T}$, but at the cost of a more complex notation.

Furthermore, recall that $\bar{B}_{ii} \neq 0$ for at least some $i \in \mathcal{N}$. Hence, $\mathcal{T}(\delta^s)$ is positive definite, i.e.,

$$v^\top \mathcal{T}(\delta^s) v > 0, \quad \forall v \in \mathbb{R}^n \setminus \{\underline{0}_n\}.$$

Moreover, from (6.4), for any $\delta_{ik} \neq 0$ (modulo 2π), $i \sim \mathcal{N}$, $k \sim \mathcal{N}_i$,

$$|(\mathcal{T}(\delta))_{ik}| < |B_{ik}|.$$

Hence, if $\delta_{ik} \neq 0$, then

$$(\mathcal{T}(\delta))_{ii} > \sum_{l \sim \mathcal{N}} |(\mathcal{T}(\delta))_{il}|, \quad (\mathcal{T}(\delta))_{kk} > \sum_{l \sim \mathcal{N}} |(\mathcal{T}(\delta))_{kl}|.$$

This, together with (6.5) implies that $v^\top \mathcal{T}(\delta) v > 0$ for any $v \in \mathbb{R}^n \setminus \{\underline{0}_n\}$ and any $\delta \in \mathbb{T}^n$, completing the proof.

□

6.3 Conditions for frequency stability of droop-controlled microgrids with distributed rotational and electronic generation (MDREGs)

The main contribution of this section is to provide a necessary and sufficient condition for local frequency stability of a lossy MDREG, i.e., an MDREG with nonzero transfer conductances. The presence of transfer conductances leads to non-symmetric network interconnections, complicating significantly the derivation of analytic stability conditions. To establish the results, no assumptions on the power line characteristics nor the voltage levels are made, but, as sometimes used in analysis of lossy conventional power systems [244], uniform damping is assumed. See Section 6.3.3 for details regarding this assumption. The provided analysis is based on [121].

The remainder of this section is structured as follows. In Section 6.3.1, the desired synchronized motion is defined. An error system for the stability analysis is constructed in Section 6.3.2. A necessary and sufficient condition for local exponential stability of a lossy MDREG is given in Section 6.3.3. Subsequently, in Section 6.3.4, the aforementioned results are applied to analyze frequency stability in lossless microgrids. In the latter case, the network interconnections are symmetric and the assumption of uniform damping is dropped. In Section 6.3.5, the obtained stability condition is then combined with Lemma 5.2.6 to give a condition, under which the frequency droop control (5.1), respectively (5.2), solves the problem of active power sharing in a lossless MDREG. Recall that the problem of active power sharing has been formulated in Problem 3.3.3.

6.3.1 Synchronized motion

To state the main results of this section, the following natural power-balance feasibility assumption is needed. Recall the system (5.13) with power flows P_i given in (4.24).

Assumption 6.3.1. *There exist constants $\delta^s \in \Theta$ and $\omega^s \in \mathbb{R}$, where*

$$\Theta := \left\{ \delta \in \mathbb{T}^n \;\middle|\; -\frac{\pi}{2} < \delta_{ik} + \phi_{ik} < \frac{\pi}{2}, i \sim \mathcal{N},\ k \sim \mathcal{N}_i \right\},$$

such that

$$\underline{1}_n \omega^s - \underline{1}_n \omega^d + K_P[P(\delta^s) - P^d] = \underline{0}_n. \tag{6.6}$$

Under Assumption 6.3.1, the motion of the system (5.13), (4.24) starting in $(\delta^s, \underline{1}_n \omega^s)$ is given by

$$\begin{aligned} \delta^*(t) &= \mathrm{mod}_{2\pi} \left\{ \delta^s + \underline{1}_n \left(\omega^s t - \int_0^t \omega^{\mathrm{com}}(\tau) d\tau \right) \right\}, \\ \omega^*(t) &= \underline{1}_n \omega^s, \end{aligned} \tag{6.7}$$

where the operator[1] $\mathrm{mod}_{2\pi}\{\cdot\}$ is added to respect the topology of the system. This desired motion is called synchronized motion and ω^s is the synchronization frequency.

Remark 6.3.2. Clearly, the synchronized motion lives in the set $\Theta \times \underline{1}_n \omega^s$.

Remark 6.3.3. There is not a unique desired synchronized motion of the system (5.13), (4.24) associated to the flow given in (6.6), but any solution with $\omega^*(t)$ as given in (6.7) and $\delta^*(t) = \mathrm{mod}_{2\pi}\{\delta^s + \underline{1}_n(\alpha + \omega^s t - \int_0^t \omega^{\mathrm{com}}(\tau)d\tau)\}$, $\alpha \in \mathbb{R}$, is a desired synchronized motion.

Remark 6.3.4. For a given constant vector δ^s, the corresponding synchronization frequency ω^s is obtained by adding up all nodes in the network. From (4.23) and (6.6) this yields

$$\sum_{i \sim \mathcal{N}} \frac{\dot{\omega}_i}{k_{P_i}} = 0 \;\Rightarrow\; \omega^s = \omega^d + \frac{\sum_{i \sim \mathcal{N}} \left(P_i^d - G_{ii} V_i^2 - \sum_{k \sim \mathcal{N}_i} V_i V_k G_{ik} \cos(\delta_{ik}^s) \right)}{\sum_{i \sim \mathcal{N}} \frac{1}{k_{P_i}}}. \tag{6.8}$$

6.3.2 Error dynamics

The main result of this section is to give conditions on the gains of the droop controllers (5.1) and (5.2) such that the synchronized motion (6.7) is locally asymptotically stable,

[1] The operator $\mathrm{mod}_{2\pi}\{\cdot\} : \mathbb{R} \to [0, 2\pi)$, is defined as follows: $y = \mathrm{mod}_{2\pi}\{x\}$ yields $y = x - k2\pi$ for some integer k, such that $y \in [0, 2\pi)$, see Section 2.4.4.

i.e., such that all solutions of the system (5.13), (4.24) starting in a neighborhood of $\mathrm{col}(\delta^s, \underline{1}_n\omega^s)$ converge to the synchronized motion (6.7) (up to a uniform shift of all angles).

It follows from inspection of (6.7) and the model derivation in Section 2.4.4, that, for the purpose of stability analysis, a suitable choice of ω^{com} is $\omega^{\mathrm{com}} = \omega^s$, since then $\delta^*(t) = \delta^s$ is a constant vector. Moreover, it is convenient to study the stability of the synchronized motion (6.37) in the coordinates $\mathrm{col}(\tilde{\delta}(t), \tilde{\omega}(t)) \in \mathbb{R}^n \times \mathbb{R}^n$ with

$$\begin{aligned} \tilde{\omega}(t) &:= \omega(t) - \underline{1}_n\omega^{\mathrm{com}} = \omega(t) - \underline{1}_n\omega^s, \\ \tilde{\delta}(t) &:= \delta(0) - \delta^s + \int_0^t (\omega - \underline{1}_n\omega^s)d\tau = \delta(0) - \delta^s + \int_0^t \tilde{\omega}(\tau)d\tau. \end{aligned} \tag{6.9}$$

In addition, the following important observation is made. The dependence with respect to δ of the dynamics (5.13), (4.24) is via angle differences δ_{ik}. This immediately leads to the following implication. Convergence of the dynamics (5.13), (4.24) to the desired synchronized motion (6.7) (up to a uniform shift of all angles) is not determined by the value of the angles, but only by their differences. Consequently, to study convergence to the synchronized motion (6.7), one node, say node n, can be arbitrarily chosen as a reference node and the remaining $\tilde{\delta}_i$ for all $i \in \mathcal{N} \setminus \{n\}$ can be expressed relative to $\tilde{\delta}_n$ via the state transformation

$$\begin{aligned} \theta := \mathcal{R}\tilde{\delta}, \quad \mathcal{R} &:= \begin{bmatrix} \mathbf{I}_{n-1} & -\underline{1}_{n-1} \end{bmatrix}, \\ \tilde{\delta} = \bar{\mathcal{R}} \begin{bmatrix} \theta \\ \tilde{\delta}_n \end{bmatrix}, \quad \bar{\mathcal{R}} &= \begin{bmatrix} \mathbf{I}_{n-1} & \underline{1}_{n-1} \\ \underline{0}_{n-1}^\top & 1 \end{bmatrix}. \end{aligned} \tag{6.10}$$

This leads to a reduced system of order $2n-1$ with $\theta = \mathrm{col}(\theta_1, \ldots, \theta_{n-1})$ replacing $\tilde{\delta}$. In the reduced coordinates, the active power flows P_i given in (4.24) read

$$\begin{aligned} P_i(\tilde{\delta}(\theta)) &:= G_{ii}V_i^2 + V_iV_n|Y_{in}|\sin(\theta_i + \delta_{in}^s + \phi_{in}) + \sum_{k\sim\mathcal{N}_i, k\neq n} V_iV_k|Y_{ik}|\sin(\theta_{ik} + \delta_{ik}^s + \phi_{ik}), \\ P_n(\tilde{\delta}(\theta)) &:= G_{nn}V_n^2 - \sum_{k\sim\mathcal{N}_n} V_nV_k|Y_{nk}|\sin(\theta_k + \delta_{kn}^s - \phi_{nk}), \quad i \sim \mathcal{N}\setminus\{n\}. \end{aligned} \tag{6.11}$$

Furthermore, written in the new coordinates $\mathrm{col}(\theta, \tilde{\omega}) \in \mathbb{R}^{n-1} \times \mathbb{R}^n$, the dynamics (5.13), (4.24) take the form

$$\begin{aligned} \dot{\theta} &= \mathcal{R}\tilde{\omega}, \\ T\dot{\tilde{\omega}} &= -\tilde{\omega} - K_P(P(\tilde{\delta}(\theta)) - P^d) + \underline{1}_n\left(\omega^d - \omega^s\right). \end{aligned} \tag{6.12}$$

The reduced system (6.12), (6.11) lives in the set $\mathbb{R}^{n-1} \times \mathbb{R}^n$. Note that this system has an equilibrium at

$$\mathrm{col}(\theta^s, \tilde{\omega}^s) = \underline{0}_{(2n-1)},$$

the local asymptotic stability of which implies asymptotic convergence of all solutions of the system (5.13), (4.24) starting in a neighborhood of $\mathrm{col}(\delta^s, \underline{1}_n \omega^s)$ to the synchronized motion (6.7) up to a uniform shift of all angles.

The following relation is used in the remainder of this section. Consider the vector P defined in (5.12) together with (6.9) and let $\tilde{L}$ be given by

$$\tilde{L} := \frac{\partial P}{\partial \tilde{\delta}}\big|_{\tilde{\delta}^s} \in \mathbb{R}^{n \times n}, \tag{6.13}$$

with entries

$$\tilde{l}_{ii} = \sum_{k \sim \mathcal{N}_i} |Y_{ik}| V_i^s V_k^s \cos(\delta_{ik}^s + \phi_{ik}), \quad \tilde{l}_{ik} = -|Y_{ik}| V_i^s V_k^s \cos(\delta_{ik}^s + \phi_{ik}).$$

Clearly, from (6.10) and (6.11),

$$\tilde{L}_R := \frac{\partial P(\tilde{\delta}(\theta))}{\partial \theta}\big|_{\theta^s} = \left(\frac{\partial P}{\partial \tilde{\delta}} \frac{\partial \tilde{\delta}}{\partial \theta} \right) \big|_{\theta^s} = \tilde{L} \begin{bmatrix} \mathbf{I}_{n-1} \\ \underline{0}_{n-1}^\top \end{bmatrix} \in \mathbb{R}^{n \times (n-1)}. \tag{6.14}$$

6.3.3 Frequency stability in lossy MDREGs

A necessary and sufficient condition for local exponential stability for lossy frequency-droop-controlled MDREGs is derived. A related work is [50], wherein, under the assumption of small inertia-over-damping ratios, conditions for frequency synchronization of a nonlinear lossy SG-based power system have been derived. The microgrid (5.13), (4.24) is very similar to the model used in [50]. The authors of [50] obtain their results via a singular perturbation approach that leads to reduced first-order dynamics of (5.13), (4.24). For the model (5.13), (4.24), the perturbation assumption of [50] reads

$$\max\big(\max_{i \sim \mathcal{N}_I} \tau_{P_i}, \max_{i \sim \mathcal{N}_{SG}} M_i k_{P_i} \big) \ll 1.$$

Another assumption sometimes used in analysis of lossy power systems is uniform damping [244]. In the present notation, this assumption reads

$$\tau_{P_i} = \tau_{P_k} = \ldots = M_l k_{P_l} = M_m k_{P_m},\ i \sim \mathcal{N}_I, k \sim \mathcal{N}_I,\ l \sim \mathcal{N}_{SG}, m \sim \mathcal{N}_{SG}.$$

None of the two assumptions is valid for generic lossy power systems, see [50] and the discussion therein. Since, in the present case, τ_{P_i} and k_{P_i} represent free design

parameters, the latter assumption can be enforced for the frequency stability analysis of a lossy MDREG. Moreover, unlike in [50], the local approximation of the reduced second-order model (6.12) corresponding to the dynamics (5.13), (4.24) is considered in the sequel.

Assumption 6.3.5. *The parameters τ_{P_i} and τ_{P_k}, $i \sim \mathcal{N}_I$, $k \sim \mathcal{N}_I$, as well as $\tilde{k}_{P_l}$ and $\tilde{k}_{P_m}$, $l \sim \mathcal{N}_{SG}$, $m \sim \mathcal{N}_{SG}$, are selected such that $\tau = \tau_{P_i} = \tau_{P_k} = \ldots = M_l k_{P_l} = M_m k_{P_m}$.*

Remark 6.3.6. The droop gains of the inverters k_{P_i}, $i \sim \mathcal{N}_I$, are not restricted by Assumption 6.3.5.

Remark 6.3.7. In practice, the low-pass filters are typically implemented in order to filter the fundamental component of the power injections [34]. Hence, Assumption 6.3.5 is usually satisfied for inverters in microgrids.

Under Assumption 6.3.5, the microgrid dynamics (6.12), (6.11) can be represented in a small neighborhood of the equilibrium $\mathrm{col}(\theta^s, \tilde{\omega}^s) = \underline{0}_{(2n-1)}$ as

$$\begin{bmatrix} \dot{\theta} \\ \dot{\tilde{\omega}} \end{bmatrix} = \underbrace{\begin{bmatrix} \mathbf{0}_{(n-1)\times(n-1)} & \mathcal{R} \\ -\frac{1}{\tau} K_P \tilde{L}_R & -\frac{1}{\tau} \mathbf{I}_{n\times n} \end{bmatrix}}_{:=A_{\mathrm{MDREG}}} \begin{bmatrix} \theta \\ \tilde{\omega} \end{bmatrix}. \tag{6.15}$$

The main result of this section is given below.

Proposition 6.3.8. *Consider the system (5.13), (4.24) satisfying Assumption 6.3.1. Fix ω^d and P^d. Select $\tau > 0$ and K_P such that Assumption 6.3.5 is satisfied. Let $\mu_i = a_i + jb_i$ be the i-th nonzero eigenvalue of $K_P\tilde{L}$. Then, $\underline{0}_{(2n-1)}$ is a locally exponentially stable equilibrium point of the system (6.12), (6.11) if and only if*

$$\tau b_i^2 < a_i \tag{6.16}$$

for all μ_i. Moreover, the equilibrium $\underline{0}_{(2n-1)}$ is locally exponentially stable for any τ if and only if $K_P\tilde{L}$ has only real eigenvalues.

Proof. Recall that, with the standing assumptions, the system (6.12), (6.11) is locally equivalent to the system (6.15). Thus, the claim is established by deriving the spectrum of A_{MDREG} defined in (6.15).

Let λ be an eigenvalue of A_{MDREG} with a corresponding right eigenvector $v = \mathrm{col}(v_1, v_2)$, $v_1 \in \mathbb{C}^{n-1}$, $v_2 \in \mathbb{C}^n$. Then,

$$\begin{aligned} \mathcal{R} v_2 &= \lambda v_1, \\ -\frac{1}{\tau}\left(K_P \tilde{L}_R v_1 + v_2\right) &= \lambda v_2. \end{aligned} \tag{6.17}$$

At first, it is proven by contradiction that zero is not an eigenvalue of A_{MDREG}. Therefore, assume $\lambda = 0$. Then,

$$\begin{aligned} \mathcal{R} v_2 &= \underline{0}_{n-1}, \\ K_P \tilde{L}_R v_1 &= -v_2. \end{aligned} \tag{6.18}$$

Multiply the second equation of (6.18) from the left by $\mathcal{R}$. Then, the first equation of (6.18) implies that

$$\mathcal{R} K_P \tilde{L}_R v_1 = -\mathcal{R} v_2 = \underline{0}_{n-1}. \tag{6.19}$$

From the definition of $\mathcal{R}$ given in (6.10), it follows that (6.19) can only be satisfied for $v_1 \neq \underline{0}_{n-1}$ if

$$K_P \tilde{L}_R v_1 = \underline{1}_n.$$

By recalling (6.14) and the fact that K_P is a diagonal matrix with positive real diagonal entries, this is equivalent to

$$\tilde{L}_R v_1 = \tilde{L} \begin{bmatrix} \mathbf{I}_{n-1} \\ \underline{0}_{n-1}^\top \end{bmatrix} v_1 = \tilde{L} w_1 = \underline{1}_n, \quad w_1 := \begin{bmatrix} \mathbf{I}_{n-1} \\ \underline{0}_{n-1}^\top \end{bmatrix} v_1. \tag{6.20}$$

It is easily verified that, under the standing assumptions, $\tilde{L}$ is the Laplacian matrix of a directed strongly connected graph. Hence, according to Lemma 2.3.14, there exists no $w_1 \neq \underline{0}_n$ satisfying (6.20). Consequently, (6.17) can only hold for $\lambda = 0$ if $v_1 = \underline{0}_{n-1}$ and $v_2 = \underline{0}_n$. Therefore, zero is not an eigenvalue of A_{MDREG}.

In the following, conditions under which all eigenvalues of A_{MDREG} have negative real part are established. Since $\lambda \neq 0$, (6.17) can be rewritten as

$$\lambda^2 v_2 + \frac{1}{\tau} \lambda v_2 + \frac{1}{\tau} K_P \tilde{L}_R \mathcal{R} v_2 = \underline{0}_n. \tag{6.21}$$

It follows from the definition of $\mathcal{R}$ given in (6.10) together with (6.14) and Lemma 2.3.15 that

$$\tilde{L}_R \mathcal{R} = \tilde{L} \begin{bmatrix} \mathbf{I}_{n-1} \\ \underline{0}_{n-1}^\top \end{bmatrix} \mathcal{R} = \tilde{L} \begin{bmatrix} \mathbf{I}_{n-1} & -\underline{1}_{n-1} \\ \underline{0}_{n-1}^\top & 0 \end{bmatrix} = \tilde{L}.$$

Hence, (6.21) is equivalent to

$$\tau \lambda^2 v_2 + \lambda v_2 + K_P \tilde{L} v_2 = \underline{0}_n. \tag{6.22}$$

This implies that v_2 must be an eigenvector of $K_P \tilde{L}$. Recall that, under the standing assumptions, $\tilde{L}$ is the Laplacian matrix of a strongly connected directed graph. Since K_P is a diagonal matrix with positive diagonal entries, $K_P \tilde{L}$ is also a Laplacian matrix of a strongly connected graph. Hence, $K_P \tilde{L}$ possesses a simple zero eigenvalue with a corresponding right eigenvector $\underline{1}_n$ and all its other eigenvalues have positive real part,

see Section 2.3.5 and also, e.g., [121, 140]. For $K_P\tilde{L}v_2 = \underline{0}_n$, (6.22) has solutions $\lambda = 0$ and $\lambda = -1/\tau$. Recall that zero is not an eigenvalue of A_{MDREG}. Hence, an eigenvalue (with unknown algebraic multiplicity) of the matrix A_{MDREG} is $\lambda_1 = -1/\tau$.

Now, the remaining $0 < m \leq 2n-2$ eigenvalues of the matrix $A_{\text{MDREG}} \in \mathbb{R}^{(2n-1)\times(2n-1)}$ are investigated. Denote the nonzero[1] eigenvalues of $K_P\tilde{L}$ by $\mu_i \in \mathbb{C}$. Let a corresponding right eigenvector be given by $w_i \in \mathbb{C}^n$, i.e., $K_P\tilde{L}w_i = \mu_i w_i$. Without loss of generality, choose w_i such that $w_i^* w_i = 1$. By multiplying (6.22) from the left with w_i^*, the remaining m eigenvalues of A_{MDREG} are the solutions $\lambda_{i_{1,2}}$ of

$$\tau\lambda_{i_{1,2}}^2 + \lambda_{i_{1,2}} + \mu_i = 0. \tag{6.23}$$

First, consider real nonzero eigenvalues, i.e., $\mu_i = a_i$ with $a_i > 0$. Then, clearly, both solutions of (6.23) have negative real parts, e.g., by the Hurwitz condition (see Theorem 2.3.12). Next, consider complex eigenvalues of $K_P\tilde{L}$, i.e., $\mu_i = a_i + jb_i$, $a_i > 0$, $b_i \in \mathbb{R} \setminus \{0\}$. Then, it follows from (6.23) that

$$\lambda_{i_{1,2}} = \frac{1}{2\tau}\left(-1 \pm \sqrt{1 - 4\tau(a_i + jb_i)}\right). \tag{6.24}$$

Let $\alpha_i := 1 - 4a_i\tau$, $\beta_i := -4b_i\tau$ and recall that the roots of a complex number $\sqrt{\alpha_i + j\beta_i}, \beta_i \neq 0$, are given by $\pm(\psi_i + j\nu_i)$, $\psi_i \in \mathbb{R}$, $\nu_i \in \mathbb{R}$, [245] with

$$\psi_i = \sqrt{\frac{1}{2}\left(\alpha_i + \sqrt{\alpha_i^2 + \beta_i^2}\right)}.$$

Thus, both solutions $\lambda_{i_{1,2}}$ in (6.24) have negative real parts if and only if

$$\sqrt{\frac{1}{2}\left(\alpha_i + \sqrt{\alpha_i^2 + \beta_i^2}\right)} < 1$$

or, equivalently,

$$\sqrt{\alpha_i^2 + \beta_i^2} < 2 - \alpha_i.$$

Inserting α_i and β_i gives

$$\sqrt{(1 - 4a_i\tau)^2 + 16b_i^2\tau^2} < 1 + 4a_i\tau,$$

where the right hand side is positive. The condition is therefore equivalent to

$$\tau < \frac{a_i}{b_i^2},$$

[1] Neither the algebraic nor the geometric multiplicities of the nonzero eigenvalues of the matrix product $K_P\tilde{L}$ are known in the present case. However, this information is not required, since, to establish the claim, it suffices to know that $\Re(\sigma(K_P\tilde{L})) \subseteq \mathbb{R}_{\geq 0}$. This follows from the facts that, under the standing assumptions, $\tilde{L}$ is the Laplacian matrix of a strongly connected graph and that K_P is a diagonal matrix with positive diagonal entries.

which is condition (6.16) for $b_i \neq 0$. Hence, A_{MDREG} is Hurwitz if and only if (6.16) holds for all μ_i. Finally, by Theorem 2.3.8, the equilibrium point $\underline{0}_{(2n-1)}$ is locally exponentially stable if and only if A_{MDREG} is Hurwitz. □

Condition (6.16) has the following immediate physical interpretation. The magnitudes of the eigenvalues μ_i of $K_P\tilde{L}$ depend on the magnitudes of the droop gains k_{P_i}. Therefore, increasing all gains contained in K_P by a factor κ, where κ is a positive real parameter, implies that all eigenvalues μ_i are increased by the same factor κ. Hence, condition (6.16) states that, in order to ensure local asymptotic stability, the larger the parameter τ is, the lower the feedback gain has to be chosen. Therefore, for the practical operation of droop-controlled inverters modeled by (5.4), condition (6.16) implies that the slower the power measurements are processed, i.e., the larger τ is, the lower the droop gains have to be chosen.

Note that, in general, a variation in K_P leads to a different synchronized motion (6.7). As a consequence, the physical interpretation of condition (6.16) given above is only valid under the assumption that a variation of the gains does not have a significant effect on the matrix $\tilde{L}$ defined in (6.13). By continuity, this is, e.g., the case for small variations of the gains.

Remark 6.3.9. Condition (6.16) can also be derived via the Routh-Hurwitz criterion for polynomials with complex coefficients given in Theorem 2.3.12, respectively for quadratic polynomials in Corollary 2.3.13. This alternative approach is illustrated when establishing the claim of Proposition 6.5.6.

Remark 6.3.10. Recall the inverter model (5.23), (4.24) which takes into account the drift of the internal clock of the inverter at the i-th node. Clearly, therein the clock drifts υ_i, $i \sim \mathcal{N}$, appear as scaling parameters. The analyis conducted in this section is based on the converse Lyapunov theorem 2.3.8, which ensures the existence of a strict Lyapunov function [128, Chapter 4]. From this Lyapunov function some robustness properties, e.g., against parameter uncertainties, can be inferred [128, Chapters 4 and 9]. The clock drifts $|\upsilon_i| \ll 1$ [213], $i \sim \mathcal{N}$, represent parameter uncertainties. Hence, Proposition 6.3.8 ensures local stability for small enough $|\upsilon_i|$, $i \sim \mathcal{N}$. Similar arguments apply to the analysis carried out in the remainder of this work. Consequently, the effect of possible clock drifts on microgrid stability is not further discussed within this chapter. For the results in Section 6.4, a detailed proof is given in [124].

6.3.4 Frequency stability in lossless MDREGs

As discussed in Section 6.2, a microgrid with inductive lines and second-order dynamics is obtained from (5.13), (4.24) by setting $G_{ik} = 0$, respectively $\phi_{ik} = 0$ for all $i \sim \mathcal{N}$, $k \sim \mathcal{N}_i$ (see Assumption 6.2.4). Recall that then the power flows (4.24) simplify to (6.2). Moreover, under Assumption 6.2.4, the reduced dynamics (6.12), (6.11) can be represented in a small neighborhood of the equilibrium $\mathrm{col}(\theta^s, \tilde{\omega}^s) = \underline{0}_{(2n-1)}$ as

$$\begin{bmatrix} \dot{\theta} \\ \dot{\tilde{\omega}} \end{bmatrix} = \underbrace{\begin{bmatrix} \mathbf{0}_{n\times n} & \mathcal{R} \\ -T^{-1}K_P\tilde{L}_R & -T^{-1} \end{bmatrix}}_{:=A_{\mathrm{MDREG,LL}}} \begin{bmatrix} \theta \\ \tilde{\omega} \end{bmatrix}, \tag{6.25}$$

with $\tilde{L}_R$ as defined in (6.14). Local exponential stability follows as a corollary to Proposition 6.3.8.

Corollary 6.3.11. *Consider the system* (5.13), (6.2) *satisfying Assumption 6.3.1. Fix* ω^d, P^d, K_P *and* T. *Then,* $\underline{0}_{(2n-1)}$ *is a locally exponentially stable equilibrium point of the system* (6.12), (6.11).

Proof. Following the proof of Proposition 6.3.8, the claim is established by deriving the spectrum of $A_{\mathrm{MDREG,LL}}$ defined in (6.25). Let λ be an eigenvalue of $A_{\mathrm{MDREG,LL}}$ with a corresponding right eigenvector $v = \mathrm{col}(v_1, v_2)$, $v_1 \in \mathbb{C}^{n-1}$, $v_2 \in \mathbb{C}^n$. Then,

$$\begin{aligned} \mathcal{R}v_2 &= \lambda v_1, \\ -T^{-1}\left(K_P\tilde{L}_R v_1 + v_2\right) &= \lambda v_2. \end{aligned} \tag{6.26}$$

As before, it is first proven by contradiction that zero is not an eigenvalue of $A_{\mathrm{MDREG,LL}}$. Therefore, assume $\lambda = 0$. Then, (6.26) becomes identical to (6.18) and the proof of Proposition 6.3.8 implies that zero is not an eigenvalue of $A_{\mathrm{MDREG,LL}}$.

To see that under Assumption 6.2.4 all eigenvalues of $A_{\mathrm{MDREG,LL}}$ have negative real part, note that for $\lambda \neq 0$, (6.26) can be rewritten as

$$T\lambda^2 v_2 + \lambda v_2 + K_P\tilde{L}_R\mathcal{R}v_2 = \underline{0}_n.$$

Recalling that $\tilde{L}_R\mathcal{R} = \tilde{L}$ and premultiplying with $v_2^* K_P^{-1}$ yields

$$v_2^* K_P^{-1} T v_2 \lambda^2 + v_2^* K_P^{-1} v_2 \lambda + v_2^* \tilde{L} v_2 = 0. \tag{6.27}$$

Recall that K_P and T are diagonal matrices with positive diagonal entries. Moreover, Assumption 6.2.4 implies that $\phi_{ik} = 0$, $i \sim \mathcal{N}$, $k \sim \mathcal{N}$ and it is easily verified that $\tilde{L}$ defined in (6.13) is a symmetric Laplacian matrix of a connected graph. Hence,

$$\tilde{L}\beta\underline{1}_n = \underline{0}_n, \quad w^*\tilde{L}w \in \mathbb{R}_{>0} \quad \forall w \in \mathbb{C}^n \setminus \{\beta\underline{1}_n\},\ \beta \in \mathbb{C}. \tag{6.28}$$

Furthermore,

$$w^* K_P^{-1} T w \in \mathbb{R}_{>0}, \quad w^* K_P^{-1} w \in \mathbb{R}_{>0} \quad \forall w \in \mathbb{C}^n \setminus \{\underline{0}_n\}. \tag{6.29}$$

Consequently, for $w = \beta \underline{1}_n$, $\beta \in \mathbb{C}$, (6.27) becomes

$$\lambda \left(w^* K_P^{-1} T w \lambda + w^* K_P^{-1} w \right) = 0,$$

which has the solutions $\lambda = 0$ and

$$\lambda = -\frac{w^* K_P^{-1} w}{w^* K_P^{-1} T w} < 0.$$

Recall that zero is not an eigenvalue of $A_{\text{MDREG,LL}}$. In addition, from (6.28), (6.29) together with the Hurwitz condition, both solutions $\lambda_{1,2}$ of (6.27) have negative real parts for any $w \in \mathbb{C}^n \setminus \{\beta \underline{1}_n\}$, $\beta \in \mathbb{C}$. This implies that $A_{\text{MDREG,LL}}$ is Hurwitz and the claim follows from Theorem 2.3.8. □

Remark 6.3.12. Assumption 6.3.5 is not needed to prove local stability in a network with inductive power lines, since $\tilde{L}$ is a symmetric Laplacian matrix if $\delta^s \in \Theta$ and $\phi_{ik} = 0$, $i \sim \mathcal{N}$, $k \sim \mathcal{N}$.

6.3.5 A solution to the problem of active power sharing in lossless MDREGs

The contribution of this section is to give a condition under which the active power sharing problem, i.e., Problem 3.3.3, is solved. The provided solution is established for an MDREG with dominantly inductive power lines operated with frequency droop control (5.1), respectively (5.2). The result follows as a corollary to the stability result in the previous section in combination with Lemma 5.2.6.

Corollary 6.3.13. *Consider the system* (5.13), (6.2) *satisfying Assumption 6.3.1. Fix* ω^d *and* T. *Furthermore, following Definition 3.3.1, select positive real constants* γ_i, $i \sim \mathcal{N}$. *Let* $U = diag(1/\gamma_i)$. *Set* $K_P = \varsigma U$ *and* $P^d = \psi U^{-1} \underline{1}_n$, *where* ς *and* ψ *are real nonzero constants. Then Problem 3.3.3 is solved locally, i.e., for all initial conditions in a neighborhood of* $col(\delta^s, \underline{1}_n \omega^s)$.

Proof. The claim is established by combining the results of Corollary 6.3.11 and Lemma 5.2.6.

First, it is shown that the suggested selection of control parameters restricts the steady-state active power flows associated with the synchronized motion (6.7) to the

desired manifold defined in Problem 3.3.3. Recall from the definition of Problem 3.3.3 that this manifold is given by

$$UP(\delta^s) = \upsilon \underline{1}_n, \quad \upsilon \in \mathbb{R},$$

with P given by (6.2). From (5.13), (6.2) with $\dot{\omega} = 0$ it follows that, along the synchronized motion (6.7),

$$\dot{\omega} = \underline{0}_n = -(\omega^s - \omega^d)\underline{1}_n - K_P(P^s - P^d),$$

which by inserting $K_P = \varsigma U$ and $P^d = \psi U^{-1}\underline{1}_n$ is equivalent to

$$\begin{aligned} \dot{\omega} = \underline{0}_n &= -(\omega^s - \omega^d)\underline{1}_n - \varsigma U(P^s - \psi U^{-1}\underline{1}_n) \\ &= -(\omega^s - \omega^d)\underline{1}_n - \varsigma(UP^s - \psi\underline{1}_n). \end{aligned} \tag{6.30}$$

It follows that

$$\begin{aligned} & UP^s = \frac{(-\omega^s + \omega^d + \varsigma\psi)}{\varsigma}\underline{1}_n \\ \Leftrightarrow \quad & UP^s = \upsilon\underline{1}_n, \quad \upsilon := \frac{(-\omega^s + \omega^d + \varsigma\psi)}{\varsigma}, \end{aligned} \tag{6.31}$$

which implies active power sharing in steady-state.

Finally, under the standing assumptions, the claimed convergence result follows directly from Corollary 6.3.11. This completes the proof. □

Remark 6.3.14. Note that the selection criterion for the parameters of the frequency droop controller given in Lemma 5.2.6 is only sufficient and not necessary to achieve a desired active power sharing. For example, for a known value of $\upsilon \in \mathbb{R}$ in (6.31), there obviously exist infinitely many other choices of P_i^d and k_{P_i}, $i \sim \mathcal{N}$, ensuring a desired power sharing in steady-state for the particular synchronized motions given by (6.7), which satisfy $UP^s = \upsilon\underline{1}_n$. The advantage of the selection criterion given in Lemma 5.2.6 is, however, that it ensures a desired power sharing in steady-state for any synchronized motion (6.7).

6.4 Conditions for stability of droop-controlled inverter-based microgrids

The main contribution of the present section is to give conditions on the parameters of the droop control (5.2)-(5.3) that ensure stability of droop-controlled inverter-based microgrids with general meshed topology and inverter models with variable frequencies, as well as variable voltage amplitudes. In contrast to [28, 29, 66, 121], no assumptions

of constant voltage amplitudes or small phase angle differences are made. In this more general scenario, the methods from graph theory and linear algebra employed in the aforementioned papers are not directly applicable. The same holds for the mathematical tools used in the previous section.

Instead, a classical Lyapunov-like approach for analysis of stability of equilibria and boundedness of trajectories is adopted. Following the interconnection and damping assignment passivity-based control approach [53, 123], the lossless microgrid system is represented in port-Hamiltonian form [129] to identify the energy-Lyapunov function and give conditions for stability of the frequency synchronization equilibrium state.

The remainder of this section is taken from [71, 123] and organized in two subsections. First, Section 6.4.1 presents conditions for global boundedness of trajectories. Second, sufficient conditions for stability for lossless inverter-based microgrids are established in Section 6.4.2.

6.4.1 Boundedness of trajectories of droop-controlled inverter-based microgrids

Consider a droop-controlled inverter-based microgrid given by (5.21), (4.24). Recall that the system (5.21), (4.24) lives in the set

$$\mathbb{M} := \mathbb{T}^n \times \mathbb{R}^n \times \mathbb{R}^n_{>0}. \tag{6.32}$$

The proposition below gives conditions for global boundedness of the trajectories of the system (5.21), (4.24) and is mainly due to Alessandro Astolfi. The formulation is taken from [71].

To establish the result, recall that Assumption 2.4.18 together with Assumption 4.4.1 implies that $B_{ik} \leq 0$, $i \sim \mathcal{N}$, $k \sim \mathcal{N}$.

Proposition 6.4.1. *Consider the system* (5.21), (4.24) *with Assumptions 2.4.18 and 4.4.1. The set* $\mathbb{M}$ *defined in* (6.32) *is positively invariant and all trajectories of* (5.21), (4.24) *are bounded if* V_i^d, k_{Q_i} *and* Q_i^d *are chosen such that*

$$V_i^d + k_{Q_i} Q_i^d > 0, \quad i \sim \mathcal{N}. \tag{6.33}$$

Proof. From (5.19), (4.24), write $\tau_{P_i} \dot{V}_i = f_{3i}(\delta, V)$, for some function $f_{3i} : \mathbb{T}^n \times \mathbb{R}^n_{>0} \to \mathbb{R}$. Note that

$$f_{3i}(V, \delta)_{|V_i=0} = V_i^d + k_{Q_i} Q_i^d,$$

which, under condition (6.33), is positive. Hence, the following implication is true

$$V_i(0) > 0 \;\Rightarrow\; V_i(t) > 0,$$

for all $t \geq 0$. This proves that the set $\mathbb{M}$ is positively invariant, cf. Definition 2.3.4.

To establish boundedness of solutions define the matrix $\Gamma := \mathrm{diag}(\tau_{P_i}/k_{Q_i})$, $i \sim \mathcal{N}$ and the function $\mathcal{W} : \mathbb{R}^n_{>0} \to \mathbb{R}_{>0}$

$$\mathcal{W}(V) = \|\Gamma V\|_1 = \sum_{i\sim\mathcal{N}} \frac{\tau_{P_i}}{k_{Q_i}} V_i.$$

Then,

$$\begin{aligned}\dot{\mathcal{W}} &= \sum_{i\sim\mathcal{N}} \left(\frac{1}{k_{Q_i}}(-V_i + V_i^d) - (Q_i(\delta, V) - Q_i^d) \right) \\ &\leq -\kappa_1 \mathcal{W} + \kappa_2 - V^\top \mathcal{T}(\delta) V,\end{aligned}$$

where

$$\kappa_1 := \min_{i\sim\mathcal{N}} \left\{ \frac{1}{\tau_{P_i}} \right\}, \quad \kappa_2 := \sum_{i\sim\mathcal{N}} \left(\frac{1}{k_{Q_i}} V_i^d + Q_i^d \right)$$

and $\mathcal{T}(\delta)$ as defined in (6.4). Here, the fact has been used that, as $G_{ik} = G_{ki}$, (4.23) implies that

$$\sum_{i\sim\mathcal{N}} Q_i = \sum_{i\sim\mathcal{N}} \left(-B_{ii} V_i^2 + \sum_{k\sim\mathcal{N}_i} B_{ik} V_i V_k \cos(\delta_{ik}) \right),$$

which are the reactive power losses in the network.

Recall that, with the given assumptions, Lemma 6.2.6 implies that

$$\mathcal{T}(\delta) \geq n\kappa_3 \Gamma^2,$$

for some $\kappa_3 > 0$. Hence,

$$\dot{\mathcal{W}} \leq -\kappa_1 \mathcal{W} + \kappa_2 - \kappa_3 \mathcal{W}^2,$$

where the third right hand term follows from the fact that[1]

$$\sqrt{n}\|x\|_2 \geq \|x\|_1, \quad \forall x \in \mathbb{R}^n$$

[1] Let $x \in \mathbb{R}^n$, $y \in \mathbb{R}^n$ and $1 \leq l < \infty$, $1 \leq q < \infty$, such that $\frac{1}{l} + \frac{1}{q} = 1$. Then, the Hölder inequality implies that $\sum_{k=1}^n |x_k y_k| \leq \left(\sum_{k=1}^n |x_k|^l\right)^{\frac{1}{l}} \left(\sum_{k=1}^n |y_k|^q\right)^{\frac{1}{q}}$ [144]. Consider any $x \in \mathbb{R}^n$ and any p-norm $\|x\|_p = \left(\sum_{i=1}^n |x_i|^p\right)^{\frac{1}{p}}$, $1 \leq p < \infty$. Let $l = \frac{r}{p}$ and $q = \frac{1}{1-p/r}$ with $1 \leq p < \infty$, $1 \leq r < \infty$. Then, by the Hölder inequality, $\|x\|_p = \left(\sum_{i=1}^n |x_i|^p 1\right)^{\frac{1}{p}} \leq \left(\left(\sum_{i=1}^n (|x_i|^p)^{r/p}\right)^{\frac{p}{r}} \left(\sum_{i=1}^n 1^{1/(1-p/r)}\right)^{1-\frac{p}{r}} \right)^{\frac{1}{p}} = n^{\left(\frac{1}{p}-\frac{1}{r}\right)} \|x\|_r$ [144]. The inequality $\sqrt{n}\|x\|_2 \geq \|x\|_1$ follows with $p = 1$ and $r = 2$. Also, the inequalities can be extended to the case $p = \infty$ by defining $\frac{1}{\infty} = 0$.

and, hence,

$$nV^\top \Gamma^2 V = n\|\Gamma V\|_2^2 \geq \|\Gamma V\|_1^2 = \mathcal{W}^2(V).$$

The differential equation

$$\dot{z} = -\kappa_1 z + \kappa_2 - \kappa_3 z^2, \quad z(0) = z_0,$$

is a scalar differential Riccati equation with constant coefficients, which has the solution

$$z(t) = \frac{2\kappa_2\left(-1+e^{\kappa_4 t}\right) + z_0\left(\kappa_1\left(1-e^{\kappa_4 t}\right) + \kappa_4\left(1+e^{\kappa_4 t}\right)\right)}{\kappa_1\left(-1+e^{\kappa_4 t}\right) + \kappa_4\left(1+e^{\kappa_4 t}\right) + 2\kappa_3 z_0\left(-1+e^{\kappa_4 t}\right)}, \tag{6.34}$$

with $\kappa_4 := \sqrt{4\kappa_2\kappa_3 + \kappa_1^2}$. Furthermore,

$$\lim_{t\to\infty} z(t) = \frac{2\kappa_2 + z_0\left(-\kappa_1 + \kappa_4\right)}{\kappa_1 + \kappa_4 + 2\kappa_3 z_0}. \tag{6.35}$$

From the Comparison Lemma [128, Chapter 3] it then follows that for $\mathcal{W}(V(0)) \leq z_0$

$$\sum_{i\sim\mathcal{N}} \frac{\tau_{P_i}}{k_{Q_i}} V_i(t) \leq z(t),$$

hence, together with (6.35), $V \in \mathcal{L}_\infty$. This, together with (4.24), implies that $P \in \mathcal{L}_\infty$. Finally, $\omega \in \mathcal{L}_\infty$ follows from (5.19), which shows that ω_i is the output of an LTI asymptotically stable system with bounded input.

□

Remark 6.4.2. Condition (6.33) in Proposition 6.4.1 has a clear physical interpretation. From the dynamics of V_i in (5.19) it follows that the equilibrium voltage is given by

$$V_i^s = V_i^d - k_{Q_i}(Q_i^s - Q_i^d),$$

where Q_i^s is the reactive power injected in steady-state to the i-th bus. Hence, (6.33) requires that the gains k_{Q_i} and the setpoints V_i^d and Q_i^d of the voltage droop control (5.3) are chosen such that $V_i^s > 0$, even if there is zero reactive power injection to the i-th bus. Note that condition (6.33) is satisfied for all k_{Q_i} if $Q_i^d \geq 0$.

6.4.2 Conditions for stability of lossless droop-controlled inverter-based microgrids

In this section conditions for frequency and voltage stability for lossless microgrids, i.e., $G_{ik} = 0$, $i \sim \mathcal{N}$, $k \sim \mathcal{N}$, are derived. The assumption of lossless admittances is further justified for the present analysis, since the droop control laws introduced in (5.2)-(5.3) are mostly used in networks with dominantly inductive, i.e., lossless, line admittances [38, 238]. Recall that under Assumption 6.2.1, the power flow equations (4.24) reduce to (6.1).

6.4.2.1 Synchronized motion

In the spirit of Section 6.3.1, the following natural power-balance feasibility assumption is needed to state the main result of this section. Recall the set Θ defined in Assumption 6.3.1.

Assumption 6.4.3. *There exist constants $\delta^s \in \Theta$, $\omega^s \in \mathbb{R}$ and $V^s \in \mathbb{R}^n_{>0}$ such that*

$$\begin{aligned} \underline{1}_n\omega^s - \underline{1}_n\omega^d + K_P[P(\delta^s, V^s) - P^d] &= \underline{0}_n, \\ V^s - V^d + K_Q[Q(\delta^s, V^s) - Q^d] &= \underline{0}_n. \end{aligned} \tag{6.36}$$

Under Assumption 6.4.3, the motion of the system (5.21), (6.1) starting in $(\delta^s, \underline{1}_n\omega^s, V^s)$ is given by

$$\begin{aligned} \delta^*(t) &= \mathrm{mod}_{2\pi}\left\{\delta^s + \underline{1}_n\left(\omega^s t - \int_0^t \omega^{\mathrm{com}}(\tau)d\tau\right)\right\}, \\ \omega^*(t) &= \underline{1}_n\omega^s, \\ V^*(t) &= V^s, \end{aligned} \tag{6.37}$$

Following the notation of Section 6.3, this desired motion is called synchronized motion and ω^s is the synchronization frequency[1].

Remark 6.4.4. Recall (6.8). Note that under Assumption 6.2.1, it is possible to uniquely determine ω^s. Towards this end, recall the well-known fact that under Assumption 6.2.1

$$\sum_{i\sim\mathcal{N}} P_i^s = 0.$$

Thus, replacing the synchronized motion (6.37) in (5.19) and adding up all the nodes yields

$$\sum_{i\sim\mathcal{N}} \frac{\dot{\omega}_i}{k_{P_i}} = 0 \quad \Rightarrow \quad \omega^s = \omega^d + \frac{\sum\limits_{i\sim\mathcal{N}} P_i^d}{\sum\limits_{i\sim\mathcal{N}} \frac{1}{k_{P_i}}}.$$

It follows that $i \sim \mathcal{N}$

$$\begin{aligned} &\frac{1}{k_{P_i}}(\omega^s - \omega^d) - P_i^d = \sum_{k\sim\mathcal{N}, k\neq i}\left(\frac{1}{k_{P_k}}(\omega^d - \omega^s) + P_k^d\right) \\ \Leftrightarrow\ &\omega^s - \omega^d - k_{P_i}P_i^d = \sum_{k\sim\mathcal{N}, k\neq i}\frac{k_{P_i}}{k_{P_k}}\left(\omega^d - \omega^s + k_{P_k}P_k^d\right). \end{aligned} \tag{6.38}$$

Remark 6.4.5. Clearly, the synchronized motion lives in the set $\Theta \times \underline{1}_n\omega^s \times \mathbb{R}^n_{>0}$.

[1] As stated in Remark 6.3.3, the desired motion (6.37) is only unique up to a uniform shift of all angles.

6.4.2.2 Error dynamics

The main result of this section is to give conditions on the setpoints and gains of the droop controllers (5.2)-(5.3) such that the synchronized motion (6.37) is locally asymptotically stable, i.e., such that all solutions of the system (5.21), (6.1) starting in a neighborhood of $\mathrm{col}(\delta^s, \underline{1}_n\omega^s, V^s)$ converge to the synchronized motion (6.37) (up to a uniform shift of all angles).

To this end, recall the matrix $\mathcal{R}$ defined in (6.10). Also recall from Section 6.3 the fact that the power flows P and Q in (5.12) are invariant to a uniform shift of all angles. Hence, δ^* is only unique up to such a shift and convergence to the desired synchronized motion (6.37) (up to a uniform shift of all angles) does not depend on the value of the angles, but only on their differences.

Recall the definition of the error states of the angles and frequencies given in (6.9). By following the approach taken in Section 6.3, it is convenient to study the stability of the synchronized motion (6.37) in the coordinates $\mathrm{col}(\tilde{\delta}(t), \tilde{\omega}(t), V(t)) \in \mathbb{R}^n \times \mathbb{R}^n \times \mathbb{R}^n_{>0}$. Furthermore, in the present case, this leads to a reduced system of order $3n-1$ with $\theta = \mathrm{col}(\theta_1, \dots, \theta_{n-1})$ replacing $\tilde{\delta}$.

For ease of notation, the following constants are introduced

$$c_{1_i} := \omega^d - \omega^s + k_{P_i} P_i^d, \quad c_{2_i} := V_i^d + k_{Q_i} Q_i^d, \quad i \sim \mathcal{N}. \tag{6.39}$$

Furthermore, let the *constant* θ_n be given by[1]

$$\theta_n := 0.$$

and let

$$\theta_{ik} := \theta_i - \theta_k,$$

which clearly verifies $\theta_{ik} = \tilde{\delta}_{ik}$ for $k \neq n$ and $\theta_{in} = \theta_i$.

Written in the new coordinates $\mathrm{col}(\theta, \tilde{\omega}, V) \in \mathbb{R}^{n-1} \times \mathbb{R}^n \times \mathbb{R}^{n_1}_{>0}$ the dynamics (5.21), (6.1) take the form

$$\begin{aligned}
\dot{\theta}_i &= \tilde{\omega}_i - \tilde{\omega}_n, \\
\tau_{P_i}\dot{\tilde{\omega}}_i &= -\tilde{\omega}_i - k_{P_i} \sum_{k \sim \mathcal{N}_i} V_i V_k |B_{ik}| \sin(\theta_{ik} + \delta^s_{ik}) + c_{1_i}, \\
\tau_{P_i}\dot{V}_i &= -V_i - k_{Q_i}\big(|B_{ii}|V_i^2 - \sum_{k \sim \mathcal{N}_i} V_i V_k |B_{ik}| \cos(\theta_{ik} + \delta^s_{ik})\big) + c_{2_i},
\end{aligned} \tag{6.40}$$

[1]The constant θ_n is not part of the state vector θ.

$i \sim \mathcal{N} \setminus \{n\}$. The dynamics of the n-th node, which serves as a reference, are given by

$$\begin{aligned}\tau_{P_n}\dot{\tilde{\omega}}_n &= -\tilde{\omega}_n + k_{P_n}\sum_{k\sim\mathcal{N}_n} V_n V_k |B_{nk}| \sin(\theta_k + \delta^s_{kn}) + c_{1_n},\\ \tau_{P_n}\dot{V}_n &= -V_n - k_{Q_n}\big(|B_{nn}|V_n^2 - \sum_{k\sim\mathcal{N}_n} V_n V_k |B_{nk}| \cos(\theta_k + \delta^s_{kn})\big) + c_{2_n}.\end{aligned} \tag{6.41}$$

The reduced system (6.40)-(6.41) lives in the set $\tilde{\mathbb{M}} = \mathbb{R}^{n-1} \times \mathbb{R}^n \times \mathbb{R}^{n_1}_{>0}$. This system has an equilibrium at

$$x^s := \mathrm{col}(\underline{0}_{n-1}, \underline{0}_n, V^s). \tag{6.42}$$

As discussed in the previous section, local asymptotic stability of x^s implies asymptotic convergence of all solutions of the system (5.21), (6.1) starting in a neighborhood of $\mathrm{col}(\delta^s, \underline{1}_n\omega^s, V^s)$ to the synchronized motion (6.37) (up to a uniform shift of all angles).

6.4.2.3 Main result

To streamline the presentation of the stability result, it is convenient to introduce the matrices $\mathbb{L} \in \mathbb{R}^{(n-1)\times(n-1)}$ and $\mathbb{W} \in \mathbb{R}^{(n-1)\times n}$ with entries

$$\begin{aligned} l_{ii} &:= \sum_{m=1}^{n} |B_{im}| V_i^s V_m^s \cos(\delta^s_{im}), \quad l_{ik} := -|B_{ik}| V_i^s V_k^s \cos(\delta^s_{ik}),\\ w_{ii} &:= \sum_{m=1}^{n} |B_{im}| V_m^s \sin(\delta^s_{im}), \quad w_{im} := |B_{im}| V_i^s \sin(\delta^s_{im}),\end{aligned} \tag{6.43}$$

where $i \sim \mathcal{N} \setminus \{n\}$, $k \sim \mathcal{N} \setminus \{n\}$ and $m \sim \mathcal{N}$, as well as

$$F := \mathrm{diag}\left(\frac{c_{2_m}}{k_{Q_m}(V_m^s)^2}\right) = \mathrm{diag}\left(\frac{V_m^d + k_{Q_m}Q_m^d}{k_{Q_m}(V_m^s)^2}\right) \in \mathbb{R}^{n\times n}. \tag{6.44}$$

Also recall the matrix $\mathcal{T}$ defined in (6.4) and denote by $\mathcal{T}(\delta^s)$ its evaluation at δ^s with entries

$$t_{ii} = |B_{ii}|, \quad t_{ik} = -|B_{ik}| \cos(\delta^s_{ik}), \quad i \neq k, \quad i \sim \mathcal{N},\ k \sim \mathcal{N}_i.$$

Recall that it follows from Lemma 6.2.6, that $\mathcal{T}(\delta^s)$ is positive definite.

Lemma 6.4.6. *Consider the system* (5.21), (6.1) *with Assumption 6.4.3. Then,* $\mathbb{L} > 0$.

Proof. Recall $\tilde{L}$ defined in (6.13). Clearly, from (6.43) and under the standing assumptions, $\tilde{l}_{ii} = l_{ii}$ and $\tilde{l}_{ik} = l_{ik}$ for $k \neq n$. Furthermore, recall that the microgrid is connected by assumption. In addition, recall from the proof of Corollary 6.3.11 that

under the given assumptions $\tilde{L}$ is a symmetric Laplacian matrix of a connected graph with the properties [140], see also, e.g., [28, 121],

$$\tilde{L}\gamma\underline{1}_n = 0,\ v^\top \tilde{L} v > 0,\ \forall v \in \mathbb{R}^n \setminus \{v = \gamma\underline{1}_n\},\ \gamma \in \mathbb{R}. \tag{6.45}$$

Recall the matrix $\mathcal{R}$ defined in (6.10), let $r := \begin{bmatrix}\underline{0}_{n-1}^\top & 1\end{bmatrix}$ and note that

$$\tilde{L}\begin{bmatrix}\mathcal{R}\\ r\end{bmatrix}^{-1} = \tilde{L}\begin{bmatrix}\mathbf{I}_{n-1} & \underline{1}_{n-1}\\ \underline{0}_{n-1}^\top & 1\end{bmatrix} = \begin{bmatrix}\mathbb{L} & \underline{0}_{n-1}\\ b^\top & 0\end{bmatrix}, \tag{6.46}$$

where $b = \mathrm{col}(\tilde{l}_{in}) \in \mathbb{R}^{n-1},\ i \sim \mathcal{N} \setminus \{n\}$. It follows from (6.45) and (6.46) that for any $\tilde{v} := \mathrm{col}(\vartheta, 0) \in \mathbb{R}^n$, $\vartheta \in \mathbb{R}^{n-1} \setminus \{\underline{0}_{n-1}\}$

$$\tilde{v}^\top \tilde{L}\begin{bmatrix}\mathcal{R}\\ r\end{bmatrix}^{-1}\tilde{v} = \tilde{v}^\top \tilde{L}\tilde{v} = \vartheta^\top \mathbb{L}\vartheta > 0. \tag{6.47}$$

Moreover, $\mathbb{L}$ is symmetric. Hence, $\mathbb{L} > 0$. □

It follows from (6.47) and the properties of spectra of symmetric matrices, see, e.g., [144], that, under the standing assumptions of Lemma 6.4.6,

$$\sigma(\mathbb{L}) \subseteq \sigma(\tilde{L}) \setminus \{0\} \subset \mathbb{R}_{>0}, \tag{6.48}$$

with $\tilde{L}$ given in (6.13). Note that the matrices $\mathbb{L}$, respectively $\tilde{L}$, correspond to the linearization of the active power flows at nodes $i \sim \mathcal{N} \setminus \{n\}$ in the reduced system (6.40)-(6.41), respectively to the linearization of the active power flows at all nodes $i \sim \mathcal{N}$ in the original system (5.21), (6.1). Hence, $\mathbb{L}$, respectively $\tilde{L}$, represent locally the network coupling strengths between the phase angles and the active power flows. Consequently, (6.48) states that the local coupling strengths between the phase angles and the active power flows in the reduced system (6.40)-(6.41) are contained within the local coupling strengths between the phase angles and the active power flows in the original system (5.21), (6.1).

The main result of this section is given below.

Proposition 6.4.7. *Consider the system* (5.21), (6.1) *with Assumption 6.4.3. Fix* ω^d, τ_{P_i}, k_{P_i} *and* P_i^d, $i \sim \mathcal{N}$. *Select* V_i^d, k_{Q_i} *and* Q_i^d *such that*

$$F + \mathcal{T}(\delta^s) - \mathbb{W}^\top \mathbb{L}^{-1}\mathbb{W} > 0. \tag{6.49}$$

Then, the equilibrium $x^s = col(\underline{0}_{n-1}, \underline{0}_n, V^s)$ *of the system* (6.40)-(6.41) *is locally asymptotically stable.*

Proof. The claim is established following the interconnection and damping assignment passivity-based control approach [53]. More precisely, the system (6.40)-(6.41) is represented in port-Hamiltonian form to identify the energy-Lyapunov function. Defining $x := \mathrm{col}(\theta, \tilde{\omega}, V)$, the system (6.40)-(6.41) can be written as

$$\dot{x} = (J - R(x))\nabla H, \tag{6.50}$$

where the Hamiltonian $H : \mathbb{R}^{n-1} \times \mathbb{R}^n \times \mathbb{R}^n_{>0} \to \mathbb{R}$ is given by

$$\begin{aligned} H(x) = &\sum_{i=1}^{n} \Big(\frac{\tau_{P_i}}{2k_{P_i}} \tilde{\omega}_i^2 + \frac{1}{k_{Q_i}} (V_i - c_{2_i} \ln(V_i)) + \frac{1}{2} |B_{ii}| V_i^2 \\ &- \frac{1}{2} \sum_{k \sim \mathcal{N}_i} V_i V_k |B_{ik}| \cos(\theta_{ik} + \delta_{ik}^s) \Big) - \sum_{i=1}^{n-1} \frac{c_{1_i}}{k_{P_i}} \theta_i \end{aligned} \tag{6.51}$$

and the interconnection and damping matrices are

$$J = \begin{bmatrix} \mathbf{0}_{(n-1)\times(n-1)} & \mathcal{J} \\ -\mathcal{J}^\top & \mathbf{0}_{2n\times 2n} \end{bmatrix}, \quad R(x) = \mathrm{blkdiag}(\mathbf{0}_{(n-1)\times(n-1)}, R_\omega, R_V) \tag{6.52}$$

with

$$\begin{aligned} \mathcal{J} &= \begin{bmatrix} \mathcal{J}_K & -\frac{k_{P_n}}{\tau_{P_n}} \underline{1}_{n-1} & \mathbf{0}_{(n-1)\times n} \end{bmatrix}, \quad \mathcal{J}_K = \mathrm{diag}\left(\frac{k_{P_k}}{\tau_{P_k}} \right) \in \mathbb{R}^{(n-1)\times(n-1)}, \\ R_\omega &= \mathrm{diag}\left(\frac{k_{P_i}}{\tau_{P_i}^2} \right) \in \mathbb{R}^{n\times n}, \quad R_V = \mathrm{diag}\left(\frac{k_{Q_i} V_i}{\tau_{P_i}} \right) \in \mathbb{R}^{n\times n}, \end{aligned}$$

$k \sim \mathcal{N} \setminus \{n\}$, $i \sim \mathcal{N}$. Note that $J = -J^\top$ and $R(x) \geq 0$. Consequently,

$$\dot{H} = -(\nabla H)^\top R(x) \nabla H \leq 0. \tag{6.53}$$

Therefore, by Lemma 2.3.11, x^s is a stable equilibrium of system (6.40)-(6.41) if $H(x)$ has a strict local minimum at the equilibrium x^s. To ensure the latter it is shown that $\nabla H(x^s) = \underline{0}_{(3n-1)}$ and $\frac{\partial^2 H(x)}{\partial x^2}\big|_{x^s} > 0$. Now,

$$\begin{aligned} \left(\frac{\partial H}{\partial \theta}\Big|_{x^s} \right)^\top &= \mathrm{col}\left(a_i - \frac{c_{1_i}}{k_{P_i}} \right) \in \mathbb{R}^{n-1}, \quad \left(\frac{\partial H}{\partial \tilde{\omega}}\Big|_{x^s} \right)^\top = \underline{0}_n, \\ \left(\frac{\partial H}{\partial V}\Big|_{x^s} \right)^\top &= \mathrm{col}\left(-b_l + |B_{ll}| V_l^s + \frac{1}{k_{Q_l}} \left(1 - \frac{c_{2_l}}{V_l^s} \right) \right) \in \mathbb{R}^n, \end{aligned}$$

where $i \sim \mathcal{N} \setminus \{n\}$, $l \sim \mathcal{N}$ and

$$a_i := \sum_{k \sim \mathcal{N}_i} V_i^s V_k^s |B_{ik}| \sin(\delta_{ik}^s), \; b_l := \sum_{k \sim \mathcal{N}_l} V_k^s |B_{lk}| \cos(\delta_{lk}^s).$$

Hence, $\nabla H(x^s) = \underline{0}_{(3n-1)}$.

The Hessian of $H(x)$ evaluated at x^s is given by

$$\frac{\partial^2 H(x)}{\partial x^2}\Big|_{x^s} = \begin{bmatrix} \mathbb{L} & \mathbf{0}_{(n-1)\times n} & \mathbb{W} \\ \mathbf{0}_{n\times(n-1)} & \Upsilon & \mathbf{0}_{n\times n} \\ \mathbb{W}^\top & \mathbf{0}_{n\times n} & F + \mathcal{T}(\delta^s) \end{bmatrix},$$

with $\mathbb{L}$, $\mathbb{W}$, F and $\mathcal{T}(\delta^s)$ as defined in (6.43), (6.44), respectively (6.4), and $\Upsilon := \operatorname{diag}(\tau_{P_i}/k_{P_i}) \in \mathbb{R}^{n\times n}$. Since Υ is positive definite, the Hessian is positive definite if and only if the submatrix

$$\begin{bmatrix} \mathbb{L} & \mathbb{W} \\ \mathbb{W}^\top & F + \mathcal{T}(\delta^s) \end{bmatrix} \tag{6.54}$$

is positive definite. Recall that Lemma 6.4.6 implies that, under the standing assumptions, $\mathbb{L}$ is positive definite. Hence, the matrix (6.54) is positive definite if and only if

$$F + \mathcal{T}(\delta^s) - \mathbb{W}^\top \mathbb{L}^{-1} \mathbb{W} > 0,$$

which is condition (6.49).

By Lemma 2.3.11, recalling (6.53) and the fact that $R(x) \geq 0$, to prove asymptotic stability it suffices to show that—along the trajectories of the system (6.50)—the implication

$$R(x(t))\nabla H(x(t)) = \underline{0}_{(3n-1)} \ \forall t \geq 0 \quad \Rightarrow \quad \lim_{t\to\infty} x(t) = x^s \tag{6.55}$$

holds. From (6.55) it follows that

$$\frac{\partial H}{\partial \tilde{\omega}} = \underline{0}_n, \quad \frac{\partial H}{\partial V} = \underline{0}_n,$$

where the first condition implies $\tilde{\omega} = \underline{0}_n$. Hence, θ is constant. The second condition implies V constant. Therefore, the invariant set where $\dot{H}(x(t)) = 0$, $\forall t \geq 0$, is an equilibrium. To prove that this is the desired equilibrium x^s recall that x^s is an isolated minimum of $H(x)$. Consequently, there is a neighborhood of x^s where no other equilibrium exists, completing the proof. □

Condition (6.49) has the following physical interpretation. The droop control laws (5.2)-(5.3) establish a feedback interconnection linking the phase angles δ, respectively θ, with the active power flows P, as well as the voltages V with the reactive power flows Q.

The matrices $\mathbb{L}$ and $\mathcal{T}(\delta^s)$ represent then the network coupling strengths between the phase angles and the active power flows, respectively, the voltages and the reactive power flows. In the same way, $\mathbb{W}$ can be interpreted as a local cross-coupling strength originating from the fact that the active power flows P are not mere functions of δ and

the reactive power flows Q are not mere functions of V, but that the active and reactive power flows are functions of both δ and V.

Condition (6.49) states that to ensure local stability of the equilibrium x^s defined in (6.42) the couplings represented by $\mathbb{L}$ and $\mathcal{T}(\delta^s)$ have to dominate the cross-couplings of the power flows contained in $\mathbb{W}$. If that is not the case the voltage variations have to be reduced by reducing the magnitudes of the gains k_{Q_i}, $i \in \mathcal{N}$.

Another possibility is to adapt Q_i^d and V_i^d. This does, however, not seem as appropriate in practice since these two parameters are typically setpoints provided by a supervisory control, which depend on the nominal voltage of the network and the expected loading conditions, see Remark 5.2.1.

Remark 6.4.8. To see that (6.50) is indeed an equivalent representation of (6.40)-(6.41), note that the part of the dynamics of $\tilde{\omega}_n$ in (6.41) resulting from $J\nabla H$ is

$$\begin{aligned}\frac{k_{P_n}}{\tau_{P_n}} \underline{1}_{n-1}^\top \left(\frac{\partial H}{\partial \theta}\right)^\top &= \frac{k_{P_n}}{\tau_{P_n}} \sum_{i=1}^{n-1} \Big(\sum_{k\sim\mathcal{N}_i} V_i V_k |B_{ik}| \sin(\theta_{ik} + \delta_{ik}^s) - \frac{c_{1_i}}{k_{P_i}} \Big) \\ &= \frac{k_{P_n}}{\tau_{P_n}} \Big(\sum_{k\sim\mathcal{N}_n} V_n V_k |B_{nk}| \sin(\theta_k + \delta_{kn}^s) - \sum_{i=1}^{n-1} \frac{c_{1_i}}{k_{P_i}} \Big),\end{aligned}$$

since $\sum_{i=1}^{n-1} \sum_{k\sim\mathcal{N}_i, k\neq n} V_i V_k |B_{ik}| \sin(\theta_{ik} + \delta_{ik}^s) = 0$. Furthermore, it follows from (6.38) that

$$c_{1_n} = \omega^d - \omega^s + k_{P_n} P_n^d = -\sum_{i=1}^{n-1} \frac{k_{P_n}}{k_{P_i}} c_{1_i}.$$

Finally, the remaining term in $\tilde{\omega}_n$ is contributed by the dissipation part $R(x)\nabla H$.

Remark 6.4.9. The analysis reveals that the stability properties of the lossless microgrid (5.21), (6.1) are independent of the frequency droop gains k_{P_i}, the active power setpoints P_i^d and the low pass filter time constants τ_{P_i}, and only condition (6.49) is imposed on V_i^d, k_{Q_i} and Q_i^d. In that regard, the result is identical to those derived for lossless first-order inverter models in [28] and lossless second-order inverter models in Section 6.3.11, respectively in [121], both assuming constant voltage amplitudes.

Remark 6.4.10. In a similar fashion to Corollary 6.3.13, a solution to Problem 3.3.5, i.e., the problem of active power sharing, can be formulated by combining the stability result given in Proposition 6.3.8 with Lemma 5.2.6. Establishing this result follows in a straightforward manner from the proof of Corollary 6.3.13 and is therefore not conducted explicitly. Furthermore, Problem 3.3.5 is considered in the next section.

Remark 6.4.11. The above given physical interpretation of the stability condition in Proposition 6.3.8 can, for example, be derived by analyzing the numerical range of the matrix condition on the left of (6.49), cf. Section 2.3.6. To see this, let $v \in \mathbb{R}^n$, $v^\top v = 1$ and multiply the matrix condition on the left of (6.49) from the left with $v^\top$ and from the right with v, which yields

$$v^\top \left(F + \mathcal{T}(\delta^s) - \mathbb{W}^\top \mathbb{L}^{-1} \mathbb{W}\right) v = v^\top \left(F + \mathcal{T}(\delta^s)\right) v - v^\top \left(\mathbb{W}^\top \mathbb{L}^{-1} \mathbb{W}\right) v > 0. \tag{6.56}$$

Without loss of generality, let $w := \mathbb{W}v \in \mathbb{R}^{n-1}$. Then, $w^\top w = v^\top \mathbb{W}^\top \mathbb{W} v = \gamma$, where $\gamma \in \mathbb{R}_{\geq 0}$, since the product of a matrix with its transposed is always positive semidefinite. Furthermore, (6.56) becomes

$$v^\top \left(F + \mathcal{T}(\delta^s)\right) v - w^\top \mathbb{L}^{-1} w > 0. \tag{6.57}$$

Clearly, $\gamma = 0$ implies $\mathbb{W}v = w = \underline{0}_{n-1}$ and the above inequality is then always true, since F and $\mathcal{T}(\delta^s)$ are positive definite matrices. Hence, assume $\gamma \neq 0$ and let $\sqrt{\gamma} b := w$, $b \in \mathbb{R}^{n-1}$. Replacing w by b in (6.57) gives

$$v^\top \left(F + \mathcal{T}(\delta^s)\right) v - \gamma b^\top \mathbb{L}^{-1} b > 0. \tag{6.58}$$

Finally, by noting that

$$\begin{aligned} v^\top \left(F + \mathcal{T}(\delta^s)\right) v = v^\top F v + v^\top \mathcal{T}(\delta^s) v \geq \min\left(\sigma\left(F\right)\right) + \min\left(\sigma\left(\mathcal{T}(\delta^s)\right)\right) > 0, \\ 0 < b^\top \mathbb{L}^{-1} b \leq \max\left(\sigma\left(\mathbb{L}^{-1}\right)\right) = \left(\min\left(\sigma(\mathbb{L})\right)\right)^{-1}, \end{aligned}$$

a (conservative) sufficient condition for the matrix inequality (6.49) to be satisfied is

$$\begin{aligned} &\min\left(\sigma(F)\right) + \min\left(\sigma\left(\mathcal{T}(\delta^s)\right)\right) - \gamma \left(\min\left(\sigma(\mathbb{L})\right)\right)^{-1} > 0 \\ \Leftrightarrow \quad &\left(\min\left(\sigma(F)\right) + \min\left(\sigma\left(\mathcal{T}(\delta^s)\right)\right)\right) \min\left(\sigma(\mathbb{L})\right) > \gamma, \end{aligned}$$

where the product $\min\left(\sigma\left(\mathcal{T}(\delta^s)\right)\right) \min\left(\sigma(\mathbb{L})\right)$ can be interpreted as a lower bound for the network coupling strength represented by $\mathbb{L}$ and $\mathcal{T}(\delta^s)$ and γ can be interpreted as the cross-coupling strength corresponding to $\mathbb{W}$.

6.4.2.4 A relaxed stability condition

Condition (6.49) is imposed to ensure $H(x)$ given in (6.51) is a positive definite function and, therefore, qualifies as a Lyapunov function candidate. This condition can be removed if, instead of Lyapunov theory, LaSalle's invariance principle (which does not require positive definiteness) is invoked, see Theorem 2.3.5. Indeed, from the proof of Proposition 6.4.7 it follows that the function $H(x)$ is still non-increasing and via LaSalle it can be concluded that all *bounded* trajectories converge to an equilibrium.

The qualifier "bounded" is, of course, critical, and its establishment is stymied by the presence of the linear term in θ contained in $H(x)$ given in (6.51). The inclusion of this term destroys the natural topology of the system, e.g., with $\theta \in \mathbb{T}^{n-1}$, and instead the system (6.40)-(6.41) with θ evolving in $\mathbb{R}^{n-1}$—which is not a bounded set—has to be considered. See Remark 7 of [49] for further discussion on this point that, unfortunately, is often overlooked in the literature.

Fortunately, due to the structure of the system, there is a particular choice of the controller gains that allows to remove this disturbing term, still preserving a port-Hamiltonian structure. It turns out that this choice of gains is of interest because it solves Problem 3.3.5, i.e., it guarantees a desired steady-state active power sharing according to Lemma 5.2.6.

The discussion above is formalized in the following corollary of Proposition 6.4.7.

Corollary 6.4.12. *Consider the system* (5.21), (6.1). *Fix* ω^d, τ_{P_i}, k_{Q_i} *and* Q_i^d, $i \sim \mathcal{N}$. *Select*

$$k_{P_i} P_i^d = \xi, \tag{6.59}$$

$i \sim \mathcal{N}$ *and some real constant* ξ. *Then, all trajectories of the system* (6.40)-(6.41) *converge to an equilibrium.*

Proof. Under condition (6.59), it follows from Remark 6.4.4 that

$$\omega^s = \omega^d + \frac{\sum_{i\sim\mathcal{N}} P_i^d}{\sum_{i\sim\mathcal{N}} \frac{1}{k_{P_i}}} = \omega^d + \frac{\xi \sum_{i\sim\mathcal{N}} \frac{1}{k_{P_i}}}{\sum_{i\sim\mathcal{N}} \frac{1}{k_{P_i}}} = \omega^d + \xi$$

and hence from (6.39) that $c_{1_i} = 0$ for all $i \in \mathcal{N}$. Consequently, it is possible to define the state $z := \operatorname{col}(\theta, \tilde{\omega}, V)$ in the set $\mathbb{D} : \mathbb{T}^{n-1} \times \mathbb{R}^n \times \mathbb{R}^n_{>0}$ and represent the system (6.40)-(6.41) in port-Hamiltonian form as

$$\dot{z} = (J - R(z))\nabla\mathcal{H},$$

with Hamiltonian $\mathcal{H} : \mathbb{T}^{n-1} \times \mathbb{R}^n \times \mathbb{R}^n_{>0} \to \mathbb{R}$ given by

$$\begin{aligned}\mathcal{H}(z) = \sum_{i=1}^{n} \Big(& \frac{\tau_{P_i}}{2k_{P_i}} \tilde{\omega}_i^2 + \frac{1}{k_{Q_i}} (V_i - c_{2_i} \ln(V_i)) + \frac{1}{2} |B_{ii}| V_i^2 \\ & - \frac{1}{2} \sum_{k\sim\mathcal{N}_i} V_i V_k |B_{ik}| \cos(\theta_{ik} + \delta_{ik}^s) \Big)\end{aligned} \tag{6.60}$$

and matrices J and $R(z)$ as defined in (6.52). Similarly to (6.53) it follows that

$$\dot{\mathcal{H}} = -(\nabla\mathcal{H})^\top R(z) \nabla\mathcal{H} \leq 0$$

and in analogy to (6.55) it holds that the invariant set where $\dot{H}(z(t)) = 0$, $\forall t \geq 0$, is an equilibrium set. Moreover, it follows from Proposition 6.4.1 that the state $z = \mathrm{col}(\theta, \tilde{\omega}, V) \in \mathbb{D}$ is globally bounded. Hence, by LaSalle's invariance principle, see Theorem 2.3.5, all trajectories of the system (6.40)-(6.41) converge to an equilibrium. □

Note, however, that the claim critically relies on the fragile assumption that $c_{1i} = 0$, $i \sim \mathcal{N}$. In the presence of small perturbations or model uncertainties, such as, for example, the presence of small conductances, the synchronization frequency is given by $\omega^s = \omega^d + \xi + \epsilon$, where ϵ is some small real nonzero constant. In that case $c_{1i} \neq 0$ under condition (6.59) and the proof of Corollary 6.4.12 is not applicable. Moreover, as usual in LaSalle's-based analysis, the absence of a *bona fide* Lyapunov function hampers the possibility of invoking a continuity argument to accommodate small disturbances.

6.5 Conditions for stability of lossless microgrids with distributed voltage control

This section is dedicated to the analysis of a microgrid operated with the DVC (5.27). Specifically, the main contributions are the following. Under the assumption of small angle differences [1, 29], it is shown that *(i)* the choice of the control parameters uniquely determines the corresponding equilibrium point of the closed-loop voltage and reactive power dynamics and that *(ii)* there exists a necessary and sufficient condition such that this equilibrium point is locally exponentially stable. In addition, by combining both aforementioned results, *(iii)* a solution to Problem 3.3.4, i.e., the problem of reactive power sharing, is given. Moreover, *(iv)*, a selection criterion for the control parameters is provided, which not only ensures reactive power sharing in steady-state, but also that the average of all voltage amplitudes in the network is equivalent to the nominal voltage amplitude for all $t \geq 0$. In addition, *(v)* the assumption of small angle differences is dropped and a necessary and sufficient condition for local exponential stability of a microgrid operated with the frequency droop control (5.2) and the DVC (5.27) is derived. By combining the latter stability result with Claim 5.3.8 and Lemma 5.2.6, *(vi)* a solution to the power sharing problem (Problem 3.3.5) is given.

It is assumed throughout this section that the power lines are dominantly inductive. Furthermore, for ease of notation, the analysis presented here is restricted to inverter-based microgrids. However, the results directly extend to MDREGs if the frequency

droop gains of the SGs are selected according to Assumption 6.3.5 and the EMFs of the SGs are controlled with the control law given by (5.30) together with (5.33).

The remainder of this section is outlined as follows. The results on existence and uniqueness properties of equilibria of the closed-loop voltage and reactive power dynamics under the DVC are given in Section 6.5.1. The corresponding stability result is presented in Section 6.5.2. The two aforementioned results are taken from [122, 125] and derived under the assumption of small angle differences. By combining these results, a solution to Problem 3.3.4 (the problem of reactive power sharing) is given in Section 6.5.3. The assumption of small angle differences is dropped in Section 6.5.4, where a condition for exponential stability of an equilibrium point of a microgrid operated with frequency droop control and DVC is provided. The section is concluded by providing a solution to the power sharing problem (Problem 3.3.5) in Section 6.5.5.

6.5.1 Existence and uniqueness of equilibria

Recall the closed-loop model of an inverter-based microgrid, i.e., $\mathcal{N} = \mathcal{N}_I$, with frequency droop control (5.2) and DVC (5.27) given with Assumption 6.2.4 by (5.36), (6.2). Furthermore, recall that under Assumption 6.2.5, the influence of the dynamics of the phase angles on the reactive power flows can be neglected. Moreover, the DVC given in (5.27) does only use reactive power measurements. Hence, by making use of Assumption 6.2.5, the voltage and reactive power dynamics of (5.36), (6.2) with $\mathcal{N} = \mathcal{N}_I$ can be analyzed independently of the angle and frequency dynamics. Therefore, the model below is considered in the following

$$\begin{aligned} \dot{V} &= -K\mathcal{L}DQ^m, \\ T\dot{Q}^m &= -Q^m + Q, \end{aligned} \tag{6.61}$$

where $Q_i = Q_i(V)$ is given by (6.3) and the initial conditions for each element of V are determined by the control law (5.27), i.e., $V(0) = V^d := \mathrm{col}(V_i^d)$, $i \sim \mathcal{N}$.

To streamline the presentation of the main result within this subsection, it is convenient to recall the matrix $\mathcal{T}(\delta) \in \mathbb{R}^{n\times n}$ defined in (6.4) and, with slight abuse of notation, denote by $\mathcal{T}$ its evaluation at $\delta_{ik} = 0$, $i \sim \mathcal{N}$, $k \sim \mathcal{N}_i$, with entries

$$\mathcal{T}_{ii} := |B_{ii}|, \quad \mathcal{T}_{ik} := -|B_{ik}|, \quad i \neq k. \tag{6.62}$$

The proposition below proves existence of equilibria of the system (6.61), (6.3). In addition, it shows that by setting $K = \kappa\mathcal{K}$, where κ is a positive real parameter and

$\mathcal{K} \in \mathbb{R}^{n\times n}$ a diagonal matrix with positive real diagonal entries, the control parameters $V(0) = V^d$, D and $\mathcal{K}$ uniquely determine the corresponding equilibrium point of the system (6.61), (6.3). It is demonstrated in the simulation study in Section 7.4 that the tuning parameter κ allows to easily shape the performance of the closed-loop dynamics.

Proposition 6.5.1. *Consider the system* (6.61), (6.3). *Fix D and a positive real constant α. Set $K = \kappa\mathcal{K}$, where κ is a positive real parameter and $\mathcal{K} \in \mathbb{R}^{n\times n}$ a diagonal matrix with positive real diagonal entries. To all initial conditions $col(V(0), Q^m(0))$ with the property*

$$\|\mathcal{K}^{-1}V(0)\|_1 = \alpha, \tag{6.63}$$

there exists a unique positive equilibrium point $col(V^s, Q^{m,s}) \in \mathbb{R}^{2n}_{>0}$. Moreover, to any α there exists a unique positive constant β such that

$$\|\mathcal{K}^{-1}V^s\|_1 = \alpha, \quad Q^s = Q^{m,s} = \beta D^{-1}\underline{1}_n. \tag{6.64}$$

Proof. To establish the claim, it is first proven that to each $Q^s \in \mathbb{R}^n_{>0}$ satisfying (6.64) there exists a unique $V^s \in \mathbb{R}^n_{>0}$. To this end, consider (5.37). Clearly, any $Q^s = \beta D^{-1}\underline{1}_n$, $\beta \in \mathbb{R}_{>0}$ satisfies (5.37) and is hence a possible vector of positive steady-state reactive power flows.

Fix a $\beta \in \mathbb{R}_{>0}$. Because of

$$Q^s_i = |B_{ii}|{V^s_i}^2 - \sum_{k\sim\mathcal{N}_i} |B_{ik}|V^s_i V^s_k, \quad i \sim \mathcal{N}, \tag{6.65}$$

no element V^s_i can then be zero. Hence, (6.65) can be rewritten as

$$-\frac{Q^s_i}{V^s_i} + |B_{ii}|V^s_i - \sum_{k\sim\mathcal{N}_i} |B_{ik}|V^s_k = 0, \quad i \sim \mathcal{N},$$

or, more compactly,

$$F(V^s) + \mathcal{T}V^s = \underline{0}_n, \tag{6.66}$$

where $F(V^s) := \mathrm{col}(-Q^s_i/V^s_i) \in \mathbb{R}^n$ and $\mathcal{T}$ is defined in (6.62). Recall that according to Lemma 6.2.6, $\mathcal{T}$ is positive definite. Consider the function $f : \mathbb{R}^n_{>0} \to \mathbb{R}$,

$$f(V) := \frac{1}{2}V^\top \mathcal{T}V - \sum_{i=1}^n Q^s_i \ln(V_i),$$

which has the property that

$$\left(\frac{\partial f(V)}{\partial V}\right)^\top = F(V) + \mathcal{T}V.$$

Hence, any critical point of f, i.e., any point $V^s \in \mathbb{R}^n_{>0}$ such that

$$\left(\frac{\partial f(V)}{\partial V}\right)^\top \Big|_{V^s} = \underline{0}_n,$$

satisfies (6.66), respectively (6.65). Moreover,

$$\frac{\partial^2 f(V)}{\partial V^2} = \operatorname{diag}\left(\frac{Q_i^s}{V_i^2}\right) + \mathcal{T} > 0,$$

which means that the Hessian of f is positive definite for all $V \in \mathbb{R}^n_{>0}$. Therefore, f is a strictly convex continuous function on the convex set $\mathbb{R}^n_{>0}$. Note that f tends to infinity on the boundary of $\mathbb{R}^n_{>0}$, i.e.,

$$\begin{aligned} f(V) &\to \infty \quad \text{as} \quad \|V\|_\infty \to \infty, \\ f(V) &\to \infty \quad \text{as} \quad \min_{i\in\mathcal{N}}(V_i) \to 0. \end{aligned}$$

Hence, there exist positive real constants $m_0 \gg 1$, $r_1 \ll 1$ and $r_2 \gg 1$, such that

$$\begin{aligned} &\mathbb{E} := \{V \in \mathbb{R}^n_{>0} \mid \min_{i\in\mathcal{N}}(V_i) \geq r_1 \wedge \|V\|_\infty \leq r_2\}, \\ &V \in \mathbb{R}^n_{>0} \setminus \mathbb{E} \quad \Rightarrow \quad f(V) > m_0, \\ &\exists V \in \mathbb{E} \quad \text{such that} \quad f(V) < m_0. \end{aligned}$$

Clearly, $\mathbb{E}$ is a compact set. Hence, by the Weierstrass extreme value theorem [246], f attains a minimum on $\mathbb{E}$. By construction, this minimum is attained at the interior of $\mathbb{E}$, which by differentiability of f implies that it is a critical point of f. Consequently, the vector $V^s := \arg\min_{V\in\mathbb{E}}(f(V))$ is the unique solution of (6.66) and thus the unique positive vector of steady-state voltage amplitudes corresponding to a given positive vector of steady-state reactive power flows Q^s. This proves existence of equilibria of the system (6.61), (6.3). Moreover, it shows that to a given $Q^s \in \mathbb{R}^n_{>0}$, there exists a unique corresponding $V^s \in \mathbb{R}^n_{>0}$.

Next, it is proven by contradiction that the constant α uniquely determines the positive equilibrium point $\operatorname{col}(V^s, Q^s) \in \mathbb{R}^{2n}_{>0}$ corresponding to all initial conditions $\operatorname{col}(V(0), Q^m(0))$ with the property (6.63). Assume that there exist two different positive equilibrium points $\operatorname{col}(V_1^s, Q_1^s) \in \mathbb{R}^{2n}_{>0}$ and $\operatorname{col}(V_2^s, Q_2^s) \in \mathbb{R}^{2n}_{>0}$ with the following property

$$\|\mathcal{K}^{-1}V_1^s\|_1 = \|\mathcal{K}^{-1}V_2^s\|_1 = \alpha. \tag{6.67}$$

It follows from (5.37) that the vectors Q_1^s and Q_2^s are identical up to multiplication by a positive real constant ϑ, i.e.,

$$Q_2^s = \vartheta Q_1^s.$$

The uniqueness result above implies $\vartheta \neq 1$, i.e., $Q_1^s \neq Q_2^s$. Otherwise V_1^s and V_2^s would coincide and the two equilibrium points would be the same.

Clearly, if $\mathrm{col}(V_1^s, Q_1^s)$ satisfies (6.65), then $\mathrm{col}(V_2^s, Q_2^s) = \mathrm{col}(\sqrt{\vartheta}V_1^s, \vartheta Q_1^s)$, $\vartheta > 0$, also satisfies (6.65) and, because of the uniqueness result, $V_2^s = \sqrt{\vartheta}V_1^s$ is the unique steady-state voltage vector corresponding to Q_2^s. As $\vartheta \neq 1$, it follows immediately that (6.67) is violated. The proof is completed by recalling that Fact 5.3.11 implies that

$$\|\mathcal{K}^{-1}V(t)\|_1 = \|\mathcal{K}^{-1}V(0)\|_1$$

for all $t \geq 0$. □

The following corollary follows immediately from the proof of Proposition 6.5.1. This result reflects the fact that the reactive power flows Q_i given in (6.3) are quadratic functions of the voltage amplitudes V_i, $i \sim \mathcal{N}$.

Corollary 6.5.2. *Consider the system* (6.61), (6.3). *Fix D and positive real constants α, β and ϑ. Set $K = \kappa\mathcal{K}$, where κ is a positive real parameter and $\mathcal{K} \in \mathbb{R}^{n\times n}$ a diagonal matrix with positive real diagonal entries. Assume col$(V^s, Q^{m,s}) \in \mathbb{R}^{2n}_{>0}$ is an equilibrium point of the system* (6.61), (6.3) *with the properties $Q^s = \beta D^{-1}\underline{1}_n$ and $\|\mathcal{K}^{-1}V^s\|_1 = \alpha$. Then, the unique equilibrium point corresponding to all initial conditions col$(V(0), Q^m(0))$ with the property $\|\mathcal{K}^{-1}V(0)\|_1 = \sqrt{\vartheta}\alpha$ is given by col$(\sqrt{\vartheta}V^s, \vartheta Q^{m,s})$.*

Proof. The last part of the proof of Proposition 6.5.1 implies that

$$\mathrm{col}(V_2^s, Q_2^{m,s}) = \mathrm{col}(\sqrt{\vartheta}V_1^s, \vartheta Q_1^{m,s})$$

is also an equilibrium point of the system (6.61), (6.3). Moreover, Fact 5.3.11 implies that

$$\|\mathcal{K}^{-1}V_2(0)\|_1 = \|\mathcal{K}^{-1}V_2^s\|_1 = \sqrt{\vartheta}\|\mathcal{K}^{-1}V_1^s\|_1 = \sqrt{\vartheta}\alpha.$$

This completes the proof. □

Remark 6.5.3. Fix a real constant α. Consider a linear first-order consensus system with state vector $x \in \mathbb{R}^n$ and dynamics

$$\dot{x} = -\mathcal{L}x, \quad x(0) = x_0, \tag{6.68}$$

where $\mathcal{L} \in \mathbb{R}^{n\times n}$ is the Laplacian matrix of the communication network. It is well-known, see, e.g., Section 2.3.5 or [85], that if the graph model of the communication network is undirected and connected, then

$$x^s = \frac{1}{n}\underline{1}_n^\top x_0 \underline{1}_n = \frac{1}{n}\left(\sum_{i=1}^n x_i(0)\right)\underline{1}_n.$$

Hence, to all x_0 with the property $\sum_{i=1}^{n} x_i(0) = \alpha$, there exists a unique x^s with $\sum_{i=1}^{n} x_i^s = \alpha$. Proposition 6.5.1 shows that the nonlinear system (6.61), (6.3) exhibits an equivalent property.

6.5.2 Voltage stability

In this section a necessary and sufficient condition for local exponential stability of equilibria of the system (6.61), (6.3) is established. To this end, the following important observation is made. It follows from Fact 5.3.11 that the motion of an arbitrary voltage V_i, $i \in \mathcal{N}$, can be expressed in terms of all other voltages V_k, $k \sim \mathcal{N} \setminus \{i\}$ for all $t \geq 0$. This implies that studying the stability properties of equilibra of the system (6.61), (6.3) with dimension $2n$, is equivalent to studying the stability properties of corresponding equilibria of a reduced system of dimension $2n-1$.

For ease of notation and without loss of generality, it is convenient to express V_n as

$$V_n = k_n \xi(V(0)) - \sum_{i=1}^{n-1} \frac{k_n}{k_i} V_i, \tag{6.69}$$

with $\xi(V(0))$ given by (5.39). Furthermore, let the reduced voltage vector $V_R \in \mathbb{R}_{>0}^{n-1}$ be given by

$$V_R := \operatorname{col}(V_1, \dots V_{n-1}), \tag{6.70}$$

and denote the reactive power flows in the reduced coordinates by

$$\begin{aligned} Q_i(V(V_R)) &= |B_{ii}| V_i^2 - \sum_{k \sim \mathcal{N}_i} |B_{ik}| V_i V_k, \\ Q_n(V(V_R)) &= |B_{nn}| V_n^2 - \sum_{k \sim \mathcal{N}_n} |B_{nk}| V_k V_n, \end{aligned} \tag{6.71}$$

where $V_n = V_n(V_R) = V_n(V_1, \dots, V_{n-1})$ and $i \sim \mathcal{N} \setminus \{n\}$.

By defining the matrix $\mathcal{L}_R \in \mathbb{R}^{(n-1)\times n}$

$$\mathcal{L}_R := \begin{bmatrix} \mathbf{I}_{n-1} & \underline{0}_{n-1} \end{bmatrix} K \mathcal{L}, \tag{6.72}$$

the system (6.61), (6.3) can be written in the reduced coordinates $\operatorname{col}(V_R, Q^m) \in \mathbb{R}_{>0}^{n-1} \times \mathbb{R}^n$ as

$$\begin{aligned} \dot{V}_R &= -\mathcal{L}_R D Q^m, \\ T\dot{Q}^m &= -Q^m + Q(V(V_R)), \end{aligned} \tag{6.73}$$

with $Q(V(V_R)) := \operatorname{col}(Q_i(V(V_R)))$ and $Q_i(V(V_R))$, $i \sim \mathcal{N}$, given in (6.71).

6.5.2.1 Error states and linearization

Recall Proposition 6.5.1. Clearly, the existence and uniqueness properties of the system (6.61), (6.3) hold equivalently for the reduced system (6.73), (6.71) with V_n given in (6.69).

Let $\mathrm{col}(V^s, Q^{m,s}) \in \mathbb{R}^{2n}_{>0}$ be a positive equilibrium point of the system (6.61), (6.3) and $\mathrm{col}(V^s_R, Q^{m,s}) \in \mathbb{R}^{(2n-1)}_{>0}$ be the corresponding equilibrium point of the system (6.73), (6.71). It follows from (6.69) that

$$\frac{\partial V_n(V_1, \ldots, V_{n-1})}{\partial V_i} = -\frac{k_n}{k_i}, \quad i \sim \mathcal{N} \setminus \{n\}.$$

Consequently, the partial derivative of the reactive power flow $Q_k(V(V_R))$, $k \sim \mathcal{N}$, given in (6.73), (6.71) with respect to the voltage $V_{R_i} = V_i$, $i \sim \mathcal{N} \setminus \{n\}$, can be written as

$$\frac{\partial Q_k(V(V_R))}{\partial V_{R_i}} = \frac{\partial Q_k}{\partial V_i}\frac{\partial V_i}{\partial V_{R_i}} + \frac{\partial Q_k}{\partial V_n}\frac{\partial V_n}{\partial V_{R_i}} = \frac{\partial Q_k}{\partial V_i} - \frac{k_n}{k_i}\frac{\partial Q_k}{\partial V_n}, \quad i \sim \mathcal{N} \setminus \{n\}. \tag{6.74}$$

Hence, by introducing the matrix

$$N := \frac{\partial Q}{\partial V}\Big|_{V^s} \in \mathbb{R}^{n \times n}$$

with entries (use (6.3))

$$n_{ii} := 2|B_{ii}|V_i^s - \sum_{k \sim \mathcal{N}_i} |B_{ik}|V_k^s, \; n_{ik} := -|B_{ik}|V_i^s, \; i \neq k, \tag{6.75}$$

as well as the matrix $\mathcal{Z} \in \mathbb{R}^{n \times (n-1)}$

$$\mathcal{Z} := \begin{bmatrix} \mathbf{I}_{n-1} \\ -g^\top \end{bmatrix}, \quad g := \mathrm{col}\left(\frac{k_n}{k_1}, \ldots, \frac{k_n}{k_{n-1}}\right), \tag{6.76}$$

and by making use of (6.74), it follows that

$$\frac{\partial Q(V(V_R))}{\partial V_R}\Big|_{V_R^s} = N\mathcal{Z}. \tag{6.77}$$

To derive an analytic stability condition, it is convenient to assume identical low pass filter time constants as stated in Assumption 6.3.5.

Furthermore, let the deviations of the system variables with respect to the equilibrium point $\mathrm{col}(V^s_R, Q^{m,s}) \in \mathbb{R}^{(2n-1)}_{>0}$ be given by

$$\tilde{V}_R := V_R - V_R^s \in \mathbb{R}^{n-1},$$
$$\tilde{Q}^m := Q^m - Q^{m,s} \in \mathbb{R}^n.$$

Linearizing the microgrid (6.73), (6.71) at this equilibrium point and making use of (6.77) together with Assumption 6.3.5 yields

$$\begin{bmatrix} \dot{\tilde{V}}_R \\ \dot{\tilde{Q}}^m \end{bmatrix} = \underbrace{\begin{bmatrix} \mathbf{0}_{(n-1)\times(n-1)} & -\mathcal{L}_R D \\ \frac{1}{\tau} N \mathcal{Z} & -\frac{1}{\tau}\mathbf{I}_n \end{bmatrix}}_{:=A_{\mathrm{DVC}}} \begin{bmatrix} \tilde{V}_R \\ \tilde{Q}^m \end{bmatrix}. \tag{6.78}$$

Note that

$$\begin{aligned} \mathcal{Z}\mathcal{L}_R &= \mathcal{Z}\begin{bmatrix} \mathbf{I}_{n-1} & \underline{0}_{n-1} \end{bmatrix} K\mathcal{L} = \begin{bmatrix} \mathbf{I}_{n-1} & \underline{0}_{n-1} \\ -g^\top & 0 \end{bmatrix} K\mathcal{L} \\ &= K \begin{bmatrix} \mathbf{I}_{n-1} & \underline{0}_{n-1} \\ -\underline{1}_{n-1}^\top & 0 \end{bmatrix} \mathcal{L} = K\mathcal{L}, \end{aligned} \tag{6.79}$$

where the last equality follows from Lemma 2.3.15 together with the fact that $\mathcal{L} = \mathcal{L}^\top$, and that

$$\mathcal{Z}^\top K^{-1} \underline{1}_n = \underline{0}_{n-1}. \tag{6.80}$$

6.5.2.2 Main result

The main contribution of this section is to give a necessary and sufficient condition for local exponential stability of an equilibrium point of the system (6.73), (6.71).

Lemma 6.5.4. *For $Q^s, V^s \in \mathbb{R}^n_{>0}$, all eigenvalues of N have positive real part.*

Proof. Dividing (6.65) by $V_i^s > 0$ yields

$$\frac{Q_i^s}{V_i^s} = |B_{ii}|V_i^s - \sum_{k\sim\mathcal{N}_i} |B_{ik}|V_k^s > 0. \tag{6.81}$$

Furthermore, from (4.21) it follows that

$$|B_{ii}|V_i^s \geq \sum_{k\sim\mathcal{N}_i} |B_{ik}|V_i^s. \tag{6.82}$$

Hence, with n_{ii} and n_{ik} defined in (6.75) we have that

$$n_{ii} = 2|B_{ii}|V_i^s - \sum_{k\sim\mathcal{N}_i} |B_{ik}|V_k^s > |B_{ii}|V_i^s \geq \sum_{k\sim\mathcal{N}\setminus\{i\}} |n_{ik}|.$$

Therefore, N is a diagonally dominant matrix with positive diagonal elements and the claim follows from Gershgorin's disc theorem [144, Chapter 6]. □

Lemma 6.5.5. *For $Q^s, V^s \in \mathbb{R}^n_{>0}$, the matrix product $ND\mathcal{L}D$ has a zero eigenvalue with geometric multiplicity one and a corresponding right eigenvector $\beta D^{-1}\underline{1}_n$, $\beta \in \mathbb{C}\setminus\{0\}$; all other eigenvalues have positive real part.*

Proof. The matrix D is diagonal with positive diagonal entries and hence positive definite. Furthermore, $\mathcal{L}$ is the Laplacian matrix of an undirected connected graph and therefore positive semidefinite. In addition, $\mathcal{L}$ has a simple zero eigenvalue with a corresponding right eigenvector $\beta \underline{1}_n$, $\beta \in \mathbb{C} \setminus \{0\}$, see Section 2.3.5. Moreover, Lemma 6.5.4 implies that N is nonsingular. Consequently, for any nonzero $v \in \mathbb{C}^n$,

$$ND\mathcal{L}Dv = \underline{0}_n \Leftrightarrow \mathcal{L}Dv = \underline{0}_n \Leftrightarrow v = \beta D^{-1}\underline{1}_n,\ \beta \in \mathbb{C} \setminus \{0\}.$$

Hence, $ND\mathcal{L}D$ has a zero eigenvalue with geometric multiplicity one and a corresponding right eigenvector $\beta D^{-1}\underline{1}_n$, $\beta \in \mathbb{C} \setminus \{0\}$.

In addition, $D\mathcal{L}D$ is positive semidefinite and by Lemma 2.3.18 it follows that

$$\sigma(ND\mathcal{L}D) \subseteq W(N)W(D\mathcal{L}D) := \{\lambda = ab \;\big|\; a \in W(N), b \in W(D\mathcal{L}D)\}. \tag{6.83}$$

By the aforementioned properties of D and $\mathcal{L}$, we have that $W(D\mathcal{L}D) \subseteq \mathbb{R}_{\geq 0}$. To prove that all nonzero eigenvalues have positive real part, it is shown that $\Re(W(N)) \subseteq \mathbb{R}_{>0}$. Clearly, from (6.83), this also implies that the only element of the imaginary axis in $W(N)W(D\mathcal{L}D)$ is the origin. Recall that the real part of the numerical range of N is given by the range of its symmetric part, i.e.,

$$\Re(W(N)) = W\left(\frac{1}{2}\left(N + N^\top\right)\right).$$

The symmetric part of N has entries

$$\bar{n}_{ii} := n_{ii}, \quad \bar{n}_{ik} := -\frac{1}{2}|B_{ik}|(V_i^s + V_k^s),$$

where n_{ii} is defined in (6.75). From (6.81) it follows that

$$|B_{ii}|V_i^s > \sum_{k \sim \mathcal{N}_i} |B_{ik}|V_k^s.$$

Hence, together with (6.82) it follows that

$$|B_{ii}|V_i^s > \frac{1}{2}\sum_{k \sim \mathcal{N}_i} |B_{ik}|(V_i^s + V_k^s) = \sum_{k \sim \mathcal{N}\setminus\{i\}} |\bar{n}_{ik}|$$

and

$$\bar{n}_{ii} = 2|B_{ii}|V_i^s - \sum_{k \sim \mathcal{N}_i} |B_{ik}|V_k^s > |B_{ii}|V_i^s > \sum_{k \sim \mathcal{N}\setminus\{i\}} |\bar{n}_{ik}|.$$

Consequently, the symmetric part of N is diagonally dominant with positive diagonal entries and by Gershgorin's disc theorem its eigenvalues are all positive real, completing the proof. □

The main result within this section is given below. It establishes a necessary and sufficient condition for local exponential stability of an equilibrium point of the system (6.61), (6.3).

Proposition 6.5.6. *Consider the system* (6.61), (6.3). *Fix D and positive real constants α and τ. Set $\tau_{P_i} = \tau$, $i \sim \mathcal{N}$ and $K = \kappa D$, where κ is a positive real parameter. Let col$(V^s, Q^{m,s}) \in \mathbb{R}^{2n}_{>0}$ be the unique equilibrium point of the system* (6.61), (6.3) *corresponding to all $V(0)$ with the property $\|D^{-1}V(0)\|_1 = \alpha$. Denote by $x^s = col(V_R^s, Q^{m,s}) \in \mathbb{R}^{(2n-1)}_{>0}$ the unique corresponding equilibrium point of the reduced system* (6.73), (6.71).

Let $\mu_i = a_i + jb_i$ be the i-th nonzero eigenvalue of the matrix product $ND\mathcal{L}D$ with $a_i \in \mathbb{R}$ and $b_i \in \mathbb{R}$. Then, x^s is a locally exponentially stable equilibrium point of the system (6.73), (6.71) *if and only if the positive real parameter κ is chosen such that*

$$\tau\kappa b_i^2 < a_i \tag{6.84}$$

for all μ_i. Moreover, the equilibrium point x^s is locally exponentially stable for any positive real κ if and only if $ND\mathcal{L}D$ has only real eigenvalues.

Proof. The proof is very similar to that of Proposition 6.3.8. With $\tau_{P_i} = \tau$, $i \sim \mathcal{N}$, the linear system (6.78) locally represents the microgrid dynamics (6.73), (6.71). The proof is thus given by deriving the spectrum of A_{DVC}, with A_{DVC} defined in (6.78). Let λ be an eigenvalue of A_{DVC} with a corresponding right eigenvector $v = \mathrm{col}(v_1, v_2)$, $v_1 \in \mathbb{C}^{n-1}$, $v_2 \in \mathbb{C}^n$. Then,

$$\begin{aligned} -\mathcal{L}_R D v_2 &= \lambda v_1, \\ \frac{1}{\tau}\left(N\mathcal{Z}v_1 - v_2\right) &= \lambda v_2. \end{aligned} \tag{6.85}$$

As done in the proof of Proposition 6.3.8, it is first shown by contradiction that zero is not an eigenvalue of A_{DVC}. Therefore, assume $\lambda = 0$. Then,

$$\mathcal{L}_R D v_2 = \underline{0}_{n-1}. \tag{6.86}$$

From the definition of $\mathcal{L}_R$ given in (6.72), it follows that (6.86) can only be satisfied if

$$K\mathcal{L}Dv_2 = \begin{bmatrix} \underline{0}_{n-1} \\ a \end{bmatrix}, \quad a \in \mathbb{C}.$$

The fact that $\mathcal{L} = \mathcal{L}^\top$ together with $\mathcal{L}\underline{1}_n = \underline{0}_n$ implies that $\underline{1}_n^\top K^{-1} K\mathcal{L}Dv = 0$ for any $v \in \mathbb{C}^n$. Therefore,

$$\underline{1}_n^\top K^{-1} K\mathcal{L}Dv_2 = \underline{1}_n^\top K^{-1} \begin{bmatrix} \underline{0}_{n-1} \\ a \end{bmatrix} = \frac{a}{k_n} = 0.$$

Hence, a must be zero. Consequently, $v_2 = \beta D^{-1}\underline{1}_n$, $\beta \in \mathbb{C}$. Inserting $\lambda = 0$ and $v_2 = \beta D^{-1}\underline{1}_n$ in the second line of (6.85) and recalling $K = \kappa D$ yields

$$N\mathcal{Z}v_1 = \beta D^{-1}\underline{1}_n = \beta\kappa K^{-1}\underline{1}_n. \tag{6.87}$$

Premultiplying with $v_1^*\mathcal{Z}^\top$ gives, because of (6.80),

$$v_1^*\mathcal{Z}^\top N\mathcal{Z}v_1 = 0.$$

As, according to the proof of Lemma 6.5.5, $\Re(W(N)) \subseteq \mathbb{R}_{>0}$, this implies

$$\mathcal{Z}v_1 = \underline{0}_n. \tag{6.88}$$

Hence, because of (6.87), $\beta = 0$ and $v_2 = \underline{0}_n$. Finally, because of (6.76), (6.88) implies $v_1 = \underline{0}_{n-1}$. Hence, (6.85) can only hold for $\lambda = 0$ if $v_1 = \underline{0}_{n-1}$ and $v_2 = \underline{0}_n$. Therefore, zero is not an eigenvalue of A_{DVC}.

Next, conditions are derived under which all eigenvalues of A_{DVC} have negative real part. Since $\lambda \neq 0$, (6.85) can be rewritten as

$$\lambda^2 v_2 + \frac{1}{\tau}\lambda v_2 + \frac{1}{\tau}N\mathcal{Z}\mathcal{L}_R D v_2 = \underline{0}_n. \tag{6.89}$$

Recall from (6.79) that $\mathcal{Z}\mathcal{L}_R = K\mathcal{L}$. Moreover, $K = \kappa D$. Hence, (6.89) is equivalent to

$$\lambda^2 v_2 + \frac{1}{\tau}\lambda v_2 + \frac{\kappa}{\tau}ND\mathcal{L}Dv_2 = \underline{0}_n. \tag{6.90}$$

This implies that v_2 must be an eigenvector of $ND\mathcal{L}D$. Recall that Lemma 6.5.5 implies that $ND\mathcal{L}D$ has a zero eigenvalue with geometric multiplicity one and all its other eigenvalues have positive real part. For $ND\mathcal{L}Dv_2 = \underline{0}_n$, (6.90) has solutions $\lambda = 0$ and $\lambda = -1/\tau$. Recall that zero is not an eigenvalue of A_{DVC}. Hence, $\lambda_1 = -1/\tau$ is the first eigenvalue (with unknown algebraic multiplicity) of the matrix A_{DVC}.

To investigate the remaining $0 \leq m \leq 2n-2$ eigenvalues of the matrix $A_{\mathrm{DVC}} \in \mathbb{R}^{(2n-1)\times(2n-1)}$, denote the remaining[1] eigenvalues of $ND\mathcal{L}D$ by $\mu_i \in \mathbb{C}$. Let a corresponding right eigenvector be given by $w_i \in \mathbb{C}^n$, i.e., $ND\mathcal{L}Dw_i = \mu_i w_i$. Without loss of generality, choose w_i such that $w_i^* w_i = 1$. By taking v_2 in (6.90) as w_i and multiplying (6.90) from the left with w_i^*, the remaining m eigenvalues of A_{DVC} are the solutions $\lambda_{i_{1,2}}$ of

$$\lambda_{i_{1,2}}^2 + \frac{1}{\tau}\lambda_{i_{1,2}} + \frac{\kappa}{\tau}\mu_i = 0. \tag{6.91}$$

[1]Neither the algebraic multiplicities of the eigenvalues of the matrix product $NDLD$ nor the geometric multiplicities of its nonzero eigenvalues are known in the present case. However, this information is not required, since, to establish the claim, it suffices to know that $\Re(\sigma(NDLD)) \subseteq \mathbb{R}_{\geq 0}$. This fact has been proven in Lemma 6.5.5.

First, consider real nonzero eigenvalues, i.e., $\mu_i = a_i$ with $a_i > 0$. Then, clearly, both solutions of (6.91) have negative real parts, e.g., by the Hurwitz condition. Next, consider complex eigenvalues of $ND\mathcal{L}D$, i.e., $\mu_i = a_i + jb_i$, $a_i > 0, b_i \in \mathbb{R} \setminus \{0\}$. Then, (6.91) is a quadratic polynomial with complex coefficients. Recall that $1/\tau$ is positive real. Hence, according to Corollary 2.3.13, both roots of (6.91) have negative real parts if and only if for $\tau >$, $\kappa > 0$,

$$\frac{1}{\tau^2}\frac{\kappa a_i}{\tau} - \frac{\kappa^2 b_i}{\tau^2} > 0 \quad \Leftrightarrow \quad a_i - \kappa\tau b_i^2 > 0, \tag{6.92}$$

which is condition (6.84). Hence, A_{DVC} is Hurwitz if and only if (6.84) holds for all μ_i. Finally, by Theorem 2.3.8, the equilibrium point x^s is locally exponentially stable if and only if A_{DVC} is Hurwitz. □

The following three observations are made with respect to Proposition 6.5.6. First, equilibria of (6.73), (6.71) are independent of the parameters τ and κ. Hence, selecting κ according to the stability condition (6.84) does not modify a given equilibrium point $\mathrm{col}(V_R^s, Q_m^s)$.

Second, condition (6.84) shows the same trade-off between the magnitude of the feedback gains (expressed by κ) and the time constant of the low pass filters (represented by τ) as does the stability condition for a lossy frequency-droop-controlled MDREG of Proposition 6.3.8. That is, the slower the power measurements are processed, the lower the feedback gains have to be chosen in order to ensure stability.

Third, for $K = \kappa D$ and a fixed α and making use of (6.69), the deviation of the voltage at the n-th node with respect to its equilibrium value V_n^s can be expressed independently of the parameter κ as

$$\tilde{V}_n := V_n - V_n^s = -\sum_{i=1}^{n-1} \frac{\chi_i}{\chi_n}\tilde{V}_i,$$

which, in accordance to Fact 5.3.11 and Proposition 6.5.1, implies that

$$\tilde{V}_n(0) = -\sum_{i=1}^{n-1} \frac{\chi_i}{\chi_n}\tilde{V}_i(0).$$

Remark 6.5.7. The selection $K = \kappa D$ is suggested in Proposition 6.5.6 based on Lemma 6.5.5, which states that $\Re(\sigma(NKLD)) \subseteq \mathbb{R}_{\geq 0}$ if $K = D$. This condition is sufficient, not necessary. Hence, there may very well exist other choices of K for which an equilibrium x^s of the system (6.61), (6.3) is stable.

6.5.3 A solution to the problem of reactive power sharing in lossless microgrids

In this section, a condition is given under which the reactive power sharing problem (Problem 3.3.4) is solved. The result follows as a corollary to Propositions 6.5.1 and 6.5.6.

Corollary 6.5.8. *Consider the system* (6.61), (6.3). *Fix D and positive real constants α and τ. Set $\tau_{P_i} = \tau$, $i \sim \mathcal{N}$ and $K = \kappa D$, where κ is a positive real parameter. Let col$(V^s, Q^{m,s}) \in \mathbb{R}^{2n}_{>0}$ be the unique equilibrium point of the system* (6.61), (6.3) *corresponding to all $V(0)$ with the property $\|D^{-1}V(0)\|_1 = \alpha$. Choose κ such that the conditions of Proposition 6.5.6 are satisfied. Then, Problem 3.3.4 is solved locally, i.e., for all initial conditions in a neighborhood of col$(V^s, Q^{m,s})$ satisfying $\|D^{-1}V(0)\|_1 = \alpha$.*

Proof. The claim is established by combining the results of Propositions 6.5.1 and 6.5.6. The result of Proposition 6.5.1 implies that, to the chosen α, there exists a positive real β, such that the equilibrium col$(V^s, Q^{m,s})$ of the system (6.61), (6.3) satisfies

$$DQ^{m,s} = DQ^s(V^s) = \beta \underline{1}_n,$$

which is equivalent to reactive power sharing as defined in Problem 3.3.4. Furthermore, under the standing assumptions, the claimed convergence result follows directly from Proposition 6.5.6. This completes the proof. □

6.5.4 Frequency and voltage stability

This section is devoted to the stability analysis of inverter-based microgrids with arbitrary meshed topologies and dominantly inductive power lines, in which the inverters are controlled via the usual frequency droop control given in (5.2) together with the proposed DVC defined in (5.27). For such networks, a necessary and sufficient condition for local frequency and voltage stability is given. Unlike in Section 6.5.2, no assumption on small angle differences is made, i.e., Assumption 6.2.5 is not used.

To establish the result, recall the closed-loop model of an inverter-based microgrid operated with the frequency droop control (5.2) and the DVC (5.27) given by (5.36), (4.24) with $\mathcal{N} = \mathcal{N}_I$, as well as Assumptions 6.2.4 and 6.3.5. Furthermore, recall that under Assumption 6.2.4, the power flow equations (4.24) simplify to (6.2).

6.5.4.1 Synchronized motion

Similar to the previous sections, the following natural power-balance feasibility assumption is made. Recall the set Θ defined in Assumption 6.4.3.

Assumption 6.5.9. *There exist constants* $\delta^s \in \Theta$, $\omega^s \in \mathbb{R}$, $V^s \in \mathbb{R}^n_{>0}$ *and* $Q^{m,s} \in \mathbb{R}^n_{>0}$, $\beta \in \mathbb{R}_{>0}$, *such that*

$$\begin{aligned} \underline{0}_n &= (\omega^d - \omega^s)\underline{1}_n - K_P(P(\delta^s, V^s) - P^d), \\ Q^{m,s} &= \beta D^{-1}\underline{1}_n, \\ \underline{0}_n &= -Q^{m,s} + Q(\delta^s, V^s), \end{aligned} \tag{6.93}$$

Under Assumption 6.5.9, the motion of the system (5.36), (6.2) starting in $\mathrm{col}(\delta^s, \underline{1}_n\omega^s, V^s, Q^{m,s})$ is given by

$$\begin{aligned} \delta^*(t) &= \mathrm{mod}_{2\pi}\left\{\delta^s + \underline{1}_n\left(\omega^s t - \int_0^t \omega^{\mathrm{com}}(\tau)d\tau\right)\right\}, \\ \omega^*(t) &= \underline{1}_n\omega^s, \\ V^*(t) &= V^s, \\ Q^{m,*}(t) &= \beta D^{-1}\underline{1}_n. \end{aligned} \tag{6.94}$$

As before, this desired motion is called synchronized motion and ω^s is the synchronization frequency.

Remark 6.5.10. The synchronized motion (6.94) lives in the set $\Theta \times \underline{1}_n\omega^s \times \mathbb{R}^n_{>0} \times \mathbb{R}^n_{>0}$ and is only unique up to a uniform shift of all angles.

6.5.4.2 Error states and linearization

Recall from Section 6.3 that the dependence with respect to δ of the dynamics (5.36), (6.2) is via angle differences δ_{ik}. Also recall the definition of the angle and frequency error states given in (6.9) and the matrix $\mathcal{R}$ defined in (6.10). For the present analysis and with slight abuse of notation, it is convenient to define the relative frequency deviation between the i-th node and the reference node n as

$$\dot{\theta}_i = \omega_i - \omega_n := \tilde{\omega}_i, \quad i \sim \mathcal{N} \setminus \{n\}. \tag{6.95}$$

Regarding the voltage dynamics, the same procedure as in Section 6.5.2 is followed and, by means of Fact 5.3.11, the voltage at the n-th bus is expressed as

$$V_n = k_n\xi(V(0)) - \sum_{i=1}^{n-1}\frac{k_n}{k_i}V_i,$$

see (6.69). Furthermore, recall the *constant* $\theta_n = 0$, the reduced voltage vector $V_R \in \mathbb{R}^{n-1}_{>0}$ defined in (6.70) as

$$V_R = \mathrm{col}(V_i), \quad i \sim \mathcal{N} \setminus \{n\},$$

as well as (6.71).

The active and reactive power flows P_i, respectively Q_i, given in (6.2) read in the new coordinates as

$$\begin{aligned} P_i(\tilde{\delta}(\theta), V(V_R)) &= G_{ii}V_i^2 + \sum_{k\sim\mathcal{N}_i} |B_{ik}|V_iV_k \sin(\theta_{ik} + \delta^s_{ik}), \\ P_n(\tilde{\delta}(\theta), V(V_R)) &= G_{nn}V_n^2 + \sum_{k\sim\mathcal{N}_n} |B_{nk}|V_nV_k \sin(\theta_{nk} + \delta^s_{nk}), \\ Q_i(\tilde{\delta}(\theta), V(V_R)) &= |B_{ii}|V_i^2 - \sum_{k\sim\mathcal{N}_i} |B_{ik}|V_iV_k \cos(\theta_{ik} + \delta^s_{ik}), \\ Q_n(\tilde{\delta}(\theta), V(V_R)) &= |B_{nn}|V_n^2 - \sum_{k\sim\mathcal{N}_n} |B_{nk}|V_kV_n \cos(\theta_{nk} + \delta^s_{nk}), \end{aligned} \tag{6.96}$$

where $V_n = V_n(V_1, \ldots, V_{n-1})$ and $i \sim \mathcal{N} \setminus \{n\}$. By defining

$$\mathcal{K}_P := \mathrm{diag}(k_{P_i}) \in \mathbb{R}^{(n-1)\times(n-1)}, \quad \tilde{\omega} := \mathrm{col}(\tilde{\omega}_i) \in \mathbb{R}^{n-1},$$

$i \sim \mathcal{N} \setminus \{n\}$, rearranging the system equations, and recalling the definition of the reduced voltage and reactive power dynamics given in (6.73), the overall microgrid dynamics (5.36), (6.2) with Assumption 6.3.5 can be written in reduced coordinates $\mathrm{col}(\theta, V_R, \tilde{\omega}, Q^m) \in \mathbb{R}^{n-1} \times \mathbb{R}^{n-1}_{>0} \times \mathbb{R}^{n-1} \times \mathbb{R}^n$ compactly as

$$\begin{aligned} \dot{\theta} &= \tilde{\omega}, \\ \dot{V}_R &= -\mathcal{L}_R D Q^m, \\ \tau\dot{\tilde{\omega}} &= -\tilde{\omega} - \mathcal{K}_P \begin{bmatrix} \mathbf{I}_{n-1} & -\mathcal{K}_P^{-1} k_{P_n} \underline{1}_{n-1} \end{bmatrix} \left(P(\tilde{\delta}(\theta), V(V_R)) - P^d \right), \\ \tau\dot{Q}^m &= -Q^m + Q(\tilde{\delta}(\theta), V(V_R)). \end{aligned} \tag{6.97}$$

The main contribution of this section is to give a condition for local exponential stability of the equilibrium $\mathrm{col}(\underline{0}_{n-1}, V_R^s, \underline{0}_{n-1}, Q^{m,s})$ of the system (6.97), (6.96). Recall that an exponentially stable equilibrium point is isolated. Hence, local exponential stability of $\mathrm{col}(\underline{0}_{n-1}, V_R^s, \underline{0}_{n-1}, Q^{m,s})$ corresponding to the reduced dynamics (6.97), (6.96) implies convergence of all trajectories of the original system (5.36), (6.2) starting in a neighborhood of $\mathrm{col}(\delta^s, \omega^s \underline{1}_n, V^s, Q^{m,s})$ to the synchronized motion (6.94) (up to a uniform constant shift of all angles). See also [247] for a discussion on the number of

states required to completely describe the dynamics of conventional SG-based power systems.

For ease of notation, it is convenient to introduce the matrices

$$\begin{aligned}
A_1 &:= \mathbf{I}_{n-1} + \mathcal{K}_P^{-1} k_{P_n} \underline{1}_{n-1} \underline{1}_{n-1}^\top \in \mathbb{R}^{(n-1)\times(n-1)}, \\
A_2 &:= \text{blkdiag}(\mathcal{K}_P A_1, -\mathbf{I}_n) \in \mathbb{R}^{(2n-1)\times(2n-1)}, \\
A_3 &:= \text{blkdiag}(\mathbf{I}_{n-1}, -\mathcal{L}_R D) \in \mathbb{R}^{(2n-2)\times(2n-1)}, \\
A_4 &:= \begin{bmatrix} \mathbf{I}_{n-1} & -\mathcal{K}_P^{-1} k_{P_n} \underline{1}_{n-1} \end{bmatrix} \in \mathbb{R}^{(n-1)\times n}, \\
A_5 &:= \text{blkdiag}(\mathbf{I}_{n-1}, \mathcal{Z}) \in \mathbb{R}^{(2n-1)\times(2n-2)}, \\
N_2 &:= \frac{\partial Q}{\partial V}\Big|_{(\delta^s, V^s)} \in \mathbb{R}^{n\times n},
\end{aligned} \tag{6.98}$$

with Q_i given in (6.2), $\mathcal{Z}$ given in (6.76) and $\mathcal{L}_R$ given in (6.72). In analogy to (6.77), it follows that

$$\frac{\partial Q(\tilde{\delta}(\theta), V(V_R))}{\partial V_R}\Big|_{(\theta^s, V_R^s)} = \left(\frac{\partial Q}{\partial V}\frac{\partial V}{\partial V_R}\right)\Big|_{(\theta^s, V_R^s)} = N_2 \mathcal{Z}.$$

Similarly,

$$\begin{aligned}
\begin{bmatrix} \mathbf{I}_{n-1} & -\mathcal{K}_P^{-1} k_{P_n} \underline{1}_{n-1} \end{bmatrix} \frac{\partial P(\tilde{\delta}(\theta), V(V_R))}{\partial V_R}\Big|_{(\theta^s, V_R^s)} &= A_4 \left(\frac{\partial P}{\partial V}\frac{\partial V}{\partial V_R}\right)\Big|_{(\theta^s, V_R^s)} \\
&= A_4 \frac{\partial P}{\partial V}\Big|_{(\theta^s, V_R^s)} \mathcal{Z}.
\end{aligned}$$

Recall $\tilde{L}$ defined in (6.13) and $\mathbb{L}$ defined in (6.43). Note that, under the made assumptions, $\phi_{ik} = 0$, $i \sim \mathcal{N}$, $k \sim \mathcal{N}$, in (6.13). Hence, with (6.14), one obtains

$$\begin{aligned}
\begin{bmatrix} \mathbf{I}_{n-1} & -\mathcal{K}_P^{-1} k_{P_n} \underline{1}_{n-1} \end{bmatrix} \frac{\partial P(\tilde{\delta}(\theta), V(V_R))}{\partial \theta}\Big|_{(\theta^s, V_R^s)} &= A_4 \left(\frac{\partial P}{\partial \tilde{\delta}}\frac{\partial \tilde{\delta}}{\partial \theta}\right)\Big|_{(\theta^s, V_R^s)} \\
&= A_4 \tilde{L} \begin{bmatrix} \mathbf{I}_{n-1} \\ \underline{0}_{n-1}^\top \end{bmatrix} = A_4 \begin{bmatrix} \mathbb{L} \\ b^\top \end{bmatrix} \\
&= \left(\mathbb{L} - \mathcal{K}_P^{-1} k_{P_n} \underline{1}_{n-1} b^\top\right),
\end{aligned} \tag{6.99}$$

where $b = \text{col}(\tilde{l}_{in}) \in \mathbb{R}^{n-1}$, $i \sim \mathcal{N} \setminus \{n\}$, see also (6.46). By noting that

$$b^\top = -\underline{1}_{n-1}^\top \mathbb{L},$$

(6.99) can be written as

$$\begin{bmatrix} \mathbf{I}_{n-1} & -\mathcal{K}_P^{-1} k_{P_n} \underline{1}_{n-1} \end{bmatrix} \frac{\partial P(\tilde{\delta}(\theta), V(V_R))}{\partial \theta}\Big|_{(\theta^s, V_R^s)} = \left(\mathbf{I}_{n-1} + \mathcal{K}_P^{-1} k_{P_n} \underline{1}_{n-1} \underline{1}_{n-1}^\top\right) \mathbb{L} = A_1 \mathbb{L}.$$

Let

$$B := \begin{bmatrix} \mathbb{L} & A_1^{-1} A_4 \frac{\partial P}{\partial V} \\ \frac{\partial Q}{\partial \theta} & N_2 \end{bmatrix} \Big|_{(\theta^s, V^s)} \in \mathbb{R}^{(2n-1)\times(2n-1)}, \tag{6.100}$$

where P_i and Q_i are given in (6.2). Finally, recall Assumption 6.5.9 and, following Section 6.5.2, let

$$\tilde{V}_R := V_R - V_R^s \in \mathbb{R}^{n-1},$$
$$\tilde{Q}^m := Q^m - Q^{m,s} \in \mathbb{R}^n.$$

By denoting the vector of the error states in the reduced coordinates by ζ, i.e.,

$$\zeta := \mathrm{col}(\theta, \tilde{V}_R, \tilde{\omega}, \tilde{Q}^m) \in \mathbb{R}^{(4n-3)},$$

the microgrid dynamics (6.97), (6.96) can be represented in a small neighborhood of the equilibrium $\mathrm{col}(\theta, \tilde{V}_R, \tilde{\omega}, \tilde{Q}^m) = \underline{0}_{(4n-3)}$ as

$$\dot{\zeta} = \underbrace{\begin{bmatrix} \mathbf{0}_{(2n-2)\times(2n-2)} & A_3 \\ -\frac{1}{\tau} A_2 B A_5 & -\frac{1}{\tau}\mathbf{I}_{(2n-1)} \end{bmatrix}}_{:=\mathcal{M}} \zeta. \tag{6.101}$$

6.5.4.3 Main result

To streamline the main result within this section, the following lemma is useful.

Lemma 6.5.11. *Select $K = D$. If the matrix $B + B^\top$ is positive definite, then the matrix product $A_2 B A_5 A_3$, the matrix components of which are defined in* (6.98) *and* (6.100)*, has a simple zero eigenvalue with a corresponding right eigenvector col($\underline{0}_{n-1}$, $\beta D^{-1}\underline{1}_n$), $\beta \in \mathbb{C} \setminus \{0\}$ and all other eigenvalues have positive real part.*

Proof. The proof is established along the lines of the proof of Lemma 6.5.5. At first, consider the matrix A_2 defined in (6.98). Note that

$$\mathcal{K}_P A_1 = \mathcal{K}_P + k_{P_n} \underline{1}_{n-1} \underline{1}_{n-1}^\top.$$

Since $\mathcal{K}_P$ is a diagonal matrix with positive diagonal entries and $k_{P_n}\underline{1}_{n-1}\underline{1}_{n-1}^\top$ is symmetric positive semidefinite [144, Example 1.3.23], $\mathcal{K}_P A_1$ is positive definite. This implies that A_2 is symmetric and invertible. Hence, via a similarity transformation with A_2, the spectrum of $A_2 B A_5 A_3$ is equivalent to that of $B A_5 A_3 A_2$. Recalling (6.79) and $K = D$, yields

$$A_5 A_3 A_2 = \mathrm{blkdiag}\left(\left(\mathcal{K}_P + k_{P_n}\underline{1}_{n-1}\underline{1}_{n-1}^\top\right), D\mathcal{L}D\right), \tag{6.102}$$

where the first block-diagonal entry is positive definite and the second is positive semidefinite. Consequently, by Lemma 2.3.18,

$$\sigma(B A_5 A_3 A_2) \subseteq W(B) W(A_5 A_3 A_2),$$

where $W(A_5A_3A_2) \subseteq \mathbb{R}_{\geq 0}$. Moreover, since $\mathcal{K}_P + k_{P_n}\underline{1}_{n-1}\underline{1}_{n-1}^\top$ is positive definite and $\mathcal{L}$ is the Laplacian matrix of a connected undirected graph, the matrix product $A_5A_3A_2$ has a simple zero eigenvalue with a corresponding right eigenvector $\mathrm{col}(\underline{0}_{n-1}, \beta D^{-1}\underline{1}_n)$, $\beta \in \mathbb{C} \setminus \{0\}$. All its other eigenvalues are positive real.

Hence, if

$$\Re(W(B)) \subseteq \mathbb{R}_{>0},$$

which is equivalent to $B+B^\top$ being positive definite, then the matrix product $BA_5A_3A_2$ has a simple zero eigenvalue with a corresponding right eigenvector $\mathrm{col}(\underline{0}_{n-1}, \beta D^{-1}\underline{1}_n)$, $\beta \in \mathbb{C} \setminus \{0\}$ and all its other eigenvalues have positive real part. This completes the proof. □

Remark 6.5.12. Recall that with Assumption 6.5.9, Lemma 6.4.6 implies that $\mathbb{L}$ is positive definite. Positive definiteness of the symmetric part of N_2 follows directly from the proof of Lemma 6.5.5 with Assumption 6.5.9. Hence, there clearly exist choices of the control parameters K_P, P^d, ω^d, V^d, K and D leading to a synchronized motion of the system (6.97), (6.2) such that $B + B^\top$ is positive definite.

Remark 6.5.13. Note that without introducing the relative frequencies $\tilde{\omega}$ in (6.95), the linearization of the microgrid dynamics would be very similar to the one given in (6.101). However, in that case the positive semidefinite Laplacian matrix $\tilde{L}$ defined in (6.13) would be contained in the matrix B rather than the positive definite matrix $\mathbb{L}$ defined in (6.43). It can then easily be verified, e.g., via the Schur complement, that with $\tilde{L}$ being the upper left entry of the matrix B, there exists no choice of control parameters such that $B + B^\top$ is positive definite. However, the stability result derived next strongly relies on the fact that all nonzero eigenvalues of $A_2BA_5A_3$ have positive real part. Therefore, the taken procedure to derive a suitable error system—although involving some rather lengthy calculations—is necessary in the present case to establish the stability claim.

Note that requiring $B + B^\top$ to be positive definite is very similar to the stability condition derived in Section 6.4 for inverter-based microgrids in which the inverters are controlled via the typical droop controls given in (5.2) and (5.3). More precisely, the matrix $B + B^\top$ being positive definite has the following physical interpretation: the control laws (5.2) and (5.27) establish a feedback interconnection linking the phase angles δ, respectively θ, with the active power flows P, as well as the voltages V with the reactive power flows Q. Recall the definition of B given in (6.100). The block-diagonal components of B are the matrices $\mathbb{L}$ and N_2 defined in (6.43), respectively (6.98). The matrices $\mathbb{L}$ and N_2 locally represent the network coupling strengths between the phase

angles and the active power flows, respectively, the voltages and the reactive power flows. In the same way, the off-block-diagonal elements of $B + B^\top$ can be interpreted as a local cross-coupling strength originating from the fact that the arguments of the functions P, respectively Q, are not merely the angles, respectively the voltage amplitudes, but that the arguments of both P and Q are both the angles and the voltage amplitudes. Hence, $B + B^\top$ being positive definite implies that the couplings represented by $\mathbb{L}$ and N_2 have to dominate the cross-couplings of the power flows contained in the off-diagonal-block elements of $B + B^\top$, see also Remark 6.4.11.

The similarity of the condition stated in Lemma 6.5.11 to condition (6.49) (ensuring stability of inverter-based microgrids operated with the droop controls (5.2) and (5.3)) is explained by the following two facts. First, both voltage controllers, the DVC (5.27) and the voltage droop control (5.2), establish a feedback interconnection of the voltages V with the reactive power flows Q. Second, the frequency droop control (5.2), which establishes a feedback interconnection between the phase angles and the active power flows, is used in both cases.

The main result of this section follows as a corollary to Proposition 6.5.6.

Corollary 6.5.14. *Consider the system* (5.36), (6.2) *under Assumption 6.5.9. Fix* ω^d, K_P, P^d, V^d *and* D. *Set* $\tau_{P_i} = \tau \in \mathbb{R}_{>0}$, $i \sim \mathcal{N}$ *and* $K = D$. *Denote the corresponding equilibrium point of the reduced system* (6.97), (6.96) *with the chosen set of control parameters by* $z^s = col(\underline{0}_{n-1}, V_R^s, \underline{0}_{n-1}, Q^{m,s})$. *Let* $\mu_i = a_i + jb_i$ *be the* i*-th nonzero eigenvalue of the matrix product* $A_2BA_5A_3$ *with* $a_i \in \mathbb{R}$ *and* $b_i \in \mathbb{R}$. *Assume that* $B + B^\top$, *with* B *defined in* (6.100), *is positive definite. Then,* z^s *is a locally exponentially stable equilibrium point of the system* (6.97), (6.96) *if and only if the parameter* τ *is chosen such that*

$$\tau b_i^2 < a_i \tag{6.103}$$

for all μ_i. *Moreover, the equilibrium point* z^s *is locally exponentially stable for any positive real* τ *if and only if* $A_2BA_5A_3$ *has only real eigenvalues.*

Proof. Following the proof of Proposition 6.5.6, the claim is established by deriving the spectrum of $\mathcal{M}$ defined in (6.101). Let λ be an eigenvalue of $\mathcal{M}$ with a corresponding right eigenvector $v = \mathrm{col}(v_1, v_2)$, $v_1 \in \mathbb{C}^{(2n-2)}$, $v_2 \in \mathbb{C}^{(2n-1)}$. Then,

$$\begin{aligned} A_3 v_2 &= \lambda v_1, \\ -\frac{1}{\tau}\left(A_2 B A_5 v_1 + v_2\right) &= \lambda v_2. \end{aligned} \tag{6.104}$$

As before, it is first shown by contradiction that zero is not an eigenvalue of $\mathcal{M}$. Therefore, assume $\lambda = 0$. Then,

$$A_3 v_2 = \underline{0}_{(2n-2)}. \tag{6.105}$$

It follows from the definition of A_3 given in (6.98) and the fact that $\mathcal{L}_R$ is given by, see (6.72),

$$\mathcal{L}_R = \begin{bmatrix} \mathbf{I}_{n-1} & \underline{0}_{n-1} \end{bmatrix} K\mathcal{L},$$

that (6.105) can only be satisfied if

$$\begin{bmatrix} \mathbf{I}_{n-1} & \mathbf{0}_{(n-1)\times n} \\ \mathbf{0}_{n\times(n-1)} & K\mathcal{L}D \end{bmatrix} v_2 = \begin{bmatrix} \underline{0}_{(2n-2)} \\ a \end{bmatrix}, \quad a \in \mathbb{C}.$$

Clearly, this implies that

$$v_2 = \mathrm{col}(\underline{0}_{n-1}, \bar{v}_2), \quad \bar{v}_2 \in \mathbb{C}^n. \tag{6.106}$$

Furthermore, from $\mathcal{L} = \mathcal{L}^\top$ and $\mathcal{L}\underline{1}_n = \underline{0}_n$, it follows that $\underline{1}_n^\top K^{-1} K\mathcal{L}D\bar{v}_2 = 0$ for any $\bar{v}_2 \in \mathbb{C}^n$. Hence, for any v_2 satisfying (6.106),

$$\begin{bmatrix} \underline{1}_{n-1}^\top & \underline{1}_n^\top K^{-1} \end{bmatrix} \begin{bmatrix} \mathbf{I}_{n-1} & \mathbf{0}_{(n-1)\times n} \\ \mathbf{0}_{n\times(n-1)} & K\mathcal{L}D \end{bmatrix} v_2 = \frac{a}{k_n} = 0.$$

Thus, a must be zero and $v_2 = \mathrm{col}(\underline{0}_{n-1}, \beta D^{-1}\underline{1}_n) \in \mathbb{C}^{(2n-1)}$, $\beta \in \mathbb{C} \setminus \{0\}$. Hence, if $\lambda = 0$, the second equation in (6.104) must satisfy

$$A_2 B A_5 v_1 = -v_2 = -\begin{bmatrix} \underline{0}_{n-1} \\ \beta D^{-1}\underline{1}_n \end{bmatrix}. \tag{6.107}$$

Recall the definition of A_2 given in (6.98). Moreover, recall that the proof of Lemma 6.5.11 implies that A_2 is invertible. Hence, multiplying (6.107) from the left with A_2^{-1} gives

$$BA_5 v_1 = -A_2^{-1} v_2 = v_2. \tag{6.108}$$

By recalling $K = D$ together with (6.80), multiplying (6.108) from the left with $v_1^* A_5^\top$ finally yields

$$v_1^* A_5^\top B A_5 v_1 = v_1^* \underline{0}_{(2n-2)} = 0,$$

which implies $w_1^* B w_1 = 0$ for $w_1 := A_5 v_1$. Since $B + B^\top$ is positive definite by assumption, $0 \notin W(B)$. Hence, $v_1 = \underline{0}_{n-1}$ and, consequently, $\lambda = 0$ is not an eigenvalue of $\mathcal{M}$.

That under condition (6.103) all eigenvalues of $\mathcal{M}$ have negative real part is a direct consequence of the following two facts. First, for $\lambda \neq 0$, note that (6.104) can be rewritten as

$$\lambda^2 v_2 + \frac{1}{\tau}\lambda v_2 + \frac{1}{\tau} A_2 B A_5 A_3 v_2 = \underline{0}_{(2n-1)}.$$

Second, recall that, under the standing assumptions, Lemma 6.5.11 implies that all nonzero eigenvalues of the matrix product $A_2 B A_5 A_3$ have positive real part. Hence, the claim follows in a straightforward manner from the proof of Proposition 6.5.6.

□

The stability condition (6.103) is in the same spirit as the previously derived stability conditions for a lossy frequency-droop-controlled MDREG in Proposition 6.3.8 and for a microgrid operated with the DVC under Assumption 6.2.5 in Proposition 6.5.6. Mainly, all conditions can be interpreted in the following way. The slower the power measurements are processed, i.e., the larger the parameter τ is chosen, the lower the feedback gains have to be chosen in order to ensure stability. Or, by invoking the argument from the opposite direction, the conditions state that the larger the controller gains are chosen, the faster the power measurements have to be processed in order to guarantee stability.

To see this in the present case, recall from the proof of Lemma 6.5.11 that the spectrum of the matrix product $A_2BA_5A_3$ is, via a similarity transformation, equivalent to that of $BA_5A_3A_2$. Furthermore, recall from (6.102) that

$$A_5A_3A_2 = \text{blkdiag}(\mathcal{K}_P + k_{P_n}\underline{1}_{n-1}\underline{1}_{n-1}^\top, D\mathcal{L}D).$$

Clearly, the eigenvalues μ_i of the matrix product $A_2BA_5A_3$ depend on the controller gains $\mathcal{K}_P$, k_{P_n} and D. Hence, by increasing all gains by a constant factor κ, all eigenvalues μ_i of the matrix product $A_2BA_5A_3$ are increased by the same factor. Consequently, τ may then have to be decreased in order for condition (6.103) to be satisfied. As discussed in Section 6.3.3 for the case of an MDREG, the above interpretation is only valid under the assumption that a variation of the gains has only a negligible effect on the entries of the matrix B defined in (6.100). By continuity, this is, e.g., the case for small gain variations. Note, however, that for $\mathcal{N} = \mathcal{N}_I$, a variation of τ does not affect equilibria of the system (6.97), (6.2).

6.5.5 A solution to the problem of power sharing in lossless microgrids

The contribution of this section is to give a condition under which the power sharing problem, i.e., Problem 3.3.5, is solved. The provided solution is established for a microgrid with dominantly inductive power lines operated with frequency droop control (5.2) and DVC (5.27). The result follows as a corollary to the stability result in the previous section in combination with Lemma 5.2.6 and Claim 5.3.8.

Corollary 6.5.15. *Consider the system* (5.36), (6.2) *under Assumption 6.5.9. Fix* ω^d, V^d, D *and positive real constants* ς *and* ψ. *Set* $\tau_{P_i} = \tau \in \mathbb{R}_{>0}$, $i \sim \mathcal{N}$ *and* $K = D$. *Furthermore, following Definition 3.3.1, select positive real constants* γ_i, $i \sim \mathcal{N}$. *Let* $U = diag(1/\gamma_i)$. *Set* $K_P = \varsigma U$ *and* $P^d = \psi U^{-1}\underline{1}_n$. *Suppose the conditions of Corollary 6.5.14 are satisfied. Then, Problem 3.3.5 is solved for all initial conditions of the system* (5.36), (6.2) *in a neighborhood of* $col(\delta^s, \underline{1}_n\omega^s, V^s, Q^{m,s})$ *satisfying* $\|D^{-1}V(0)\|_1 = \|D^{-1}V^s\|_1$.

Proof. The proof follows in an analogous manner to those of Corollaries 6.3.13 and 6.5.8 and is therefore omitted. □

6.6 Summary

This chapter has been dedicated to the problems of frequency and voltage stability in microgrids. Several conditions have been derived for stability of microgrids operated with the different control laws presented in Chapter 5, i.e., the droop controls (5.1), (5.2) and (5.3), as well as the DVC (5.27). To establish these results mainly mathematical tools from linear algebra, as well as port-Hamiltonian systems have been used. In all cases, the stability condition has been obtained via converse Lyapunov theorems.

More precisely, it has been shown that for all analyzed control schemes there exist selections of the control parameters and setpoints such that the closed-loop microgrid possesses a locally asymptotically stable synchronized motion. Note that most of the derived conditions are necessary and sufficient. In addition, under the assumption of small angle differences, it has been proven that the choice of the control parameters of the DVC uniquely determines the equilibrium point of the voltage and reactive power dynamics.

Furthermore, a condition has been derived, under which the problem of active power sharing, i.e., Problem 3.3.3, is solved in a microgrid with dominantly inductive power lines by means of the frequency droop control. This latter claim has been established by combining the derived stability results with the selection criterion for the frequency droop control parameters provided in Lemma 5.2.6. In a similar fashion, a condition has been derived under which Problem 3.3.4, i.e., the problem of reactive power sharing, is solved by the DVC in microgrids with dominantly inductive power lines. A solution to Problem 3.3.5 (the problem of joint active and reactive power sharing) has been provided by combining both aforementioned approaches.

In the case of inverter-based microgrids operated with frequency droop control and DVC, the derived necessary and sufficient stability conditions can be interpreted as: "the slower the power measurements are processed, i.e., the larger the low pass filter time constants are, the lower the feedback gains have to be chosen". Recall that both, the low pass filter time constants and the feedback gains, are design parameters, which can be set by the operator.

The sufficient stability condition derived for the case of a lossless droop-controlled inverter-based microgrid states that local asymptotic stability is independent of the choice of the controller gains and setpoints of the frequency droop controller as well as of the low pass filter time constants, but does depend on the choice of the controller gains and setpoints of the voltage droop controller. This coincides with the result obtained for frequency stability of frequency droop-controlled lossless MDREGs under the assumption of constant voltage amplitudes.

Moreover, the following conclusion can be drawn from the analysis of microgrids with variable frequencies and voltages operated either with the droop controls or the frequency droop control and the DVC. The analyzed control laws have in common that they establish a feedback interconnection of the voltage amplitudes with the reactive power flows and of the phase angles with the active power flows. These specific pairings have been chosen on the basis of the physical relation of the power flows with the phase angles and voltage amplitudes in the corresponding electrical network. However, both the active and the reactive power flows are nonlinear functions of the phase angles and the voltage amplitudes. Therefore, the derived stability conditions state that, in order to ensure local stability, the local coupling-strengths between the active power flows and the phase angles, as well as between the reactive power flows and the voltage amplitudes have to dominate the cross-couplings originating from the common dependence of the power flows from both variables, i.e., from phase angles and voltage amplitudes.

The obtained results show two parallels to classical control design methods for MIMO systems. A common procedure in MIMO control design is to seek a decomposition of the MIMO control design problem into several decoupled SISO control problems. Typically, such a design procedure is feasible if it is possible to identify input-output pairings of the open-loop system, which exhibit a strong coupling between each other, but are only loosely coupled with the remaining inputs and outputs of the system. Two popular and traditional representatives of such methods are the Dynamic Nyquist Array

[248] and the Relative Gain Array [249, Chapter 10]. As has been described in Chapter 5, the frequency and voltage droop controls (5.2) and (5.3), respectively the DVC (5.27), are derived following the exact same goal, i.e., to formulate a MIMO control design problem as a set of decoupled SISO control design problems. The main difference in the design of the controls (5.2), (5.3), respectively the DVC (5.27), compared to standard control theory methods is that the input-output couplings are determined by a heuristic inspection of the power flow equations over a power line, rather than by analyzing the frequency response of a MIMO plant.

The second parallel to classical MIMO control design is as follows. If decoupled SISO controllers have been designed for an LTI MIMO system, then asymptotic stability of the equilibrium of the resulting closed-loop system can, e.g., be verified via the generalized Nyquist theorem in combination with the concept of generalized diagonal dominance, see e.g., [250, 251, 252]. Roughly speaking, one requirement for stability is then, that the diagonal elements of the closed-loop system dominate over the off-diagonal elements. As has been discussed above, this requirement is similar to the stability conditions for microgrids with variable frequencies and voltages obtained in this chapter.

7

Illustrative simulation examples

7.1 Introduction

The theoretical analysis is illustrated via simulation examples based on the three-phase islanded Subnetwork 1 of the CIGRE benchmark medium voltage distribution network [253, 254]. Following the outline of the previous chapter, at first a simulation study for a microgrid operated with the droop controls (5.2) and (5.3) is conducted. Subsequently, the performance of the voltage droop control (5.3) with respect to the control objective of reactive power sharing is compared to that of the DVC (5.27) proposed in this work.

As discussed in Section 5.2, the voltage droop control (5.3) is mainly used for inverter-interfaced units. Therefore, the considered system for the simulations is a purely inverter-based microgrid. Recall, however, that an SG operated with frequency droop control (5.1) and the voltage control law given by (5.30) together with (5.33) has equivalent dynamics to an inverter with the respective controls.

All simulations are carried out in Plecs [255]. Compared to the representation of the power flows given by (4.24) used for the analysis, the inductances are represented by first-order ODEs in the model used for the simulations rather than constants as in (4.24), see also Section 2.4.4. Hence, the simulations also serve to evaluate *(i)* the validity of the model (5.21), (4.24), respectively (5.36), (4.24) and *(ii)* the robustness of the stability conditions derived in Chapter 6 with respect to model uncertainties.

This chapter is based on [71, 125] and structured as follows. The model setup is described in Section 7.2. The simulation results for droop-controlled microgrids are discussed in Section 7.3. Finally, the performance of the proposed DVC is evaluated in Section 7.4.

7.2 Benchmark model setup

The benchmark microgrid is a meshed network and consists of 11 main buses, see Fig. 7.1. The following two modifications are made compared to the original system given in [253, 254]: first, at bus 9b the combined heat and power (CHP) diesel generator is replaced by an inverter–interfaced CHP fuel cell (FC). Second, since the original network given in [253] stems from a distribution network connected to a transmission system, the power ratings of the generation units are scaled by a factor four compared to [253], such that the controllable units (CHPs, batteries, FC) can satisfy the load demand in autonomous operation mode at least during some period of time.

Furthermore, it is assumed that the PV units connected at buses 3, 4, 6, 8 and 11 are not equipped with any storage device. It is therefore assumed that these PV units are not operated in grid-forming, but in grid-feeding mode. This is standard practice and means that the PV units are controlled in such way that they deliver a fixed amount of power to an energized grid, see Section 4.2 or, e.g., [81]. Since the PV units can then not be represented by (4.16), they are denoted as non-controllable units.

Hence, the network in Fig. 7.1 possesses a total of six controllable generation sources of which two are batteries at buses 5b ($i = 1$) and 10b ($i = 5$), two are FCs in households at buses 5c ($i = 2$) and 10c ($i = 6$) and two are FC CHPs at buses 9b ($i = 3$) and 9c ($i = 4$). It is assumed that all controllable generation units are equipped with the frequency droop control given in (5.2). The voltage is controlled either by the DVC (5.27) or the voltage droop control (5.3) depending on the simulation scenario. To each inverter its power rating $S_i^N \in \mathbb{R}_{>0}$, $i \sim \mathcal{N}$, is associated and, for simplicity, it is assumed that the transformer power rating is equivalent to that of the corresponding generation source. The transformer impedances of the generation units are modeled based on the IEEE standard 399-1997 [256]. Since the apparent power ratings of the generation sources are not specified in [253], S_i^N is set to the maximum active power given for each source in Table 2 of [253]. The main system data are given in Table 7.1.

The loads at nodes 3-11 represent industrial and household loads as specified in Table 1 of [253], besides the load at node 1, which is neglected. It is assumed that all PV units work at 50% of their nominal power with $\cos(\phi) := P/S = 0.98$ and are treated as negative loads, while the wind power plant is not generating any power[1].

[1]The nominal power of the wind power plant at node 8 is equivalent to approximately 79 times the installed load at that node. Hence, in order to be able to compute an equivalent impedance corresponding to the sum of generation and load at that node, the wind power plant would have to be operated below 1.2% of its rated power. Therefore, the wind power plant is assumed to not generate

Table 7.1: Main test system parameters

Base values	$S_{\text{base}} = 4.75$ MVA, $V_{\text{base}} = 20$ kV
S_i^N	$[0.505, 0.028, 0.261, 0.179, 0.168, 0.012]$ pu

The corresponding shunt-admittance representing a load at a node is computed at nominal frequency and voltage and by summing the load demand and the PV generation at each node. Then, in the corresponding Kron-reduced network all nodes represent controllable DGs, see Section 2.4.4.3.

The line parameters and lengths are as given in [253]. The total length of the lines is approximately 15 km. As outlined in Section 6.2, the transformer impedances of the inverters are merged with the line impedances. The largest R/X ratio of an admittance in the network is then 0.30. For HV transmission lines it is typically 0.31 [212]. Hence, the assumption of dominantly inductive admittances is satisfied.

7.3 Droop-controlled microgrids

To illustrate the analysis carried out in Section 6.4, an extensive simulation study of a droop-controlled microgrid is performed. The study mainly aims at *(i)* evaluating the conservativeness of the sufficient stability condition (6.49) and *(ii)* demonstrating that the frequency droop control (5.2) achieves the objective of active power sharing if the corresponding parameters are chosen according to Lemma 5.2.6. More precisely, the following two scenarios for droop-controlled microgrids are considered.

1) Lossless scenario. All loads and uncontrollable generation sources (PV, wind turbine) of the test system given in Fig. 7.1 are neglected. Also in that case the largest R/X ratio of an admittance in the network is 0.30. Consequently, the droop control laws given in (5.2) are adequate and the stability analysis of Section 6.4 applies.

The batteries at nodes 5b and 10b are operated in charging mode, hence functioning as loads. The frequency droop gains and setpoints of the inverters are designed according to Lemma 5.2.6 with $\chi_i = S_i^N$, $P_i^d = \alpha_i S_i^N$ pu and $k_{P_i} = 0.2/S_i^N$ Hz/pu, $i \sim \mathcal{N}$, where pu denotes per unit values with respect to the common system base power S_{base} given in Table 7.1. Hence, the inverters should supply the requested power, respectively

any power at all in the considered simulation scenarios.

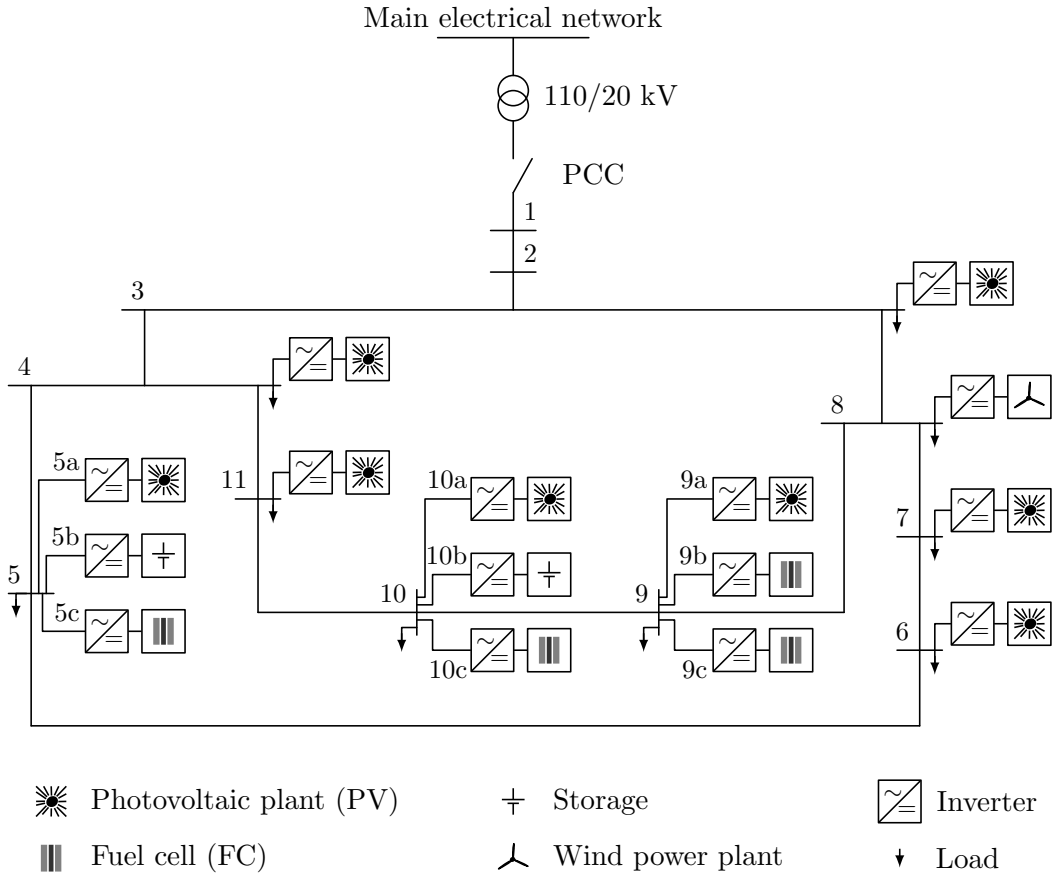

Figure 7.1: 20 kV MV benchmark model adapted from [253] with 11 main buses and several inverter-interfaced DG and storage units. The controllable units are located at buses 5b, 5c, 9b, 9c, 10b and 10c. The sign ↓ denotes loads. PCC denotes the point of common coupling to the main grid. The switch at the PCC is open and, hence, the microgrid is operated in islanded-mode. The numbering of the main buses is according to [253].

be charged, in proportion to their power ratings. It is assumed that the power setpoints have been provided by some sort of high-level control or energy management system, see Remark 5.2.1, with $\alpha_i = 0.3$ for inverters in generation mode ($i = 2, 3, 4, 6$) and $\alpha_i = -0.4$ for inverters in charging mode, i.e., $i = 1, 5$.

The reactive power setpoints are set to $Q_i^d = \beta_i S_i^N$ pu with $\beta_i = 0.025$, $i \sim \mathcal{N}$, to account for the inductive behavior of the lines. The voltage droop gains are chosen in the same relation as the frequency droop gains, i.e., $k_{Q_i} = 0.1/S_i^N$ pu/pu and $V_i^d = 1$, $i \sim \mathcal{N}$. The low pass filter time constants are set to $\tau_P = \text{col}(\tau_{P_i}) = 0.2[1, 2, .5, 3, 4, 1]$ s, $i \sim \mathcal{N}$. This choice is motivated by the fact that for a European grid with nominal frequency $f^d = 50$ Hz, this is equivalent to $\tau = 10/f^d = 0.2$ s.

The simulation results are shown in Fig. 7.2. After a transient the frequencies synchronize and the voltage amplitudes become constant. The latter satisfy the usual requirement of $0.9 < V_i^s < 1.1$ for V_i^s in pu and $i \sim \mathcal{N}$. The initial conditions have been chosen arbitrarily. Condition (6.49) is satisfied and, hence, the synchronized motion is locally asymptotically stable.

Furthermore, the batteries are charged in proportion to their power ratings with the active power also being supplied proportionally, as stated in Lemma 5.2.6. Hence, the simulation confirms that the frequency droop control, as given in (5.2), is suited to achieve the desired objective of active power sharing. But, as discussed in Section 5.3, the reactive power is not shared proportionally, limiting the overall performance of the voltage droop control law (5.3).

The obtained experience in numerous simulations with large variety of control gains, setpoints, low pass filter time constants and initial conditions is that whenever the solutions of the system converge to a synchronized motion as defined in Assumption 6.4.3, the latter is locally asymptotically stable by condition (6.49). However, there exist gain settings such that the solutions of the system exhibit limit-cycle behavior. As one would expect, this is the case for very large control gains and low pass filter time constants.

2) Scenario with constant impedance loads. In this simulation scenario the robustness of the stability condition (6.49) with respect to loads represented by constant impedances is evaluated. The system setup is as described in Section 7.2. The control gains are chosen as specified in the lossless scenario with $\alpha_i = 0.6$ and $\beta_i = 0.25$, $i \sim \mathcal{N}$. Hence, all inverters operate in generation mode. The voltage setpoints and low pass filter time constants are as in the lossless case.

The simulation results are displayed in Fig. 7.3. All trajectories converge to a synchronized motion satisfying condition (6.49), indicating that the condition is robust—to a certain extent—to the presence of transfer and load conductances. The inverters share the active power demand of the loads as stated in Lemma 5.2.6. Compared to the lossless scenario, all inverters provide positive reactive power. However, as in the lossless scenario, the reactive power sharing is not proportional among all units since in steady-state the voltage amplitudes are not equal at all buses.

Furthermore, numerous simulations with different parameters indicate that the stability condition (6.49) is satisfied in all cases in which the solutions of the system converge to a synchronized motion. As in the lossless case, there are gain settings such that the solutions of the system do not converge to a desired synchronized motion as defined in Assumption 6.4.3, but show a limit cycle behavior. This is typically the case for very large control gains and/or large low pass filter time constants.

7.4 Microgrids with frequency droop control and distributed voltage control

In this section the performance of the proposed DVC (5.27) is demonstrated via simulations. The main purpose of the simulation analysis is four-fold: *(i)* to evaluate the performance of the DVC (5.27) compared to the voltage droop control (5.3); *(ii)* to investigate the ability of the DVC to quickly achieve a desired reactive power distribution after changes in the load; *(iii)* to test the compatibility of the DVC (5.27) with the frequency droop control (5.2); *(iv)* to analyze the influence of control design parameters on convergence properties of the closed-loop system. These are main criteria for a practical implementation of the DVC (5.27). To this end, a large number of simulations with a variety of initial conditions, control parameters and load changes have been performed.

Recall that the DVC is a distributed control, which requires communication. The graph model of the distributed communication network required for the implementation of the DVC (5.27) together with the electrical network is depicted in Fig. 7.4. Nodes that are connected with each other exchange their local reactive power measurements. Note that the communication is not all-to-all and that there is no central unit. Furthermore, to obtain a practically relevant setup, it is assumed that the phase angles of the inverters are controlled by the typical frequency droop control given in (5.2). Hence, the closed-loop system is of the form (5.36), (4.24).

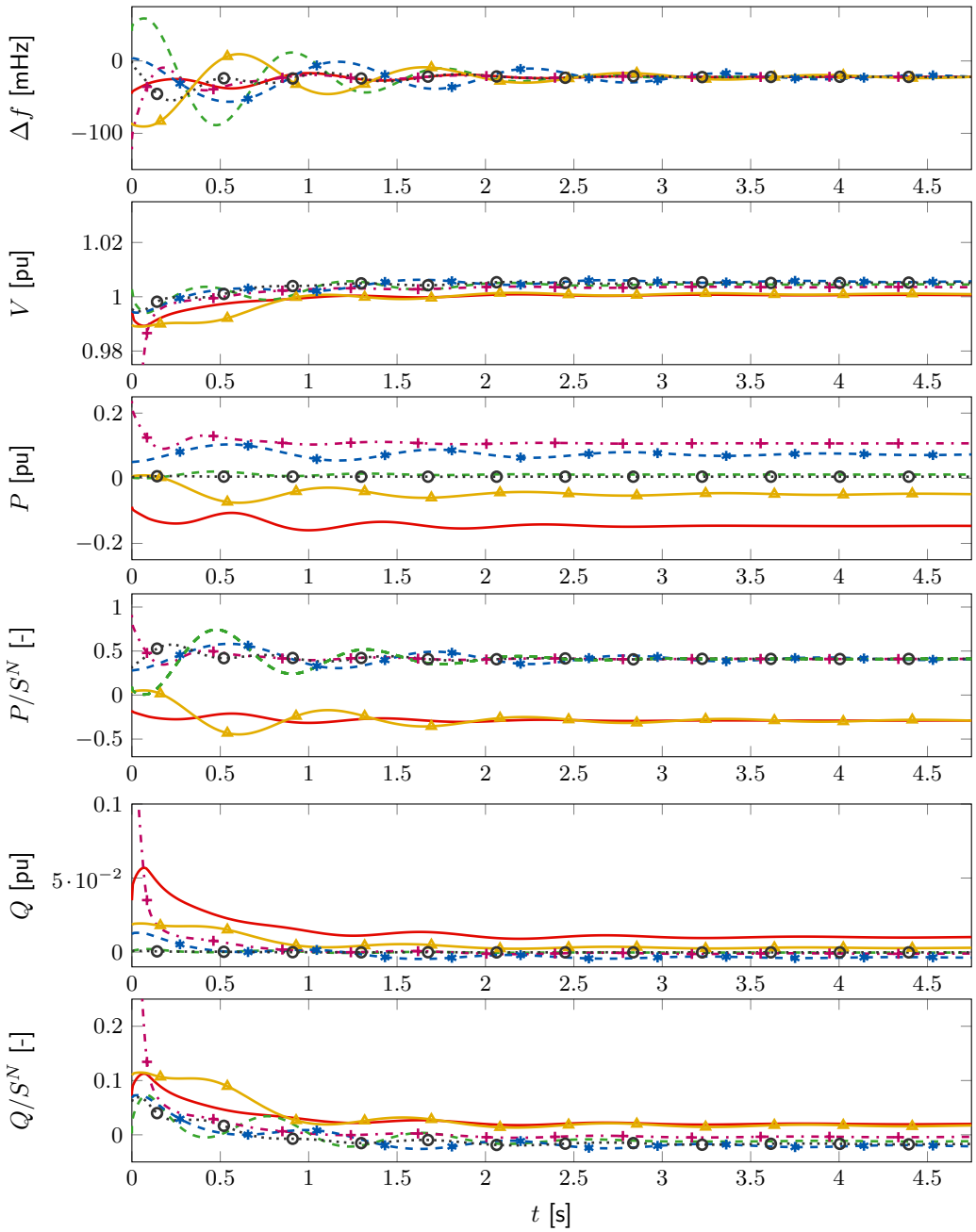

Figure 7.2: Simulation example of a droop-controlled microgrid - lossless scenario. Trajectories of the power outputs P_i and Q_i in pu, the power outputs relative to source rating P_i/S_i^N and Q_i/S_i^N, the internal relative frequencies $\Delta f_i = (\omega_i - \omega^d)/(2\pi)$ in mHz and the voltage amplitudes V_i in pu of the controllable sources in the microgrid given in Fig. 7.1, $i = 1, \ldots, 6$. The active power is shared by the generating sources in proportion to their ratings in steady-state, i.e., $P_i^s/S_i^N = P_k^s/S_k^N$ for $i, k = 2, 3, 4, 6$, while the batteries are charged in proportion to their ratings, i.e., $P_1^s/S_1^N = P_5^s/S_5^N$. The lines correspond to the following sources: battery 5b, $i = 1$ '–', FC 5c, $i = 2$ '- -', FC CHP 9b, $i = 3$ '+-', FC CHP 9c, $i = 4$ '* -', battery 10b, $i = 5$ '△ -' and FC 10c, $i = 6$ 'o-'. The initial conditions have been chosen arbitrarily.

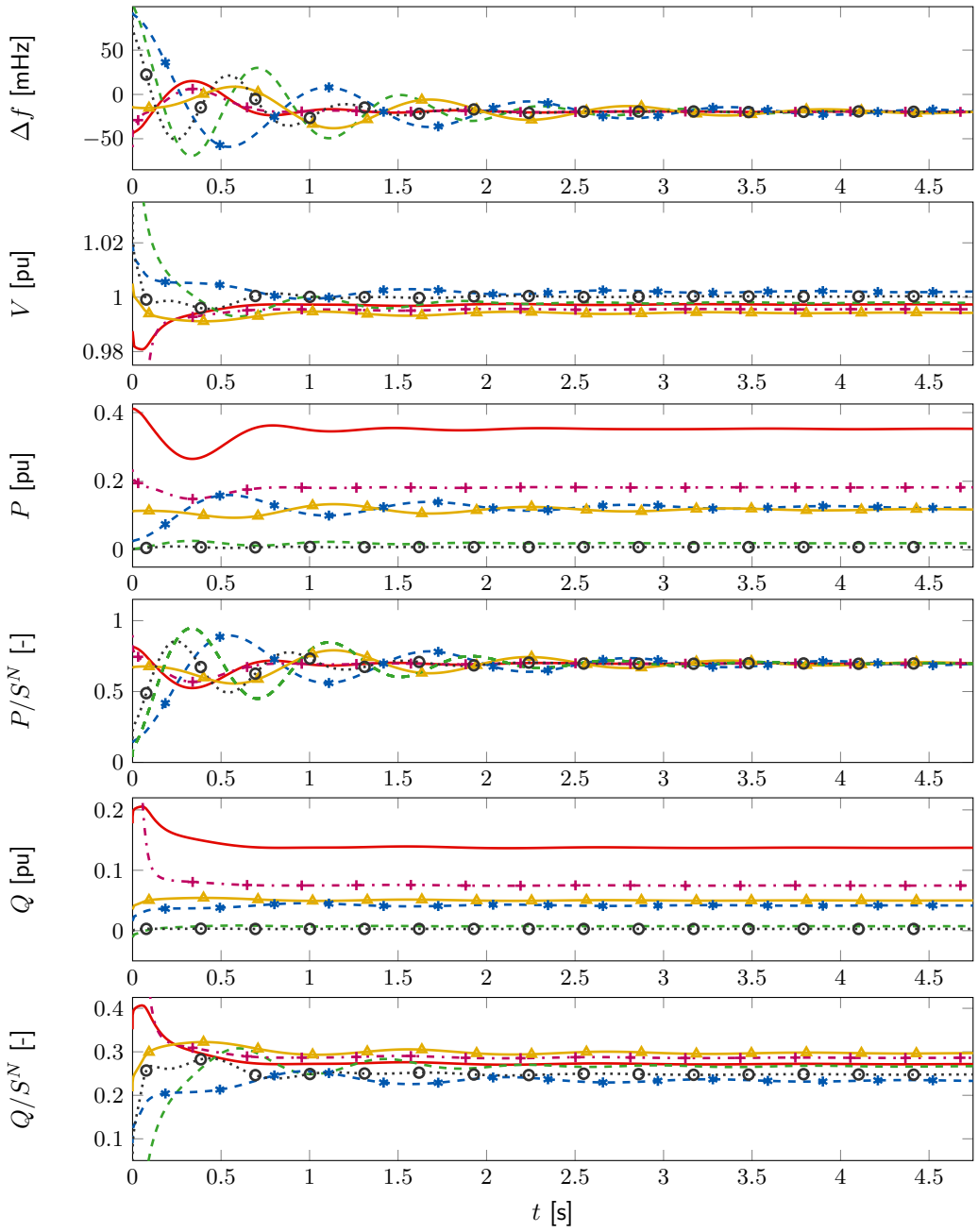

Figure 7.3: Simulation example of a droop-controlled microgrid - scenario with constant impedance loads. Trajectories of the power outputs P_i and Q_i in pu, the power outputs relative to source rating P_i/S_i^N and Q_i/S_i^N, the internal relative frequencies $\Delta f_i = (\omega_i - \omega^d)/(2\pi)$ in mHz and the voltage amplitudes V_i in pu of the controllable sources in the microgrid given in Fig. 7.1, $i = 1, \ldots, 6$. The active power is shared by the sources in proportion to their ratings in steady-state, i.e., $P_i^s/S_i^N = P_k^s/S_k^N$ for all $i, k = 1, \ldots, 6$. The lines correspond to the following sources: battery 5b, $i = 1$ '–', FC 5c, $i = 2$ '- -', FC CHP 9b, $i = 3$ '+-', FC CHP 9c, $i = 4$ '* -', battery 10b, $i = 5$ '△ -' and FC 10c, $i = 6$ 'o-'. The initial conditions have been chosen arbitrarily.

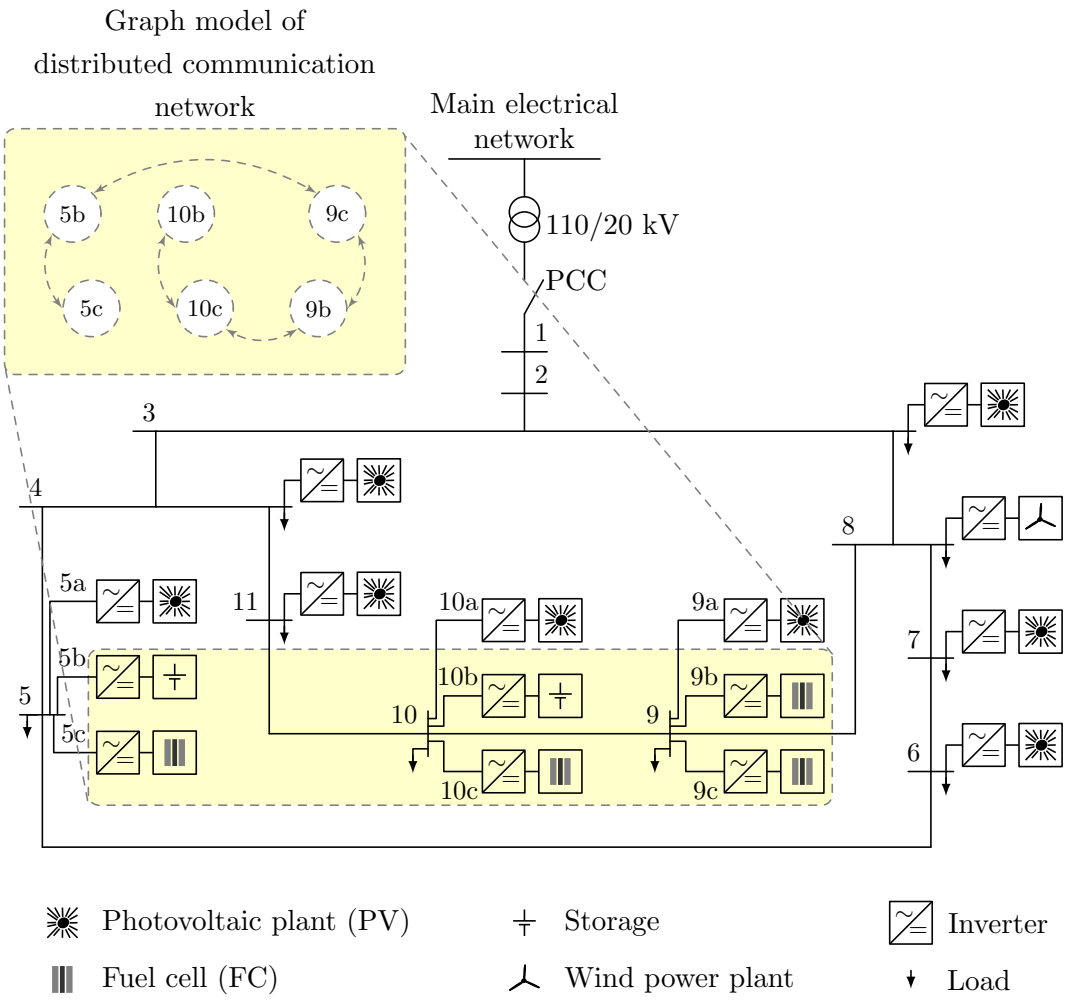

Figure 7.4: 20 kV MV benchmark model adapted from [253] with 11 main buses and inverter-interfaced DG units. The controllable units are located at buses 5b, 5c, 9b, 9c, 10b and 10c. The sign ↓ denotes loads. PCC denotes the point of common coupling to the main grid. The switch at the PCC is open and, hence, the microgrid is operated in islanded-mode. The numbering of the main buses is according to [253]. The communication infrastructure is connected. The communication is not all-to-all, neither is there a central unit.

The following representative scenario is considered to illustrate the results obtained in Section 6.5: at first, the system is operated under nominal loading conditions; then, at $t = 0.5$ s there is an increase in load at bus 9; at $t = 2.5$ s, the load at bus 4 is disconnected. The magnitude of each change in load corresponds to approximately $0.1S_{\text{base}}$. From a practical point of view, this represents a significant change in load. Furthermore, the total length of the power lines connecting bus 5 and 9, i.e., the two most remote nodes with grid-forming units, is 2.15 km with a total impedance of $0.014 + j0.005$ pu (without considering the transformers). Hence, the electrical distance between the buses is small and the requirement of reactive power sharing is practically meaningful in the considered scenario.

The gains and setpoints of the frequency droop controllers are selected as in the previous section. The same holds for the parameters of the voltage droop control (5.3).

For the DVC (5.27), the nominal power rate of each source is selected as weighting coefficient, i.e., $\chi_i = S_i^N$, $i \sim \mathcal{N}$ (see also Remark 3.3.2) and, following Proposition 6.5.6, K is set to $K = \kappa D$ with $\kappa = 0.04$. For both voltage controls, the voltage setpoint is chosen as $V_i^d = 1$ pu, $i \sim \mathcal{N}$. To satisfy Assumption 6.3.5, the low pass filter time constants are set to $\tau_{P_i} = 0.2$ s, $i \sim \mathcal{N}$.

The simulation results are shown for the system (4.16), (4.24) operated with the voltage droop control (5.3) in Fig. 7.5a and with the DVC (5.27) in Fig. 7.5b. The system quickly reaches a steady-state under both controls, also after the changes in load at $t = 0.5$ s and $t = 2.5$ s. Local exponential stability of the reduced-dimension closed-loop system (6.97), (6.96) operated with the controls (5.2) and (5.27) is confirmed for both operating points via condition (6.103) given in Corollary 6.5.14. Moreover, the conservativeness of the sufficient condition in Lemma 6.5.11 has been evaluated in numerous further simulations with different parameters and load changes. The condition of the lemma has been satisfied in all performed simulations. This indicates that *(i)* the condition is practically applicable and that *(ii)* it is robust with respect to model uncertainties, e.g., the presence of transfer conductances.

As already observed in the previous section, under the voltage droop control (5.3), the reactive power is not shared by all inverters in the desired manner, i.e., in the present case in proportion of their ratings. On the contrary and as predicted, the DVC (5.27) does achieve a desired reactive power distribution in steady-state. Moreover, when the system is operated with the DVC (5.27), the voltage levels remain very close

to the nominal value $V^d = 1$ pu. This is not the case if the system is operated with the voltage droop control (5.3).

Consider for example the voltage trajectories after the load step at $t = 0.5$ s. There, all voltage amplitudes are decreased under the voltage droop control (5.3), while the DVC (5.27) merely causes small variations in the voltage amplitudes in order to satisfy the increased reactive power demand by the loads. This additional undesired behavior of the voltage droop control (5.3) is explained as follows: the voltage droop control is a proportional control the input of which is the deviation of the reactive power injection with respect to a desired setpoint. Ideally this setpoint would correspond exactly to the reactive power injection of the inverter to supply the load demand. However, as mentioned earlier, such setpoint is difficult—if even possible—to obtain in practice. Furthermore, the network considered here is dominantly inductive with inductive loads. In general, the reactive power injection of the sources is positive in such networks, see Fig. 7.5. Hence, any increase in reactive power demand beyond the magnitude of the chosen setpoint Q_i^d may lead to a significant decrease in magnitude of the voltage amplitudes. This is not desired in operation. Therefore, [27, 82, 83] propose the use of a secondary control loop with an integrator to restore the voltage amplitudes to acceptable values.

The DVC (5.27) does not produce such undesired large decreases in voltage amplitudes. This is an indication that no additional control is necessary to restore the voltage amplitudes within a desired range—a clear advantage over the voltage droop control (5.3). Furthermore, this fact also explains why the overall power demand is higher if the network is operated with the DVC (5.27), instead of the voltage droop control (5.3).

In addition, the simulation results show a good compatibility of the DVC (5.27) and the frequency droop control (5.2). Recall that the frequency droop control (5.2) is a proportional control, the input of which is the deviation of the active power injection relative to a desired setpoint. Hence, a higher active power demand leads to a lower synchronization frequency, as can be seen in Fig. 7.5. Under each of the voltage controls, the active power is shared in a desired proportional manner.

Numerous further simulation scenarios confirm that the voltage droop control does not achieve a desired reactive power sharing. The obtained experience shows that the relative deviations of the weighted reactive powers $\bar{Q}_i$, $i \sim \mathcal{N}$, in a steady-state, i.e.,

$$\frac{\max_{i\sim\mathcal{N}} \bar{Q}_i^s}{\min_{i\sim\mathcal{N}} \bar{Q}_i^s},$$

can be as low as a few percent, but also go beyond 30% for control parameters chosen within a practically reasonable range. The specific value depends on the selection of the control parameters, as well as the initial conditions and location of simulated changes in load.

In contrast and as predicted, the DVC (5.27) achieves a desired reactive power sharing in the sense of Definition 3.3.1 in steady-state. Furthermore, with the choice of $\kappa = 0.04$ a steady-state is typically reached within a few seconds. The exact convergence time depends on initial conditions, as well as magnitude and location of the changes in load. As outlined in Section 6.5.2, there exist other meaningful choices for K, for example, $K = \kappa I$. Overall, the best performance has been obtained with $K = \kappa D$ and $0.05 < \kappa < 0.15$.

Furthermore, κ is a very intuitive tuning parameter. In analogy to linear SISO control systems, low values of κ lead to relatively long settling times, but little overshoot. On the contrary, the larger κ is chosen, the shorter is the settling time at the cost of a higher overshoot and a broader error band. This effect is illustrated for different values of κ in Fig. 7.6.

Moreover, the robustness with respect to the presence of transfer conductances of the closed-loop microgrid operated with the frequency droop control (5.2) and the DVC (5.27) has been evaluated in numerous simulations. More precisely, the R/X ratios of the power lines have been varied in a range of $[0.3, 3]$. In all simulated cases, the trajectories of the closed-loop microgrid converge to a synchronized motion. Furthermore, a desired active and reactive power sharing is always achieved and the voltage amplitudes remain close to the nominal value of 1 pu. Hence, the simulations demonstrate that the investigated control scheme is also well-suited for networks with larger R/X ratios.

In addition, the convergence speed depends on the connectivity properties of the communication network, as well as on the physical characteristics of the electrical network. A detailed evaluation of the influence of these two points is subject of future research.

7.5 Summary

The analysis performed in the previous chapters has been illustrated via simulation examples based on the the CIGRE benchmark MV distribution network. In the case of a droop-controlled microgrid, the derived stability condition is satisfied and a desired

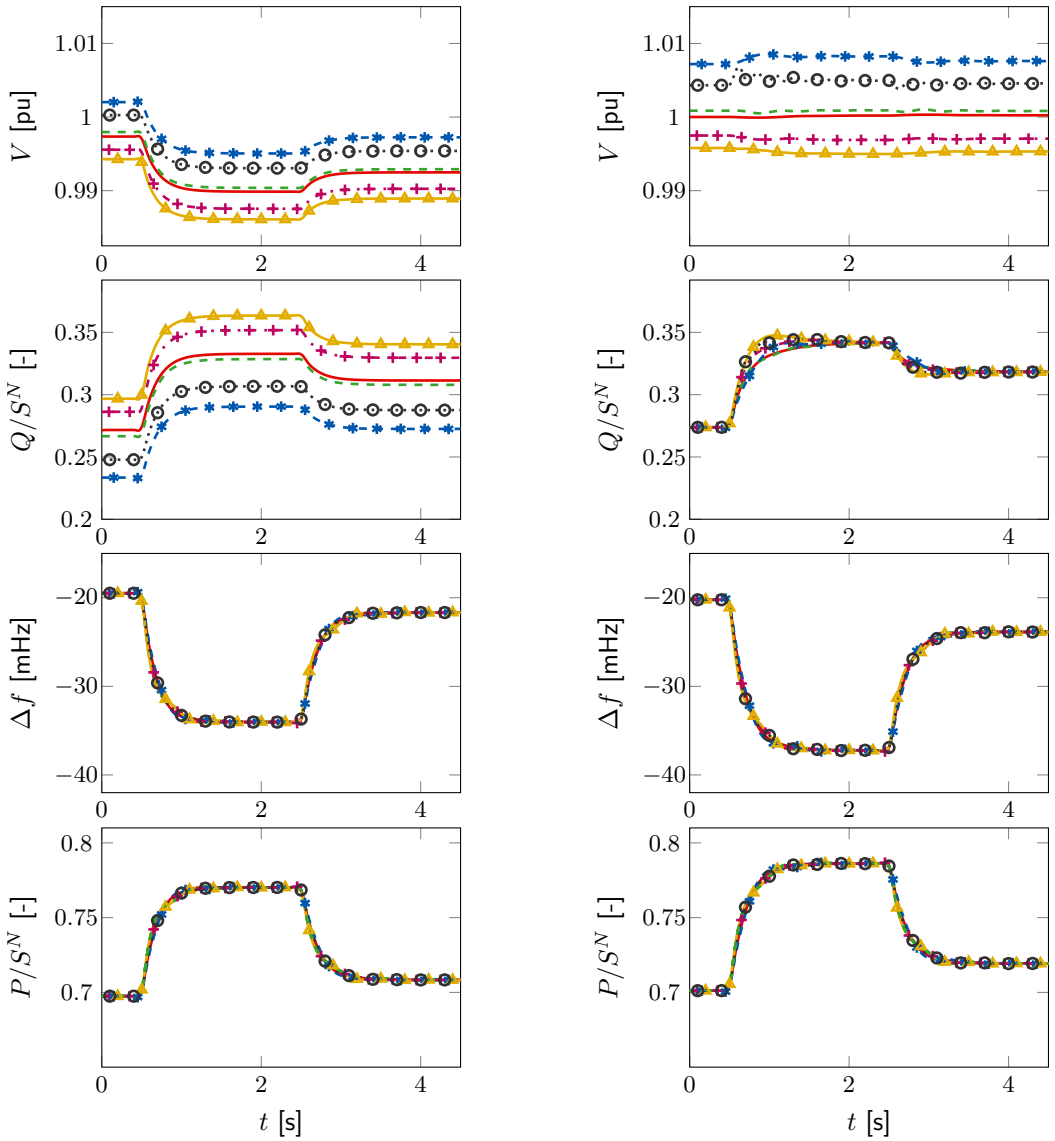

(a) Trajectories of the system (4.16), (4.24) operated with the frequency droop control (5.2) and the voltage droop control (5.3)

(b) Trajectories of the system (4.16), (4.24) operated with the frequency droop control (5.2) and the DVC (5.27)

Figure 7.5: Comparison of voltage droop control and DVC. In both cases, the system reaches quickly a steady-state after a change in load. However, as can be clearly seen, the proposed DVC (5.27) achieves the objective of reactive power sharing, while the voltage droop control (5.3) does not. Trajectories of the power outputs relative to source rating P_i/S_i^N and Q_i/S_i^N, the voltage amplitudes V_i in pu and the internal relative frequencies $\Delta f_i = (\omega_i - \omega^d)/(2\pi)$ in mHz of the controllable sources in the microgrid given in Fig. 7.4, $i = 1, \ldots, 6$. The lines correspond to the following sources: battery 5b, $i = 1$ '–', FC 5c, $i = 2$ '- -', FC CHP 9b, $i = 3$ '+-', FC CHP 9c, $i = 4$ '* -', battery 10b, $i = 5$ '△ -' and FC 10c, $i = 6$ 'o-'.

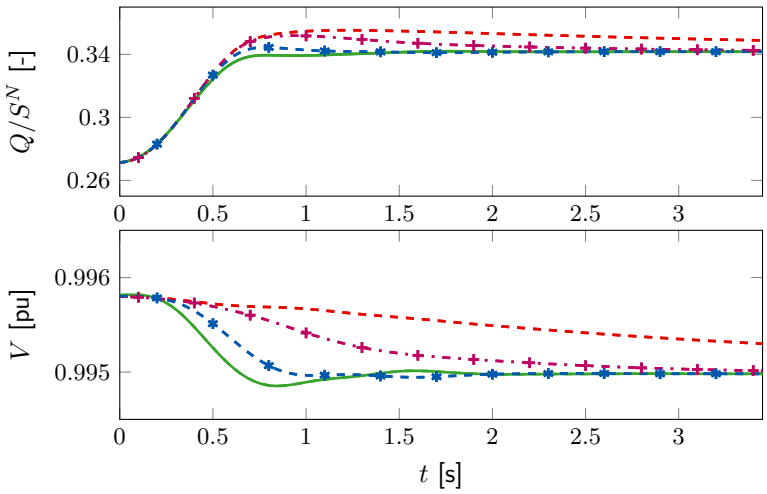

Figure 7.6: Responses of the voltage amplitude V_5 and the weighted reactive power Q_5/S_5^N of the inverter 5 at bus 10b to a load step at bus 9 for different values of κ : $\kappa = 0.005$ '- -', $\kappa = 0.02$ '-+', $\kappa = 0.07$ '-*', $\kappa = 0.15$ '–'.

steady-state active power distribution is achieved in simulation for a wide selection of different control gains, setpoints, low pass filter time constants and initial conditions.

The simulations also show that, despite the observation that meshed microgrids with droop control possess a locally stable synchronized motion for a wide range of control gains, the conventional voltage droop control does, in general, not guarantee proportional reactive power sharing. This observation has been confirmed in a second simulation study in which the performance in terms of reactive power sharing of the usual voltage droop control has been compared to the DVC proposed in Section 5.3.

Furthermore, it has been demonstrated that, as predicted, the DVC achieves reactive power sharing and, hence, clearly outperforms the usual voltage droop control. In addition, the simulations show good compatibility of the proposed voltage control with the typical frequency droop control. Furthermore, some intuition for the choice of the control parameters of the proposed DVC has been provided. Overall, the evaluation of the simulation results together with the experiences from numerous further simulation scenarios lead to the conclusion that the DVC is a well-suited control scheme for voltage control and reactive power sharing in microgrids.

8

Discussion and conclusion

8.1 Summary

The microgrid concept, introduced in Chapter 3, represents a promising solution to facilitate the integration of renewable DG units into the electrical grid. In this work three fundamental challenges in microgrids have been considered: *(i)* frequency stability, *(ii)* voltage stability and *(iii)* power sharing. As in any system, stability is a basic criterion for a reliable and secure operation. The relevance of power sharing is given by the fact that it permits to prespecify the utilization of the diverse generation units in the network. Furthermore, it has been shown, that power sharing essentially is an agreement problem.

As a basis for the analysis and control design, a generic modular model of an uncontrolled microgrid has been derived in Chapter 4. The main model components are generation units interfaced to the network via AC inverters or SGs, as well as loads and power lines. Inverters are modeled as controllable AC voltage sources. A detailed derivation of this model representation of an inverter together with the main underlying assumptions is given in Section 4.2. SGs, power lines and loads are modeled following standard procedures in power system stability studies.

Based on the derived microgrid model, suitable control schemes to address the aforementioned control objectives are discussed in Chapter 5. One important contribution of this work is the design of a consensus-based distributed voltage control (DVC), which ensures a desired reactive power sharing in steady-state. The control design is motivated for microgrids with dominantly inductive power lines. However, it is proven in Section 5.3 that the DVC achieves reactive power sharing in steady-state independently of the line admittances. Furthermore, frequency and voltage droop control are

discussed. In particular, a selection of control parameters for the frequency droop controller is given, which ensures desired active power sharing in steady-state. As in the case of the DVC, this criterion is also independent of the line admittances.

The main contributions of this thesis are conditions for frequency and voltage stability of microgrids operated with the aforementioned control schemes. The derived results have been established in Chapter 6 by using tools of linear algebra, as well as port-Hamiltonian systems in combination with converse Lyapunov theorems. Most of the results are derived under the assumption of lossless line admittances. Furthermore, conditions are given, under which the frequency droop control, respectively the proposed DVC, solve the problem of active, respectively reactive, power sharing in microgrids with dominantly inductive power lines. These results are derived by combining the obtained stability conditions with the aforementioned selection criterion for the parameters of the frequency droop controller, respectively the inherent properties of the DVC.

For lossless microgrids with inverters with variable frequencies and voltage amplitudes, the derived stability conditions have the following common physical interpretation. The analyzed control schemes share the property that they establish a feedback interconnection of the voltage amplitudes with the reactive power flows and of the phase angles with the active power flows. The derived stability conditions state that—in order to ensure stability—the local coupling-strengths between the active power flows and the phase angles, as well as between the reactive power flows and the voltage amplitudes have to dominate the cross-couplings originating from the common dependence of the power flows from both variables, i.e., from phase angles and voltage amplitudes. In the case of lossless droop-controlled inverter-based microgrids, this is sufficient for local stability. In the case of lossless microgrids operated with frequency droop control and DVC, the control parameters and the time constants of the low-pass filters can then be chosen such that local stability is ensured.

The analysis has been illustrated via extensive simulation studies in Chapter 7. The derived stability conditions for the different investigated network configurations are satisfied and a desired steady-state active power distribution is achieved in simulation for a wide selection of different control gains, setpoints, low pass filter time constants and initial conditions.

The simulations also show that, despite the observation that meshed microgrids with droop control possess a locally stable synchronized motion for a wide range of

control gains, the conventional voltage droop control does, in general, not achieve proportional reactive power sharing. On the contrary, it has been demonstrated that the DVC proposed in this work does guarantee reactive power sharing. In addition, the simulations show good compatibility of the proposed DVC with the typical frequency droop control. Furthermore, some intuition for the choice of the control parameters of the proposed DVC has been provided. Overall, the evaluation of the simulation results together with the experiences from numerous further simulation scenarios lead to the conclusion that the DVC is a well-suited control scheme for voltage control and reactive power sharing in microgrids.

In summary, models, control solutions and stability conditions for a wide spectrum of microgrid configurations have been elaborated in this thesis. The considered networks comprise frequency droop-controlled MDREGs, droop-controlled inverter-based microgrids and microgrids operated with frequency droop control and the DVC proposed in this work.

8.2 Future research directions

The focus of this work is on the problems of frequency stability, voltage stability and power sharing in microgrids. In this section, extensions of the presented results are indicated. At first, proximate extensions are described. Then, more distant research directions are outlined.

Most of the stability conditions in this work have been derived under the assumption of dominantly inductive admittances. The results have been established via Lyapunov theory, from which some robustness properties can be inferred. A case of particular interest is robustness in the presence of conductances. However, robustness-based analysis usually only allows to consider small perturbations. Hence, a nearby extension of the present work is the explicit consideration of conductances in the analysis. As discussed in Section 6.2, this is a long-standing problem in power system analysis, see, e.g. [36, 44]. Recent work [50, 64] provides a partial solution to this problem. However, the results of [50, 64] are derived for first-order models of SGs, respectively inverters. In addition, the authors of [50] assume constant voltage amplitudes, while the results of [64] are very conservative.

Another direction of research in which the derived results should be extended is with regards to the considered load models. In this work, it has been assumed that all loads can be represented by constant impedances. While this assumption is frequently used

in power system stability analysis [3, 4, 6], it does, in general, not permit to accurately describe all possible loads. The main reason for this is that, as discussed in Chapter 4, there usually is a large variety of different loads connected within one microgrid. Hence, the individual loads may have very different characteristics. An extension of the presented results to constant current loads seems straight-forward and is currently being investigated by the author. An extension to constant power loads seems more difficult, since in that case it is not possible to work with the Kron-reduced network representation. Therefore, in that scenario, the microgrid model to be considered is a DAE system. Analytical stability analysis of such systems is mathematically very challenging, see, e.g., [257]. This is one reason why researchers have pursued modeling loads as dynamical systems. Another reason is that load dynamic response may have a strong effect on power system stability and, in particular, on voltage stability [232, 258]. Frequency- and voltage-dependent dynamic load models are discussed, e.g., in [1, 6, 232, 233, 240, 258, 259, 260]. However, the derivation of stability conditions for power systems with dynamic frequency- and voltage-dependent load models is rather complicated. As a consequence and as pointed out in Chapter 6, the load models are usually, somehow artificially, adapted to fit the theoretical framework used for the construction of energy-Lyapunov functions, see, e.g., [47, 243]. Hence, the investigation of power system and, in particular, microgrid stability using more detailed load models is a close-by open direction of research.

Furthermore, the DVC proposed in this work also offers room for several proximate extensions. One such extension, which is currently under investigation, is the design of a DVC for SG-interfaced units that does not require a feedback linearization. Moreover, the DVC is a communication-based control, which requires information exchange over a network. In practice, this often implies the presence of some sort of feedback delay, which can severely affect the control performance [85, 88]. Conditions for convergence of consensus protocols for multi-agent systems under the presence of delays have been widely investigated in the literature, see, e.g., [95, 96, 97, 104, 105]. The effect of communication delays on the convergence properties of the average consensus protocol used to design the DVC has been analyzed for uniform delays, e.g., in [88], and for heterogeneous time-varying delays, e.g., in [92, 93]. One conclusion of the results derived in [88] is that there is a trade-off between the degree of the nodes and the robustness with respect to delays. However, all of the aforementioned results are restriced to purely multi-agent systems, while in the present case an additional physi-

cal layer corresponding to the electrical network has to be considered in the analysis. Therefore, it is interesting to extend the analysis of a microgrid operated with the DVC conducted in this thesis to communication networks with time-delay. Also, the present control approach is derived under the assumption that only the power outputs of the DG units can be measured instantaneously. Yet, it is foreseen that in future power networks instantaneous measurements of the load consumption will be available, too [18]. Extending the DVC to incorporate load measurements would, e.g., allow to determine the desired reactive power distribution in dependency of the load demand and its electrical distance to the respective DG units. This is a relevant criterion, since the load demand usually changes over time. An exemplary scenario, in which such an extension could be beneficial, is the following. Consider a microgrid, where the load demand is concentrated at one specific location in the network at a point in time $t_0 \in \mathbb{R}$. Suppose that at $t_1 \in \mathbb{R}$, $t_1 \gg t_0$, the main load demand shifts to another location in the network. If this information would be available, the weighting gains of the respective DG units could be adapted to the new situation. This would, e.g., allow to minimize losses.

The abovementioned difficulties regarding conditions for stability in networks with highly resistive power lines also raise the question of whether the controls discussed in this work are well-suited for such networks. Highly resistive power lines may, for example, appear in small microgrids at the LV level. Inspired by the droop control laws discussed in this work, controls for inverter-interfaced units in networks with highly resistive power lines have been proposed, e.g., in [72, 237, 238, 261]. However, no thorough network stability analysis has been carried out. Hence, the design of specific control laws together with corresponding conditions for stability in microgrids with highly resistive power lines is a further promising field of research.

Another relevant direction of future research is the extension of the present analysis to more detailed microgrid models, e.g., networks with time-varying power line models. Only very recently there have been some partially successful reports on this topic [175, 262, 263, 264, 265, 266, 267]. However, to the best of the author's knowledge, all these results are restricted to very special cases. For example, in [262] a port-Hamiltonian model of a power system with SGs is derived. Yet, the stability analysis is restricted to the special case of an SG connected to a constant linear load. A similar approach is followed in [264, 265], where a sufficient condition for global asymptotic stability of a generic SG-based power system is derived. Building on [262], the authors

of [264, 265] also follow a port-Hamiltonian modeling approach to establish their result. However, the main stability claim in [264, 265] critically relies on the assumption of a constant field winding current, as well as on the definition of a very specific value for the mechanical torque of each SG in the system. This torque not only depends on the constant field current, but also on an arbitrarily chosen synchronization frequency and arbitrarily prespecified steady-state terminal voltages for all SGs.

In [263, 266] the problem of synchronization of DG units with identical dynamics connected to a single load over a dynamic parallel network with identical power lines is considered. To derive their synchronization result, the authors of [263, 266] model all DG units as nonlinear oscillators and introduce a new mathematical framework named passivity with respect to manifolds.

Similarly, [175, 267] provide synchronization conditions in networks with identical node dynamics using $\mathcal{L}_2$ methods. The node dynamics are modeled as nonlinear circuits consisting of a passive impedance connected in parallel to a nonlinear voltage-dependent current source. Hence, practically the approach is restricted to networks with inverter-based generation sources. Furthermore, the synchronization conditions provided in [267] are restricted to networks with star topology, i.e., to parallel networks. The more recent work [175] extends the results of [267] to networks with general topology. However, the synchronization results therein are restriced to networks with identical power lines or with power lines, which share a uniform line impedance per length and the lengths of the lines may vary. In addition, the authors of [175] themselves conclude that their approach cannot be extended to more general heterogeneous networks using the methods employed in [175].

Moreover, [175, 263, 266, 267] have in common that the analysis and provided solutions are limited to the problem of network synchronization, while other practically relevant performance criteria such as power sharing are not considered. In addition, as done explicitly in [263, 266] and implicitly in [175, 267], modeling a grid-forming inverter as a controllable voltage source may not be adequate, when considering fast line dynamics. This latter observation follows from the fact that typically the dynamics of the internal inverter controls together with the inverter output filter are slower than the line dynamics, see the model derivation in Chapter 4 for details. Hence, in summary, the problem of stability analysis in microgrids with heterogeneous generation pool and time-varying power line models is still a challenging open problem.

Furthermore, based on the hierarchical control architecture for microgrids described in Section 3.4, the investigated problems in this work are associated with the primary control layer. The control actions and associated dynamics at the higher control layers, i.e., secondary and tertiary control, have not been considered in this work. The performance analysis of interactions of the primary control layer with higher control layers is therefore a further interesting direction of future research.

Control schemes for secondary frequency control are, e.g., proposed in [28, 77, 78, 119]. The problem of optimal dispatch, i.e., tertiary control, is considered, e.g., in [7, 79, 195, 268]. In [28, 119] the interaction of the primary and secondary frequency control levels are also considered. But, the analysis therein is conducted under the assumptions of first-order inverter models, lossless admittances, as well as constant voltage amplitudes. Under equivalent assumptions, the recent work [66] further untertakes the aforementioned endeavor by extending the analysis of [28, 119] to additionally consider the tertiary control layer. Yet, the analysis therein is restricted to active power flows. Furthermore, neither load nor generation uncertainties nor storage capacities are considered.

Finally, the hierarchical control architecture presented in Section 3.4 following [38, 191, 192] is strongly influenced by the well-established hierarchical control architecture in large transmission systems, see, e.g., [6, 190]. However, as discussed in Section 3.2, the properties of microgrids clearly differ from those of conventional large power systems. Another relevant question, also raised, e.g., in [66] and Section 3.4, therefore is, whether the hierarchical control architecture proposed in [38, 191, 192] is adequate to assess the operational objectives and constraints in microgrids.

In conclusion, there are many challenging open questions regarding a reliable, safe and efficient operation of microgrids, as well as generic power systems with large amount of renewable DG. The author hopes that the work conducted in this thesis may help to answer some of these questions and serve as a base for a large variety of challenging future research directions.

References

[1] P. Kundur. *Power system stability and control*. McGraw-Hill, 1994. 1, 5, 6, 7, 27, 35, 37, 40, 47, 58, 59, 63, 79, 84, 85, 86, 87, 89, 93, 95, 117, 119, 143, 184

[2] D. A. Jones. **Electrical engineering: the backbone of society**. In *IEE Proceedings A, Science, Measurement and Technology*, **138**, pages 1–10. IET, 1991. 1

[3] P. Anderson and A. Fouad. *Power System Control and Stability*. J.Wiley & Sons, 2002. 1, 6, 8, 27, 31, 32, 34, 35, 36, 37, 39, 40, 41, 58, 59, 84, 85, 86, 87, 91, 93, 184

[4] J. D. Glover, M. S. Sarma, and T. J. Overbye. *Power system analysis and design*. Cengage Learning, 2011. 1, 8, 27, 29, 31, 34, 35, 36, 37, 39, 40, 43, 52, 53, 55, 56, 63, 65, 184

[5] J. J. Grainger and W. D. Stevenson. *Power system analysis*, **621**. McGraw-Hill New York, 1994. 1, 27, 34, 35, 37

[6] J. Machowski, J. Bialek, and J. Bumby. *Power system dynamics: stability and control*. J.Wiley & Sons, 2008. 1, 2, 6, 7, 8, 9, 27, 31, 34, 35, 37, 40, 47, 63, 65, 84, 85, 86, 87, 91, 93, 95, 96, 184, 187

[7] P. P. Varaiya, F. F. Wu, and J. W. Bialek. **Smart operation of smart grid: Risk-limiting dispatch**. *Proceedings of the IEEE*, **99**(1):40–57, 2011. 1, 2, 3, 55, 187

[8] J. T. Houghton. *Climate change 1995: The science of climate change: contribution of working group I to the second assessment report of the Intergovernmental Panel on Climate Change*, **2**. Cambridge University Press, 1996. 1

[9] J. Hansen, M. Sato, R. Ruedy, L. Nazarenko, A. Lacis, G. Schmidt, G. Russell, I. Aleinov, M. Bauer, S. Bauer, et al. **Efficacy of climate forcings**. *Journal of Geophysical Research: Atmospheres (1984–2012)*, **110**(D18), 2005. 1

[10] S. Solomon. *Climate change 2007-the physical science basis: Working group I contribution to the fourth assessment report of the IPCC*, **4**. Cambridge University Press, 2007. 1

[11] M. R. Raupach, G. Marland, P. Ciais, C. Le Quéré, J. G. Canadell, G. Klepper, and C. B. Field. **Global and regional drivers of accelerating CO2 emissions**. *Proceedings of the National Academy of Sciences*, **104**(24):10288–10293, 2007. 1

[12] United Nations Framework Convention on Climate Change (UNFCCC). **Kyoto Protocol to the united nations framework convention on climate change**. In *United Nations Framework Convention on Climate Change (http://unfccc. int)*, 1997. 2

[13] C. Breidenich, D. Magraw, A. Rowley, and J. W. Rubin. **The Kyoto protocol to the United Nations framework convention on climate change**. *American Journal of International Law*, pages 315–331, 1998. 2

[14] International Energy Agency. **Topics: Renewables**. http://www.iea.org/topics/renewables/, retrieved 04.05.2014. 2

[15] R. Teodorescu, M. Liserre, and P. Rodriguez. *Grid converters for photovoltaic and wind power systems*, **29**. John Wiley & Sons, 2011. 2, 27, 28, 31, 32, 33, 34, 53

[16] T. Klaus, C. Vollmer, K. Werner, H. Lehmann, and K. Müschen. **Energy target 2050: 100% renewable electricity supply**. Federal Environment Agency, 2010. 2

[17] Communication from the commission. **EUROPE 2020 - A European strategy for smart, sustainable and inclusive growth (COM(2010) 2020)**. European Commission, 2010. 2

[18] H. Farhangi. **The path of the smart grid**. *IEEE Power and Energy Magazine*, **8**(1):18 –28, january-february 2010. 2, 3, 53, 55, 56, 185

[19] X. Fang, S. Misra, G. Xue, and D. Yang. **Smart grid - the new and improved power grid: a survey**. *Communications Surveys & Tutorials, IEEE*, **14**(4):944–980, 2012. 2, 3, 55

[20] T. Ackermann, G. Andersson, and L. Söder. **Distributed generation: a definition**. *Electric power systems research*, **57**(3):195–204, 2001. 3

[21] T. Green and M. Prodanovic. **Control of inverter-based micro-grids**. *Electric Power Systems Research*, **Vol. 77**(9):1204–1213, july 2007. 3, 51, 52, 53, 55, 56, 60, 62, 67, 74, 77

[22] R. Lasseter. **MicroGrids**. In *IEEE Power Engineering Society Winter Meeting, 2002*, **1**, pages 305 – 308 vol.1, 2002. 3, 52, 53, 55, 56

[23] N. Hatziargyriou, H. Asano, R. Iravani, and C. Marnay. **Microgrids**. *IEEE Power and Energy Magazine*, **5**(4):78–94, 2007. 3, 52, 53, 55, 56

[24] F. Katiraei, R. Iravani, N. Hatziargyriou, and A. Dimeas. **Microgrids management**. *IEEE Power and Energy Magazine*, **6**(3):54–65, 2008. 3, 52, 53, 55, 56, 59, 60, 62, 68, 73, 77

[25] R. H. Lasseter. **Smart distribution: Coupled microgrids**. *Proceedings of the IEEE*, **99**(6):1074–1082, 2011. 3, 56

[26] M. Marwali, J.-W. Jung, and A. Keyhani. **Control of distributed generation systems - Part II: Load sharing control**. *IEEE Transactions on Power Electronics*, **19**(6):1551 – 1561, nov. 2004. 5, 107

[27] A. Micallef, M. Apap, C. Spiteri-Staines, and J. M. Guerrero. **Secondary control for reactive power sharing in droop-controlled islanded microgrids**. In *IEEE International Symposium on Industrial Electronics (ISIE)*, pages 1627–1633, 2012. 5, 107, 177

REFERENCES

[28] J. W. Simpson-Porco, F. Dörfler, and F. Bullo. **Synchronization and power sharing for droop-controlled inverters in islanded microgrids**. *Automatica*, **49**(9):2603 – 2611, 2013. 5, 7, 9, 10, 12, 52, 77, 94, 98, 103, 104, 116, 117, 130, 137, 140, 187

[29] J. W. Simpson-Porco, F. Dörfler, and F. Bullo. **Voltage stabilization in microgrids using quadratic droop control**. In *52nd Conference on Decision and Control*, pages 7582–7589, Florence, Italy, 2013. 5, 9, 10, 77, 94, 105, 116, 117, 119, 130, 143

[30] F. Katiraei and M. Iravani. **Power Management Strategies for a Microgrid With Multiple Distributed Generation Units**. *IEEE Transactions on Power Systems*, **21**(4):1821 –1831, nov. 2006. 6, 9, 67, 95

[31] F. Katiraei, M. Iravani, and P. Lehn. **Small-signal dynamic model of a micro-grid including conventional and electronically interfaced distributed resources**. *IET Generation, Transmission Distribution*, **1**(3):369–378, May 2007. 6, 9, 67

[32] Z. Miao, A. Domijan, and L. Fan. **Investigation of Microgrids With Both Inverter Interfaced and Direct AC-Connected Distributed Energy Resources**. *IEEE Transactions on Power Delivery*, **26**(3):1634 –1642, july 2011. 6, 9, 67

[33] E. Coelho, P. Cortizo, and P. Garcia. **Small-signal stability for parallel-connected inverters in standalone AC supply systems**. *IEEE Transactions on Industry Applications*, **38**(2):533 –542, 2002. 6, 9, 75, 76, 77, 93, 95, 97, 98

[34] N. Pogaku, M. Prodanovic, and T. Green. **Modeling, Analysis and Testing of Autonomous Operation of an Inverter-Based Microgrid**. *IEEE Transactions on Power Electronics*, **22**(2):613 –625, march 2007. 6, 9, 52, 73, 74, 76, 77, 93, 124

[35] J. Lopes, C. Moreira, and A. Madureira. **Defining control strategies for MicroGrids islanded operation**. *IEEE Transactions on Power Systems*, **21**(2):916 – 924, may 2006. 6, 11, 58, 59, 60, 62, 63, 68, 73, 74, 75, 77

[36] P. Varaiya, F. F. Wu, and R.-L. Chen. **Direct methods for transient stability analysis of power systems: Recent results**. *Proceedings of the IEEE*, **73**(12):1703–1715, 1985. 6, 87, 98, 118, 183

[37] M. Chandorkar, D. Divan, and R. Adapa. **Control of parallel connected inverters in standalone AC supply systems**. *IEEE Transactions on Industry Applications*, **29**(1):136 –143, jan/feb 1993. 7, 10, 11, 93, 94, 95, 96, 97

[38] J. Guerrero, P. Loh, M. Chandorkar, and T. Lee. **Advanced Control Architectures for Intelligent MicroGrids – Part I: Decentralized and Hierarchical Control**. *IEEE Transactions on Industrial Electronics*, **60**(4):1254–1262, 2013. 7, 9, 56, 60, 63, 64, 65, 78, 96, 97, 133, 187

[39] P. Kundur, J. Paserba, V. Ajjarapu, G. Andersson, A. Bose, C. Canizares, N. Hatziargyriou, D. Hill, A. Stankovic, C. Taylor, T. Van Cutsem, and V. Vittal. **Definition and classification of power system stability IEEE/CIGRE joint task force on stability terms and definitions**. *IEEE Transactions on Power Systems*, **19**(3):1387–1401, 2004. 8, 47, 48, 58, 59

[40] G. Andersson, P. Donalek, R. Farmer, N. Hatziargyriou, I. Kamwa, P. Kundur, N. Martins, J. Paserba, P. Pourbeik, J. Sanchez-Gasca, et al. **Causes of the 2003 major grid blackouts in North America and Europe, and recommended means to improve system dynamic performance**. *IEEE Transactions on Power Systems*, **20**(4):1922–1928, 2005. 8

[41] S. V. Buldyrev, R. Parshani, G. Paul, H. E. Stanley, and S. Havlin. **Catastrophic cascade of failures in interdependent networks**. *Nature*, **464**(7291):1025–1028, 2010. 8

[42] R. Rüdenberg. *Elektrische Schaltvorgänge und verwandte Störungserscheinungen in Starkstromanlagen*. Julius Springer, Berlin, 1923. 8

[43] R. Rüdenberg. *Transient Performance of Electric Power Systems*. , McGraw-Hill, New York, 1950. 8

[44] N. Bretas and L. F. C. Alberto. **Lyapunov function for power systems with transfer conductances: extension of the Invariance principle**. *IEEE Transactions on Power Systems*, **18**(2):769–777, 2003. 9, 118, 183

[45] T. Shen, R. Ortega, Q. Lu, S. Mei, and K. Tamura. **Adaptive L2 disturbance attenuation of hamiltonian systems with parametric perturbation and application to power systems**. *Asian Journal of Control*, **5**(1):143–152, 2003. 9

[46] A. Zecevic, G. Neskovic, and D. Siljak. **Robust decentralized exciter control with linear feedback**. *IEEE Transactions on Power Systems*, **19**(2):1096 – 1103, may 2004. 9

[47] R. Guedes, F. Silva, L. Alberto, and N. Bretas. **Large disturbance voltage stability assessment using extended Lyapunov function and considering voltage dependent active loads**. In *IEEE PESGM*, pages 1760–1767, 2005. 9, 118, 184

[48] R. Ortega, M. Galaz, A. Astolfi, Y. Sun, and T. Shen. **Transient stabilization of multimachine power systems with nontrivial transfer conductances**. *IEEE Transactions on Automatic Control*, **50**(1):60 – 75, jan. 2005. 9, 87, 118

[49] W. Dib, R. Ortega, A. Barabanov, and F. Lamnabhi-Lagarrigue. **A Globally Convergent Controller for Multi-Machine Power Systems Using Structure-Preserving Models**. *IEEE Transactions on Automatic Control*, **54**(9):2179 –2185, sept. 2009. 9, 142

[50] F. Dörfler and F. Bullo. **Synchronization and Transient Stability in Power Networks and Non-uniform Kuramoto Oscillators**. *SIAM Journal on Control and Optimization*, **50**(3):1616–1642, 2012. 9, 10, 12, 98, 118, 123, 124, 183

[51] D. Casagrande, A. Astolfi, R. Ortega, and D. Langarica. **A solution to the problem of transient stability of multimachine power systems**. In *51st Conference on Decision and Control*, pages 1703–1708. IEEE, 2012. 9, 87, 94, 109

[52] W. Dib, R. Ortega, and D. Hill. **Transient Stability Enhancement of Multi-Machine Power Systems: Synchronization via Immersion of a Pendular System**. *Asian Journal of Control*, **16**(1):50–58, 2014. 9

[53] R. Ortega, A. van der Schaft, B. Maschke, and G. Escobar. **Interconnection and damping assignment passivity-based control of port-controlled Hamiltonian systems**. *Automatica*, **38**(4):585–596, 2002. 9, 116, 131, 138

[54] A. Tuladhar, H. Jin, T. Unger, and K. Mauch. **Parallel operation of single phase inverter modules with no control interconnections**. In *Applied Power Electronics Conference and Exposition*, **1**, pages 94 –100, feb 1997. 9, 95

[55] J. Guerrero, J. Matas, L. de Vicuna, M. Castilla, and J. Miret. **Wireless-Control Strategy for Parallel Operation of Distributed-Generation Inverters**. *IEEE Transactions on Industrial Electronics*, **53**(5):1461 –1470, oct. 2006. 9, 95

[56] N. L. Soultanis, S. A. Papathanasiou, and N. D. Hatziargyriou. **A Stability Algorithm for the Dynamic Analysis of Inverter Dominated Unbalanced LV Microgrids**. *IEEE Transactions on Power Systems*, **22**(1):294 –304, feb. 2007. 9, 95

[57] M. Marwali, J.-W. Jung, and A. Keyhani. **Stability Analysis of Load Sharing Control for Distributed Generation Systems**. *IEEE Transactions on Energy Conversion*, **22**(3):737–745, Sept 2007. 9

[58] E. Barklund, N. Pogaku, M. Prodanovic, C. Hernandez-Aramburo, and T. Green. **Energy Management System with Stability Constraints for Stand-alone Autonomous Microgrid**. In *IEEE International Conference on System of Systems Engineering*, pages 1–6, April 2007. 9

[59] Y. Mohamed and E. El-Saadany. **Adaptive Decentralized Droop Controller to Preserve Power Sharing Stability of Paralleled Inverters in Distributed Generation Microgrids**. *IEEE Transactions on Power Electronics*, **23**(6):2806 –2816, nov. 2008. 9, 10, 73, 74, 75, 76, 77, 94

[60] E. Barklund, N. Pogaku, M. Prodanovic, C. Hernandez-Aramburo, and T. Green. **Energy Management in Autonomous Microgrid Using Stability-Constrained Droop Control of Inverters**. *IEEE Transactions on Power Electronics*, **23**(5):2346 –2352, sept. 2008. 9, 95

[61] S. Iyer, M. Belur, and M. Chandorkar. **A Generalized Computational Method to Determine Stability of a Multi-inverter Microgrid**. *IEEE Transactions on Power Electronics*, **25**(9):2420 –2432, sept. 2010. 9, 95

[62] G. Diaz, C. Gonzalez-Moran, J. Gomez-Aleixandre, and A. Diez. **Scheduling of Droop Coefficients for Frequency and Voltage Regulation in Isolated Microgrids**. *IEEE Transactions on Power Systems*, **25**(1):489 –496, feb. 2010. 9, 10, 103

[63] N. Ainsworth and S. Grijalva. **A Structure-Preserving Model and Sufficient Condition for Frequency Synchronization of Lossless Droop Inverter-Based AC Networks**. *IEEE Transactions on Power Systems*, **28**(4):4310–4319, Nov 2013. 9, 10

[64] Z. Wang, M. Xia, and M. Lemmon. **Voltage stability of weak power distribution networks with inverter connected sources**. In *American Control Conference*, pages 6577–6582, June 2013. 9, 10, 183

[65] S. Krishnamurthy, T. Jahns, and R. Lasseter. **The operation of diesel gensets in a CERTS microgrid**. In *IEEE PESGM-Conversion and Delivery of Electrical Energy in the 21st Century*, pages 1 –8, july 2008. 9, 84

[66] F. Dörfler, F. Bullo, et al. **Breaking the Hierarchy: Distributed Control & Economic Optimality in Microgrids**. *arXiv preprint arXiv:1401.1767*, 2014. 9, 10, 63, 64, 130, 187

[67] F. Dörfler, M. Chertkov, and F. Bullo. **Synchronization in complex oscillator networks and smart grids**. *Proceedings of the National Academy of Sciences*, **110**(6):2005–2010, 2013. 10, 12

[68] F. Dörfler. *Dynamics and Control in Power Grids and Complex Oscillator Networks*. Ph.d. thesis, University of California at Santa Barbara, September 2013. 10, 12

[69] J. W. Simpson-Porco, F. Dörfler, and F. Bullo. **Droop-controlled inverters are Kuramoto oscillators**. In *IFAC Workshop on Distributed Estimation and Control in Networked Systems*, pages 264–269, Santa Barbara, CA, USA, 2012. 10, 12

[70] J. Schiffer, A. Anta, T. D. Trung, J. Raisch, and T. Sezi. **On power sharing and stability in autonomous inverter-based microgrids**. In *51st Conference on Decision and Control*, pages 1105–1110, Maui, HI, USA, 2012. 10, 68, 77

[71] J. Schiffer, R. Ortega, A. Astolfi, J. Raisch, and T. Sezi. **Conditions for stability of droop-controlled inverter-based microgrids**. *Automatica*, **50**(10):2457–2469, 2014. 10, 58, 68, 77, 94, 105, 115, 117, 131, 167

[72] Q.-C. Zhong. **Robust Droop Controller for Accurate Proportional Load Sharing Among Inverters Operated in Parallel**. *IEEE Transactions on Industrial Electronics*, **60**(4):1281–1290, 2013. 10, 11, 94, 97, 104, 105, 185

[73] Y. W. Li and C.-N. Kao. **An Accurate Power Control Strategy for Power-Electronics-Interfaced Distributed Generation Units Operating in a Low-Voltage Multibus Microgrid**. *IEEE Transactions on Power Electronics*, **24**(12):2977 –2988, dec. 2009. 10, 94, 105

[74] C. K. Sao and P. W. Lehn. **Autonomous load sharing of voltage source converters**. *IEEE Transactions on Power Delivery*, **20**(2):1009–1016, 2005. 10, 94

[75] W. Yao, M. Chen, J. Matas, J. Guerrero, and Z.-M. Qian. **Design and Analysis of the Droop Control Method for Parallel Inverters Considering the Impact of the Complex Impedance on the Power Sharing**. *IEEE Transactions on Industrial Electronics*, **58**(2):576 –588, feb. 2011. 10, 94

[76] C.-T. Lee, C.-C. Chu, and P.-T. Cheng. **A new droop control method for the autonomous operation of distributed energy resource interface converters**. In *IEEE Energy Conversion Congress and Exposition (ECCE)*, pages 702–709, 2010. 10, 94

[77] A. Bidram, A. Davoudi, F. L. Lewis, and Z. Qu. **Secondary control of microgrids based on distributed cooperative control of multi-agent systems**. *IET Generation, Transmission & Distribution*, **7**(8):822–831, 2013. 11, 12, 187

REFERENCES

[78] A. Bidram, A. Davoudi, F. Lewis, and J. Guerrero. **Distributed Cooperative Secondary Control of Microgrids Using Feedback Linearization**. *IEEE Transactions on Power Systems*, **28**(3):3462–3470, 2013. 11, 12, 187

[79] S. Bolognani and S. Zampieri. **A Distributed Control Strategy for Reactive Power Compensation in Smart Microgrids**. *IEEE Transactions on Automatic Control*, **58**(11):2818–2833, Nov 2013. 11, 70, 97, 187

[80] S. Bolognani, G. Cavraro, R. Carli, and S. Zampieri. **A distributed feedback control strategy for optimal reactive power flow with voltage constraints**. *arXiv preprint arXiv:1303.7173*, 2013. 11, 107

[81] J. Rocabert, A. Luna, F. Blaabjerg, and P. Rodriguez. **Control of Power Converters in AC Microgrids**. *IEEE Transactions on Power Electronics*, **27**(11):4734–4749, Nov 2012. 11, 58, 60, 62, 68, 70, 71, 72, 73, 77, 78, 168

[82] Q. Shafiee, J. Guerrero, and J. Vasquez. **Distributed Secondary Control for Islanded Microgrids – A Novel Approach**. *IEEE Transactions on Power Electronics*, **29**(2):1018–1031, 2014. 11, 113, 116, 177

[83] L.-Y. Lu. **Consensus-based P-f and Q-V droop control for multiple parallel-connected inverters in lossy networks**. In *IEEE International Symposium on Industrial Electronics (ISIE)*, pages 1–6, 2013. 11, 116, 177

[84] L.-Y. Lu and C.-C. Chu. **Autonomous power management and load sharing in isolated micro-grids by consensus-based droop control of power converters**. In *1st International Future Energy Electronics Conference (IFEEC)*, pages 365–370, Nov 2013. 11, 116

[85] R. Olfati-Saber, J. A. Fax, and R. M. Murray. **Consensus and cooperation in networked multi-agent systems**. *Proceedings of the IEEE*, **95**(1):215–233, 2007. 11, 12, 23, 25, 26, 107, 147, 184

[86] R. Olfati-Saber and R. M. Murray. **Consensus protocols for networks of dynamic agents**. In *American Control Conference*, 2003. 11

[87] I. Lestas and G. Vinnicombe. **Scalable robust stability for nonsymmetric heterogeneous networks**. *Automatica*, **43**(4):714–723, 2007. 11

[88] R. Olfati-Saber and R. M. Murray. **Consensus problems in networks of agents with switching topology and time-delays**. *IEEE Transactions on Automatic Control*, **49**(9):1520–1533, 2004. 11, 184

[89] F. Xiao and L. Wang. **State consensus for multi-agent systems with switching topologies and time-varying delays**. *International Journal of Control*, **79**(10):1277–1284, 2006. 11

[90] A. Jadbabaie, J. Lin, and A. S. Morse. **Coordination of groups of mobile autonomous agents using nearest neighbor rules**. *IEEE Transactions on Automatic Control*, **48**(6):988–1001, 2003. 11

[91] F. Xiao and L. Wang. **Consensus protocols for discrete-time multi-agent systems with time-varying delays**. *Automatica*, **44**(10):2577–2582, 2008. 11

[92] P.-A. Bliman and G. Ferrari-Trecate. **Average consensus problems in networks of agents with delayed communications**. *Automatica*, **44**(8):1985–1995, 2008. 11, 184

[93] Y. G. Sun, L. Wang, and G. Xie. **Average consensus in networks of dynamic agents with switching topologies and multiple time-varying delays**. *Systems & Control Letters*, **57**(2):175–183, 2008. 11, 184

[94] Y.-P. Tian and C.-L. Liu. **Consensus of multi-agent systems with diverse input and communication delays**. *IEEE Transactions on Automatic Control*, **53**(9):2122–2128, 2008. 11

[95] Y. G. Sun and L. Wang. **Consensus of multi-agent systems in directed networks with nonuniform time-varying delays**. *IEEE Transactions on Automatic Control*, **54**(7):1607–1613, 2009. 11, 184

[96] U. Münz, A. Papachristodoulou, and F. Allgöwer. **Delay robustness in consensus problems**. *Automatica*, **46**(8):1252–1265, 2010. 11, 184

[97] U. Münz, A. Papachristodoulou, and F. Allgöwer. **Robust consensus controller design for nonlinear relative degree two multi-agent systems with communication constraints**. *IEEE Transactions on Automatic Control*, **56**(1):145–151, 2011. 11, 184

[98] W. Ren. **On Consensus Algorithms for Double-Integrator Dynamics**. *IEEE Transactions on Automatic Control*, **53**(6):1503 –1509, july 2008. 11

[99] W. Ren and R. Beard. *Distributed consensus in multi-vehicle cooperative control: theory and applications*. Springer, 2007. 11, 23

[100] W. Yu, G. Chen, and M. Cao. **Some necessary and sufficient conditions for second-order consensus in multi-agent dynamical systems**. *Automatica*, **46**(6):1089–1095, 2010. 11

[101] D. Goldin and J. Raisch. **Consensus for Agents with Double Integrator Dynamics in Heterogeneous Networks**. *Asian Journal of Control*, 2012. 11

[102] D. Goldin. *Stability and Controllability of Double Integrator Consensus Systems in Heterogeneous Networks*. Ph.d. thesis, TU Berlin, 2013. 11, 25

[103] L. Moreau. **Stability of continuous-time distributed consensus algorithms**. In *43rd Conference on Decision and Control*, **4**, pages 3998–4003. IEEE, 2004. 11, 12

[104] N. Chopra and M. W. Spong. **Output synchronization of nonlinear systems with time delay in communication**. In *45th IEEE Conference on Conference on Decision and Control*, pages 4986–4992. IEEE, 2006. 11, 184

[105] E. Nuno, R. Ortega, L. Basañez, and D. Hill. **Synchronization of networks of nonidentical Euler-Lagrange systems with uncertain parameters and communication delays**. *IEEE Transactions on Automatic Control*, **56**(4):935–941, 2011. 11, 184

[106] P. Wieland, J.-S. Kim, H. Scheu, and F. Allgöwer. **On consensus in multi-agent systems with linear high-order agents**. In *Proc. IFAC World Congress*, pages 1541–1546, 2008. 11

[107] J. H. Seo, H. Shim, and J. Back. **Consensus of high-order linear systems using dynamic output feedback compensator: low gain approach**. *Automatica*, **45**(11):2659–2664, 2009. 11

[108] I. Lestas. **Large Scale Heterogeneous Networks, the Davis–Wielandt Shell, and Graph Separation**. *SIAM Journal on Control and Optimization*, **50**(4):1753–1774, 2012. 11

[109] Y. Cao, W. Yu, W. Ren, and G. Chen. **An overview of recent progress in the study of distributed multi-agent coordination**. *IEEE Transactions on Industrial Informatics*, **9**(1):427–438, 2013. 12

[110] M. Bürger and C. De Persis. **Internal models for nonlinear output agreement and optimal flow control**. *arXiv preprint arXiv:1302.0780*, 2013. 12

[111] M. Bürger and C. De Persis. **Dynamic coupling design for nonlinear output agreement and time-varying flow control**. *Automatica*, **51**:210–222, 2015. 12

[112] D. J. Hill and G. Chen. **Power systems as dynamic networks**. In *IEEE International Symposium on Circuits and Systems (ISCAS)*, pages 4–pp. IEEE, 2006. 12

[113] F. Dörfler and F. Bullo. **Synchronization and transient stability in power networks and non-uniform Kuramoto oscillators**. In *American Control Conference*, pages 930 –937, 30 2010-july 2 2010. 12, 98

[114] F. Dörfler and F. Bullo. **On the Critical Coupling for Kuramoto Oscillators**. *SIAM Journal on Applied Dynamical Systems*, **10**(3):1070–1099, 2011. 12

[115] M. Andreasson, H. Sandberg, D. V. Dimarogonas, and K. H. Johansson. **Distributed Integral Action: Stability Analysis and Frequency Control of Power Systems**. In *51st Conference on Decision and Control*, Maui, HI, USA, 2012. 12, 116

[116] M. Andreasson, D. V. Dimarogonas, K. H. Johansson, and H. Sandberg. **Distributed vs. Centralized Power Systems Frequency Control under Unknown Load Changes**. In *12th European Control Conference*, pages 3524–3529, Zürich, Switzerland, 2013. 12, 116

[117] U. Münz and D. Romeres. **Region of Attraction of Power Systems**. In *Estimation and Control of Networked Systems*, **4**, pages 49–54, 2013. 12

[118] J. W. Simpson-Porco, F. Dörfler, Q. Shafiee, J. M. Guerrero, and F. Bullo. **Stability, power sharing, & distributed secondary control in droop-controlled microgrids**. In *IEEE International Conference on Smart Grid Communications (SmartGridComm)*, pages 672–677, Vancouver, BC, Canada, 2013. 12

[119] H. Bouattour, J. W. Simpson-Porco, F. Dörfler, and F. Bullo. **Further results on distributed secondary control in microgrids**. In *52nd Conference on Decision and Control*, pages 1514–1519, Dec 2013. 12, 187

[120] A. Bidram, F. Lewis, and A. Davoudi. **Distributed Control Systems for Small-Scale Power Networks: Using Multiagent Cooperative Control Theory**. *IEEE Control Systems*, **34**(6):56–77, 2014. 12, 64

[121] J. Schiffer, D. Goldin, J. Raisch, and T. Sezi. **Synchronization of droop-controlled microgrids with distributed rotational and electronic generation**. In *52nd Conference on Decision and Control*, pages 2334–2339, Florence, Italy, 2013. 12, 94, 98, 115, 116, 120, 126, 130, 137, 140

[122] J. Schiffer, T. Seel, J. Raisch, and T. Sezi. **A consensus-based distributed voltage control for reactive power sharing in microgrids**. In *13th European Control Conference*, pages 1299–1305, Strasbourg, France, 2014. 58, 62, 94, 105, 106, 109, 115, 116, 117, 144

[123] J. Schiffer, R. Ortega, A. Astolfi, J. Raisch, and T. Sezi. **Stability of synchronized motions of inverter-based microgrids under droop control**. In *19th IFAC World Congress*, pages 6361–6367, Cape Town, South Africa, 2014. 94, 115, 131

[124] J. Schiffer, R. Ortega, C. Hans, and J. Raisch. **Droop-controlled inverter-based microgrids are robust to clock drifts**. In *American Control Conference*, pages 2341–2346, Chicago, IL, USA, 2015. 79, 82, 104, 127

[125] J. Schiffer, T. Seel, J. Raisch, and T. Sezi. **Voltage stability and reactive power sharing in inverter-based microgrids with consensus-based distributed voltage control**. *IEEE Transactions on Control Systems Technology*, 2015. To appear. 62, 94, 105, 106, 109, 115, 116, 117, 119, 144, 167

[126] J. Schiffer, D. Zonetti, R. Ortega, A. Stanković, J. Raisch, and T. Sezi. **Modeling of microgrids - from fundamental physics to phasors and voltage sources**. 2015. Submitted. 28, 51, 67, 68

[127] R. Sepulchre, M. Jankovic, and P. Kokotovic. *Constructive nonlinear control*. Springer, Berlin, 1997. 16

[128] H. K. Khalil. *Nonlinear systems*, **3**. Prentice Hall, 2002. 16, 17, 19, 20, 37, 38, 76, 127, 133

[129] A. van der Schaft. *L2-Gain and Passivity Techniques in Nonlinear Control*. Springer, 2000. 16, 20, 21, 22, 131

[130] S. Sastry. *Nonlinear systems: analysis, stability, and control*, **10**. Springer New York, 1999. 16

[131] E. J. Routh. *A treatise on the stability of a given state of motion: particularly steady motion*. Macmillan and Company, 1877. 22

[132] A. Hurwitz. **Über die Bedingungen unter welchen eine Gleichung nur Wurzeln mit negativen reellen Teilen besitzt**. *Math. Ann.*, **46**:273–284, 1895. 22

[133] E. Frank. **On the zeros of polynomials with complex coefficients**. *Bulletin of the American Mathematical Society*, **52**(2):144–157, 1946. 22, 23

[134] M. Bodson and O. Kiselychnyk. **Analytic conditions for spontaneous self-excitation in induction generators**. In *American Control Conference*, pages 2527–2532, 2010. 22

[135] Z.-J. Tang, T.-Z. Huang, J.-L. Shao, and J.-P. Hu. **Leader-following consensus for multi-agent systems via sampled-data control**. *IET control theory & applications*, **5**(14):1658–1665, 2011. 22

[136] M. Bodson and O. Kiselychnyk. **The complex Hurwitz test for the analysis of spontaneous self-excitation in induction generators**. *IEEE Transactions on Automatic Control*, **58**(2):449–454, 2013. 22

REFERENCES

[137] A. Doria-Cerezo and M. Bodson. **Root locus rules for polynomials with complex coefficients**. In *21st Mediterranean Conference on Control & Automation (MED)*, pages 663–670. IEEE, 2013. 22

[138] A. Doria-Cerezo, M. Bodson, C. Batlle, and R. Ortega. **Study of the Stability of a Direct Stator Current Controller for a Doubly Fed Induction Machine Using the Complex Hurwitz Test**. *IEEE Transactions on Control Systems Technology*, **21**(6):2323–2331, Nov 2013. 22

[139] S. Hara, H. Tanaka, and T. Iwasaki. **Stability Analysis of Systems With Generalized Frequency Variables**. *IEEE Transactions on Automatic Control*, **59**(2):313–326, Feb 2014. 22

[140] C. Godsil and G. Royle. *Algebraic Graph Theory*. Springer, 2001. 23, 24, 126, 137

[141] M. Mesbahi and M. Egerstedt. *Graph theoretic methods in multiagent networks*. Princeton University Press, 2010. 23, 24

[142] W. Ren, R. W. Beard, and E. M. Atkins. **Information consensus in multivehicle cooperative control**. *IEEE Control Systems*, **27**(2):71–82, 2007. 23, 24

[143] H. Roger and R. J. Charles. *Topics in matrix analysis*. Cambridge University Press, 1991. 27

[144] R. A. Horn and C. R. Johnson. *Matrix analysis*. Cambridge university press, 2012. 27, 132, 137, 150, 159

[145] W. D. Stevenson. *Elements of power system analysis*. McGraw Hill Kogakusha Limited, 1975. 27

[146] P. Sauer and M. Pai. *Power system dynamics and stability*. Prentice Hall, 1998. 27, 35, 37, 38, 84, 85, 86, 87

[147] H. Akagi, E. H. Watanabe, and M. Aredes. *Instantaneous power theory and applications to power conditioning*. John Wiley & Sons, 2007. 27, 28, 29, 32, 33, 34

[148] Q.-C. Zhong and T. Hornik. *Control of power inverters in renewable energy and smart grid integration*. John Wiley & Sons, 2012. 27, 29, 31, 32, 34, 39, 68, 74

[149] K. Heuck, K.-D. Dettmann, and D. Schulz. *Elektrische Energieversorgung: Erzeugung, Übertragung und Verteilung elektrischer Energie für Studium und Praxis*. Springer DE, 2013. 27, 29, 31

[150] **DIN 40110-1:1994 - Wechselstromgrößen; Zweileiter-Stromkreise, (engl: "Quantities used in alternating current theory; two-line circuits)**, march 1994. 28, 35

[151] R. H. Park. **Two-reaction theory of synchronous machines generalized method of analysis-part I**. *Transactions of the American Institute of Electrical Engineers*, **48**(3):716–727, 1929. 31, 32

[152] G. C. Paap. **Symmetrical components in the time domain and their application to power network calculations**. *IEEE Transactions on Power Systems*, **15**(2):522–528, 2000. 31, 32

[153] G. Andersson. **Dynamics and control of electric power systems**. *Lecture notes, EEH - Power Systems Laboratory, ETH Zürich*, 2012. 31, 32

[154] S. Fryze. **Wirk-, Blind-und Scheinleistung in elektrischen Stromkreisen mit nichtsinusförmigem Verlauf von Strom und Spannung**. *Elektrotechnische Zeitschrift*, **25**:569–599, 1932. 33

[155] F. Buchholz. *Das Begriffssystem Rechtleistung, Wirkleistung, totale Blindleistung*. Selbstverl.;[Lachner in Komm], 1950. 33

[156] M. Depenbrock. *Untersuchungen über die Spannungs-und Leistungsverhältnisse bei Umrichtern ohne Energiespeicher*. PhD thesis, Mikrokopie GmbH, 1962. 33

[157] H. Akagi, Y. Kanazawa, and A. Nabae. **Generalized theory of the instantaneous reactive power in three-phase circuits**. In *International Power Electronic Conference (IPEC)*, **83**, pages 1375–1386, 1983. 33, 34

[158] J. L. Willems. **A new interpretation of the Akagi-Nabae power components for nonsinusoidal three-phase situations**. *IEEE Transactions on Instrumentation and Measurement*, **41**(4):523–527, 1992. 33, 34

[159] M. Depenbrock. **The FBD-method, a generally applicable tool for analyzing power relations**. *IEEE Transactions on Power Systems*, **8**(2):381–387, 1993. 33

[160] F. Z. Peng and J.-S. Lai. **Generalized instantaneous reactive power theory for three-phase power systems**. *IEEE Transactions on Instrumentation and Measurement*, **45**(1):293–297, 1996. 33, 34

[161] H. Kim and H. Akagi. **The instantaneous power theory on the rotating pqr reference frames**. In *International Conference on Power Electronics and Drive Systems (PEDS)*, **1**, pages 422–427. IEEE, 1999. 33

[162] M. Depenbrock, V. Staudt, and H. Wrede. **Concerning" Instantaneous power compensation in three-phase systems by using pqr theory"**. *IEEE Transactions on Power Electronics*, **19**(4):1151–1152, 2004. 33

[163] M. Aredes, H. Akagi, E. H. Watanabe, E. Vergara Salgado, and L. F. Encarnacao. **Comparisons Between the p–q and p–q–r Theories in Three-Phase Four-Wire Systems**. *IEEE Transactions on Power Electronics,*, **24**(4):924–933, 2009. 33

[164] A. E. Emanuel. **Summary of IEEE standard 1459: definitions for the measurement of electric power quantities under sinusoidal, nonsinusoidal, balanced, or unbalanced conditions**. *IEEE Transactions on Industry Applications*, **40**(3):869–876, 2004. 34

[165] J. L. Willems, J. A. Ghijselen, and A. E. Emanuel. **The apparent power concept and the IEEE standard 1459-2000**. *IEEE Transactions on Power Delivery*, **20**(2):876–884, 2005. 34

[166] W. H. Kersting. *Distribution system modeling and analysis*. CRC press, 2012. 35

[167] N. Mohan and T. M. Undeland. *Power electronics: converters, applications, and design*. John Wiley & Sons, 2007. 36, 68

[168] P. Sauer, D. LaGesse, S. Ahmed-Zaid, and M. Pai. **Reduced order modeling of interconnected multimachine power systems using time-scale decomposition**. *IEEE Transactions on Power Systems*, **2**(2):310–319, 1987. 37

[169] P. W. Sauer. **Time-scale features and their applications in electric power system dynamic modeling and analysis**. In *American Control Conference*, pages 4155–4159. IEEE, 2011. 37

[170] P. Kokotovic, H. K. Khali, and J. O'reilly. *Singular perturbation methods in control: analysis and design*, **25**. Siam, 1999. 37, 76

[171] V. Venkatasubramanian, H. Schattler, and J. Zaborszky. **Fast time-varying phasor analysis in the balanced three-phase large electric power system**. *IEEE Transactions on Automatic Control*, **40**(11):1975–1982, 1995. 38

[172] P. Sauer, S. Ahmed-Zaid, and P. Kokotovic. **An integral manifold approach to reduced order dynamic modeling of synchronous machines**. *IEEE Transactions on Power Systems*, **3**(1):17–23, 1988. 38

[173] P. Kokotovic and P. Sauer. **Integral manifold as a tool for reduced-order modeling of nonlinear systems: A synchronous machine case study**. *IEEE Transactions on Circuits and Systems*, **36**(3):403–410, 1989. 38

[174] M. Hazewinkel. *Encyclopaedia of Mathematics (9)*, **9**. Springer, 1993. 39

[175] S. Dhople, B. Johnson, F. Dörfler, and A. Hamadeh. **Synchronization of Nonlinear Circuits in Dynamic Electrical Networks with General Topologies**. *IEEE Transactions on Circuits and Systems I: Regular Papers*, **61**(9):2677–2690, October 2014. 46, 185, 186

[176] F. Dörfler and F. Bullo. **Kron reduction of graphs with applications to electrical networks**. *IEEE Transactions on Circuits and Systems I: Regular Papers*, **60**(1):150–163, 2013. 47, 98

[177] S. Chowdhury and P. Crossley. *Microgrids and active distribution networks*. The Institution of Engineering and Technology, 2009. 52

[178] N. Lidula and A. Rajapakse. **Microgrids research: A review of experimental microgrids and test systems**. *Renewable and Sustainable Energy Reviews*, **15**(1):186–202, 2011. 52, 53

[179] M. Barnes, J. Kondoh, H. Asano, J. Oyarzabal, G. Ventakaramanan, R. Lasseter, N. Hatziargyriou, and T. Green. **Real-World MicroGrids-An Overview**. In *IEEE Int. Conf. on System of Systems Engineering, 2007. SoSE '07*, pages 1 –8, april 2007. 53

[180] E. Planas, A. Gil-de Muro, J. Andreu, I. Kortabarria, and I. Martínez de Alegría. **General aspects, hierarchical controls and droop methods in microgrids: A review**. *Renewable and Sustainable Energy Reviews*, **17**:147–159, 2013. 53, 63, 64, 65

[181] D. Salomonsson. *Modeling, Control and Protection of Low-Voltage DC Microgrids*. PhD thesis, KTH, Electric Power Systems, 2008. 53

[182] D. Salomonsson, L. Soder, and A. Sannino. **Protection of low-voltage DC microgrids**. *IEEE Transactions on Power Delivery*, **24**(3):1045–1053, 2009. 53

[183] A. Kwasinski and C. N. Onwuchekwa. **Dynamic behavior and stabilization of DC microgrids with instantaneous constant-power loads**. *IEEE Transactions on Power Electronics*, **26**(3):822–834, 2011. 53

[184] X. Wang, J. M. Guerrero, F. Blaabjerg, and Z. Chen. **A review of power electronics based microgrids**. *Journal of Power Electronics*, **12**(1):181–192, 2012. 53, 68, 73

[185] J. J. Justo, F. Mwasilu, J. Lee, and J.-W. Jung. **AC-microgrids versus DC-microgrids with distributed energy resources: A review**. *Renewable and Sustainable Energy Reviews*, **24**:387–405, 2013. 53

[186] G. Joos, B. Ooi, D. McGillis, F. Galiana, and R. Marceau. **The potential of distributed generation to provide ancillary services**. In *IEEE Power Engineering Society Summer Meeting*, **3**, pages 1762–1767. IEEE, 2000. 55, 73

[187] R. C. Dugan, M. F. McGranaghan, and H. W. Beaty. **Electrical power systems quality**. *New York, McGraw-Hill*, **1**, 1996. 56

[188] I. D. Margaris, S. A. Papathanassiou, N. D. Hatziargyriou, A. D. Hansen, and P. Sorensen. **Frequency control in autonomous power systems with high wind power penetration**. *IEEE Transactions on Sustainable Energy*, **3**(2):189–199, 2012. 59

[189] **DIN EN 50160:2010 - Merkmale der Spannung in öffentlichen Elektrizittsversorgungsnetzen, (engl: "Voltage characteristics of electricity supplied by public distribution networks)**, february 2011. 62

[190] ENTSO-E. **Operation Handbook**, 2013. Online: www.entsoe.eu/publications/system-operations-reports/operation-handbook/. 63, 65, 187

[191] J. Guerrero, J. Vasquez, J. Matas, L. de Vicuna, and M. Castilla. **Hierarchical Control of Droop-Controlled AC and DC Microgrids; A General Approach Toward Standardization**. *IEEE Transactions on Industrial Electronics*, **58**(1):158 –172, jan. 2011. 63, 64, 65, 187

[192] A. Bidram and A. Davoudi. **Hierarchical structure of microgrids control system**. *IEEE Transactions on Smart Grid*, **3**(4):1963–1976, 2012. 63, 64, 65, 187

[193] O. Palizban, K. Kauhaniemi, and J. M. Guerrero. **Microgrids in active network managementPart I: Hierarchical control, energy storage, virtual power plants, and market participation**. *Renewable and Sustainable Energy Reviews*, 2014. 64

[194] R. W. Erickson and D. Maksimovic. *Fundamentals of power electronics*. Springer, 2001. 68, 74

[195] C. A. Hans, V. Nenchev, J. Raisch, and C. Reincke-Collon. **Minimax Model Predictive Operation Control of Microgrids**. In *19th IFAC World Congress*, pages 10287–10292, Cape Town, South Africa, 2014. 70, 97, 187

[196] M. Prodanovic and T. C. Green. **Control and filter design of three-phase inverters for high power quality grid connection**. *IEEE Transactions on Power Electronics*, **18**(1):373–380, 2003. 73

[197] F. Blaabjerg, R. Teodorescu, M. Liserre, and A. V. Timbus. **Overview of control and grid synchronization for distributed power generation systems**. *IEEE Transactions on Industrial Electronics*, **53**(5):1398–1409, 2006. 73

[198] H.-P. Beck and R. Hesse. **Virtual synchronous machine**. In *9th Int. Conf. on Electr. Power Quality and Utilisation.*, pages 1 –6, oct. 2007. 73, 94, 100

[199] K. Visscher and S. De Haan. **Virtual synchronous machines for frequency stabilisation in future grids with a significant share of decentralized generation**. In *SmartGrids for Distribution, 2008. IET-CIRED. CIRED Seminar*, pages 1 –4, june 2008. 73, 100

[200] Q. Zhong and G. Weiss. **Synchronverters: Inverters That Mimic Synchronous Generators**. *IEEE Transactions on Industrial Electronics*, **58**(4):1259 – 1267, april 2011. 73, 94, 100

[201] S. Fukuda and T. Yoda. **A novel current-tracking method for active filters based on a sinusoidal internal model [for PWM invertors]**. *IEEE Transactions on Industry Applications*, **37**(3):888–895, 2001. 74

[202] R. Teodorescu, F. Blaabjerg, M. Liserre, and P. C. Loh. **Proportional-resonant controllers and filters for grid-connected voltage-source converters**. *IEE Proceedings-Electric Power Applications*, **153**(5):750–762, 2006. 74

[203] G. Weiss, Q.-C. Zhong, T. C. Green, and J. Liang. **$H\infty$ repetitive control of DC-AC converters in microgrids**. *IEEE Transactions on Power Electronics*, **19**(1):219–230, 2004. 74

[204] T. Hornik and Q.-C. Zhong. **A Current-Control Strategy for Voltage-Source Inverters in Microgrids Based on and Repetitive Control**. *IEEE Transactions on Power Electronics*, **26**(3):943–952, 2011. 74

[205] P. C. Loh and D. G. Holmes. **Analysis of multiloop control strategies for LC/CL/LCL-filtered voltage-source and current-source inverters**. *IEEE Transactions on Industry Applications*, **41**(2):644–654, 2005. 74

[206] S. Chiniforoosh, J. Jatskevich, A. Yazdani, V. Sood, V. Dinavahi, J. Martinez, and A. Ramirez. **Definitions and Applications of Dynamic Average Models for Analysis of Power Systems**. *Power Delivery, IEEE Transactions on*, **25**(4):2655–2669, Oct 2010. 74

[207] S. Chiniforoosh, J. Jatskevich, A. Yazdani, V. Sood, V. Dinavahi, J. Martinez, and A. Ramirez. **Definitions and applications of dynamic average models for analysis of power systems**. *IEEE Transactions on Power Delivery*, **25**(4):2655–2669, 2010. 74

[208] U. Münz and M. Metzger. **Voltage and Angle Stability Reserve of Power Systems with Renewable Generation**. In *19th IFAC World Congress*, pages 9075–9080, Cape Town, South Africa, 2014. 77

[209] H. Kopetz. *Real-time systems: design principles for distributed embedded applications*. Springer, 2011. 78, 79

[210] L. Schenato and G. Gamba. **A distributed consensus protocol for clock synchronization in wireless sensor network**. In *46th IEEE Conference on Decision and Control*, pages 2289–2294. IEEE, 2007. 78, 81

[211] L. Schenato and F. Fiorentin. **Average timesynch: A consensus-based protocol for clock synchronization in wireless sensor networks**. *Automatica*, **47**(9):1878–1886, 2011. 78, 81

[212] A. Engler. **Applicability of droops in low voltage grids**. *International Journal of Distributed Energy Resources*, **1**(1):1–6, 2005. 78, 96, 97, 169

[213] Anritsu. **Understanding Frequency Accuracy in Crystal Controlled Instruments - Application Note**. Technical report, Anritsu EMEA Ltd., 2001. 78, 79, 80, 127

[214] R. H. Bishop. *Mechatronic systems, sensors, and actuators: fundamentals and modeling*. CRC press, 2007. 79

[215] J. G. Webster and H. Eren. *Measurement, Instrumentation, and Sensors Handbook: Spatial, Mechanical, Thermal, and Radiation Measurement*, **1**. CRC press, 2014. 79

[216] J. C. Butcher. *Numerical methods for ordinary differential equations*. John Wiley & Sons, 2008. 80

[217] O. Kukrer. **Discrete-time current control of voltage-fed three-phase PWM inverters**. *IEEE Transactions on Power Electronics*, **11**(2):260–269, 1996. 82

[218] D. Maksimovic and R. Zane. **Small-signal discrete-time modeling of digitally controlled PWM converters**. *IEEE Transactions on Power Electronics*, **22**(6):2552–2556, 2007. 82

[219] T. Nussbaumer, M. L. Heldwein, G. Gong, S. D. Round, and J. W. Kolar. **Comparison of prediction techniques to compensate time delays caused by digital control of a three-phase buck-type PWM rectifier system**. *IEEE Transactions on Industrial Electronics*, **55**(2):791–799, 2008. 82

[220] D. Angeli and D. Efimov. **On Input-to-State Stability with respect to decomposable invariant sets**. In *52nd Conference on Decision and Control*, pages 5897–5902. IEEE, 2013. 82

[221] D. Efimov, R. Ortega, and J. Schiffer. **ISS of multistable systems with delays: application to droop-controlled inverter-based microgrids**. In *American Control Conference*, pages 4664–4669, Chicago, IL, USA, 2015. 82

[222] I. Langmuir. **The relation between contact potentials and electrochemical action**. *Transactions of the American Electrochemical Society*, **29**:125–180, 1916. 84

[223] N. Tsolas, A. Arapostathis, and P. Varaiya. **A structure preserving energy function for power system transient stability analysis**. *IEEE Transactions on Circuits and Systems*, **32**(10):1041–1049, Oct 1985. 87

[224] Y. Wang, L. Xie, D. Hill, and R. Middleton. **Robust nonlinear controller design for transient stability enhancement of power systems**. In *31st Conference on Decision and Control*, pages 1117–1122. IEEE, 1992. 87, 109

[225] Y. Wang, D. J. Hill, R. H. Middleton, and L. Gao. **Transient stability enhancement and voltage regulation of power systems**. *IEEE Transactions on Power Systems*, **8**(2):620–627, 1993. 87, 109

[226] H.-D. Chang, C.-C. Chu, and G. Cauley. **Direct stability analysis of electric power systems using energy functions: theory, applications, and perspective**. *Proceedings of the IEEE*, **83**(11):1497–1529, Nov 1995. 87

[227] Y. Wang, G. Guo, and D. J. Hill. **Robust decentralized nonlinear controller design for multimachine power systems**. *Automatica*, **33**(9):1725–1733, 1997. 87, 109

[228] Y. Guo, D. J. Hill, and Y. Wang. **Nonlinear decentralized control of large-scale power systems**. *Automatica*, **36**:1275–1289, 2000. 87, 109

[229] Y. Guo, D. Hill, and Y. Wang. **Global transient stability and voltage regulation for power systems**. *IEEE Transactions on Power Systems*, **16**(4):678–688, Nov 2001. 87

[230] M. Galaz, R. Ortega, A. S. Bazanella, and A. M. Stankovic. **An energy-shaping approach to the design of excitation control of synchronous generators**. *Automatica*, **39**(1):111–119, 2003. 87

[231] D. Casagrande, A. Astolfi, and R. Ortega. **Global stabilization of non-globally linearizable triangular systems: Application to transient stability of power systems**. In *50th Conference on Decision and Control and European Control Conference*, pages 331–336, 2011. 87, 94, 109

[232] T. Van Cutsem and C. Vournas. *Voltage stability of electric power systems*, **441**. Springer, 1998. 87, 184

[233] **Load representation for dynamic performance analysis [of power systems]**. *IEEE Transactions on Power Systems*, **8**(2):472–482, May 1993. 87, 184

[234] K. Turitsyn, P. Sulc, S. Backhaus, and M. Chertkov. **Options for control of reactive power by distributed photovoltaic generators**. *Proceedings of the IEEE*, **99**(6):1063–1073, 2011. 89

[235] A. Krishna. *Voltage Stability and Reactive Power Sharing in Microgrids with Distributed Rotational and Electronic Generation*. Master's thesis, TU Berlin/ Indian Institute of Technology Roorkee, 2014. 94, 105, 106, 109

[236] P. Villenueve. **Concerns generated by islanding [electric power generation]**. *Power and Energy Magazine, IEEE*, **2**(3):49 – 53, may-june 2004. 95

[237] K. De Brabandere, B. Bolsens, J. Van den Keybus, A. Woyte, J. Driesen, and R. Belmans. **A Voltage and Frequency Droop Control Method for Parallel Inverters**. *IEEE Transactions on Power Electronics*, **22**(4):1107 –1115, july 2007. 97, 185

[238] J. Guerrero, J. Matas, L. G. de Vicuna, M. Castilla, and J. Miret. **Decentralized Control for Parallel Operation of Distributed Generation Inverters Using Resistive Output Impedance**. *IEEE Transactions on Industrial Electronics*, **54**(2):994 –1004, april 2007. 97, 133, 185

[239] J. Guerrero, L. Garcia de Vicuna, J. Matas, M. Castilla, and J. Miret. **Output Impedance Design of Parallel-Connected UPS Inverters With Wireless Load-Sharing Control**. *IEEE Transactions on Industrial Electronics*, **52**(4):1126 – 1135, aug. 2005. 97, 104

[240] A. Bergen and D. Hill. **A Structure Preserving Model for Power System Stability Analysis**. *IEEE Transactions on Power Apparatus and Systems*, **PAS-100**(1):25 –35, jan. 1981. 98, 184

[241] C. Hernandez-Aramburo, T. Green, and N. Mugniot. **Fuel consumption minimization of a microgrid**. *IEEE Transactions on Industry Applications*, **41**(3):673 – 681, may-june 2005. 103

[242] W. Ren. **Synchronization of coupled harmonic oscillators with local interaction**. *Automatica*, **44**(12):3195 – 3200, 2008. 116

[243] R. J. Davy and I. A. Hiskens. **Lyapunov functions for multimachine power systems with dynamic loads**. *IEEE Transactions on Circuits and Systems I: Fundamental Theory and Applications*, **44**(9):796–812, 1997. 118, 184

[244] H.-D. Chiang, F. Wu, and P. Varaiya. **A BCU method for direct analysis of power system transient stability**. *IEEE Transactions on Power Systems*, **9**(3):1194 –1208, aug 1994. 120, 123

[245] S. Rabinowitz. **How to find the square root of a complex number**. *Mathematics and Informatics Quarterly*, **3**:54–56, 1993. 126

[246] D. P. Bertsekas, A. Nedić, and A. E. Ozdaglar. *Convex analysis and optimization*. Athena Scientific Belmont, 2003. 146

[247] J. Willems. **A partial stability approach to the problem of transient power system stability**. *International Journal of Control*, **19**(1):1–14, 1974. 157

[248] H. Rosenbrock. **Design of multivariable control systems using the inverse Nyquist array**. In *Proceedings of the Institution of Electrical Engineers*, **116**, pages 1929–1936. IET, 1969. 166

[249] S. Skogestad and I. Postlethwaite. *Multivariable Feedback Control: Analysis and Design*. John Wiley & Sons, 2005. 166

[250] A. Mees. **Achieving diagonal dominance**. *Systems & Control Letters*, **1**(3):155–158, 1981. 166

[251] D. J. Limebeer. **The application of generalized diagonal dominance to linear system stability theory**. *International Journal of Control*, **36**(2):185–212, 1982. 166

[252] J. Raisch. *Mehrgrößenregelung im Frequenzbereich*, **98**. Oldenbourg Verlag, 1994. 166

[253] K. Rudion, A. Orths, Z. Styczynski, and K. Strunz. **Design of benchmark of medium voltage distribution network for investigation of DG integration**. In *IEEE PESGM*, 2006. 167, 168, 169, 170, 175

[254] Z. Styczynski, A. Orths, K. Rudion, A. Lebioda, and O. Ruhle. **Benchmark for an Electric Distribution System with Dispersed Energy Resources**. In *IEEE PES Transmission and Distribution Conference and Exhibition*, pages 314–320, May 2006. 167, 168

[255] Plexim GmbH. **Plecs software, www.plexim.com**, 2013. 167

[256] IEEE. **IEEE Recommended Practice for Industrial and Commercial Power Systems Analysis (Brown Book)**. *IEEE Standard 399-1997*, pages 1–488, Aug 1998. 168

[257] D. J. Hill and I. M. Mareels. **Stability theory for differential/algebraic systems with application to power systems**. In *Robust Control of Linear Systems and Nonlinear Control*, pages 437–445. Springer, 1990. 184

[258] D. Karlsson and D. J. Hill. **Modelling and identification of nonlinear dynamic loads in power systems**. *IEEE Transactions on Power Systems*, **9**(1):157–166, 1994. 184

[259] **Standard load models for power flow and dynamic performance simulation**. *IEEE Transactions on Power Systems*, **10**(3):1302–1313, Aug 1995. 184

[260] H. Renmu, M. Jin, and D. J. Hill. **Composite load modeling via measurement approach**. *IEEE Transactions on Power systems*, **21**(2):663–672, 2006. 184

[261] T. L. Vandoorn, B. Renders, L. Degroote, B. Meersman, and L. Vandevelde. **Active load control in islanded microgrids based on the grid voltage**. *IEEE Transactions on Smart Grid*, **2**(1):139–151, 2011. 185

[262] S. Fiaz, D. Zonetti, R. Ortega, J. Scherpen, and A. van der Schaft. **A port-Hamiltonian approach to power network modeling and analysis**. *European Journal of Control*, **19**(6):477–485, 2013. 185

[263] L. A. Tôrres, J. P. Hespanha, and J. Moehlis. **Power supply synchronization without communication**. In *IEEE Power and Energy Society General Meeting*, pages 1–6. IEEE, 2012. 185, 186

[264] S. Y. Caliskan and P. Tabuada. **Towards a compositional analysis of multi-machine power systems transient stability**. In *52nd Conference on Decision and Control*, pages 3969–3974. IEEE, 2013. 185, 186

[265] S. Caliskan and P. Tabuada. **Compositional Transient Stability Analysis of Multimachine Power Networks**. *IEEE Transactions on Control of Network Systems*, **1**(1):4–14, March 2014. 185, 186

[266] L. Tôrres, J. P. Hespanha, and J. Moehlis. **Synchronization of Oscillators Coupled through a Network with Dynamics: A Constructive Approach with Applications to the Parallel Operation of Voltage Power Supplies**. *IEEE Transactions on Automatic Control. Current status: under review*, 2013. 185, 186

[267] B. Johnson, S. Dhople, A. Hamadeh, and P. Krein. **Synchronization of nonlinear oscillators in an LTI power network**. *IEEE Transactions on Circuits and Systems I: Regular Papers*, **61**(3):834–844, 2014. 185, 186

[268] S. Bolognani, G. Cavraro, and S. Zampieri. **A distributed feedback control approach to the optimal reactive power flow problem**. In *Control of Cyber-Physical Systems*, pages 259–277. Springer, 2013. 187